EPIDEMIOLOGY AND BIOMECHANICAL ANALYSIS OF FACIAL FRACTURES

Joseph M Cormier

Dissertation submitted to the faculty of the Virginia Polytechnic Institute and State University in partial fulfillment of the requirements for the degree of

Doctor of Philosophy

In

Biomedical Engineering

Committee

Dr. Stefan M. Duma, Ph.D., Chair
Dr. H. Clay Gabler, Ph.D., Co-chair
Dr. James R. Funk, Ph.D.
Dr. Michael L. Madigan, Ph.D.
Dr. Joel D. Stitzel, Ph.D.

February 6, 2009
Blacksburg, Virginia

Keywords: face, risk, frontal, nasal, maxilla, mandible, FOCUS, NASS

EPIDEMIOLOGY AND BIOMECHANICAL ANALYSIS OF FACIAL FRACTURES

Joseph M Cormier

(ABSTRACT)

The purpose of this dissertation is to examine the occurrence of facial fractures in automotive collisions and to determine the tolerance of the facial bones to blunt impact. The effects of restraint use, impact severity and impact direction on facial fractures were evaluated using the NASS-CDS database. The association between brain injury and facial fractures was also examined. The tolerance of the frontal bone, nasal bone, maxilla and mandible was determined using the flat surface of a cylindrical impactor. The influence of anthropometric measures and geometrical descriptors on the tolerance of the facial bones is also presented. The force-displacement response of each impacted region was also determined and response corridors were created. These corridors were used to evaluate the biofidelity of the FOCUS headform under the same impact conditions. Mathematical models were also created to predict the force and displacement resulting from facial impact. The data contained in this dissertation can be used to determine the risk of facial fracture as a function of impact force and evaluate the biofidelity of models simulating facial impact.

ACKNOWLEDGEMENTS

There are a lot of people who helped me through my doctorial career. At work, the employees at BRC were always supportive and willing to help in any way possible and at Virginia Tech the students and professors at the Center for Injury Biomechanics went out of their way to help me with my experiments and improve the analyses involved in the work.

My advisor, Stefan Duma has been involved in my academic career since beginning my master's degree. He has always wanted me to excel and without his support, I would not have made it through my doctorial pursuit. His support and guidance has helped make me a better researcher and will continue to help me throughout my career.

Dr. Joel Stitzel has been an inspiration to me since working with him while obtaining my master's degree. He has always been very willing to help and cared about the success of the other students as much as his own.

I would like to thank the remainder of my committee, Dr. Michael Madigan, Dr. Clay Gabler and Dr. Jim Funk for their help in making the dissertation better and their willingness to take the time to help me during my graduate studies.

Lastly, I owe a great deal of thanks to my friends and family for their continued support throughout my academic career. Especially my mom and sister for always giving me a reason to continue and look forward to the too few times we could see each other. Thank you very much for all your love and support.

TABLE OF CONTENTS

LIST OF FIGURES

LIST OF TABLES

CHAPTER 1:
THE EPIDEMIOLOGY OF FACIAL INJURIES IN AUTOMOTIVE COLLISIONS

INTRODUCTION

The four most common sources of facial trauma are Motor Vehicle Collision (MVC), assault, sports and falls (Lim 1993; Muraoka 1995; Jayamanne and Gillie 1996; Shapiro 2001; Gassner 2003). Facial fractures incurred due to a MVC are more likely to result in associated head injury; therefore, the identification of parameters associated with facial fracture will reduce the likelihood of more severe head injuries (Lim 1993). A study of over 3,000 hospital ER patients found that the zygoma is the most frequently fractured facial bone (Hackle 2001). Orbital blow-out fractures have also been shown to be among the most common facial fractures due to a MVC (Jayamanne and Gillie 1996; Hackle 2001). Studies examining the effects of restraint systems have found that the presence of an airbag and seatbelt use reduced the likelihood of sustaining a facial fracture (Murphy 2000; Shapiro 2001). Examining hospital records with a focus on age, one study found that older patients were more likely to die as a result of facial and related trauma (Haymond 1988).

The majority of the previous work on facial fractures is limited to a review of a series of trauma cases. These offer no information regarding the relationship between facial trauma and the collision event. The National Automotive Sampling System – Crashworthiness Data System (NASS-CDS) represents a sample of vehicular crashes in the United States that is weighted to represent national trends. Approximately half of these provide information regarding the severity of the collision in terms of Delta-V (ΔV) and the Principal Direction of Force (PDOF). These variables, among others, are frequently utilized to estimate the risk of occupant injury in automotive impacts. Knowing the ΔV of impacts that cause facial fractures will also help relate the occurrence of these injuries to testing performed by the NHTSA to evaluate vehicle performance using crash test dummies. The purpose of this chapter is to examine the patterns of facial injury, occupant characteristics and concomitant injuries within the NASS – CDS.

METHODOLOGY

The data for this study were obtained from the NASS-CDS database for years 1993 to 2007. All data were processed using the Statistical Analysis Software (SAS Institute, Cary N.C). Unless stated otherwise all analyses were limited to occupants 18 years of age or older. Events including a rollover or ejected occupants were excluded. The "system / organ" definition within the SAS data files was used to determine whether the occupant incurred a facial injury. Facial fracture was further determined using the "lesion" variable, with the exception of teeth fractures and rupture of the mucosal membranes of the nose which were not included in the analysis as a facial fracture. Frontal bone fracture does not have a specific AIS Code within NASS; therefore, these fractures were identified by the body region and aspect for each injury. A vault fracture with an anterior aspect is the designation for a frontal bone fracture and these were identified within the NASS dataset and included within the facial fracture variable. Frontal bone fractures and facial fractures were combined to create a single variable indicating whether or not a person incurred a facial fracture. The final dataset included a total of 93,339 occupants weighted to 43,325,675.

The influence of vehicle and occupant parameters on the risk of facial fracture was assessed using risk ratios. Confidence intervals for risk ratios were determined using the unweighted data and risks were determined using weighted data. Using the unweighted data for risk ratios maintains the correct distribution of occupant and vehicle parameters, which is disturbed by weighting the data. Using the weighted data for the overall risk produces more conservative risks because low-severity impacts in the NASS-CDS database are underrepresented in the raw data. The correlation between variables was assessed using Pearson's test for correlation.

For frontal and rear impacts, occupants seated in the front outboard positions were analyzed separately. For side impacts, occupants seated in the outboard position of the front and rear seats were grouped into near and far side impacts. Variables describing the

availability of side airbags and deployment status were combined to assess the effects of side airbags. The BAGAVOTH variable in the NASS database specifies the availability of other airbags besides a frontal airbag. The BAGDEPOT variable can then be used to determine if the denoted bag deployed during the event (NHTSA 1997). The variable RESTYPE identifies the type of airbags available within the vehicle; therefore, when combined with BAGAVOTH, the type of side airbag available to an occupant can be determined. Injury sources for occupants in frontal impacts were analyzed separately for drivers and right front passengers. No methods were utilized to account for missing data. Observations missing data of interest were not utilized for that particular analysis.

Statistical models were created to estimate the risk of facial injuries and the influence on vehicle and occupant descriptors. Non-parametric models were created using the Consistent Threshold method described by Nusholtz and Mosier (Nusholtz and Mosier 1999). The CT method is designed to determine the risk of an outcome based on doubly censored data. The data obtained from NASS CDS are doubly censored because the only measure of exposure is a single number describing the change in velocity of the vehicle which is not a measure of the exact exposure level necessary to cause the injury. The methodology for calculating the CT risk function was implemented into a custom algorithm in Matlab (The Mathworks, Natick MA) to determine the risk of injury for various occupant groups as a function of delta-V (ΔV). Survival analysis was also performed using a parametric approach for determining the risk of facial injury.

A Weibull model was chosen because of its increasing hazard model with severity and the closed form solution of its Cumulative Distribution Function (Lee 2003). The Weibull CDF is given by,

$$CDF = 1 - \exp -(\lambda \cdot \Delta V)^{\gamma} \qquad \text{(Equation 1)}$$

where λ and γ are the scale and shape parameters respectively and ΔV is the change in velocity of the vehicle. This function will provide an estimate of risk of injury using the maximum likelihood estimate of the scale and shape parameters. The LIFEREG

procedure within SAS accounts for left and right censoring and, therefore will be used to determine the parameter estimates (Allison 1995; Cantor 2003).

RESULTS

Trends in facial injury and facial fracture were examined utilizing the NASS CDS data set for years 1993 to 2007. In NASS the frontal bone is not designated as a facial structure, therefore, facial injuries do not include an injury to the frontal bone. In this study, a facial fracture can include the frontal bone. Facial injuries of AIS = 1 comprise 91% of all facial injuries, whereas for facial fractures, AIS = 1 comprises only 39%.

Overall Trends

Overall trends in facial injuries were investigated by examining various parameters for all occupants, without regard for impact direction. This dataset contained 93,339 unweighted occupants, and was the largest dataset because of the lack for a need of a vehicle inspection to determine a ΔV. The frequency of facial fractures by year has decreased by approximately 1,000 weighted cases over the last four years (Figure 1). During 2007 there were 8000 weighted cases of facial fracture due to frontal impacts and 1350 during side impacts. Both weighted and unweighted (Figure 2) data demonstrated an increase between 1995 and 1997 with a sharp decline after 1997. These trends were present within after examining the data for unrealistic weighting factors. The unweighted counts for frontal impacts did not demonstrate the same decreasing trend as the weighted data.

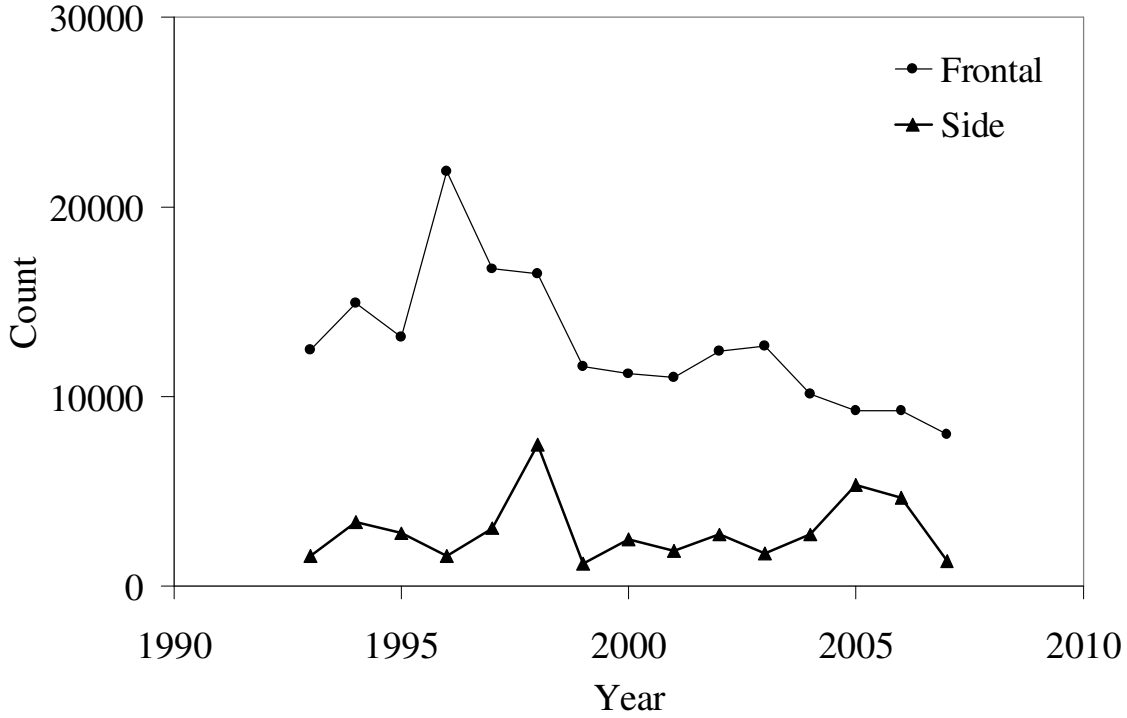

Figure 1: Weighted number of facial fractures by year and impact direction.

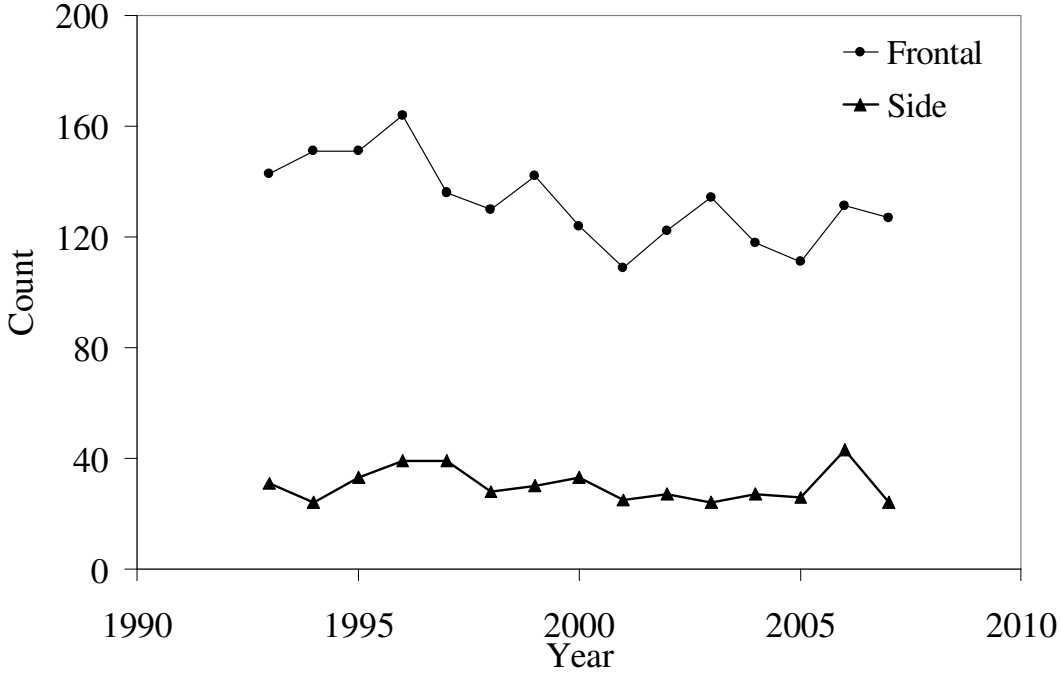

Figure 2: Unweighted number of facial fractures by year and impact direction.

The most common facial injuries were abrasions (21%), contusions (32%), lacerations (32%) and fractures (11%). Belt use reduced the risk of facial injury (**R**isk **R**atio RR: 0.5, 95% **C**onfidence **I**nterval CI: 0.47-0.51), facial fracture (RR: 0.36 CI: 0.34-0.39) and

brain injury (RR: 0.51 CI: 0.49-0.52) ($p<0.0001$ for all comparisons). There was no statistical difference in risk of facial injury between drivers and right front passengers. Males over the age of 18 had a statistically higher risk of facial fractures (RR: 1.47 CI: 1.4-1.6) and brain injuries (RR: 1.14 CI: 1.1-1.2) than females.

Facial fracture is 1.5 times ($p<0.0001$) more likely in a frontal impact than a side impact and has an overall risk of 1% in the NASS-CDS database.

Frontal Impacts

Within the dataset containing known ΔVs, there were a total of 37,630 drivers (weighted = 17,073,744) and 8,700 right front passengers (weighted = 3,469,836). Frontal impacts posed the greatest risk of any facial injury (6%), facial injury of AIS 2+ (1%) and facial fracture (1%) compared to other impact directions. The most common facial fractures sustained by drivers (Figure 3) and right front passengers (Figure 4) were to the nose, mandible, orbit and maxilla. Restraint use had only marginal effects on the distribution of facial injuries to drivers in frontal impacts. Right front passengers who were restrained by an airbag and seatbelt did not incur any frontal or zygomatic fractures. Maxilla fractures were most common for unbelted occupants exposed to an airbag. This trend was present for drivers, but not as pronounced.

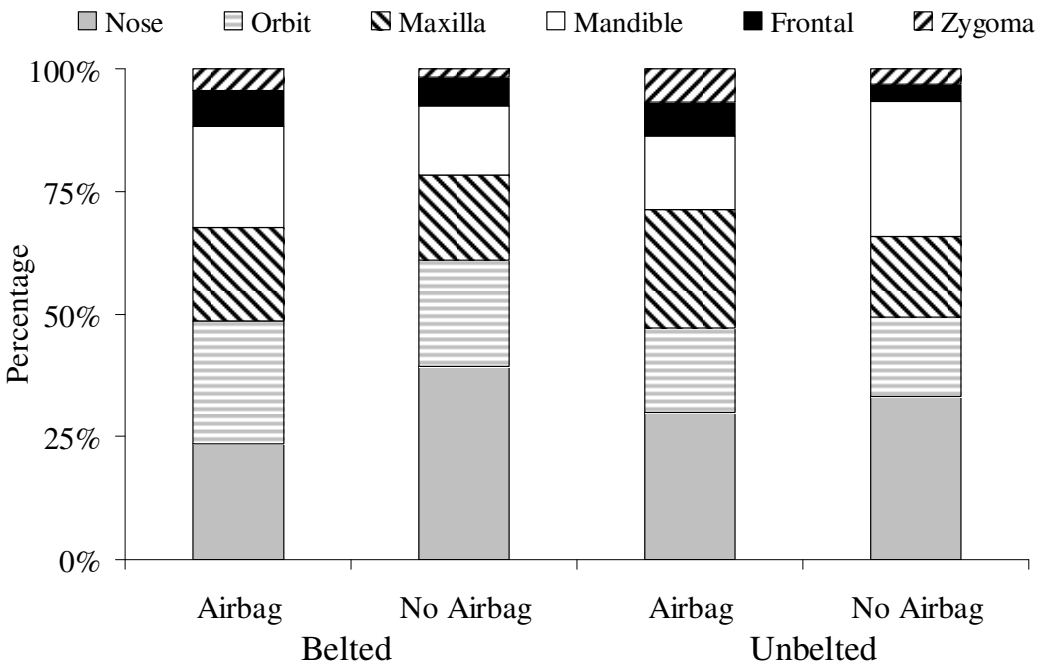

Figure 3: Distribution of facial bone fractures for adult drivers in frontal impacts using unweighted data.

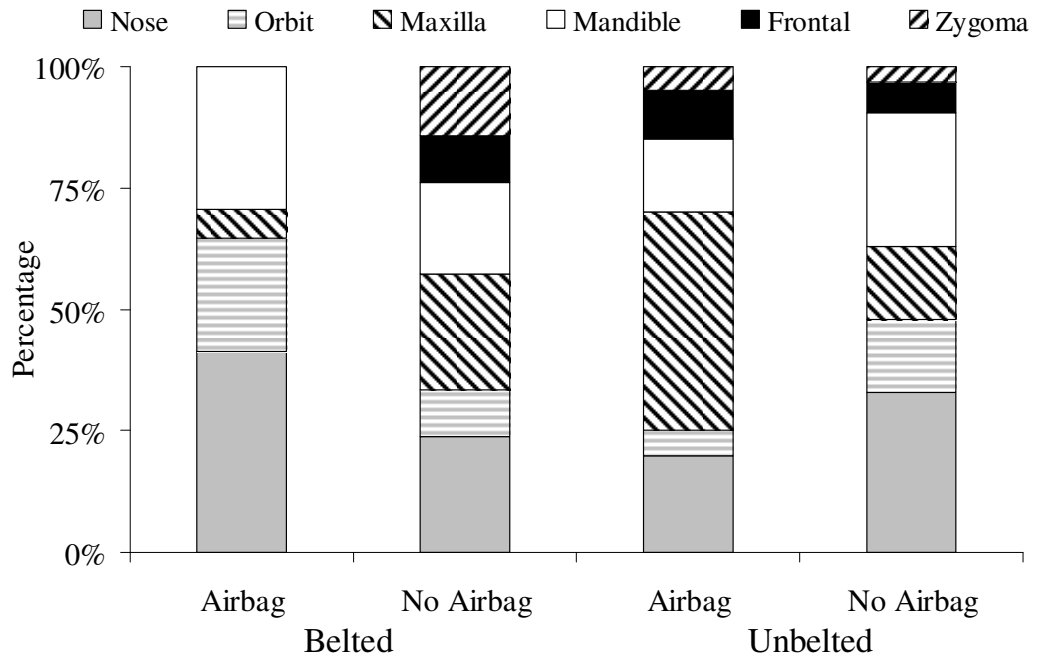

Figure 4: Distribution of facial bone fractures for adult right front passengers in frontal impacts using unweighted data.

Risk ratios were determined to illustrate the effects of various restraint parameters (Table 1). As an example, airbags were more effective in reducing the risk of facial injury (RR:

0.73 CI: 0.68-.0.79) in belted (RR: 0.5 CI: 0.42-.077) than unbelted (RR: 0.65 CI: 0.56-.075) occupants. If the risk ratio is less than one, the reference group has a lower risk than the comparison. The closer the risk ratio and confidence intervals are to 1, the smaller the difference between the reference and comparison groups. Seat position, BMI and gender did not have a significant influence on the risk of sustaining a facial injury.

Table 1: Risk ratios by injury type for adult occupants in frontal impacts.

Facial Fracture

Data Segment	Reference	Comparison	Risk Ratio	95% Confidence Interval		P value
All	Belted	Unbelted	0.26	0.23	0.28	< 0.0001
Belted	Airbag	No Airbag	0.51	0.43	0.59	< 0.0001
Unbelted			0.65	0.57	0.76	< 0.0001

Facial Fracture (AIS 3+)

Data Segment	Reference	Comparison	Risk Ratio	95% Confidence Interval		P value
All	Belted	Unbelted	0.26	0.23	0.30	< 0.0001
Belted	Airbag	No Airbag	0.58	0.48	0.71	< 0.0001
Unbelted			0.80	0.67	0.96	0.015

Injury Sources

Injury sources were identified for occupants sustaining a facial fracture by seating position in frontal impacts (Figure 5 - Figure 6). In order to normalize for collision severity when analyzing the effect of airbag deployments, frontal collisions with a ΔV less than 25 km/h were excluded for the injury source analyses. Among belted occupants sustaining a facial fracture that were exposed to an airbag, 7% were defined as having a "same occupant contact" and 4% sustained their facial fracture as a result of contact with the B pillar. Same occupant contact indicates that the injury source was attributed to contact with some part of the occupant incurring the facial fracture. For passengers, sections of the roof became more prominent injury sources, including the sunvisor and header regions.

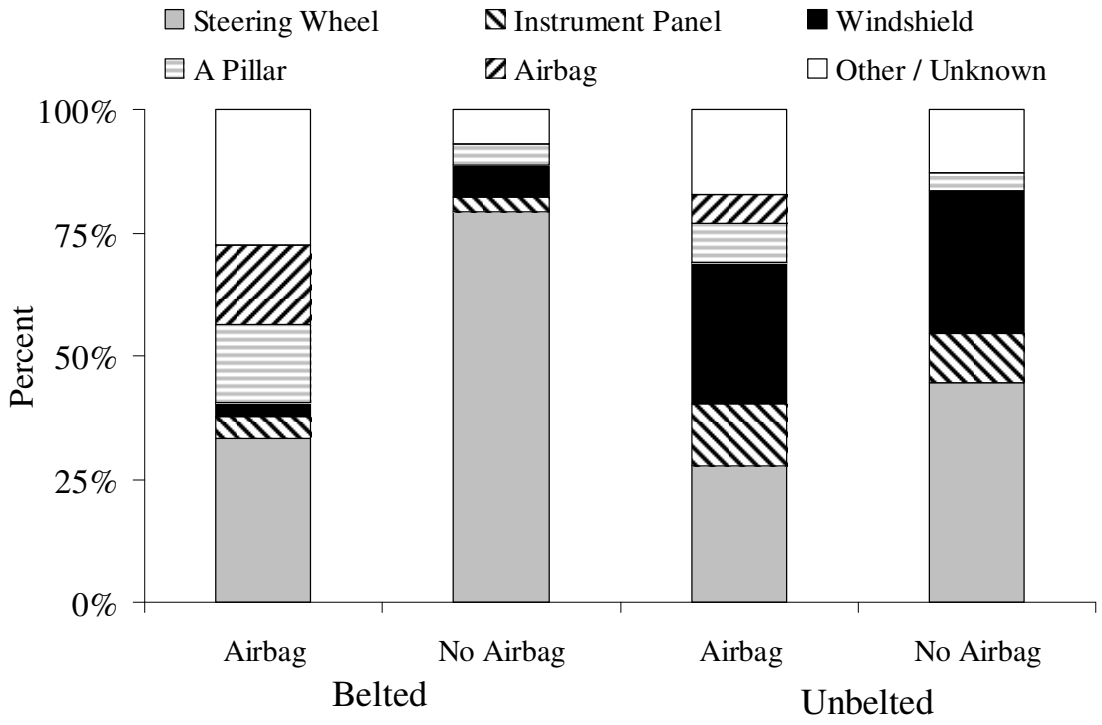

Figure 5: Injury sources for drivers in frontal impacts with a facial fracture.

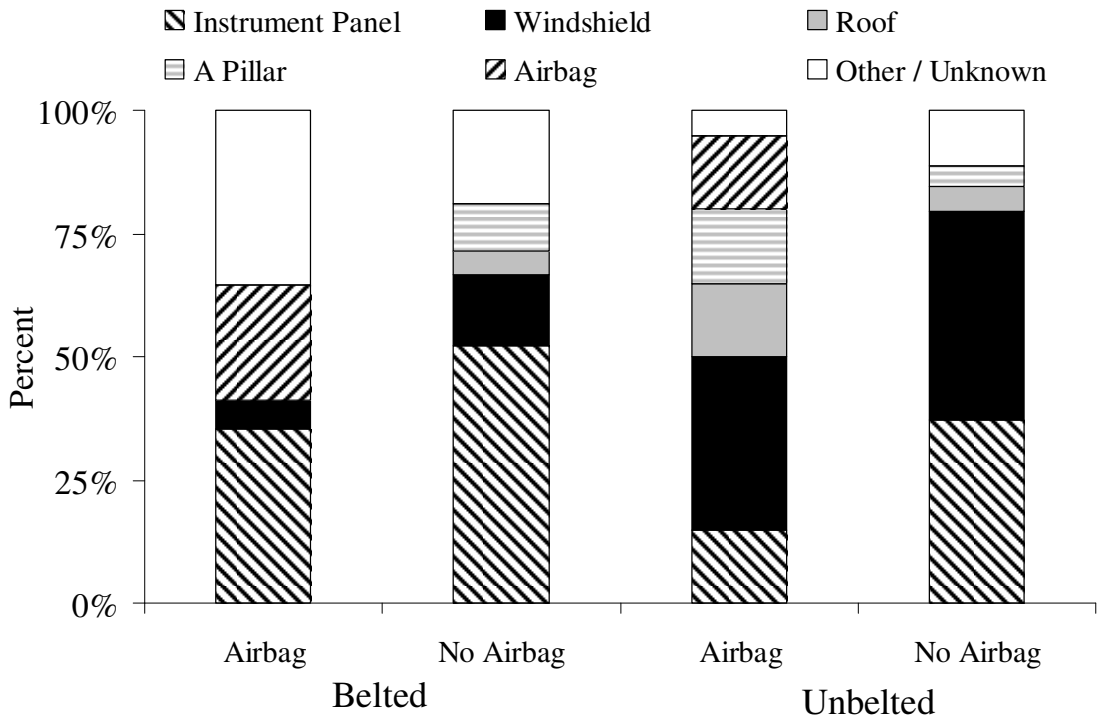

Figure 6: Injury sources for right front passengers in frontal impacts with a facial fracture.

Risk of Facial Fracture

In frontal impacts, approximately 50% of the facial fractures occur at a ΔV less than 35 km/h (Figure 7). As a comparison, 50% of the occupants with a maximum AIS of 3+ occurred at a ΔV less than 26 km/h indicating that facial fractures are associated with higher severity crashes than other injuries. Vehicle ΔV was used to predict the risk of facial fracture (Figure 8) and facial injury (AIS 3+) for belted and unbelted occupants (Figure 9). These risks were generated by using the weighted data within the NASS-CDS dataset.

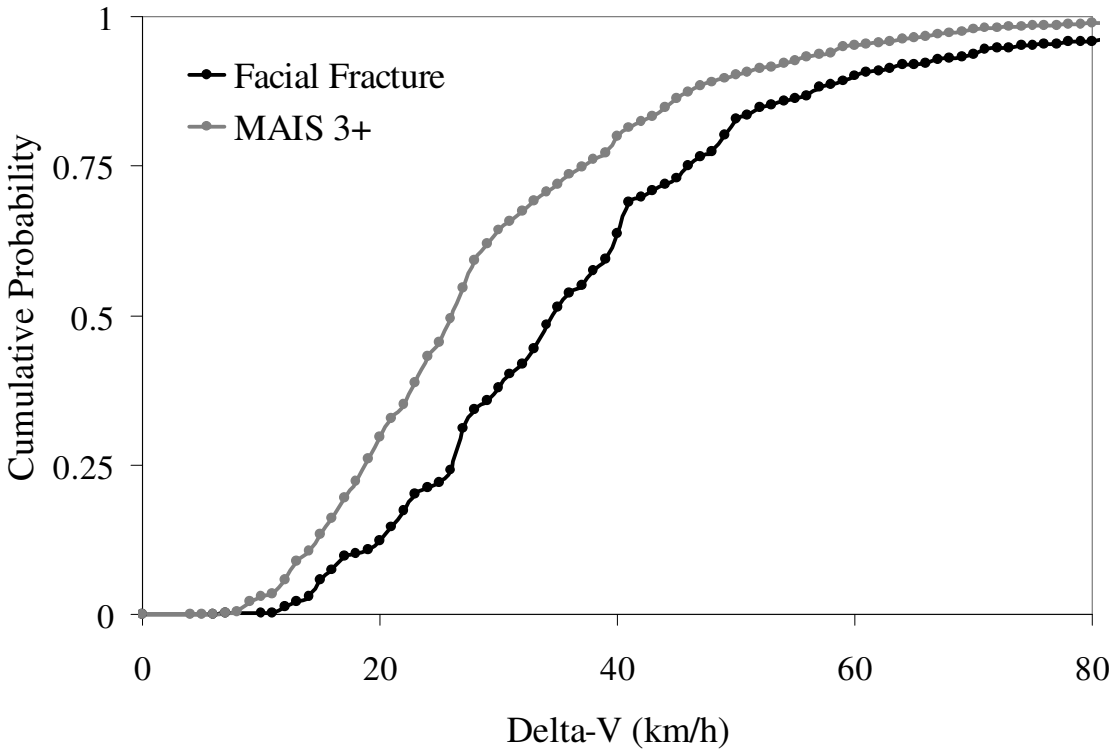

Figure 7: Cumulative distribution of facial fractures in frontal impacts.

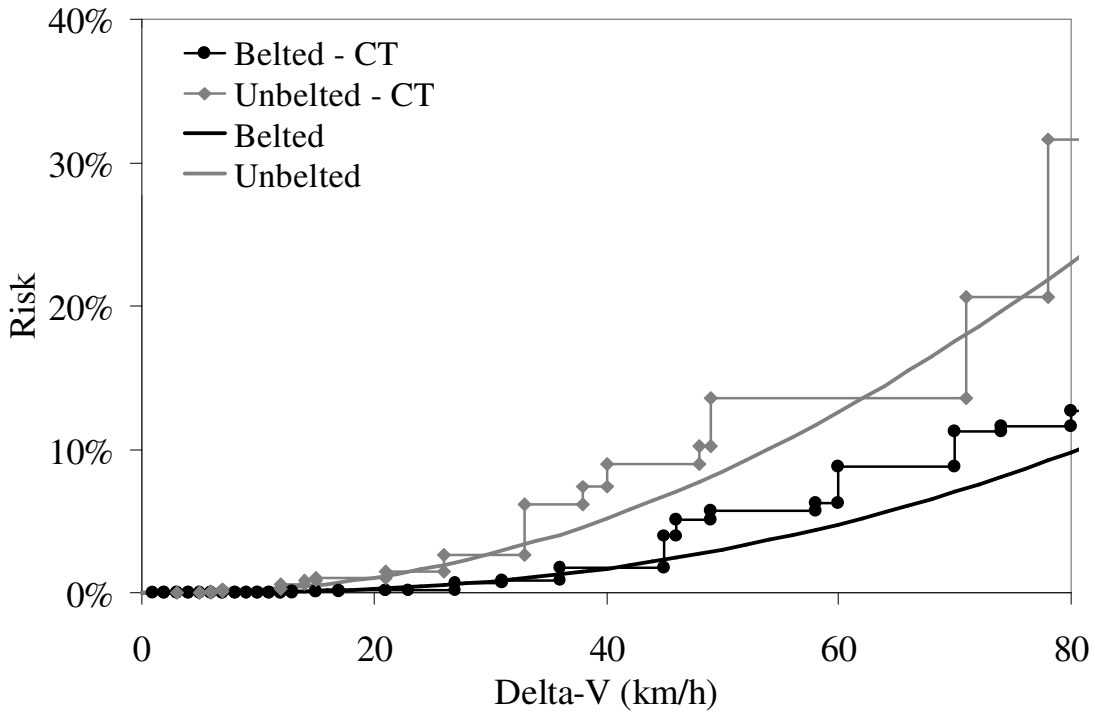

Figure 8: Risk of facial fracture in frontal impacts generated using CT and Weibull models.

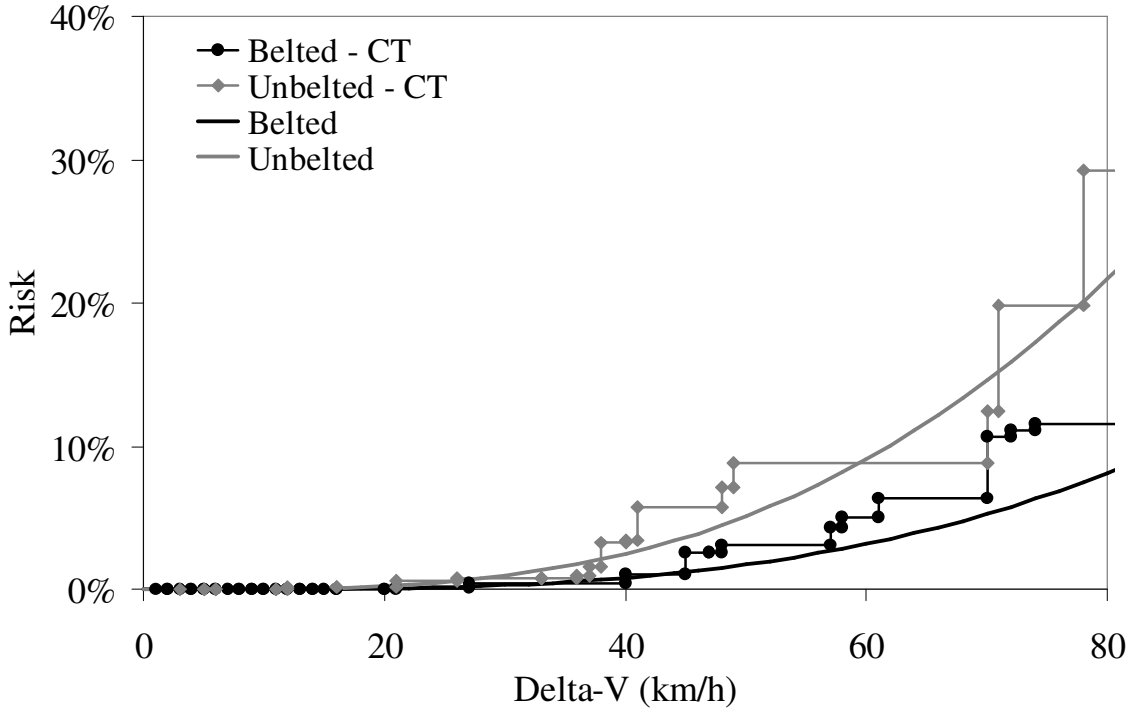

Figure 9: Risk of facial injury (AIS 3+) in frontal impacts generated using CT and Weibull models.

Side Impacts

Side impacts were analyzed by dividing them into near and far side categories for outboard occupants in the first and second rows. There was no difference in the risk of minor (AIS 2+) or severe (AIS 3+) facial injury or facial fracture between near and far side occupants. Fractures to the frontal bone and mandible were more common in side impacts compared to frontal impacts. Trends in facial bone fracture were examined by restraint and impact type. Each subset contained between 95 and 120 raw observations (Figure 10).

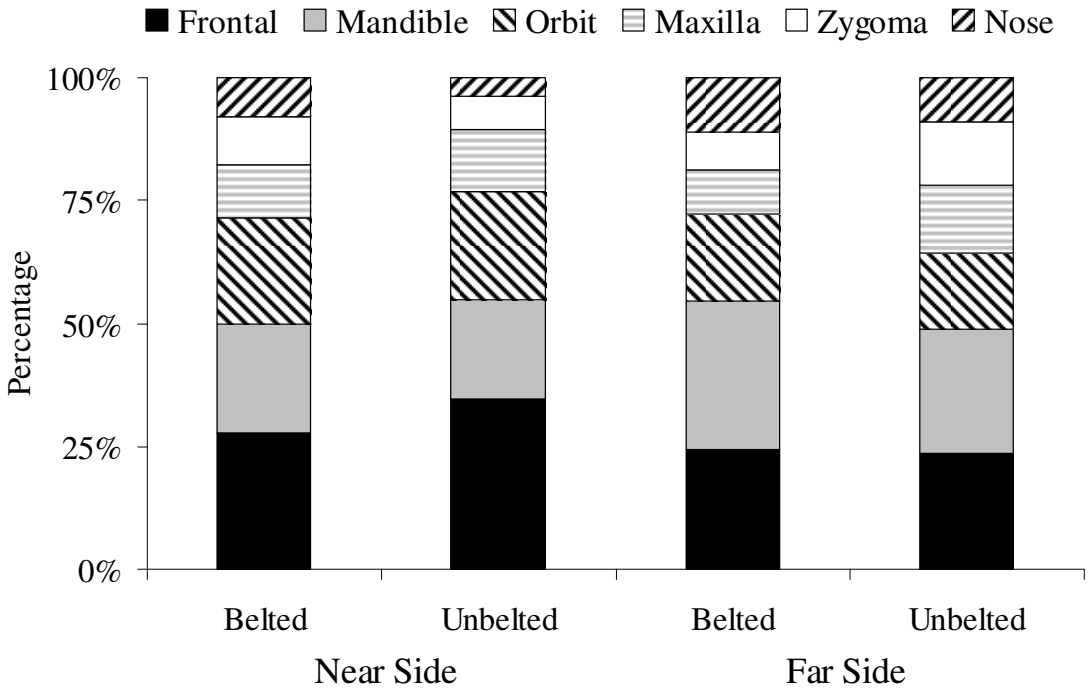

Figure 10: Distribution of facial fractures in near and far side impacts.

Only 6% of near side impacts were classified as being equipped with some type of a side airbag. Approximately 50% of these side airbags were classified as being deployed; of these 43% deployed at a ΔV less than 16 km/h, 37% between 16 and 32 and 16% between 32 and 48 km/h. Side airbag deployment did not statistically alter the risk of facial injury or fracture. Belt use was found to play a significant role in reducing the risk of facial injuries and fracture in side impacts (Table 2). Belt use reduced the risk of

sustaining a facial fracture by 64% in near side and 73% in far side impacts, both statistically significant ($p < 0.0001$).

Table 2: Risk ratios by injury type for adult occupants in side impacts.

Facial Fracture

Data Segment	Reference	Comparison	Risk Ratio	95% Confidence Interval		P value
Near Side	Belted	Unbelted	0.36	0.28	0.46	< 0.0001
Far Side	Belted	Unbelted	0.27	0.21	0.36	< 0.0001

Facial Fracture (AIS 3+)

Data Segment	Reference	Comparison	Risk Ratio	95% Confidence Interval		P value
Near Side	Belted	Unbelted	0.38	0.20	0.71	0.002
Far Side	Belted	Unbelted	0.23	0.11	0.48	< 0.0001

Injury Sources

Injury sources were identified for occupants with a facial fracture by impact direction and belt status (Figure 11). For these distributions, contact with the instrument panel was included under "interior". Due to the wide range of injury sources, identification of the six most frequent injury sources did not encompass the majority.

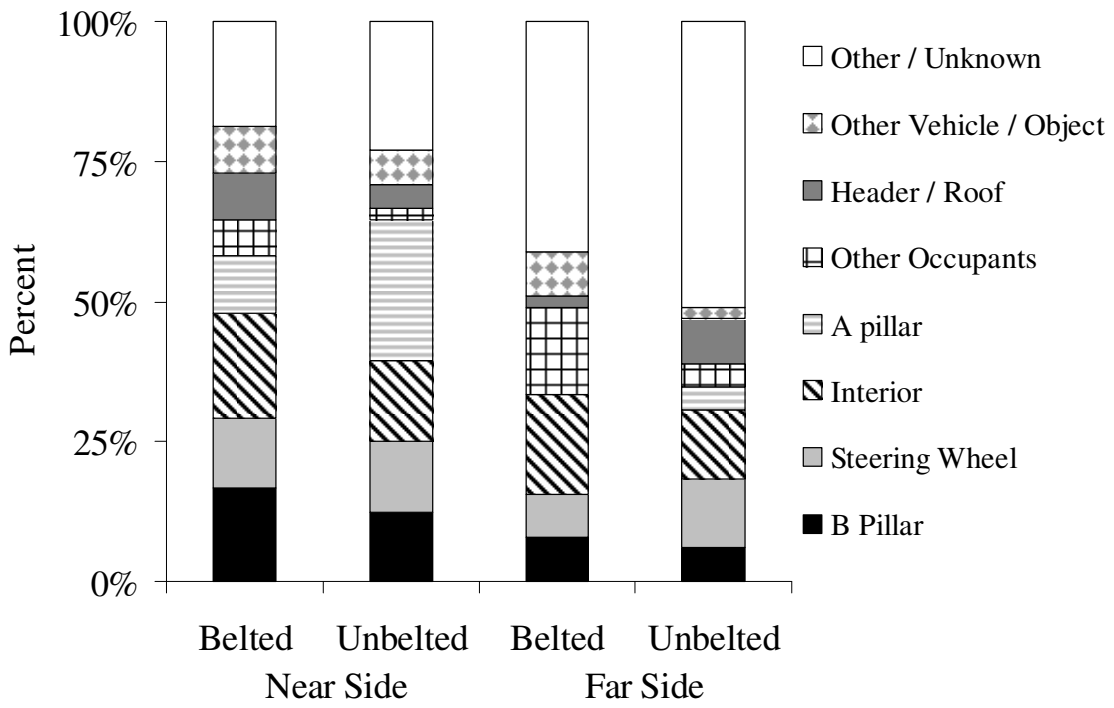

Figure 11: Injury source for adult occupants sustaining a facial fracture without brain injury in side impacts.

Risk of Facial Fracture

The risk of sustaining a facial fracture as a function of ΔV in near and far-side impacts was evaluated using the NASS-CDS database. The risk of facial fracture by ΔV and impact direction was determined using the raw and weighted data for belted and unbelted occupants (Table 3). At a ΔV above 64 km/h, the risk the risk estimates produced inconsistent results. For example, the risk to unbelted far side occupants decreased for the raw and weighted groups. As a result, risk curves were generated only using side impacts with a ΔV less than 64 km/h (Figure 12, Figure 13). Good agreement was achieved between the risks estimated using the Weibull and CT methods.

Table 3: Risk of facial fracture by side impact direction, severity and restraint use.

	Near-Side Impacts				Far-Side Impacts			
	Raw		Weighted		Raw		Weighted	
ΔV (km/h)	**Belted**	**Unbelted**	**Belted**	**Unbelted**	**Belted**	**Unbelted**	**Belted**	**Unbelted**
< 16	0.35%	1.32%	0.44%	0.05%	0.39%	2.03%	0.12%	0.46%
16 - 32	1.29%	2.45%	0.52%	0.56%	0.91%	3.70%	0.81%	1.33%
32 - 48	4.71%	9.33%	1.48%	5.77%	2.43%	10.0%	0.56%	4.17%
48 - 64	7.38%	7.79%	3.54%	4.84%	7.95%	14.3%	5.25%	10.0%
> 64	12.5%	18.8%	15.8%	14.1%	20.5%	6.25%	7.32%	0.82%

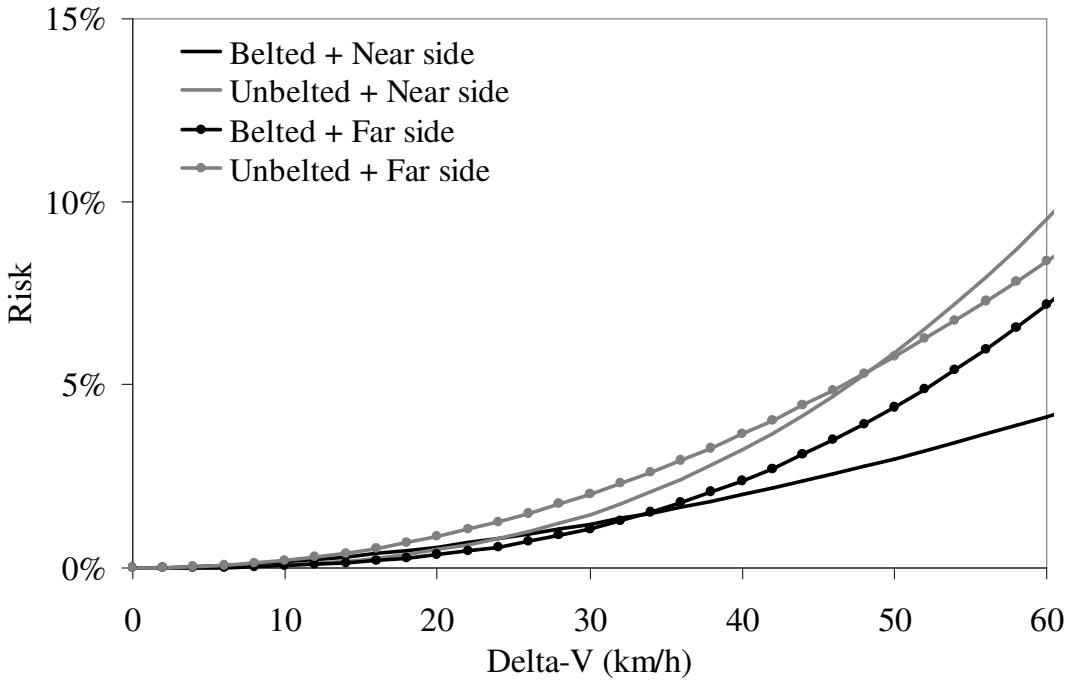

Figure 12: Risk of facial fracture in side impacts using Weibull model.

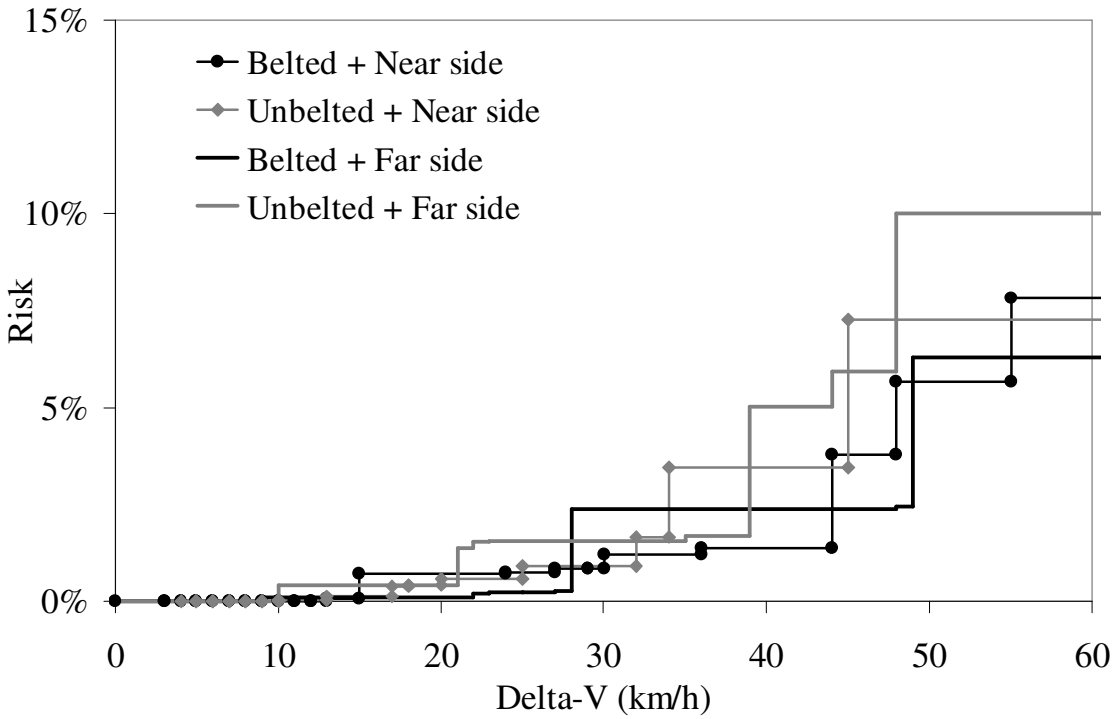

Figure 13: Risk of facial fracture in side impacts using the CT method.

DISCUSSION

The results of this study demonstrate the importance of seat belt use in the mitigation of facial injuries. In frontal impacts the exposure to an airbag deployment did decrease the risk of facial injury or fracture, but its influence was greater for belted occupants (Table 1). The results of this study are similar to those of a similar study utilizing the NASS-CDS database to examine facial fractures in frontal impacts (Cox 2004). The previous study found that seatbelt use had a statistically significant influence on the risk of facial injury and fracture, but an airbag alone did not significantly reduce the risk of facial injury compared to unrestrained occupants. The current study compared the risk of facial injury or fracture for unbelted occupants with and without airbag deployment and found that the airbag statistically reduced the risk of injury. The previous study (Cox 2004) included data up to 2000, while the current study contained NASS data up to 2007. The larger sample of airbag deployments in the current study is likely the major reason for the differences considering that the risk ratios of the previous study were similar in magnitude, but lacked the confidence to be statistically significant.

There were interesting differences in the distribution of facial fractures between frontal and side impacts. In frontal impacts, the nose was by far the most common bone fractured regardless of restraint use (Figure 3). This is consistent with the fact that the nasal bone is among the weaker structures of the face (Nahum 1975). Despite this, in side impacts the nasal bone was the least common bone fractured, and the frontal bone and mandible were the most frequently fractured bones. The more frequent occurrence of frontal bone fracture in side impacts is not surprising when considering that most side collisions classified as a side impact have a frontal component, as well.

An important aspect of the side impacts in this study was that almost all (81%) of the facial injuries occurred in vehicles that had some frontal component to the PDOF. The majority of facial fractures occurred in vehicles with higher degrees of a frontal component (Figure 14).

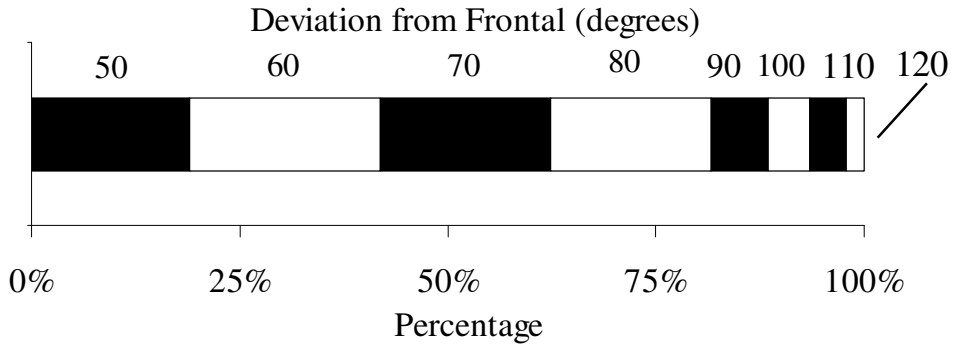

Figure 14: Distribution of facial fractures in side impacts by PDOF.

Unbelted occupants most frequently incurred a facial fracture as a result of the A-pillar in near side impacts and the interior in far-side impacts. The B-pillar was the most common injury source for belted occupants in near side impacts. The prevalence of impacts with a frontal component also explains the effectiveness in belt use (Table 2).

Problems were encountered when calculating risks with respect to ΔV when raw sample sizes become small (Table 3). As a result, risks of facial fracture in side impacts were only valid up to 64 km/h. When assessing the risk of an outcome at high ΔVs, one should examine the raw and weighted data to ensure that the weighting factors are creating a

distribution that agrees with the raw data. This applies to all cases when the raw numbers are small because the weighting factors are applied to a smaller subset of data.

Within the adult population, age did not increase the likelihood of sustaining a facial fracture. When considering younger occupants however, those less than 10 years of age had the lowest risk ($p<0.0001$) for facial fracture.

CONCLUSIONS

This study demonstrates trends in facial injury severity, source and their association with restraint use in frontal and side impacts. The A-pillar was among the most common injury source for belted occupants exposed to an airbag in frontal impacts and unbelted occupants in near-side impacts. Windshield contact was more prevalent for right front passengers in frontal impacts than drivers. The majority of injury sources for occupants in side impacts were located toward the front of the vehicle. When evaluating the potential for facial fracture, particularly to the frontal bone, it is important to consider impacts not normally defined as frontal. Impacts with a PDOF that differs from frontal by 50^{o} or more contained a higher proportion of frontal bone fractures than impacts closer to frontal.

Facial fractures are more common in impacts with a frontal component and belt use is the most effective way to reduce an occupant's risk of sustaining a facial fracture. In frontal impacts, airbags have a greater influence on the risk of sustaining a facial fracture for belted occupants. The risk of sustaining a facial fracture was equal for drivers and right front passengers. Overall, severe facial fractures are rare and are associated with more severe impacts and lack of restraints.

REFERENCES

Allison PD: Survival Analysis Using SAS: A Practical Guide, Cary, SAS Press; 1995.

Cantor AB: Analysis Techniques for Medical Research, 2nd, Cary SAS Press; 2003.

Cox D, Vincent DG, McGwin G, MacLennan PA, Holmes JD, Rue LW, 3rd: Effect of restraint systems on maxillofacial injury in frontal motor vehicle collisions, *J Oral Maxillofac Surg*, 62(5), 571-5; 2004.

Gassner R, Tuli T, Hächl O, Rudisch A, Ulmer H: Cranio-Maxillofacial Trauma: A 10 Year Review of 9543 cases with 21067 Injuries, *Cranial and Maxillofacial Surgery*, 31, 51-61; 2003.

Hackle W, Hausberger K, Sailer R, Ulmer H, Gassner R: Prevalence of Cervical Spine Injuries in Patients with Facial Trauma, *Oral and Maxillofacial Surgery*, 92(4), 370-6; 2001.

Haymond C, Nicholson C, Kiyak A, D T: Age Differences in Response to Facial Trauma, *Special Care in Dentistry*,(May-June); 1988.

Jayamanne DGR, Gillie RF: Do Patients with Facial Trauma to the Orbito-Zygomatic Region also Sustain Significant Ocular Injuries?, *Coll. Surg. Eding.*, 41, 200-3; 1996.

Lim LH, Lam LK, Moore MH, Trott JA, David DJ: Associated Injuries in Facial Fractures: A Review of 839 Patients, *British J. Plast. Surg.*, 46, 365-38; 1993.

Muraoka M, Nakai Y, Nakagawa K, Yoshioka N, Nakaki Y, Yabe T, Hyodo T, Kamo R, Wakami S: Fifteen – Year Statistics and Observation of Facial Bone Fracture, *Osaka City Med. J.*, 41(2), 49-61; 1995.

Murphy RX, Birmingham KL, Okunski WJ, Wasser T: The Influence of Airbag and Restraining Devices on the Patterns of Facial Trauma in Motor Vehicle Collisions, *Plast. Reconstr. Surg.*, 105, 516-20; 2000.

Nahum AM: The Biomechanics of Facial Bone Fracture, *Laryngoscope*, 85(1), 140-56; 1975.

NHTSA: NASS-CDS Data Collection, Coding, and Editing Manual; 1997.

Nusholtz G, Mosier R: Consistent Threshold Estimate for Doubly Censored Biomechanical Data, *Society of Automotive Engineers* SAE No. 1999-01-0714; 1999.

Shapiro AJ, Johnson RM, Miller SF, McCarthy MC: Facial Fractures in a Level I Trauma Centre: The Importance of Protective Devices and Alcohol Abuse, *Injury Int. J. Care Injured*, 32, 353-56; 2001.

CHAPTER 2:
THE RELATIONSHIP BETWEEN FACIAL FRACTURES AND BRAIN INJURIES IN AUTOMOTIVE COLLISIONS

INTRODUCTION

The four most common sources of facial trauma are Motor Vehicle Collision (MVC), assault, sports and falls (Lim 1993; Muraoka 1995; Jayamanne and Gillie 1996; Shapiro 2001; Gassner 2003). A study of over 3,000 hospital ER patients found that the zygoma is the most frequently fractured facial bone (Hackle 2001). Orbital blow-out fractures have also been shown to be among the most common facial fractures due to a MVC (Jayamanne and Gillie 1996; Hackle 2001). Studies examining the effects of restraint systems have found that airbag deployment and seatbelt use reduced the likelihood of sustaining a facial fracture (Murphy 2000; Shapiro 2001). Examining hospital records with a focus on age, one study found that older patients were more likely to die as a result facial and related trauma (Haymond 1988).

The majority of the previous work on facial fractures is limited to a review of a series of trauma cases. These offer no information regarding the relationship between facial trauma and collision event. The National Automotive Sampling System – Crashworthiness Data System (NASS-CDS) represents a large sample of vehicular crashes in the United States. Approximately half of these provide information regarding the severity of the collision in terms of Delta-V (ΔV) and the Principal Direction of Force. These variables, among others are frequently utilized to estimate the risk of occupant injury in automotive impacts. Knowing the ΔV of impacts that cause facial fractures will also help relate the occurrence of these injuries to testing performed by the NHTSA to evaluate vehicle performance using crash test dummies. The purpose of this chapter is to examine the patterns of facial injury, occupant characteristics and concomitant injuries and their association with brain injury.

METHODOLOGY

The data for this study were obtained from the NASS-CDS database for years 1993 to 2007. All data were processed using the Statistical Analysis Software (SAS Institute, Cary N.C). Unless stated otherwise, all analyses were limited to occupants 18 years of age or older. Rollover and ejected occupants were excluded. The system / organ definition within the SAS data files was used to determine whether the occupant incurred a facial injury. Facial fracture was further determined using the lesion variable, with the exception of teeth fractures and rupture of the mucosal membranes of the nose which were not included in the analysis as a facial fracture. Frontal bone fracture does not have a specific AIS Code within NASS; therefore, these fractures were identified by the AIS code and aspect for each injury. A vault fracture with an anterior aspect is the designation for a frontal bone fracture and these were identified within the NASS dataset and included within the facial fracture variable. Frontal bone fractures and facial fractures were combined to create a single variable indicating whether or not a person incurred a facial fracture. The final dataset included a total of 105,416 occupants.

The influence of vehicle and occupant parameters on the risk of facial fracture was assessed using risk ratios. Confidence intervals for risk ratios were determined using the unweighted data and quoted risks using weighted data. Using the unweighted data for ratios maintains the correct distribution of occupant and vehicle parameters that is disturbed by weighting the data. Using the weighted data for the overall risk produces more conservative risks because of the lack of low-severity impacts in the NASS CDS database. The correlation between variables was assessed using Pearson's test for correlation.

For frontal and rear impacts, occupants seated in the front outboard positions were analyzed seperately. For side impacts, occupants seated in the outboard position of the front and rear seats were grouped into near and far side impacts. Variables describing the availability of side airbags and deployment status were combined to assess the effects of side airbags. The BAGAVOTH variable in the NASS database specifies the availability

of other airbags besides a frontal airbag. The BAGDEPOT variable can then be used to determine if the denoted bag deployed during the event (NHTSA 1997). The variable RESTYPE identifies the type of airbags available within the vehicle; therefore, when combined with BAGAVOTH, the type of side airbag available to an occupant can be determined.

RESULTS

Overall Trends

Trends in facial fracture and brain injury were examined utilizing the NASS CDS data set for years 1993 to 2007. Brain injury (AIS 1+) was over 2 times ($p<0.0001$) more likely in a side impact than a frontal impact. The overall risk of an AIS 1+ injury was 8%, and the overall risk of an AIS 3+ brain injury was 0.8%. The same trend in facial and brain injury was also demonstrated though risk ratios. Occupants with a facial injury (AIS 2+) had a risk of brain injury (AIS 2+) that was over 6 times (RR: 6.83 CI: 6.5-7.2) higher than occupants without a facial injury. This same trend was similar for occupants with and without facial fractures (RR: 6.24 CI: 5.9-6.5).

Dividing facial fractures into upper and lower regions (lower being everything but the frontal bone), demonstrated that upper facial fractures are more likely (RR: 8.2 CI: 7.3-9.2) to be associated with a brain injury than lower facial fractures (RR: 6 CI: 5.7-6.3). This trend is also demonstrated in the distribution of upper and lower facial fractures associated with each AIS level of brain injury. Facial injuries (AIS 2+) showed a differing trend, in that the majority of facial injuries were within the lower brain injury severity. In the overall dataset, facial fracture was associated with higher severity brain injuries. The trend in facial and brain AIS demonstrated that increasing facial injury severity was associated with a more severe brain injury. These trends were examined by impact direction as well.

Frontal Impacts

Occupants sustaining a facial fracture in a frontal impact were more likely to have incurred a brain injury. On average, 72% of occupants with facial injuries of AIS 3 or greater also incurred a brain injury. Examining the distribution of brain injury severity by facial fracture severity demonstrated a prevalence of higher severity brain injuries as facial fracture severity increased (Figure 15).

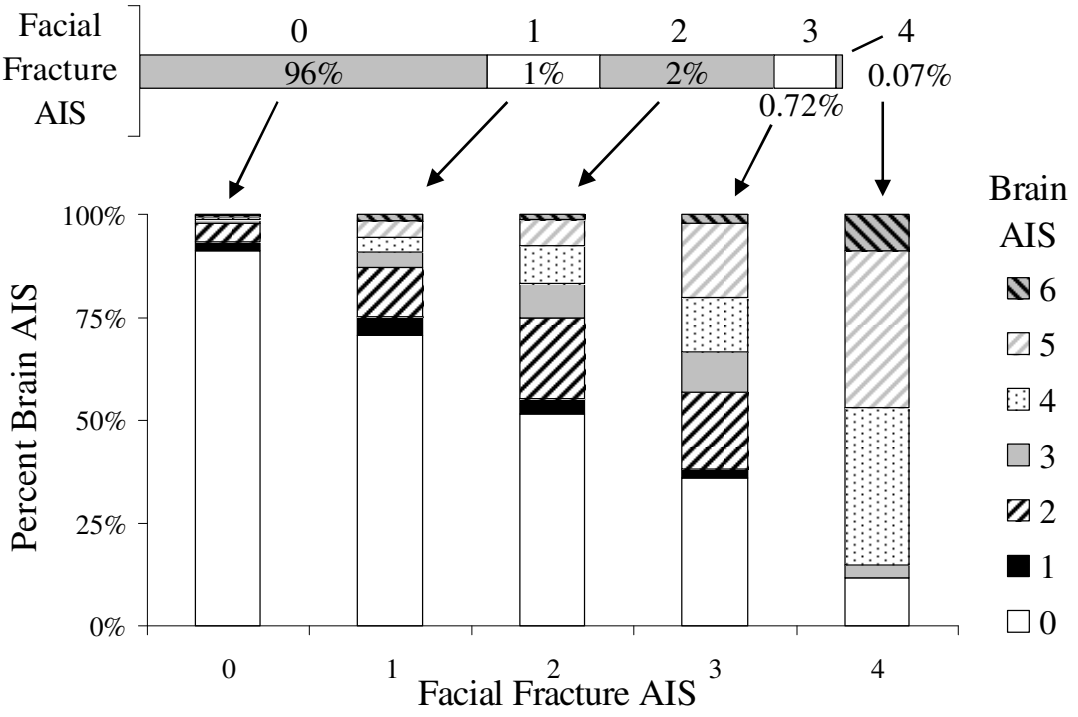

Figure 15: Relationship between facial fracture and brain injury AIS in frontal impacts.

In contrast, the majority of occupants sustaining a brain injury did not incur a facial injury as well. An increase in brain AIS did not result in the same increase in facial injury potential. In general, occupants sustaining a brain injury did not demonstrate an increasing risk of sustaining a facial fracture. Occupants with higher severity brain injuries did demonstrate a higher percentage of facial fractures; however, the relationship was fairly constant above an AIS of 3 (Figure 16).

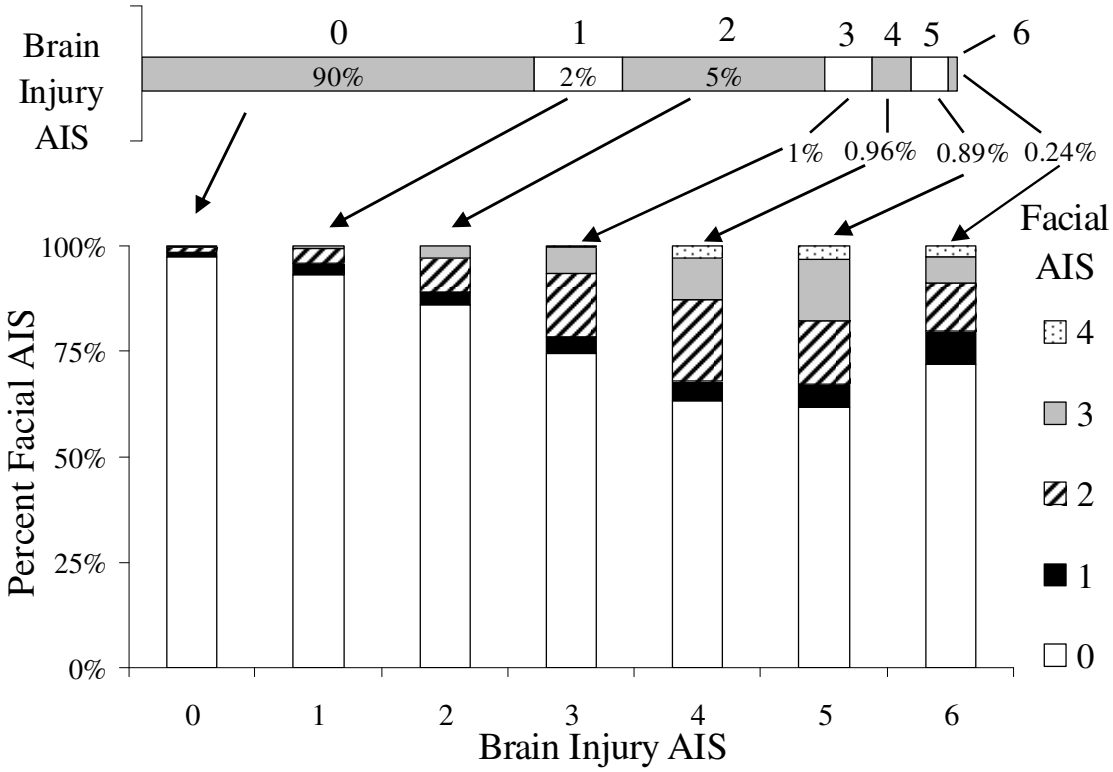

Figure 16: Distribution of facial fractures by brain injury severity in frontal impacts.

Upper facial fractures were more represented in higher severity brain injuries than lower facial fractures and all facial injuries (Figure 17). The number of occupants with a brain injury was lowest within those with lower facial fractures. Upper facial fractures were more likely to be associated with a brain injury than lower facial fractures in frontal impacts (RR: 1.7 CI: 1.5-1.8). Upper facial fractures were also more likely to be associated with a brain injury than minor facial injuries (AIS 2+) (RR: 1.4 CI: 1.5-1.9) and severe facial injuries (AIS 3+) (RR: 1.2 CI: 1.0-1.3).

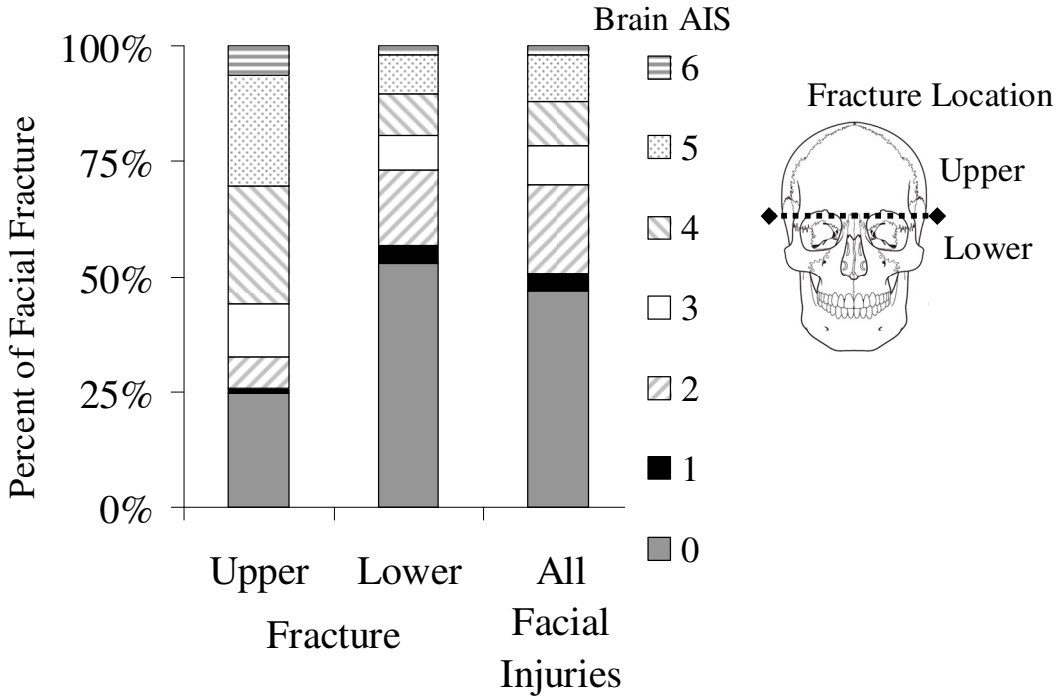

Figure 17: Upper and lower facial fractures within each brain AIS for frontal impacts.

Injury Sources

Injury sources for occupants sustaining a facial fracture and brain injury were investigated for frontal impacts. For occupants sustaining a facial fracture and brain injury, the steering wheel was the most common injury source; secondary sources depended on restraint type (Figure 20). Injury sources for occupants sustaining only a brain injury were more varied, with the front header accounting for more of the injuries than for occupants sustaining both a facial fracture and brain injury (Figure 22).

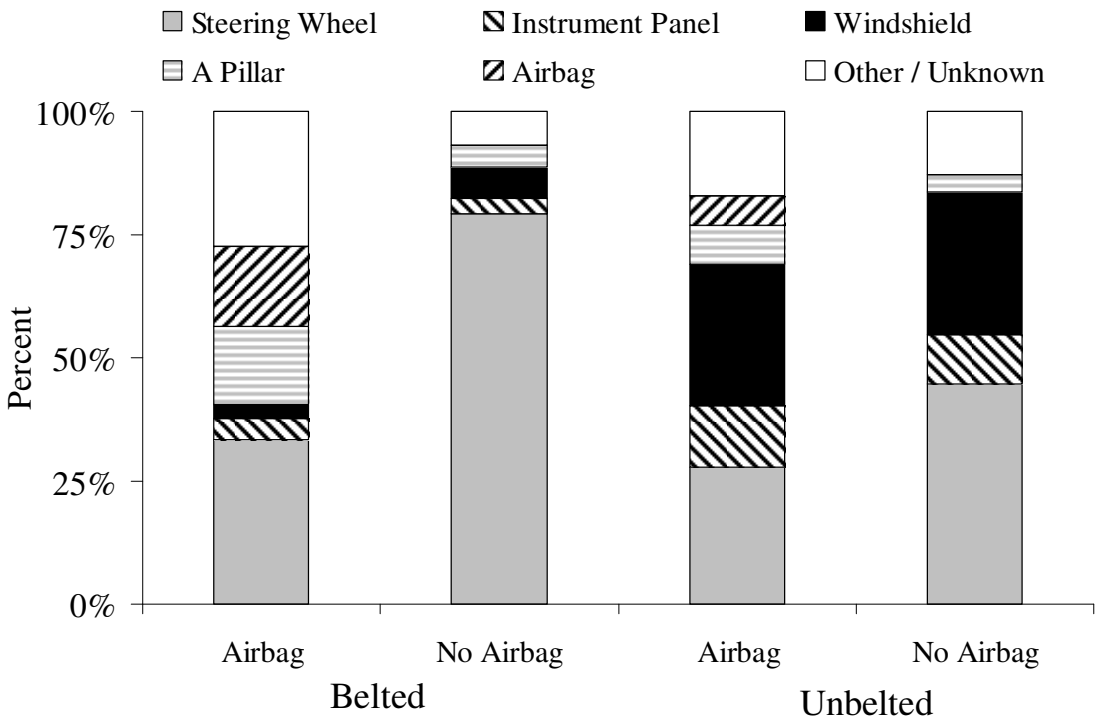

Figure 18: Injury sources for drivers in frontal collisions sustaining a facial fracture (no brain injury).

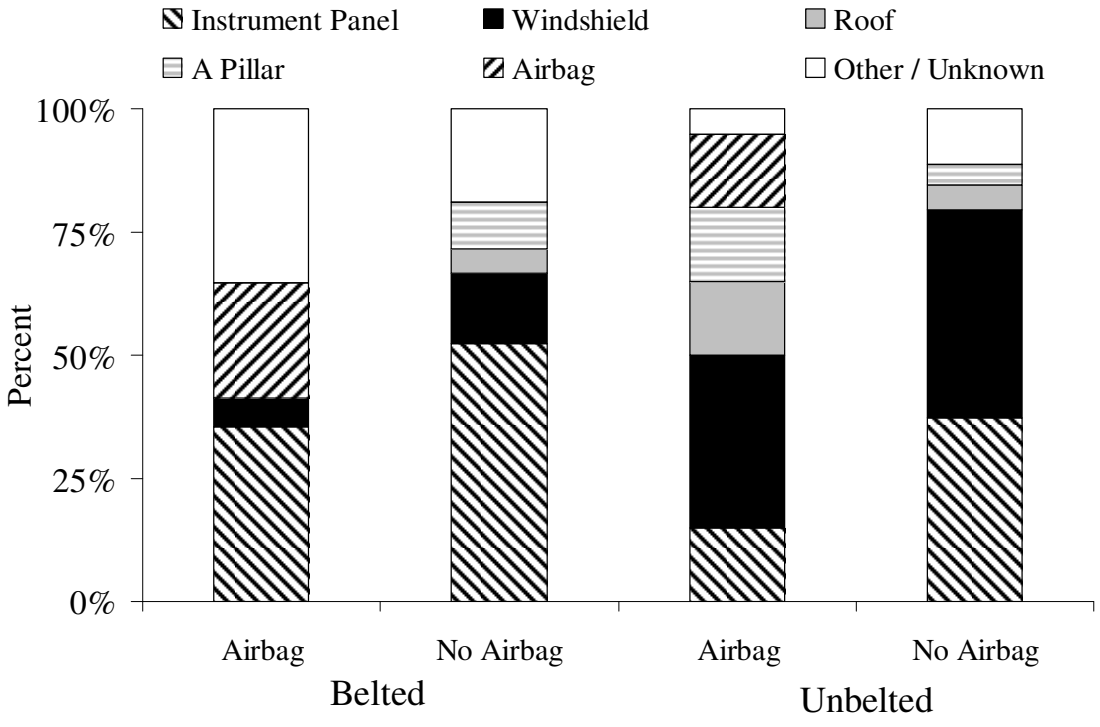

Figure 19: Injury sources for right front passengers in frontal collisions sustaining a facial fracture (no brain injury).

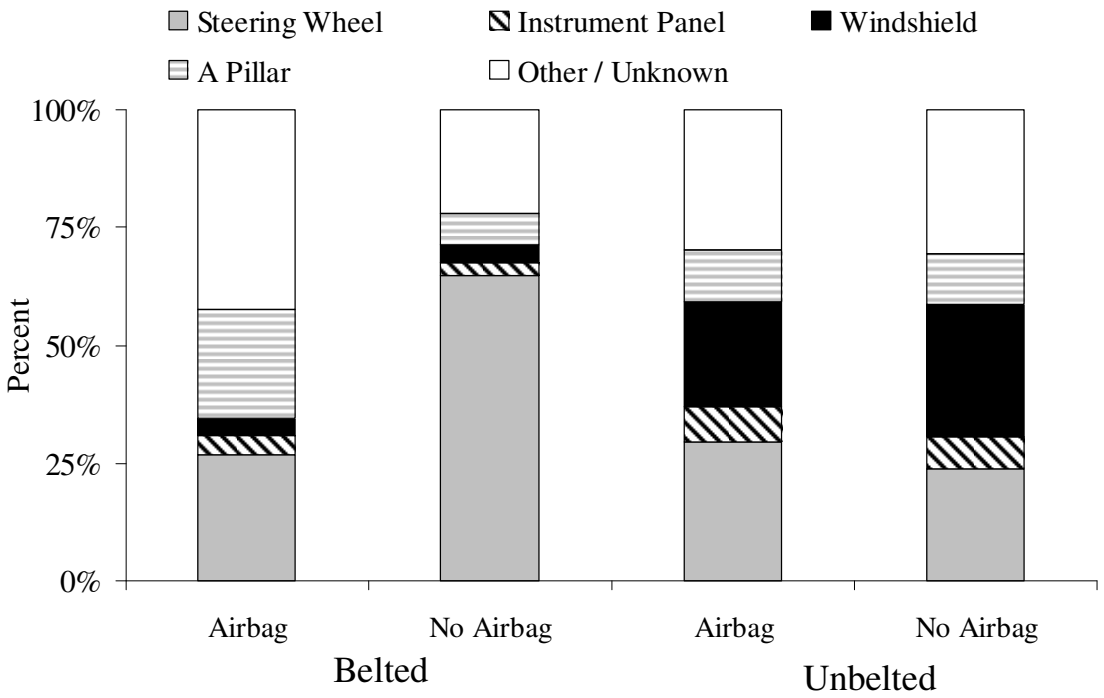

Figure 20: Injury sources for drivers in frontal impacts with a facial fracture and brain injury (AIS 3+).

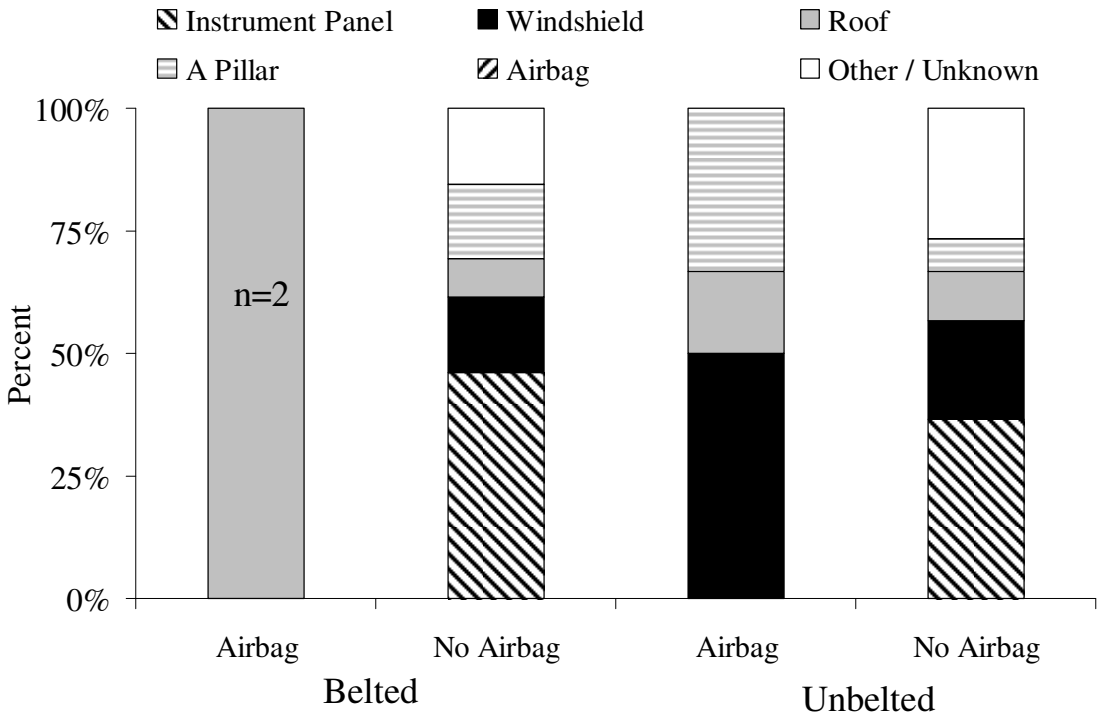

Figure 21: Injury sources for passengers in frontal impacts with a facial fracture and brain injury (AIS 3+).

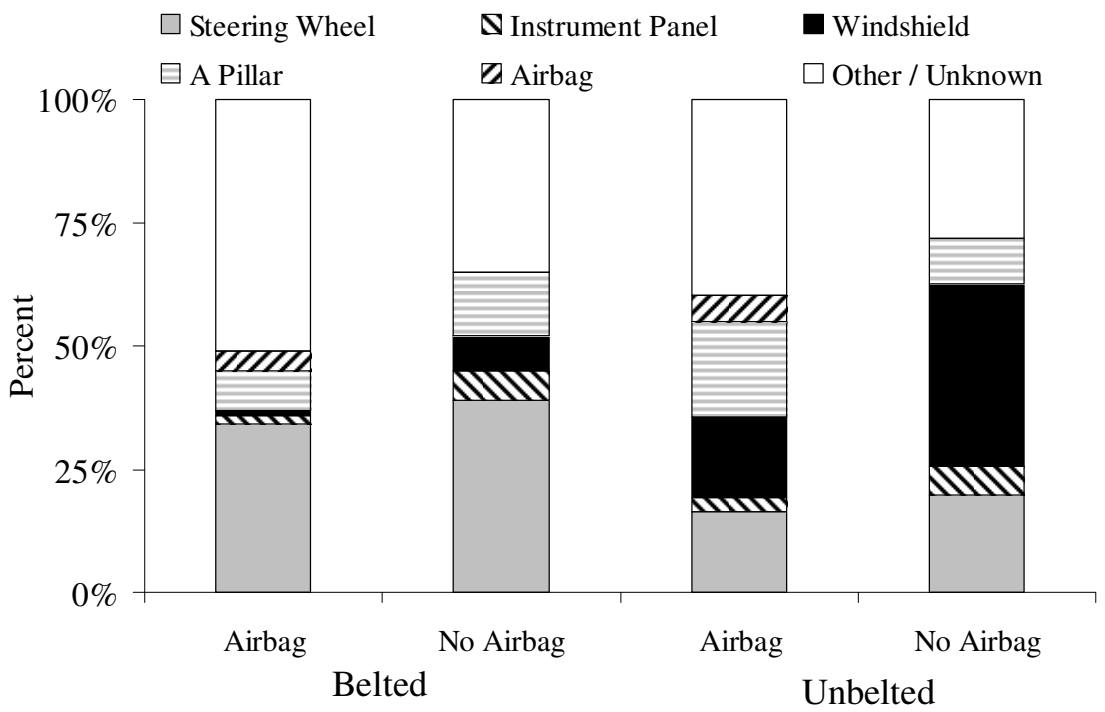

Figure 22: Injury sources for drivers in frontal impacts with a brain injury (AIS 3+) and no facial fracture.

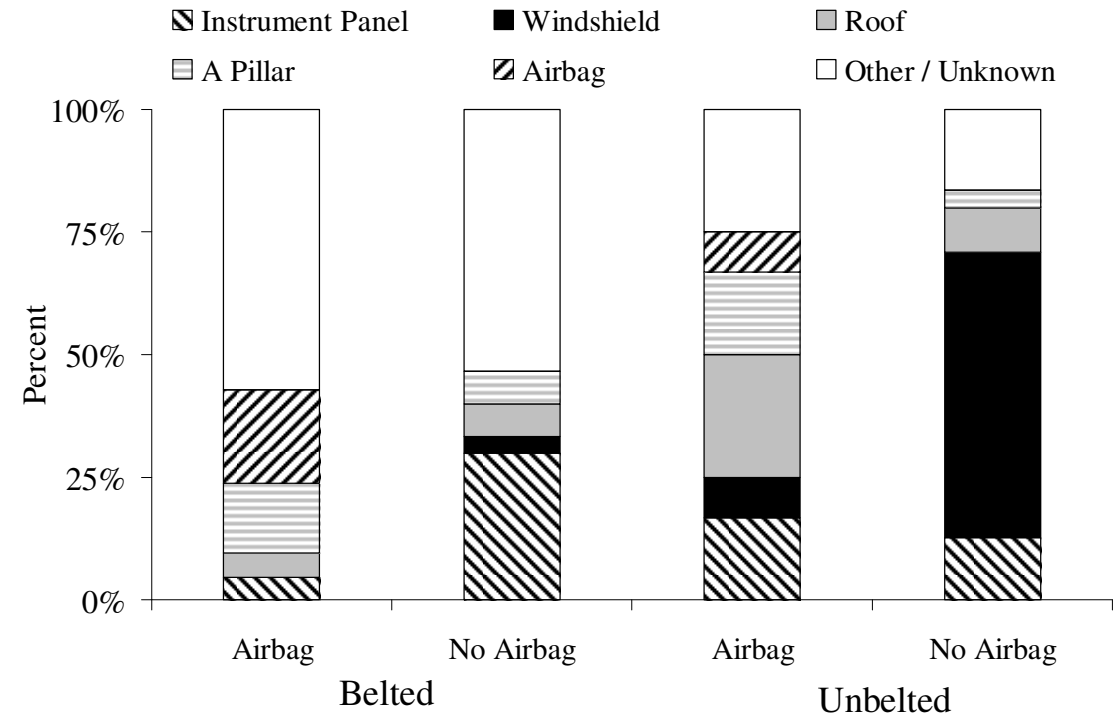

Figure 23: Injury sources for passengers in frontal impacts with a brain injury (AIS 3+) and no facial fracture.

Among passengers belted without an airbag, the right B pillar (17%) was the second most common source of a brain injury without facial fracture.

Side Impacts

The relationship between facial and brain injury was investigated in side impacts as well. There was a positive relationship between the severity of facial fracture AIS and brain injury AIS in side impacts (Figure 24).

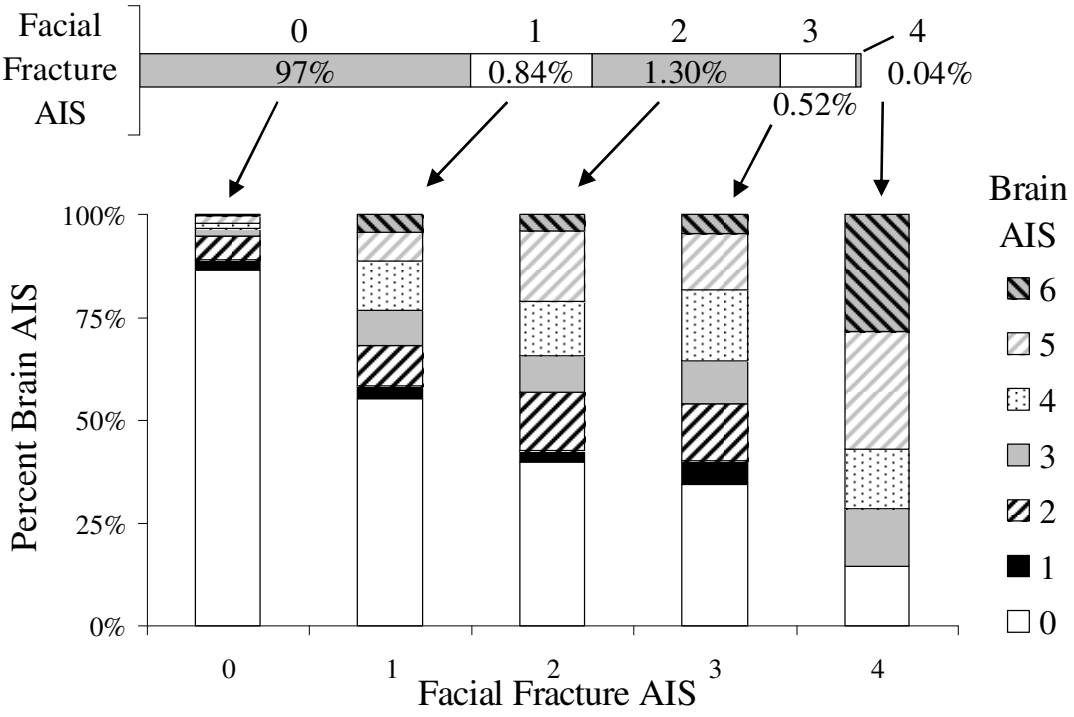

Figure 24: Distribution of brain injuries by facial fracture AIS in side collisions.

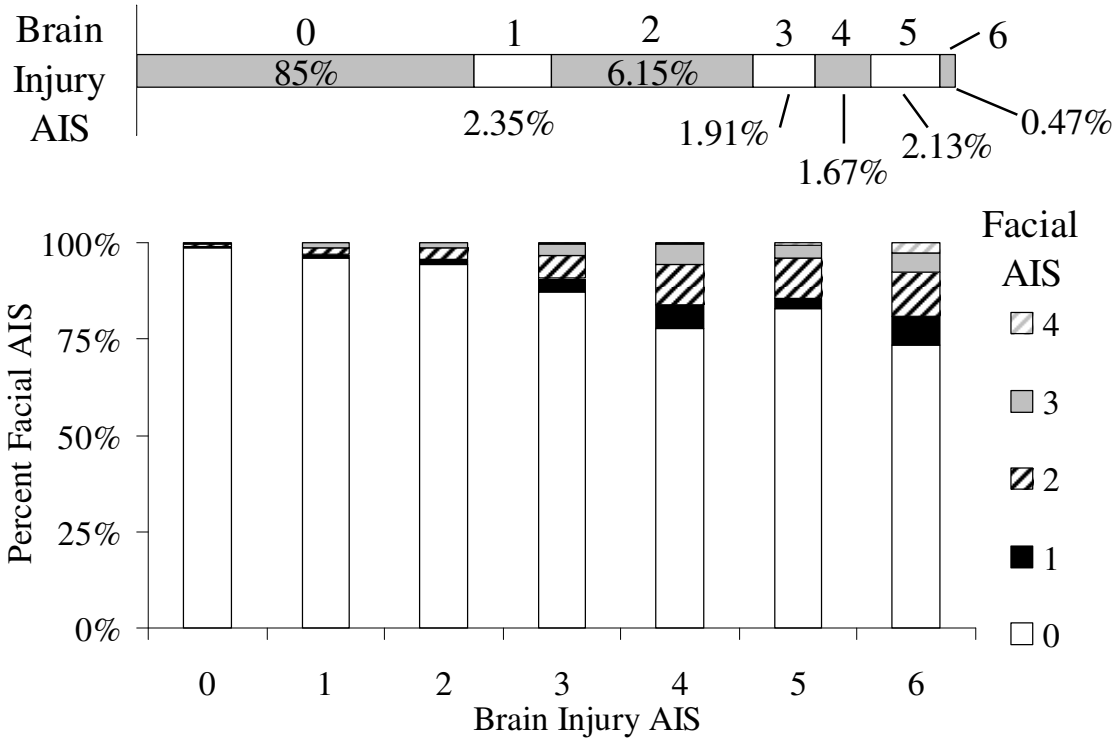

Figure 25: Distribution of facial fractures by brain injury severity in side impacts.

Fractures to the upper portion of the face (frontal bone) were statistically (p=0.01) more likely (RR: 1.4 CI: 1.1-1.64) to be associated with a brain injury than fractures to the lower face.

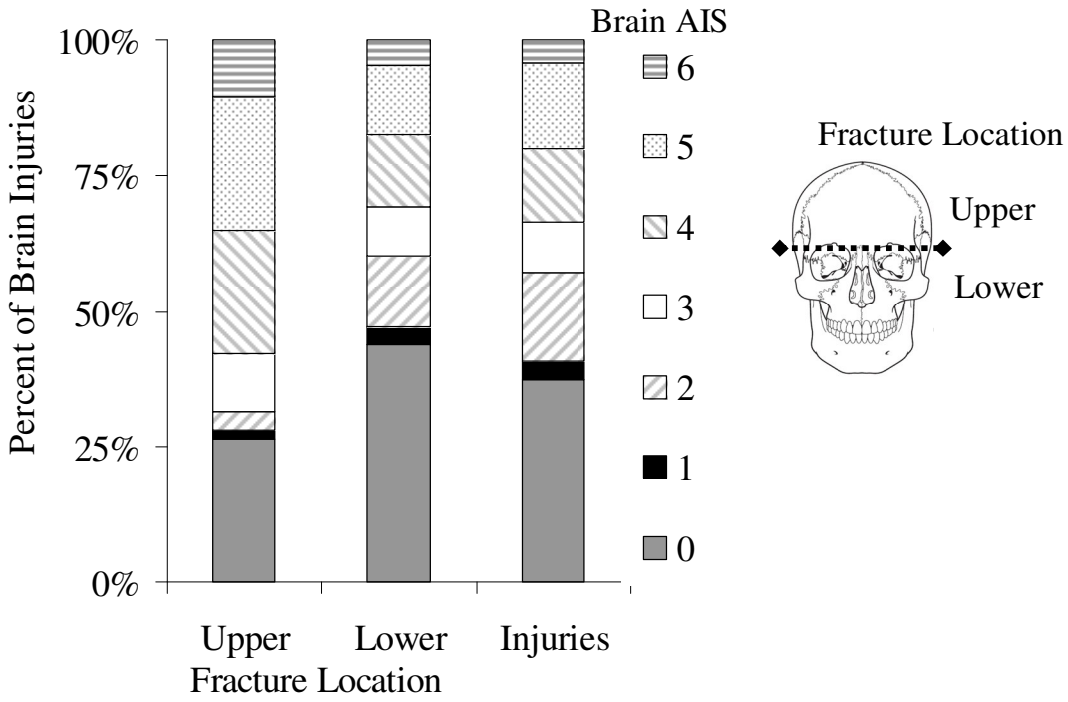

Figure 26: Upper and lower facial fracture and facial injuries (AIS 2+) associated with each brain AIS level in side impacts.

Injury Sources

The source of injury for occupants sustaining a facial fracture and brain injury was investigated for side impacts. Other occupants were a more common injury source for occupants sustaining both a facial fracture and brain injury than those with a brain injury alone (Figure 27, Figure 28, Figure 29). The B-pillar and instrument panel were the most common injury sources for both injury patterns. For far-side impacts, the instrument panel was more prominent and for near-side impacts, the B-pillar was a more frequent injury source.

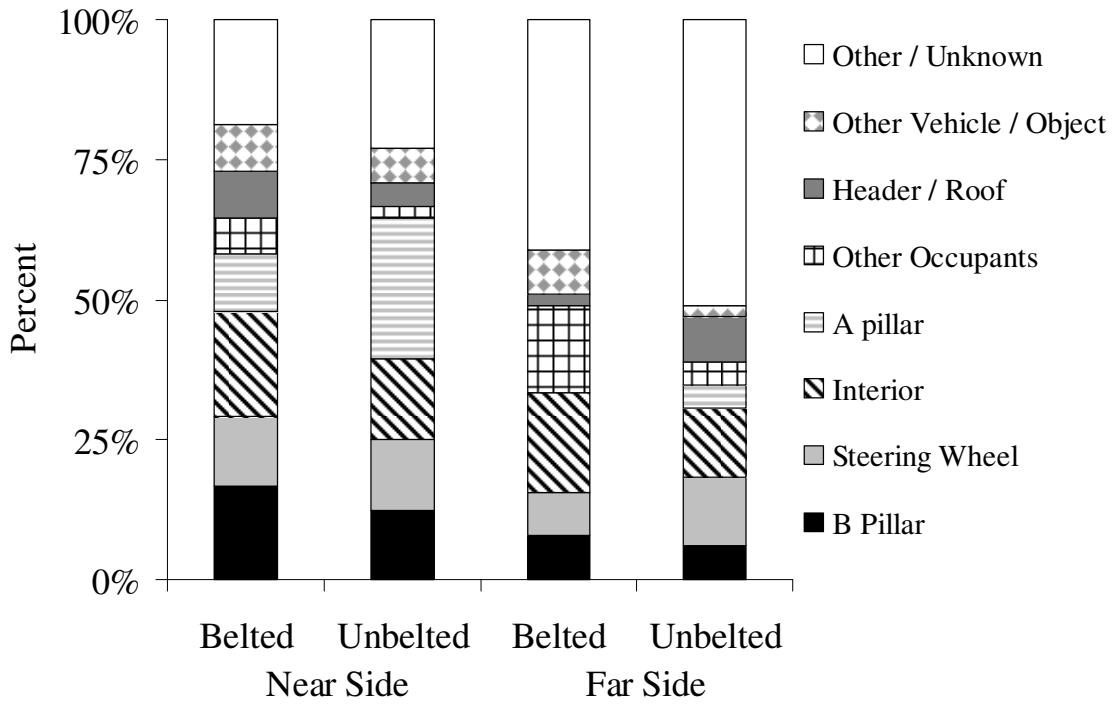

Figure 27: Injury sources for occupants with a facial fracture alone.

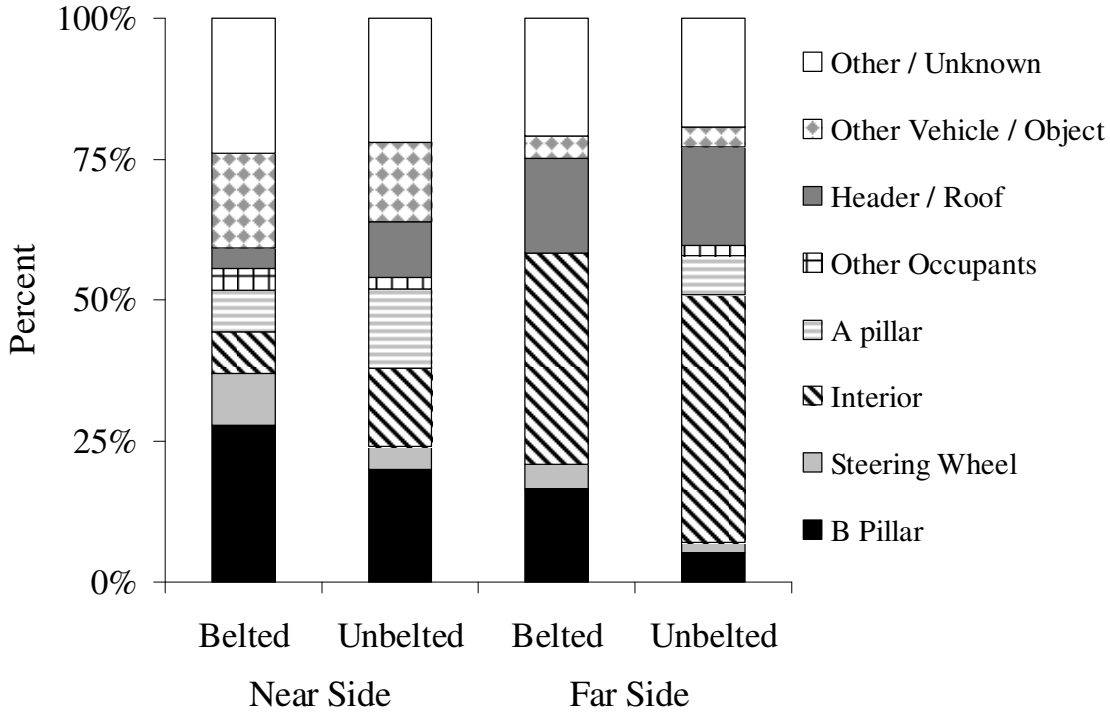

Figure 28: Injury sources for occupants with a facial fracture and brain injury (AIS 3+) in side impacts.

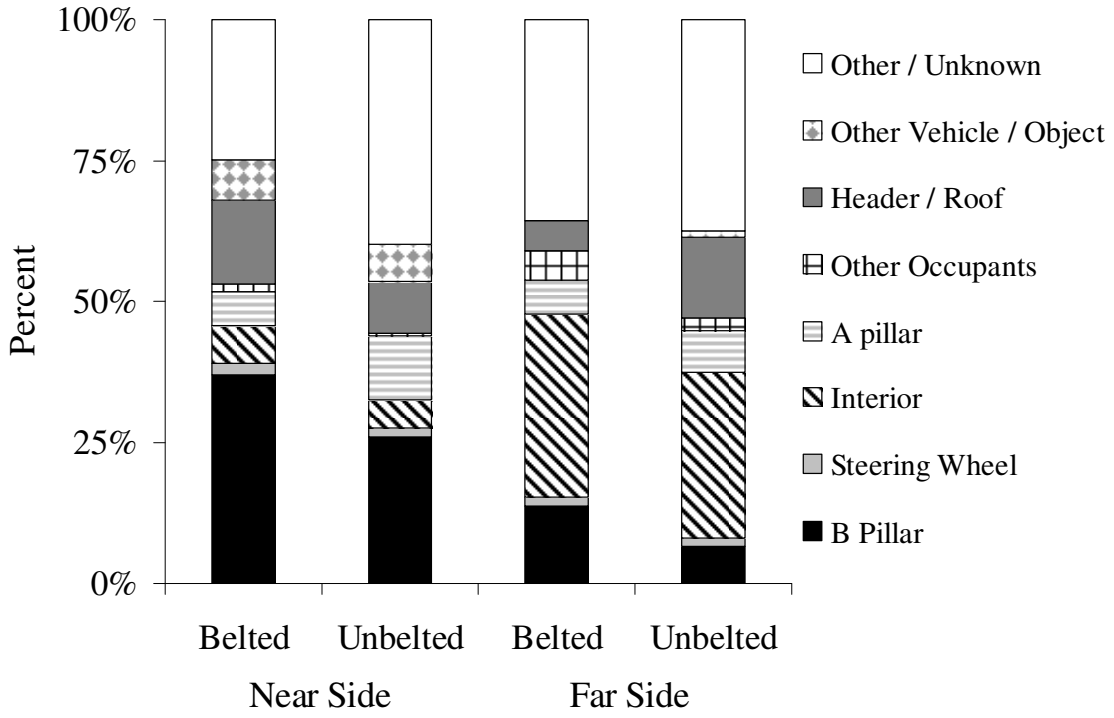

Figure 29: Injury sources for occupants with a brain injury (AIS 3+) and no facial fracture in side impacts.

DISCUSSION

Occupants with a facial fracture were more likely to have incurred a brain injury than occupants without a facial fracture. The converse was not true, indicating that occupants with a brain injury were not more likely to have sustained a facial fracture. When fractures were separated between the upper and lower face, upper facial fractures were more likely to be associated with a brain injury than lower. This is consistent with the idea that frontal bone fractures will be more likely to cause a brain injury than any other facial fracture. This trend has been demonstrated by others using hospital data (Lee 1987). Injury sources differed slightly between occupants with a facial fracture and no brain injury, both injuries and only a brain injury. In frontal impacts, the steering wheel was the most common source for injury when a facial fracture was incurred, and the windshield was the most common injury source when a facial fracture was not present. In frontal impacts, the A-pillar and steering wheel were the most common injuries sources for belted occupants exposed to an airbag deployment.

The relationship between facial fracture and brain injury was examined more closely for a smaller segment of crashes. These crashes were limited to frontal impacts with a ΔV greater than 16 and less than 48 km/h in which a restrained driver sustained any facial injury as a result of steering rim impact without airbag deployment. A total of 719 occupants met these criteria. Within this subset 8 incurred an AIS = 3 facial injury, 49 incurred an AIS = 2 injury and the remaining 662 sustained an AIS = 1 facial injury. Within this subset, the risk of sustaining a brain injury was 50% higher (RR: 1.5 CI: 1.4-1.9) than sustaining a facial fracture. Additionally, occupants were over twice as likely to sustain a brain injury if they sustained a facial fracture as opposed to any facial injury (RR: 2.2 CI: 1.6-3.1). This demonstrates that for impacts of similar severity, to similar objects, the risk of sustaining a brain injury is not reduced when a facial fracture occurs, but rather that a brain injury is more likely for occupants with a facial fracture. This is an intuitive result since the presence of a facial fracture is indicative of a severe head impact.

CONCLUSIONS

Regardless of impact type, there was a positive correlation between facial injury severity and brain injury. The distribution of injury sources in frontal and side impacts was demonstrated by restraint use. The distribution in injury source was different between occupants with a facial fracture and those with and without a concomitant brain injury. For occupants sustaining a brain injury alone (no facial fracture), the airbag was not listed as a source of the brain injury. The windshield and steering wheel were among the more common sources of a brain injury alone in frontal collisions.

The occurrence of a facial fracture is related to the applied stress, so that higher forces can be applied without fracture if the area of contact is increased. Based on the results of this study, including a detailed examination of brain injuries by injury source, it appears that brain injuries frequently occur in the absence of facial fractures. The vehicle interior seems to be applying forces to the occupant's face over a sufficient area that the brain is being injured without concomitant facial fractures. When facial fractures do occur, a brain injury is more likely suggesting that facial fractures are associated with more severe

impacts and, therefore, brain injury is likely. There is no evidence to suggest that facial fractures decrease the likelihood of brain injury in automotive impacts.

REFERENCES

Gassner R, Tuli T, Hächl O, Rudisch A, Ulmer H: Cranio-Maxillofacial Trauma: A 10 Year Review of 9543 cases with 21067 Injuries, *Cranial and Maxillofacial Surgery*, 31, 51-61; 2003.

Hackle W, Hausberger K, Sailer R, Ulmer H, Gassner R: Prevalence of Cervical Spine Injuries in Patients with Facial Trauma, *Oral and Maxillofacial Surgery*, 92(4), 370-6; 2001.

Haymond C, Nicholson C, Kiyak A, D T: Age Differences in Response to Facial Trauma, *Special Care in Dentistry*,(May-June); 1988.

Jayamanne DGR, Gillie RF: Do Patients with Facial Trauma to the Orbito-Zygomatic Region also Sustain Significant Ocular Injuries?, *Coll. Surg. Eding.*, 41, 200-3; 1996.

Lee KF, Wagner LK, Lee YE, Suh JH, Lee SR: The impact-absorbing effects of facial fractures in closed-head injuries. An analysis of 210 patients, *J Neurosurg*, 66(4), 542-7; 1987.

Lim LH, Lam LK, Moore MH, Trott JA, David DJ: Associated Injuries in Facial Fractures: A Review of 839 Patients, *British J. Plast. Surg.*, 46, 365-38; 1993.

Muraoka M, Nakai Y, Nakagawa K, Yoshioka N, Nakaki Y, Yabe T, Hyodo T, Kamo R, Wakami S: Fifteen – Year Statistics and Observation of Facial Bone Fracture, *Osaka City Med. J.*, 41(2), 49-61; 1995.

Murphy RX, Birmingham KL, Okunski WJ, Wasser T: The Influence of Airbag and Restraining Devices on the Patterns of Facial Trauma in Motor Vehicle Collisions, *Plast. Reconstr. Surg.*, 105, 516-20; 2000.

NHTSA: NASS-CDS Data Collection, Coding, and Editing Manual; 1997.

Shapiro AJ, Johnson RM, Miller SF, McCarthy MC: Facial Fractures in a Level I Trauma Centre: The Importance of Protective Devices and Alcohol Abuse, *Injury Int. J. Care Injured*, 32, 353-56; 2001.

CHAPTER 3:
A REVIEW OF STUDIES INVESTIGATING FACIAL TOLERANCE

INTRODUCTION

Research concerning facial bone tolerance received considerable attention between 1965 and 1995. In the past, there has been little work focusing on facial fracture research and therefore, there is a lack of detailed information necessary to determine the force at which a given facial bone is expected to fracture. The risk of sustaining a facial fracture is dependent on the level of stress imposed on the underlying bone. Independent of the geometrical differences among human facial structures, the imposed stress can be influenced by impactor shape and size as well as loading direction and location. These complicating factors necessitate the use of simplistic testing procedures that introduce little variation into a statistical analysis of the resulting data. Unfortunately, the several groups that have performed biomechanical testing of facial bones did not utilize symbiotic methods which would allow their data to be pooled together. This was also observed in a literature review published previously (Hampson 1995).

The literature concerning facial fracture tolerance consists of two main categories. One involves the use of a cylindrical impactor to simulate facial impacts with an automotive steering wheel (Allsop 1988, Bermond 1989, Bruyere 2000, Cesari 1989, Hodgson 1965, Welbourne 1989, Yoganandan 1993). The second category involves the use of a flat, round impacting surface (Nahum 1975, Nahum 1968, Schneider 1972, Viano 2004). The advantage of the flat impactor is that it is usually smaller and applies an impact that is isolated to a single facial bone or region. Cylindrical impacts are typically performed by striking across the entire face. This can add variation in the amount of force that each side of the head is exposed to and it can also apply load across multiple bones, making it difficult to determine tolerances for an individual bone. Additional information concerning the tolerance of the frontal bone can be gleaned from previous studies utilized in the development of the Head Injury Criterion (HIC).

A significant amount of frontal bone impacts were incorporated in the development of the HIC as well. These ranged from cylindrical impactors (Hodgson 1973a, Hodgson 1973b) to windshield impacts using sled tests (Hodgson 1973a). Several published analyses were performed to determine a statistical relationship between impact severity (HIC, acceleration, etc.) and the risk of frontal bone fracture. The results of these studies will be reviewed and compared with more recent studies.

Facial bone tolerance has been investigated by several researchers using a variety of methods. Despite these efforts, a clear understanding of facial tolerance has yet to be defined. The purpose of this study is to utilize the previous work to improve our current understanding of facial bone tolerance. A brief summary of the previous work will be provided.

LITERATURE REVIEW

Flat Impactors

Hodgson reported some of the earliest research on facial bone tolerance (Hodgson 1967, Hodgson 1965). Their experiments maximized the resources available by performing several impacts at each location. Repeated testing can compromise the integrity of a bone, causing it to fracture at a lower force which negates the usefulness of the fracture test data generated. Two different circular contact areas were tested, 6.5 cm^2 (1 in^2) and 34 cm^2 (5.2 in^2). Minimal force fracture values for the frontal, mandible and zygomatic bones were 4194 N, 1600 N, and 1600 N respectively. For matched impact locations, impactor size was varied to measure its affect on fracture tolerance. Tests with the larger contact area had a fracture load 1.5 to 2.5 times the original value. This exemplifies the importance of impact area which has been found to increase facial bone tolerance in other studies as well (Swearingen 1965).

A comprehensive study by Nahum and Gadd in the late 1960's expanded on previous work (Nahum 1968). Minimal force tolerance levels were established for the frontal bone (3560-7117 N), maxilla (667-1334 N), mandible (2447-4000 N) and zygoma (890-

2890 N). A circular impactor tip with a contact area of 6.5 cm^2 (1 in^2) was used for all impacts. A crushable nickel pad added to the impactor distributed the load more evenly over the contact area and provided a secondary measure of force. Results from these tests established minimal fracture tolerances for the frontal, zygoma, and temporo-parietal regions to be 4000 N, 2000 N, and 890 N respectively.

Further development in fracture tolerances was provided by Schneider in 1972 by testing additional impact directions and locations using a similar apparatus as Nahum and Gadd (Schneider 1972). The tests performed included anterior-posterior and lateral loading of the mandible, oblique impacts to the maxilla, and lateral loading of the zygomatic arch. From 106 impacts the minimal force tolerances described by the authors were 1780 N for the mandible in the anterior-posterior loading direction, 890 N for the mandible in the lateral loading direction (rectangular plate), 668 N for the maxilla, and 890 N for the zygomatic arch. Between 6 six female subjects and 11 male subjects, a trend indicated females have a lower load tolerance for all impact locations than the males.

Cylindrical Impactors

Several previous studies have examined the tolerance of facial bones using cylindrical impactors which simulated impact with a steering wheel (Allsop 1988, Bermond 1989, Bruyere 2000, Cesari 1989, Hodgson 1965, Nyquist 1986, Welbourne 1989, Yoganandan 1988, Yoganandan 1993). As is the case for flat impactors, each study utilized slightly different methods to perform the experiments. These variations include methods used to support the head, angle of impact, unilateral versus bilateral contact and padded or rigid surfaces. It is reasonable to assume that each of these variations has an effect on facial tolerance; however, the extent is unknown due to insufficient sample sizes.

The NHTSA and Wayne State University collaborated on an investigation of facial fractures due to steering wheel impacts (Nyquist et al. 1986). A rigid bar, simulating a steering wheel, had a 25 mm diameter and impacted the face horizontally in the infra-orbital region. Two impactor masses, 32 kg and 64 kg, were used for the tests. Every

impact resulted in at least a nasal bone fracture but sometimes more extensive damage occurred to the facial bones. Overall, it was determined that below 3000 N only minor injuries occurred and at forces over 3000 N more seriously injury was a result. Additionally, force deflection data were collected for each impact. Their data demonstrated that stiffness increases with increasing impactor penetration. This is an important result and is probably related to impactor area.

Horizontal bar experiments continued with impacts to the maxilla and nasal region (Welbourne et al. 1989). The primary objective of this research was to compare the performance of a surrogate device to cadaver responses. Although only 1 fracture was produced from the eight maxilla impacts, the nasal impacts produced 6 fractures from eight subjects. Fracture force values for this region ranged from 1875 N to 3760 N. To account for head rotation during a frontal collision, Bruyere *et al.* performed impacts at an angle of 30 degrees from the A-P direction (Bruyere et al. 2000). Logistic regression was used to determine the risk of frontal bone fracture. Their results suggested that a force of 7500 N had a 50% chance of causing a fracture. This force corresponded to an impactor energy of 265 J. Most studies do not have sufficient data to produce risk curves, so the threshold for fracture is usually stated. Using an unpadded cylindrical impactor, Nyquist *et al.* estimated a 3 kN threshold for severe facial fracture (Nyquist et al. 1986). Their subjects were struck in the suborbital region, so that the bones involved could vary by subject geometry and orientation.

Similar to the studies described previously, Allsop *et al.* performed facial impacts using a cylindrical impactor (Allsop 1988). They used an array of semi-circular disks instrumented with load cells to measure impact force. Unlike any previous study however, an Acoustic Emission (AE) sensor was used to "listen" to the facial bones during impact. This was done because unlike long bones like the femur, facial bones present a curved shell structure that can continue to support load after fracture. This creates difficulties when attempting to measure the force that caused a facial fracture. If a bone is exposed to a measured impulse (force over time) resulting in fracture, but the force at which the fracture occurred is unknown, this produces left-censored data. Left

censoring indicates that the force necessary to cause a bone to fracture is an unknown force less than the maximum force. Right censoring occurs when a bone does not fracture and, therefore, the force necessary to cause fracture is higher than the maximum force, but unknown. The AE sensors were used by Allsop *et al.* to estimate the time at which fracture occurred and utilized the force at that time as the fracture force. The measured AE during fracture was representative of a burst emission consistent with other studies (Wright 1981).

HIC Development

Early facial fracture research focused on the frontal bone and lead to the development of the Head Injury Criterion (HIC). Currently, the HIC plays an important role in vehicle design and the implementation of Federal Motor Vehicle Safety Standards (FMVSS). The HIC developed from the Wayne State Tolerance Curve (WSTC) which was meant to predict skull fracture as a function of anterior–posterior head acceleration and the duration over which the acceleration is applied (Lissner 1960).

In 1971 Versace proposed the use of the HIC as a measure of the average acceleration which corresponded to the WSTC (Versace 1971). Then, in 1985 Prasad and Mertz analyzed a series of 54 head impacts obtained by four different studies and recommended that the calculation of HIC should be limited to a duration of 15 ms (Prasad 1985b). This duration was chosen because the duration of the impacts analyzed in which a skull fracture occurred was less than 15 ms and if used for long durations, a low-level acceleration would result in a high HIC if applied for the necessary duration. The authors also found that a HIC of 1500 was not acceptable due to the presence of skull fractures at a HIC between 1000 and 1500. The dataset used to derive the risk of brain injury was an amalgamation of several studies utilizing different methods to impact the frontal bone. The estimated risk functions demonstrated that the risk of frontal bone fracture was similar to the risk of a brain injury. The aim of these studies was to determine skull fracture thresholds or brain injury thresholds using cadavers.

Two of the studies incorporated into the original HIC analysis by Prasad and Mertz (1985) were performed by Hodgson *et al.* (Hodgson 1973a, Hodgson 1973b). The Hodgson *et al.* study in 1973 determined the fracture tolerance of the frontal bone by dropping cadavers onto surfaces of varying shape and stiffness. The subjects were positioned such that the aspect of the frontal bone with the smallest radius struck first. With respect to impact surface, a flat rigid surface produced fractures at impacts speeds near 2.2 m/s (7.3 ft/s) and by comparison fractures were produced at impact speeds of 3 to 4 m/s (10 to 12 ft/s) and 5.5 m/s (18 ft/s) for the flat 90 and 60 durometer rubber surfaces respectively.

A second study considered by Prasad and Mertz (1985) in the development of HIC was performed by Hodgson by performing sled tests that resulted in cadaver head impacts into High Penetration Resistant (HPR) windshields (Hodgson 1973a). A total of 19 tests were conducted using 5 embalmed cadavers instrumented with four accelerometers on one side of the skull. Head acceleration from windshield impact was typically characterized by a large initial spike followed by a longer duration sinusoidal response.

None of the tests resulted in fracture. The average peak head acceleration was 230 G (Standard Deviation = 55 G) with an average HIC of 600 (S.D. = 600). The average pulse duration of the initial spike was 2.4 ms (S.D. = 1.2). The authors concluded that the mechanism for concussion is the initial spike and not the longer duration pulse which occurs as the interlayer of the windshield bulges forward. All impacts were performed at a speed of approximately 8 m/s (27 ft/s) and there was no relationship between peak head acceleration and the resulting level of windshield damage.

Additional studies of interest in the development of the HIC threshold were performed through the Association Peugeot Renault (APR) by Got *et al.* (1978 and 1983). Unlike the studies by Hodgson *et al.,* these studies were performed to determine the cadaver tolerance to brain injury. The data gathered during these studies were used in both the skull fracture tolerance curve and the brain injury tolerance curve developed by Prasad and Mertz (1985). The 25 drop tests within the APR dataset consisted of impacts to

various aspects of the skull and face and utilized padded surfaces or helmeted cadavers. All impacts were utilized by Prasad and Mertz (1985) in their initial analysis, but only 18 were utilized in the reanalysis by Mertz *et al*. (Mertz 1996). Two additional studies concerned with brain injury in cadavers were performed by Nahum *et al.* (Nahum 1976, Nahum 1977). These two studies provided a total of 18 tests performed by impacting the frontal bone with a padded or rigid surface. The articles published by Nahum *et al.* did not mention the occurrence of skull fracture in any test. Their data were only utilized to determine brain injury tolerance by Prasad and Mertz (1985), and not skull tolerance by Mertz *et al.* (1996).

The studies described above were analyzed using the Mertz-Weber method (Mertz 1982), which demonstrated that a HIC of 1000 corresponded to a 16% risk of incurring a life-threatening brain injury. The risk of sustaining a skull fracture or brain injury was relatively equivalent based on the data available. The Mertz-Weber method accounts for data censoring in order to estimate the cumulative distribution of the data by assuming a normal distribution. It was assumed that the weakest specimen was the one that failed at the lowest force and the strongest specimen the one exposed to the highest force without fracture. The normal distribution was then fit between those two data points.

Mertz *et al.* (1996) utilized the same dataset as Prasad and Mertz (1985) and estimated the risk of skull fracture using the certainty method (Figure 30). Under the certainty method, the risk of fracture is determined for a defined set of intervals of the loading stimulus. A certainty group is obtained for each interval and observation depending on the outcome of each test. If a test resulted in failure, then it is known with certainty that it would fail at all stimuli above the fracture stimulus and so by the certainty method, that single test would be counted as a failure for all intervals above the fracture stimulus. Conversely for a non-fracture test, it would be counted as a non-fracture for all intervals less than the peak stimulus. To determine the risk of fracture at each interval the number of certain failures is divided by the sum of certain failures and non-failures within a given interval. A normal cumulative distribution function was also fit to the certainty data. This demonstrated that the data analyzed did not have a normal distribution. Risk

functions were also developed using different combinations of observations by removing assumed outliers and adding additional data from a study by Ono (Ono 1996) (Figure 31).

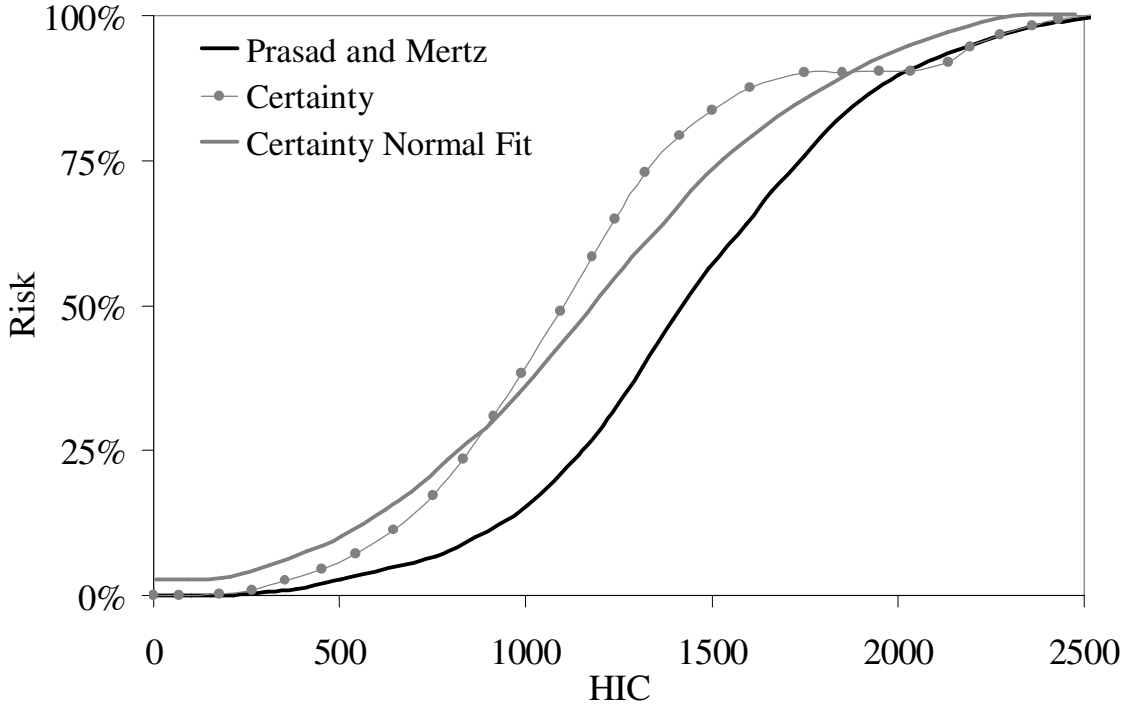

Figure 30: Original risk estimation by Prasad and Mertz with reanalysis by Mertz using certainty method.

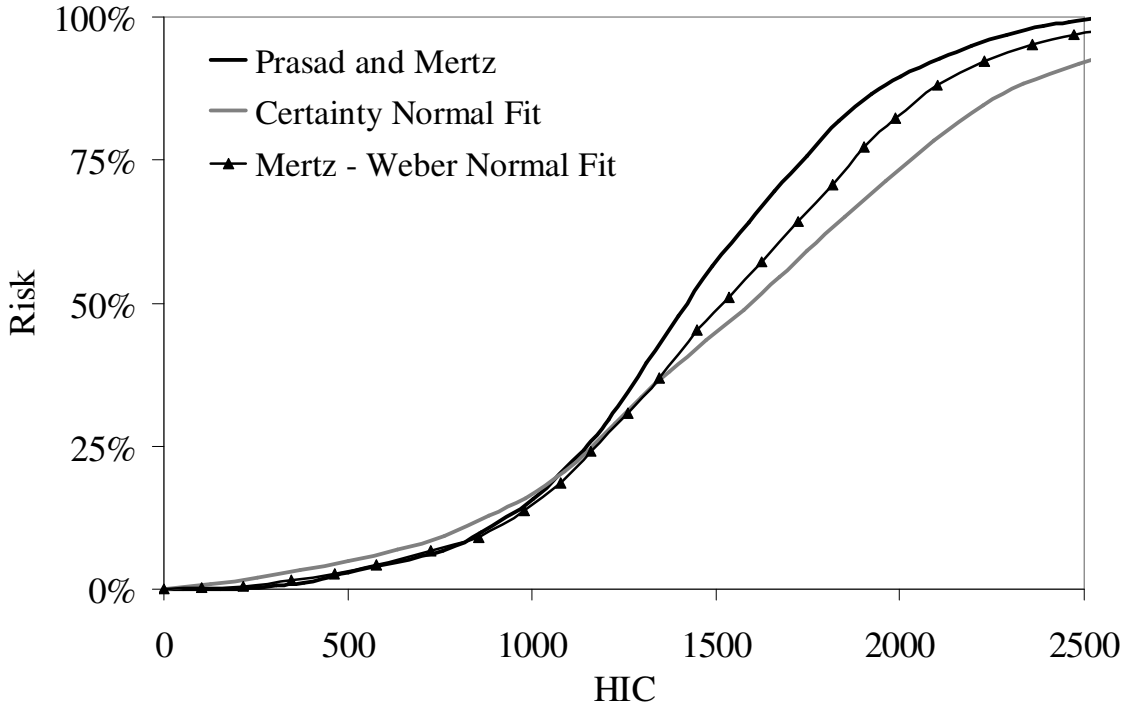

Figure 31: Original risk estimation by Prasad and Mertz with analysis of expanded dataset by Mertz.

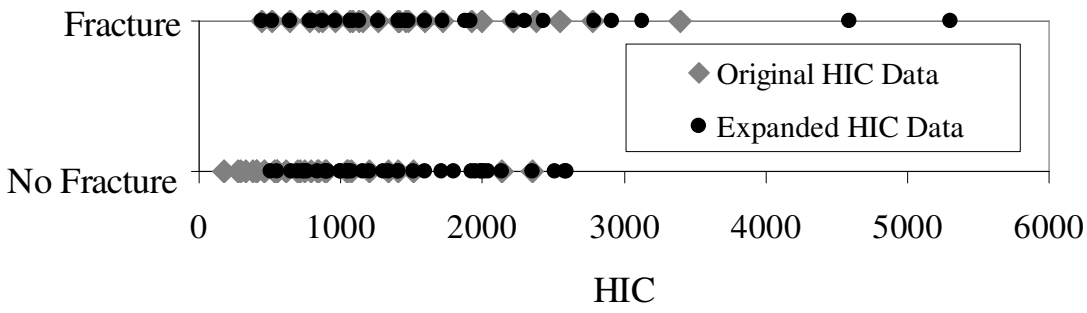

Figure 32: Distribution of original and expanded datasets used by Mertz *et al.* (1996).

The reanalysis by Mertz *et al.* (1996) produced values similar to the original estimate by Prasad and Mertz (1985). The expanded dataset showed a clear shift in fracture forces toward higher values than the original data (Figure 32). In some instances the expanded dataset contained two impacts for a single subject, consisting of a fracture and no fracture test. The resulting decrease in risk of injury with the expanded data set was not unexpected. The authors note that as the number of observations increase, the efficacy of the certainty method will decrease and may produce a biased threshold distribution. A detailed critique of the certainty method is found in a 2001 report by TNO Automotive Crash Safety Center (Van Ratingen 2000). They found that the certainty method can

produce statistically significant risk functions when there is no association between stimulus and outcome. They recommended that the certainty method not be used for risk function development and a probit or logit analysis be used instead. A similar analysis was also performed by Eppinger *et al.* in which they came to the same conclusion (Eppinger 1999). Similar to the TNO report, they found that the certainty method ignored a lot of the data and increases in sample size did not alter the estimated risks.

In the same report, the NHTSA described the development of injury criteria for automotive restraint systems (Eppinger 1999). The analysis of the HIC dataset by Hertz was described and demonstrated that a HIC of 700 corresponded to a 31% risk of skull fracture (AIS $\geq$ 2) for the mid-sized male (Hertz 1993). A log-normal curve was used to fit the previous data and was determined to provide the best fit when compared to a normal and two-parameter Weibull models. In the Final Economic Assessment for FMVSS 208 on Advanced Airbags, the NHTSA stated that Hertz had expanded the Prasad/Mertz curves to include all AIS levels (NHTSA 2000). The risk estimates developed by Mertz *et al.* (1996) were similar to the estimates by Hertz for a MAIS 3 head injury.

The preceding was a brief summary of studies examining human tolerance to facial impact; additional reviews are available in the literature (Allsop 2002, Eppinger 1999, Hampson 1995). Continuing with the purpose of this study, the methods utilized to analyze the previous work will be described.

METHODOLOGY

The current study began with a review of the literature and a compilation of data reported in each study of interest (Appendix A). The data from multiple studies were pooled when impacts were performed on the same facial region, in the same direction and using the same type of impactor. These datasets were then analyzed in an attempt to estimate the fracture tolerance of each region using parametric and non-parametric techniques.

Analysis of HIC Development

An analysis of the HIC development was performed using survival analysis methods to estimate the risk of fracture using average acceleration and HIC. Since all the data utilized to generate the HIC risk curve were censored, statistical techniques meant for this type of data were used. The Consistent Threshold (CT) method was used to determine a non-parametric estimate of risk based on HIC and the average acceleration data also provided within the Prasad / Mertz datasets. A Weibull model was also fit to the data to generate parametric risk curves. The LIFEREG procedure within SAS can account for left and right censoring and, therefore was used to determine the parameter estimates (Allison 1995, Cantor 2003). Comparisons between risk curves generated by the expanded dataset and original Prasad / Mertz datasets were also performed.

Analysis of Facial Impact Studies

Beginning with the frontal bone, two studies by Nahum *et al.* represented the largest sample performed by one investigator (Nahum 1975, Nahum 1968). No other study was similar enough to facilitate combining their data with another. The two studies consisted of 37 frontal bone impacts, 31 of which resulted in fracture. The data reported consisted of multiple impacts to a single subject.

Three previous studies evaluating the tolerance of the frontal bone using a cylindrical impactor were reviewed (Allsop 1988, Bermond 1989, Bruyere 2000). As described previously, the Allsop data are uncensored due to the use of acoustic emission sensors. Since the Allsop *et al.* data were not censored, the non-parametric, Kaplan-Meier method was chosen along with the parametric Weibul model to estimate risk of fracture as a function of force. The Kaplan-Meier method is meant for data which are left censored and non-censored and estimates the risk of fracture at intervals based on the number of subjects that failed and the number of subjects at risk at each interval (Kleinbaum 2005). The Kaplan-Meier estimates were determined using the lifetest procedure within SAS (Allison 1995).

RESULTS

Facial Impact Studies

The data from several studies were combined to obtain an estimate of fracture risk as a function of impact force by facial bone or region.

Frontal Bone

Two studies by Nahum *et al.* represent the largest sample performed by one investigator (Nahum 1975, Nahum 1968). Their data consisted of 37 frontal bone impacts, 31 of which resulted in fracture (Table 4).

Table 4: Summary of frontal bone impact data within Nahum studies.

	Peak Force (N)		**Kinetic Energy (N-m)**	
	Fracture	**No Fracture**	**Fracture**	**No Fracture**
Mean	5285	6093	51.0	41.1
Min	2669	4217	28.2	25.3
Max	9875	7429	133.8	55.9
Std Deviation	1633	1221	22.5	10.7

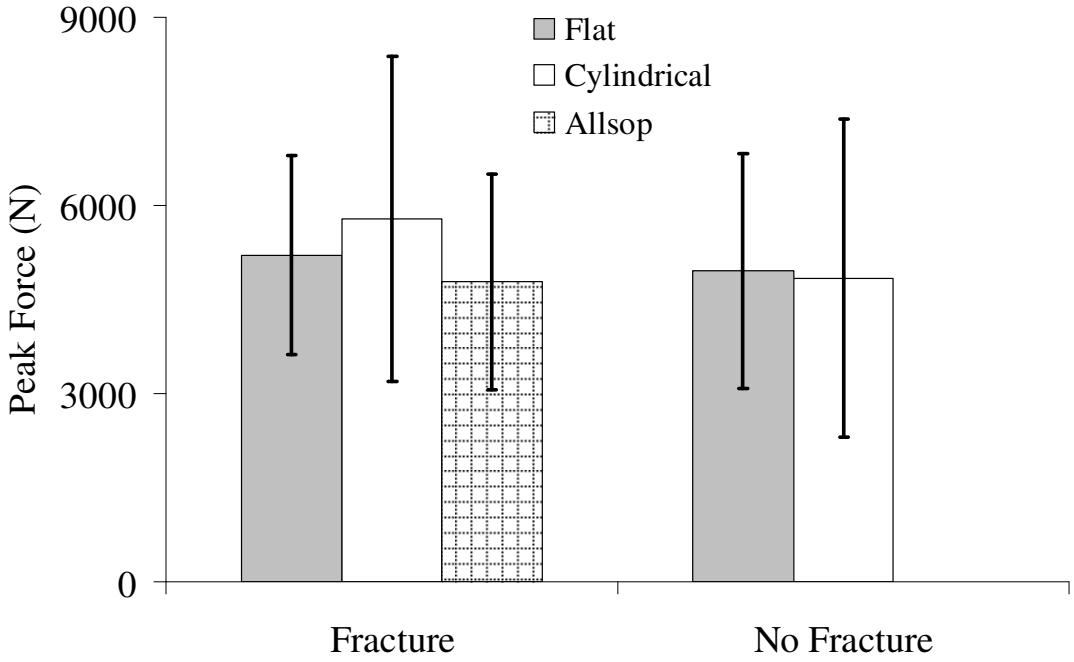

Figure 33: Frontal bone peak forces by impactor shape.

The kinetic energy of the impactor was estimated using the impact velocity and impactor mass when provided in the study. These values show little correlation with the peak force resulting from a frontal bone impact (Figure 34, Figure 35).

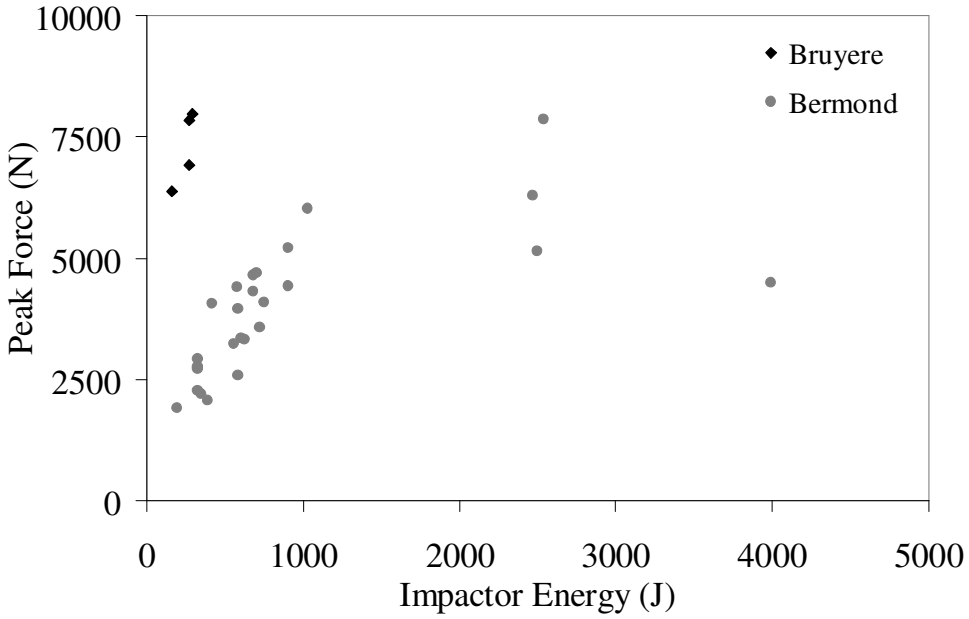

Figure 34: Impactor energy and peak force for two studies utilizing a cylindrical impactor.

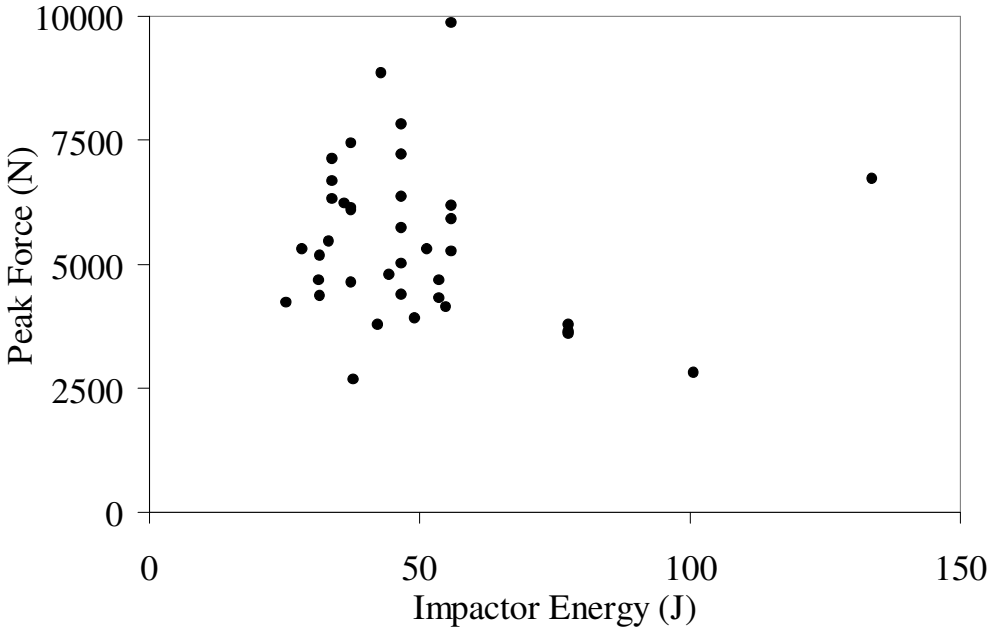

Figure 35: Impactor energy and resulting peak force during frontal bone impact with a flat impactor (Nahum 1968 and 1975).

A weibul model and the CT method was used to estimate the risk of fracture as a function of peak force (Figure 36). The resulting relationship demonstrates the limitation in calculating risk functions based on limited data that is doubly censored. Based on these data, the authors suggested a fracture threshold for the frontal bone of 4,000 N.

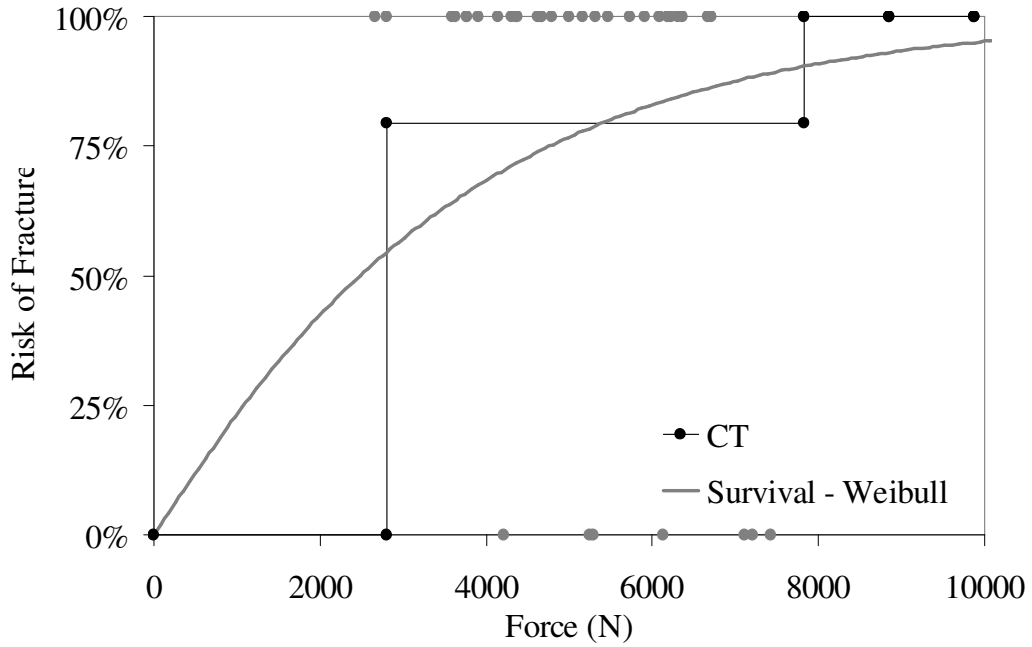

Figure 36: Analysis of Nahum et al. (1968, 1975) frontal bone impact data.

Risk curves were developed using survival methods for doubly censored data for the Bermond *et al.* data alone (Figure 37) and together (Figure 38) with the Bruyere *et al.* data due to the use of similar methods.

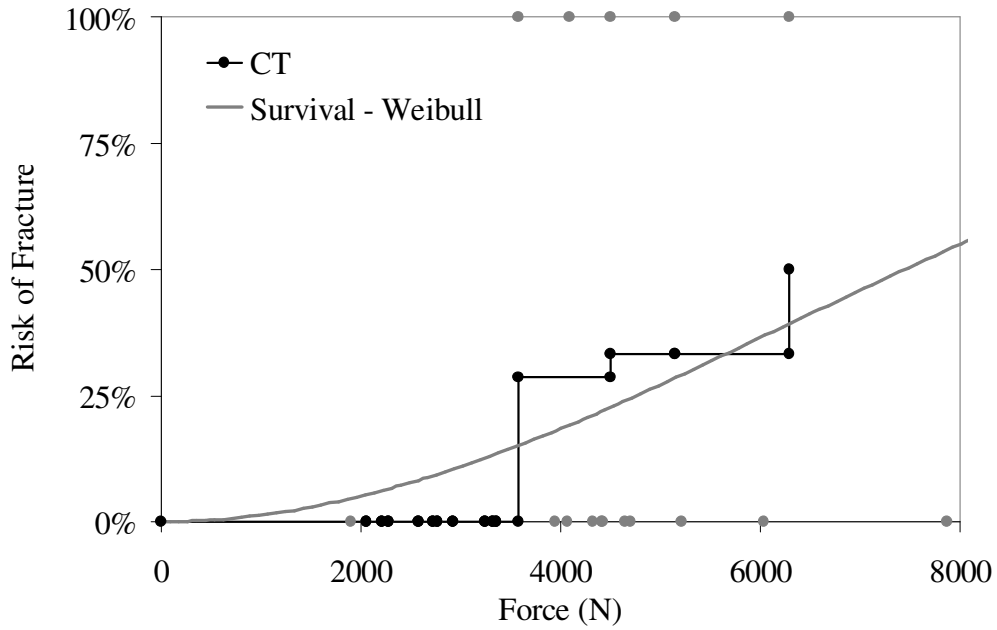

Figure 37: Survival analysis of frontal bone impacts using a cylindrical impactor (Bermond 1989).

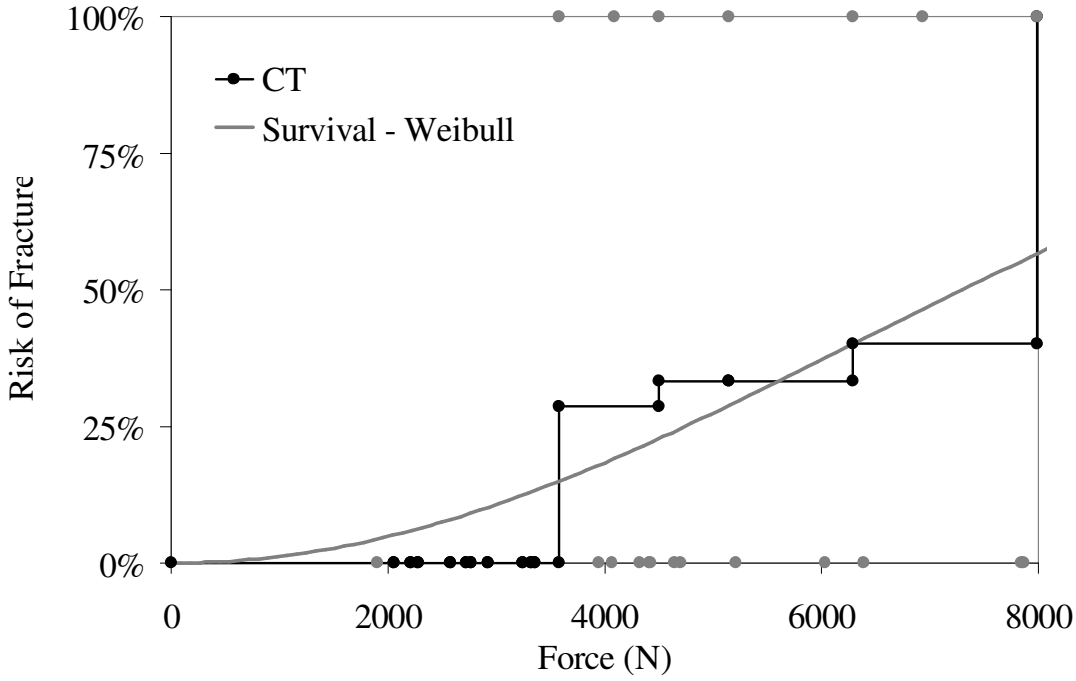

Figure 38: Survival analysis of frontal bone impacts using a cylindrical impactor (Bermond 1989, Bruyere 2000).

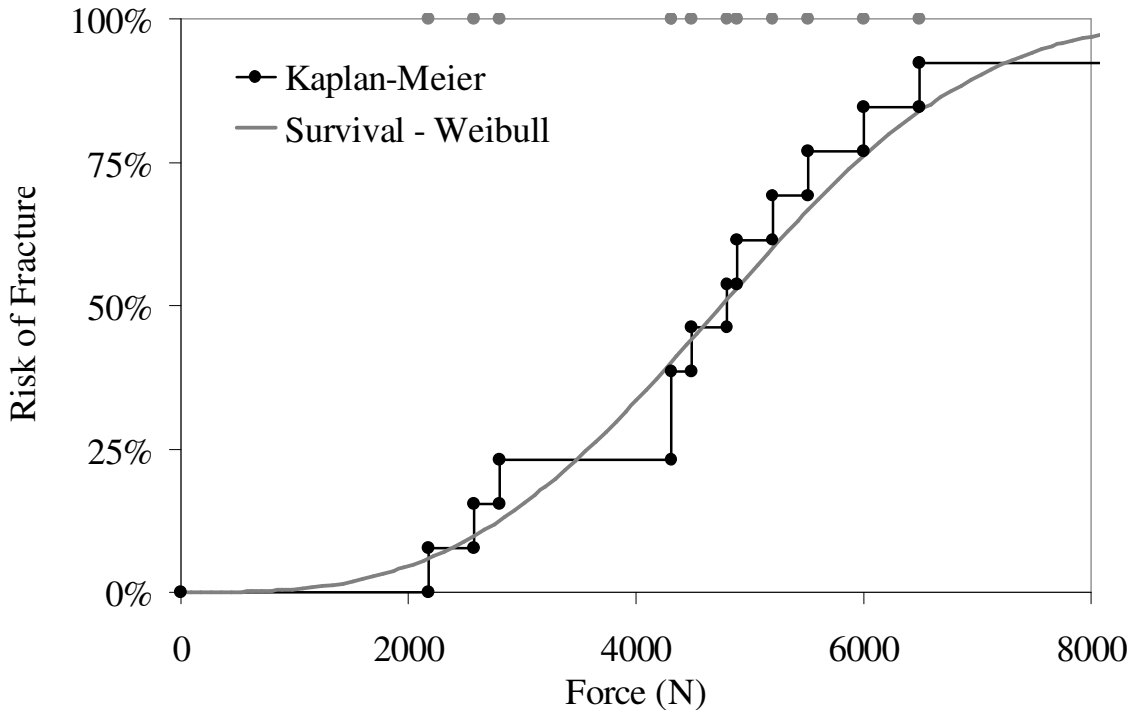

Figure 39: Survival analysis of frontal bone impacts using a cylindrical impactor (Allsop 1988).

Nasal Bone

One study in the literature was found to have performed a series of tests on the nasal bone (Cesari 1989) (Table 5). Due to the use of a cylindrical impactor some impacts resulted in fractures of the maxilla as well. The CT method produced an estimated risk of 67% for the available tests which resulted in peak forces between 1790 and 3760 N. Impactor energies were comparable to those of studies causing fractures in the maxilla and frontal bone which is consistent with the occurrence of maxilla fractures in these tests as well (Figure 40).

Table 5: Summary of nasal impact data using a cylindrical impactor (Cesari 1989).

Peak Force (N)	Impact Energy (J)	Fracture	Nasal fracture only
2503	87	1	1
2918	79	0	0
2781	123	1	0
3403	76	0	0
3760	112	1	1
2225	112	1	0
1875	43	1	1
1790	42	0	1

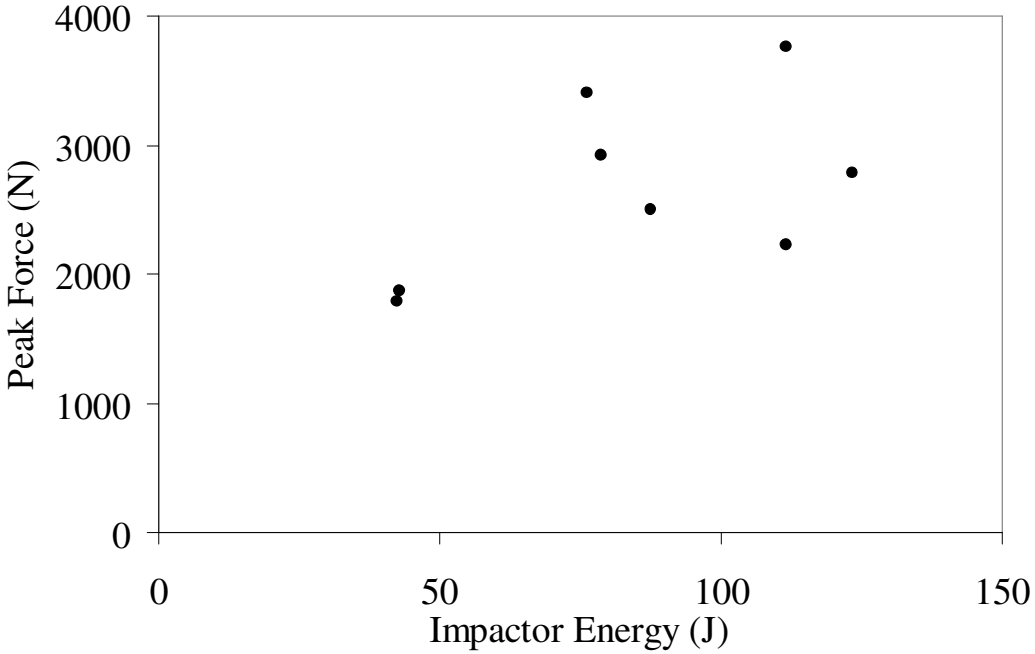

Figure 40: Impactor energy and peak force for nasal impacts by Cesari *et al.* 1989.

Maxilla

A total of four studies investigating the tolerance of the maxilla were assessed (Allsop 1988, Bruyere 2000, Cesari 1989, Nahum 1975) (Figure 41). The Allsop *et al.* data were non-censored and were not combined with the other studies utilizing a cylindrical impactor (Figure 42).

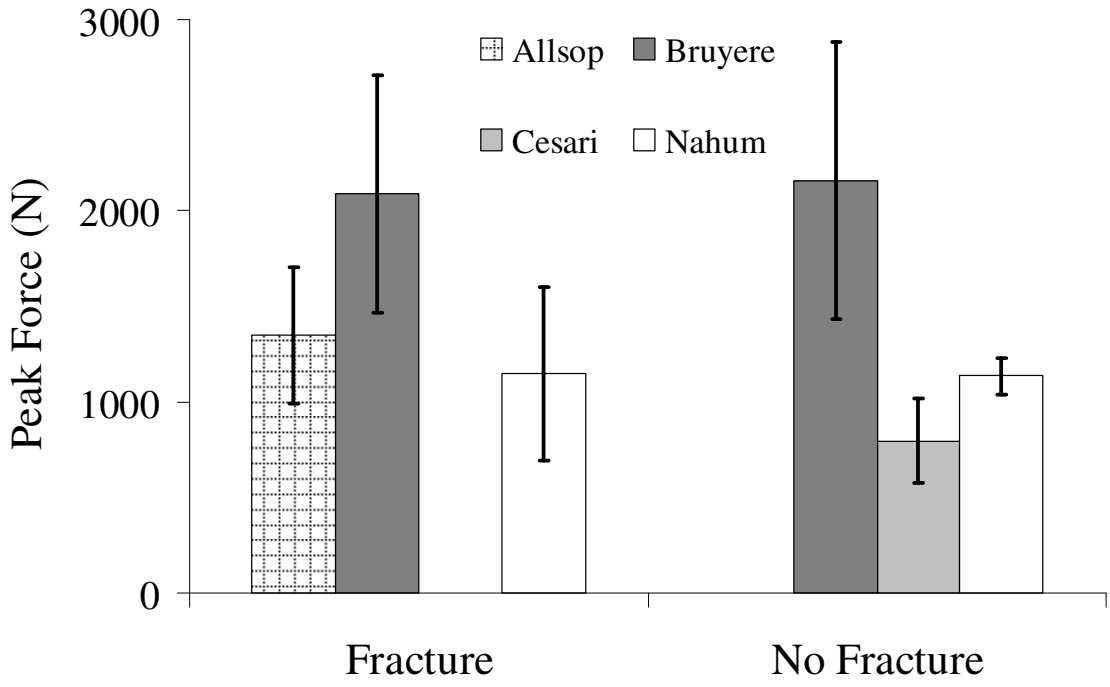

Figure 41: Peak forces during maxilla impact by study.

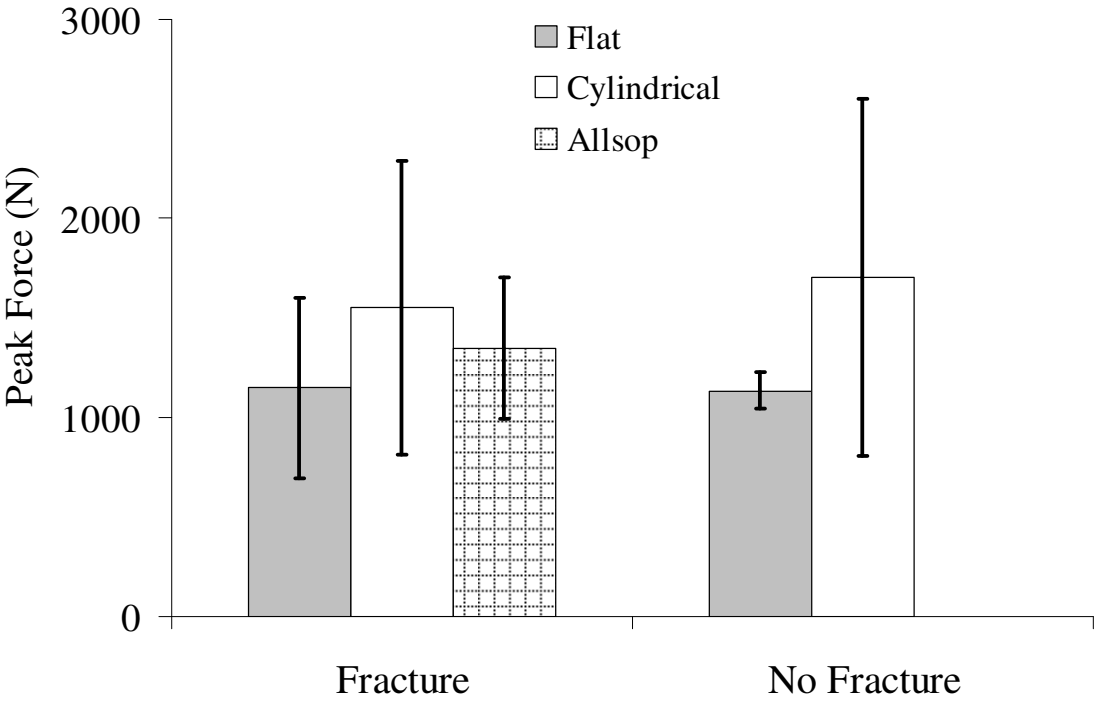

Figure 42: Maxilla peak forces by impactor shape.

HIC Development Studies

The previous datasets generated by Mert *et al.* and utilized to determine risk curves as a function of HIC and peak head acceleration were assembled and analyzed. The original dataset used by Prasad and Mertz in 1985 to determine the risk of facial fracture and brain injury was analyzed using survival analysis techniques (Figure 43). Mertz *et al.* created a larger dataset by combining several studies examining the tolerance of the frontal bone to various types of impact (Mertz 1996). Even though the individual studies used markedly different methods, the data were combined to generate a single function for the risk of frontal bone fracture. Applying accepted statistical techniques to the Mertz *et al.* datasets demonstrates the effect of adding and removing observations to create the "expanded" dataset (Figure 44).

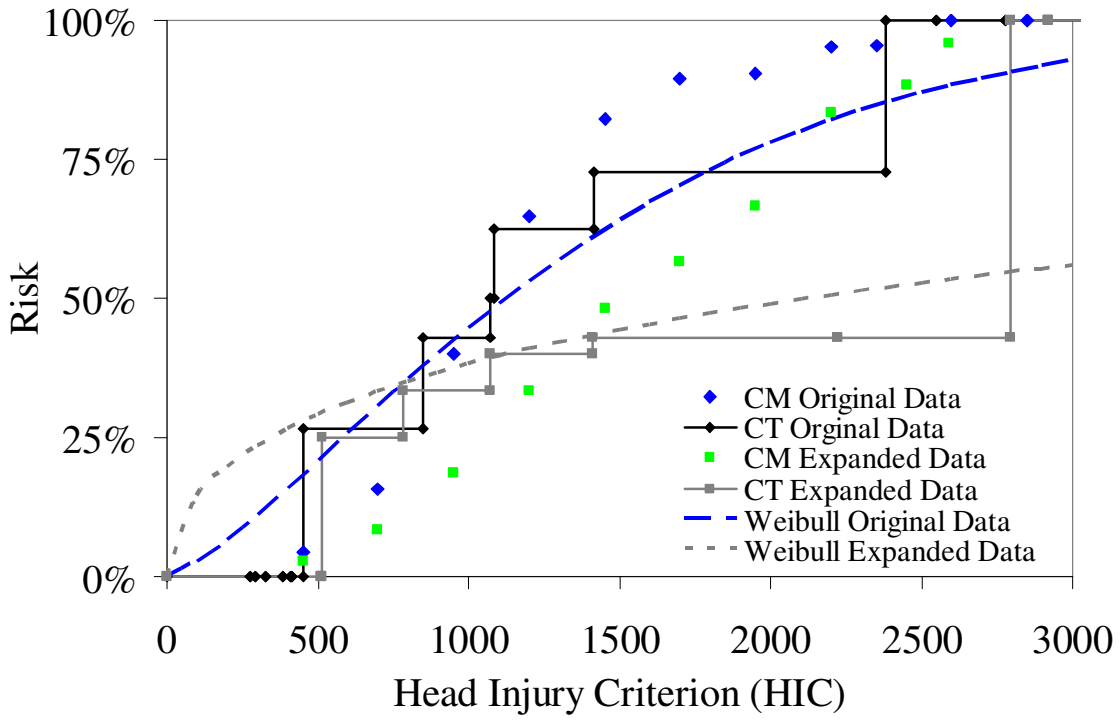

Figure 43: Analysis of original and expanded HIC development datasets.

The Kaplan-Meier method was used because in the analysis by Mertz *et al.* it was assumed that the fracture tests produced non-censored data. It is unclear if these data are uncensored due to the use of peak acceleration as the injury predictor. Survival analyses were also created using a Weibull distribution and assuming doubly censored data.

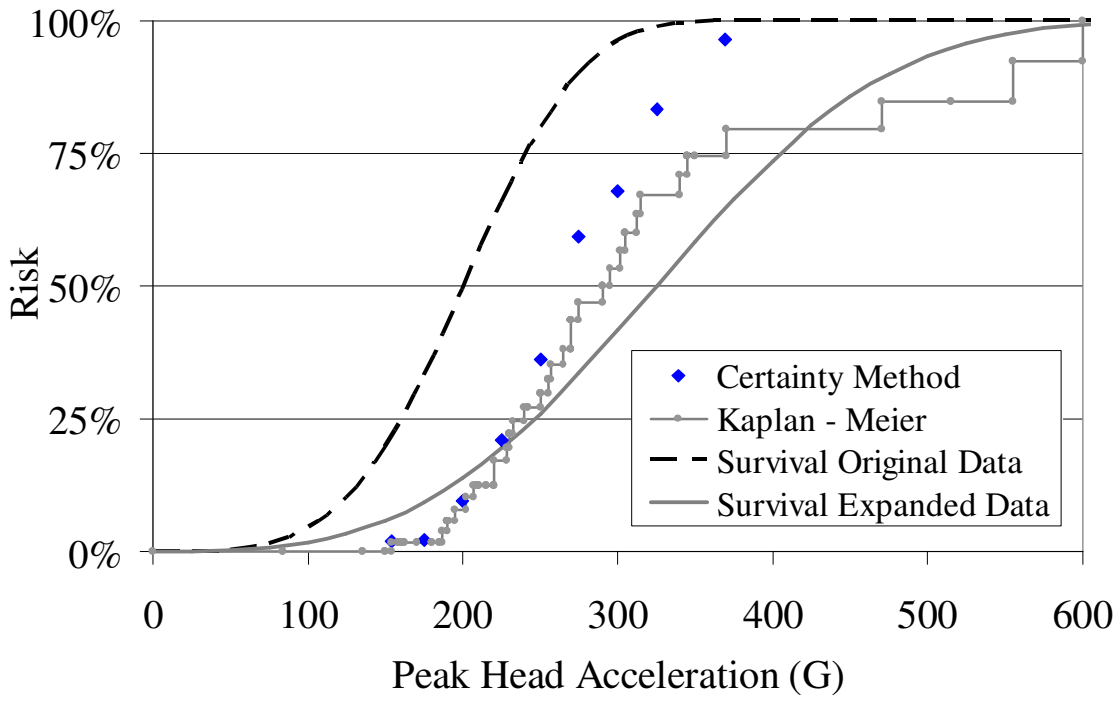

Figure 44: Analysis of original and expanded datasets utilized by Mertz *et al.* (1996).

DISCUSSION

The development of the HIC is convoluted because the risk of a fracture and brain injury was assumed to have the same relationship to HIC (Prasad 1985a). Biomechanically this is nonsensical sense it is known that higher forces can be applied over greater area which will reduce the risk of fracture while increasing head acceleration and, therefore, the risk of a brain injury.

A similar analysis of the Mertz / Prasad dataset was performed in a previous study (Hertz 1993). Similar to this study, proc LIFEREG in SAS was utilized to fit various models that predict the occurrence of skull fracture using HIC. The results of the previous study demonstrated that the Weibull and lognormal distributions fit the Mertz / Prasad data better than a normal and the Mertz / Prasad method.

In a Preliminary Regulatory Evaluation by the NHTSA, risk functions for various levels of brain AIS injuries were presented (NHTSA 2008). The origin of the data used to

support these various estimates is unclear. The risk of an AIS 4, 5 and fatal brain injury were very similar for all values of HIC (Figure 45). The risk of AIS 4, 5 and fatal brain injury is very similar for all values of HIC according to the risk functions. These values are fairly similar to those in the previous analyses by Mertz *et al.* (1996).

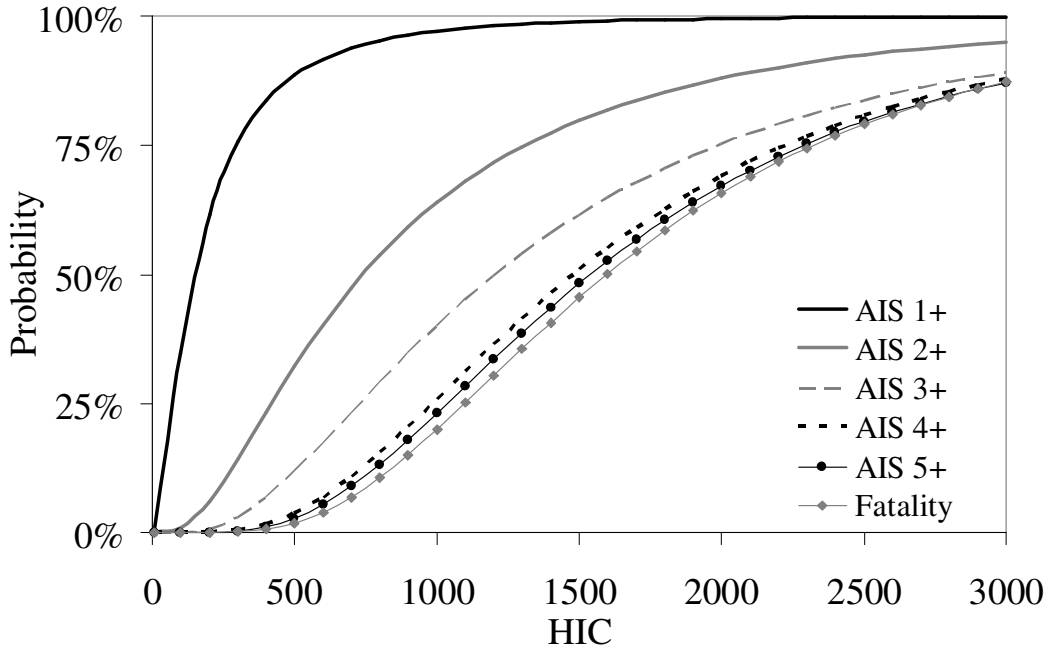

Figure 45: Risk of various AIS level brain injuries.

The 25 drop tests within the APR dataset consisted of impacts to various aspects of the skull and face and utilized padded surfaces or helmeted cadavers. A second study considered by Prasad and Mertz (1985) in the development of HIC was performed by Hodgson by performing sled tests that resulted in cadaver head impacts into High Penetration Resistant (HPR) windshields (Hodgson 1973a). The risk curves by Mertz *et al.* (1996) estimated that the risk of fracture at a head acceleration of 230 G would be 20%.

With the exception of the study by Allsop *et al.*, all the previous literature concerning facial fracture contains data that are doubly censored (Allsop 1988). This means that all observations are either right or left censored and there are no non-censored observations. As a result of variable methods and lack of data, statistical analyses to estimate the risk of fracture as a function of impact severity are unavailable in the current literature. The

current knowledge is also lacking in an understanding of the overall response of the frontal bone to impact. The development of finite element models or Anthropomorphic Test Devices (ATD) for fracture prediction is limited by the lack of a quantitative measure of frontal bone response to impact. Defining force-deflection corridors and creating simple mathematical models of the frontal bone response will provide a basis for the development of more advanced models and ATDs.

CONCLUSIONS

An analysis of the previous literature demonstrates a lack in the number of samples and consistency in test methods used in determining the tolerance of facial bones to impact. The previous data does provide valuable information concerning the response of the facial bones to impact and the limitations associated with structures that continue to support load after fracture. The obvious differences in structural composition are demonstrated in the varying tolerances by facial region.

The importance of obtaining non-censored fracture data is demonstrated through two aspects in the current review. In one aspect, peak force is not influenced by the occurrence of fracture and, therefore, the peak force during a test is more a function of the structural stiffness of the face and the methods used by investigator the (Figure 41). Compared to the study by Allsop *et al.* which acquired non-censored data, fracture forces by the other studies were higher when using similar methods. This was demonstrated for tests on the frontal bone and maxilla. Secondly, the calculation of risk curves was facilitated by the availability of non-censored data, whereas studies with censored data did not allow for the calculation of risk functions, even with larger sample sizes.

Appendix A

Table A.1: Prasad / Mertz data used in preliminary HIC analysis (Prasad 1985).

Source	HIC	Average Acceleration (G)	Fracture
2	175	105	0
2	278	90	0
2	291	106	0
2	326	116	0
2	384	101	0
2	411	128	0
2	413	124	0
1	450	125	1
2	461	104	0
3	516	76	1
2	531	97	0
2	554	128	0
2	554	138	0
2	611	225	0
1	640	140	1
3	692	104	0
2	711	151	0
3	750	108	0
3	781	96	1
2	791	183	0
3	839	96	0
2	845	159	0
1	850	150	1
1	870	175	1
2	892	185	0
3	900	173	0
1	965	200	1
3	1042	125	0
2	1050	197	0
1	1070	185	1
3	1078	126	0
3	1085	116	1
1	1130	175	1
3	1156	120	1

Source	HIC	Average Acceleration (G)	Fracture
3	1200	139	0
3	1270	137	1
3	1334	136	0
1	1410	215	1
3	1411	154	0
3	1416	156	1
1	2000	185	1
3	2138	191	0
1	2220	190	1
3	2351	224	0
1	2380	205	1
1	2550	280	1
3	1460	118	1
3	1483	176	1
2	1520	231	0
1	1600	235	1
3	1720	189	1
1	1930	150	1
1	2780	295	1
1	3400	290	1

Source	Study
1	Hodgson 1977
2	Hodgson 1973
3	Lissner 1960

Table A.2: Tests impacting the frontal bone with a flat impactor

Study	ID	Peak Force (N)	Impact Energy (J)	Fracture
Nahum 68	1	5311	28	1
Nahum 68	1	4795	44	1
Nahum 68	2	7117	34	0
Nahum 68	2	6672	34	1
Nahum 68	3	6316	34	1
Nahum 68	3	5471	33	1
Nahum 68	4	3772	42	1
Nahum 68	4	2669	38	1
Nahum 68	5	8852	43	1
Nahum 68	5	6717	134	1
Nahum 68	6	4671	31	1
Nahum 68	6	2802	101	1
Nahum 68	7	4359	32	1
Nahum 68	7	3914	49	1
Nahum 68	8	4217	25	0
Nahum 68	8	3585	78	1
Nahum 68	9	6228	36	1
Nahum 68	9	3630	78	1
Nahum 68	10	5160	32	1
Nahum 68	10	3772	78	1
Nahum 75	1	5738	47	1
Nahum 75	1	6183	56	1
Nahum 75	2	4626	37	1
Nahum 75	2	9875	56	1
Nahum 75	3	5916	56	1
Nahum 75	4	6139	37	0
Nahum 75	4	6361	47	1
Nahum 75	5	4671	54	1
Nahum 75	5	4315	54	1
Nahum 75	6	7429	37	0
Nahum 75	6	7206	47	0
Nahum 75	7	7829	47	1
Nahum 75	8	4381	47	1
Nahum 75	9	5004	47	1
Nahum 75	9	4137	55	1
Nahum 75	10	5293	51	0
Nahum 75	10	5249	56	0
Nahum 75	11	6094	37	1

Table A.3: Tests impacting the frontal bone with a cylindrical impactor

Study	ID	Peak Force (N)	Impact Energy (J)	Fracture
Allsop 88	1	5204	-	1
Allsop 88	2	2580	-	1
Allsop 88	3	2802	-	1
Allsop 88	4	2180	-	1
Allsop 88	5	4893	-	1
Allsop 88	6	4804	-	1
Allsop 88	7	8585	-	1
Allsop 88	8	4315	-	1
Allsop 88	9	4493	-	1
Allsop 88	10	4315	-	1
Allsop 88	11	6494	-	1
Allsop 88	12	6005	-	1
Allsop 88	13	5516	-	1
Bruyere 00	1	6387	157	0
Bruyere 00	1	6932	270	1
Bruyere 00	2	7849	270	0
Bruyere 00	3	7988	289	1
Bermond 89	1	1900	195	0
Bermond 89	2	4410	575	0
Bermond 89	3	2280	327	0
Bermond 89	4	3580	726	1
Bermond 89	5	2920	327	0
Bermond 89	6	4320	682	0
Bermond 89	7	2770	327	0
Bermond 89	8	4650	682	0
Bermond 89	9	2720	327	0
Bermond 89	10	3240	558	0
Bermond 89	11	2210	345	0
Bermond 89	12	4700	699	0
Bermond 89	13	2060	389	0
Bermond 89	14	4090	752	1
Bermond 89	15	4070	416	0
Bermond 89	16	4420	903	0
Bermond 89	17	2576	584	0
Bermond 89	18	6031	1027	0
Bermond 89	19	3944	584	0
Bermond 89	20	4503	3992	1
Bermond 89	21	3352	602	0
Bermond 89	22	5149	2496	1
Bermond 89	23	3317	628	0
Bermond 89	24	7866	2540	0
Bermond 89	25	5210	903	0
Bermond 89	26	6293	2469	1

Table A.4: Tests impacting the maxilla with a flat impactor

Study	ID	Peak Force (N)	Impact Energy (J)	Fracture
Nahum75	1	1846	18	1
Nahum75	2	1979	26	1
Nahum75	3	1366	8	1
Nahum75	3	943	5	1
Nahum75	4	979	5	1
Nahum75	5	1201	5	0
Nahum75	5	1157	6	1
Nahum75	6	943	6	1
Nahum75	7	1068	6	0
Nahum75	7	1370	10	1
Nahum75	8	658	5	1
Nahum75	9	623	5	1
Nahum75	9	765	5	1

Table A.5: Tests impacting the maxilla with a cylindrical impactor

Study	ID	Peak Force (N)	Impact Energy (J)	Fracture
Cesari 89	1	516	16	1
Cesari 89	2	660	15	0
Cesari 89	3	673	32	0
Cesari 89	4	1254	82	1
Cesari 89	5	788	31	1
Cesari 89	6	1148	44	1
Cesari 89	7	1361	88	1
Cesari 89	8	1049	90	0
Allsop 88	1	1000	-	1
Allsop 88	2	1200	-	1
Allsop 88	3	1200	-	1
Allsop 88	4	1800	-	1
Allsop 88	5	1800	-	1
Allsop 88	6	1100	-	1
Bruyere 00	1	2085	152	1
Bruyere 00	2	1572	106	0
Bruyere 00	2	1462	189	1
Bruyere 00	3	1394	130	0
Bruyere 00	3	1802	287	1
Bruyere 00	4	1972	286	1
Bruyere 00	5	1842	248	0
Bruyere 00	6	2615	282	0
Bruyere 00	7	3116	289	1
Bruyere 00	8	2187	298	0
Bruyere 00	9	3331	291	0

REFERENCES

Allison PD: Survival Analysis Using SAS: A Practical Guide, Cary, SAS Press; 1995.

Allsop D, Kennett K: Skull and Facial Bone Trauma. Accidental Injury: Biomechanics and Prevention. A. Nahum and J. Melvin. New York, Springer-Verlag. 2nd Edition**,** 254-76; 2002.

Allsop D, Warner C, Wille M, Schneider D, Nahum A: Facial Impact Response – A Comparison of the Hybrid 3 Dummy and Human Cadaver, *Society of Automotive Engineers*, SAE No. 881719; 1988.

Bermond F, Kallieris D, Mattern R, Ramet M, Bouquet R, Caire Y, Voiglio E: Human Face Response at an Angle to the Fore-aft Vertical Plane Impact, *Proceedings of the IRCOBI*; 1989.

Bruyere K, Bermond F, Bouguet R, Caire Y, Ramet M, Voiglio E: Human Maxilla Bone Response to 30 degree Oriented Impacts and Comparison with Frontal Bone Impacts, *Proceedings of the 44th Association for the Advancement of Automotive Medicine Conference*, 219-34; 2000.

Cantor AB: Analysis Techniques for Medical Research, 2nd, Cary SAS Press; 2003.

Cesari D, Ramet M, Welbourne E: Experimental Evaluation of Human Facial Tolerance to Injuries, *Proceedings of the IRCOBI*, Stockholm, Sweden; 1989.

Eppinger R, Sun E, Bandak F, Haffner M, Khaewpong N, Maltese M, Kuppa S, Nguyen T, Takhounts E, Tannous R, Zhang A, Saul R: Development of Improved Injury Criterial for the Assessment of Advanced Automotive Restraint Systems - II, *NHTSA*; 1999.

Hampson D: Facial Injury: A Review of Biomechanical Studies and Test Procedures for Facial Injury Assessment, *Journal of Biomechanics*, 28(1), 1-7; 1995.

Hertz E: A Note on the Head Injury Criteria (HIC) as a Predictor of the Risk of Skull Fracture, *37th Annual Proceedings of the Association for the Advancement of Automotive Medicine*; 1993.

Hodgson V, Thomas L, Brinn J: Concussion Levels Determined by HPR Windshield Impacts, *Proceedings of the 17 Stapp Car Crash Conference*, SAE No. 730970; 1973.

Hodgson VR: Tolerance of the facial bones to impact, *Am. J. Anat*, 120(1), 113-22; 1967.

Hodgson VR, Lange WA, Talwalker RK: Injury to the Facial Bones, *Proceedings of the 9th Stapp Car Crash Conference*, SAE No. 650957; 1965.

Hodgson VR, Thomas LM: Breaking Strength of the Human Skull Versus Impact Surface Curvature, *Wayne State University Report* DOT-HS-146-2-230; 1973.

Kleinbaum D, Klein M: Survival Analysis: A Self-Learning Text, 2nd, New York, Springer Science; 2005.

Lissner HR, Lebow M, Evans FG: Experimental Studies on the Relation Between Acceleration and Intracranial Pressure Changes in Man, *Surg. Gynec. Obs.*, 3, 329-38; 1960.

Mertz HJ, Prasad P, Nusholtz G: Head Injury Risk Assessment for Forehead Impacts, *Society of Automotive Engineers*, No. 96099; 1996.

Mertz HJ, Weber DA: Interpretations of the Impact Responses of a 3-Year-Old Child Dummy Relative to Child Injury Potential, *Society of Automotive Engineers*, SAE No. 826048; 1982.

Nahum AM: The biomechanics of facial bone fracture, *Laryngoscope*, 85(1), 140-56; 1975.

Nahum AM, Gatts JD, Gadd CW, Danforth J: Impact tolerance of the skull and face, *Proceedings of the 12th Stapp Car Crash Conference,* October 22-23, New York; 1968.

Nahum AM, Smith RW: An Experimental Model for Closed Head Impact Injury, *Proceedings of the 20th Stapp Car Crash Conference,* SAE No. 760825; 1976.

Nahum AM, Smith RW, Ward CC: Intracranial Pressure Dynamics During Head Impact, *Proceedings of the 21st Stapp Car Crash Conference,* SAE No. 770922; 1977.

NHTSA: Final Economic Assessment FMVSS 208 Advanced Airbags, Docket: NHTSA-00-7013-2; 2000.

NHTSA: Preliminary Regulatory Evaluation FMVSS 218 Motorcycle Helmet Labeling; 2008.

Nyquist GW, Cavanaugh JM, Goldberg SJ, King AI: Impact Tolerance and Response of the Face, *Proceedings of the Advances in Bioengineering Conference*, Anaheim, CA; 1986.

Ono (1996). Personal Communication from Mr. Stan Backaitis, NHTSA.

Prasad P, Mertz H: The Position of the United States Delegation to the ISO Working Group 6 on the Use of HIC in the Automotive Environment, *Society of Automotive Engineers*,(851246); 1985a.

Prasad P, Mertz HJ: The position of the United States Delegation to the ISO Working Group 6 on the use of HIC in the automotive environment, *Presented at the Government/Industry Meeting & Exposition, Washington, D.C., May 20-23, 1985*

(Society of Automotive Engineers Technical Paper Series). Warrendale, PA, Society of Automotive Engineers, 1-11; 1985b.

Schneider DC, Nahum AM: Impact Studies of Facial Bones and Skull, *Proceedings of the 16th Stapp Car Crash Conference,* SAE No. 720965; 1972.

Swearingen JJ: Tolerances of the Human Face to Crash Impact, *Office of Aviation Medicine, Federal Aviation Agency*; 1965.

Van Ratingen M, Compigne S, Hynd D, Edlund L: SID 2000 – Side Impact Dummy Enhancements for Improved Occupant Protection for the Year 2000 and Beyond, No. BE97-4355; 2000.

Versace J: A Review of the Severity Index, *Proceedings of the 15th Stapp Car Crash Conference,* SAE No. 710881; 1971.

Viano DC, Bir C, Walilko T, Sherman D: Ballistic Impact to the Forehead, Zygoma, and Mandible: Comparison of Human and Frangible Dummy Face Biomechanics, *J. Trauma Inj. Inf. Crit.Care*, 56(6), 1305-11; 2004.

Welbourne ER, Ramet M, Zarebski M: A Comparison of Human Facial Fracture Tolerance with the Performance of a Surrogate Test Device, *Proceedings of the 12th ESV,* 89-4A-0-004, Gothenberg, Sweden; 1989.

Wright TM, Vosburgh F, Burstein AH: Permanent Deformation of Compact Bone Monitored by Acoustic Emission, *J. Biomech.*, 14(6), 405-9; 1981.

Yoganandan N, Fintar F, Sances A, Myklebust J, Schmaltz D: Steering Wheel Induced Facial Trauma, *Proceedings of the 32nd Stapp Car Crash Conference,* SAE No. 881712; 1988.

Yoganandan N, Pintar FA, Reinartz J, Sances A: Human facial tolerance to steering wheel impact: A biomechanical study., *Journal of Safety Research*, 24(2), 77-85; 1993.

CHAPTER 4:
ACOUSTIC EMISSION IN FACIAL FRACTURE DETECTION

INTRODUCTION

The use of AE to detect incipient failure of a structure is based on the hypothesis that crack nucleation and propagation within a material results in the release of acoustic emissions. One large advantage of using AE to detect microdamage in a material is that an AE sensor does not have to be in the immediate vicinity of the defect in order to detect a change. Studies using AE analysis to detect the presence of microfractures in bone have found that it is more accurate than using techniques sensitive to a reduction in elastic modulus under fatigue loading (Rajachar 1999). This suggests that AE can detect microstructural defects that are not large enough to affect the structural integrity of the material.

An acoustic emission is an acoustic wave brought about by the release of energy from a localized source within the material (Kohn 1995). In metal failure, the release of energy is of the form of dislocation motion, microcracking and twinning that occurs in multiple but localized zones simultaneously to produce an AE signal perceivable by an AE sensor. The energy contained within the acoustic wave represents a portion of the energy released at the source. Energy is also dissipated in the form of dislocations, plastic flow, crack extension and heat. There are several mechanisms that can generate an acoustic emission within a material: mechanical, thermal, physical / chemical, electrical and magnetic.

Acoustic emission is measured in terms of volts, the magnitude of which is related to the magnitude of the waves encountering the sensor. An AE event is defined by the number and duration of acoustic waves that are above a specified threshold. A single rise and fall of an AE signal that has a magnitude higher than the threshold voltage is called a count.

In bone, AE is produced by the nucleation and propagation of microfractures in the interstitial matrix between osteons as well as the fracture of osteons. Monitoring of bone

under fatigue loading has demonstrated that AE analysis has the capacity to detect the presence of microcracks as small as 25 μm (Rajachar 1999). In the same study, the onset of AE occurred at 20 to 30 thousand cycles before the elastic modulus was changed by 1% through the fatigue process. This suggests that AE signal prior to changes in elastic modulus represent the nucleation, growth and coalescence of microfractures before structural integrity is affected. Histological and AE data suggest that the fatigue process of bone begins with a diffuse region of matrix damage. Coupling information from several AE sensors, the authors found that as the loading cycles continued beyond the initiation of AE, the location of AE centered on the primary fracture process zone.

In the context of impact biomechanics, acoustic emission presents itself in the form of high-amplitude bursts with a large number of AE events, differentiating itself with the AE response seen under fatigue or static loading scenarios. Studies using cortical bone have found that the onset of AE begins just prior to maximum force or specimen failure (Allsop 1988a, Allsop 1988b, Fischer 1986, Funk 2002). Additional studies using bovine femoral bone in torsion and tension found that significant AE signal was only created during plastic deformation and fracture (Knets 1975, Peters 1982, Wright 1981).

In contrast, a study using metal pins embedded in cancellous bone found that AE began at low forces with the number of counts increasing exponentially as maximum force was reached.

This finding is similar to that of Wright *et al.* (1981) who found that AE during yield occurred at a lower amplitude than AE during fracture. Similarly, Schwalbe *et al.* (Schwalbe 1999) found AE to occur at low load levels when performing torsional tests on human femur; however, the amplitude or frequency of the signal was not described. An explanation for the lack of AE during yielding of human bone was offered by Knets *et al.* (1974). They attributed the lack of AE to the Kaiser effect which was discovered in 1953 (Kaiser 1953). The Kaiser effect is similar to the response of a plastically deformed specimen. Once the specimen is reloaded, plastic deformation will not begin until the force at which plasticity was initiated in the previous loading cycle. In the same manner,

the Kaiser effect states that AE will not be produced in a specimen during a secondary loading cycle until the force experienced during the previous cycle is exceeded. Knets *et al.* (1953) hypothesis was that no AE signal is produced at low forces because the human bone is loaded constantly and, therefore, AE signal is only produced when the forces of daily activity are exceeded. In their study of cortical bone from human femurs, no AE occurred until 94% of the failure strain was reached. The authors also determined that the number of AE counts is directly related to the number of microcracks within the bone and the number of pulses generated by the surface of a crack.

Examining the effects of loading rate, the study by Wells and Rawlings (1984) noted that the total number of counts decreased with an increase in loading rate, which they attributed to a decrease in the number of trabeculae fractured during the test. This finding was supported through microstructural analysis. They hypothesized that the initial low level of AE was due to fluid being forced between trabeculae. This study is an example of using the number of AE event counts to assess its relationship to mechanical stress.

The study by Fischer *et al.* (1986) defined a cumulative event amplitude distribution to analyze the AE response of a given material (Equation 2).

$$F(V) = F(V_o)(\frac{V}{V_o})^{-b} \qquad \text{(Equation 2)}$$

where, V is the highest voltage during an AE event, V_o is the voltage threshold for an event to be considered, F(V) is the number of events with an amplitude above V. Plotting this distribution on a log-log scale will produce a straight line if F(V) follows the power-law relationship given by the –b value.

A previous study has shown that the slope of the line given by b is determined by the material and deformation characteristics of the specimen (Pollock). High b values are associated with ductile materials which generally produce lower amplitude emissions compared to those of brittle materials that generally have lower b values, producing a

higher amplitude emission. The power law relationship was developed by researches in seismology, demonstrating the history and wide application of AE technology (Ishimoto 1939). This finding is also consistent with the study by Rajachar *et al.* (1999) who associated an increase in AE response with plastic deformation.

Using a single loading rate, Wright *et al.* (1981) examined the AE response of cortical bone specimens with chemically altered mechanical properties. This study was performed by removing specimens from bovine femoral bone. A control group of specimens was compared to specimens that were fully decalcified and a third group of specimens that was created by partially removing the collagen using hydrazine. The specimens were loaded in tension to failure and the AE response was monitored using sensors attached to the specimen grips. The AE response was recorded in terms of number of counts at a given specimen strain. The control specimens demonstrated the typical elastic-plastic response, while the decalcified specimens did not undergo plastic deformation and exhibited a drastically reduced elastic modulus. Similar to the decalcified specimens, the partially deproteinized specimens (half of the collagen was actually removed) did not undergo plastic deformation, but maintained an elastic modulus similar to the control specimens.

Similar to the previous studies, AE in the control specimens initiated just prior to the yield point with a large increase in counts at failure. The emissions during yield were also found to have a lower amplitude than those at fracture. The partially deproteinized specimens exhibited no AE during loading except at fracture. The response of the decalcified specimens was similar to the response of the control specimens after yield in that they produced continuous low amplitude AE prior to fracture with an increase in AE closer to fracture.

The results of this study are consistent with the idea that compact bone can be thought of as a two phase model composed of an elastic-perfectly plastic mineral matrix and linearly elastic collagen. The similarity between post-yield response of control specimens and the modulus of the decalcified specimens supports the idea that the plastic response of

cortical bone is dependent on the collagen fibers. In addition to the mechanical response, both specimens also exhibited similar AE responses.

The above review represents a small number of studies that have utilized acoustic emission technology for biomechanical research; however, these studies show that AE can reveal more about the fracture process of bone than a simple stress-strain diagram. The majority of previous studies are involved in monitoring the failure of bone over several loading cycles in order to gain insight into the failure mechanism of bone. The use of AE demonstrated the initial presence of a diffuse array of microfractures within the bone, the coalescence of fractures and finally a dominating source of AE at the fracture site. The AE under different loading rates suggest that at higher rates, fewer events are produced at higher amplitudes. The majority of studies performed at the higher rates also demonstrated that the onset of AE occurs immediately prior to fracture. This finding is very significant for the application of AE in impact biomechanics in which the timing of fracture is crucial. During the Allsop *et al.* (1988) study, it was found that the bones typically fractured at a force less than the peak force for a given test.

METHODOLOGY

This study comprises a total of 91 tests performed on 14 unembalmed human heads. All the heads had been previously frozen and thawed prior to testing. Each head was instrumented with two Acoustic Emission (AE) sensors (Micro30S, Physical Instruments, New Jersey) mounted to the mandible at the angle and to the frontal bone just posterior to the apex of the forehead. The sensors were mounted directly to the bone by removing the soft tissue and periosteum and gluing the sensor in place with cyanoacrylate adhesive. The heads were mounted in place using Bondo which provided a rigid support, eliminating the variability induced using a padded support. The orientation of the head was such that the Frankfort plane was approximately vertical. In each test, anatomical landmarks were used to determine impact location. For frontal impacts, the impactor was positioned such that its lower edge was centered to and just superior to the supraorbital ridge. For a nasal impact, the impactor was positioned such that the lower edge of the

nasal bone, located by palpation was centrally located on the impactor. A maxilla test was performed by aligning the impactor to strike just below the inferior orbital ridge at its midpoint with the orbit. For the mandible tests, the impactor was positioned to strike midline with the skull, between the alveolar processes and the bottom of the chin. A 7 lb impactor was used to apply the impact to each of the facial bones. The impacting surface had a circular cross section with an area of 1 in^2 and was machined with a slight bevel around its surface to reduce edge effects. Impactor force was measured by multiplying the average acceleration measured by two accelerometers (Endevco 7264B-2000, Endevco Corp., San Juan Capistrano CA) mounted to the free-falling impactor (Figure 46).

Two data acquisition systems were utilized for the current study, one for the accelerometers (Iotech WBK16, Cleveland,OH) and one for the acoustic emission sensors (PCI-2, Physical Instruments, New Jersey). A preamplifier was also used in conjunction with the AE sensors. An initial matrix of testing was performed to assess any delay that may exist between the accelerometer and AE data acquisition systems. This was performed by triggering both systems, as would occur in an actual test and applying an input to the accelerometer and an AE sensor simultaneously. This ensured that both sensors received an input at the same instant in time and, therefore, if any delay was present it would be a result of a triggering artifact and not the timing of the input signal. A total of 15 tests were performed to characterize this delay so that it could be accounted for when determining the time of fracture onset.

An additional 18 tests were performed to evaluate the AE signal that is produced from a preexisting facial fracture when impacted at a sub-threshold velocity. This was done to determine if the AE signal during a fracture is actually the result of crack propagation or a byproduct of the higher force necessary to produce the fracture. Therefore, if a low-level impact on a preexisting fracture produces a similar AE response as a high-level fracture-producing impact, the resulting AE is associated with the fracture process and is not a function of impactor force. To perform this analysis, the fractured frontal bones of two heads were exposed to repeated testing at the lowest drop height available.

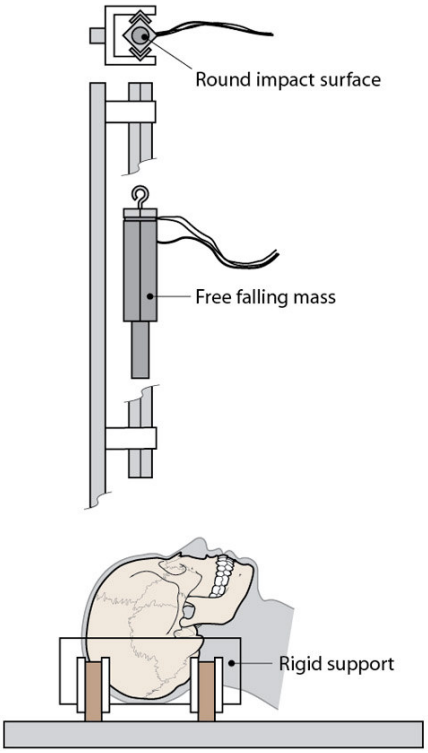

Figure 46: Schematic of test apparatus used in the current study.

Data Processing

To utilize AE data as a method of estimating the time at which fracture begins, a threshold must be established that differentiates normal background emissions from those associated with the fracture event. This was established *post hoc* by examining the maximum voltage of the AE signal and the number of counts above a given threshold. Signal processing techniques will also be used to attempt to isolate non-fracture AE from fracture AE as a function of time.

RESULTS

A facial fracture was produced in 29 tests. No fracture occurred in 62 tests. 18 tests were performed on regions with pre-existing fractures. An Acoustic Emission (AE) signal was measured in every test using a sensor mounted on the frontal bone and mandible. Unlike previous studies utilizing AE sensors (Allsop 1988) both fracture and non-fracture tests in

the current study resulted in some level of AE. Therefore, a threshold had to be determined that differentiated normal background emissions from those associated with the fracture event. This was established after the test series was complete by examining the maximum voltage of the AE signal and the number of counts (single emission) above a given threshold. The voltage threshold was defined to be the same for all bones and the value was chosen to differentiate as many fracture and non-fracture tests as possible for each bone. The voltage measured by the AE sensor ranged from 0 to 10 volts, with the majority of fracture tests reaching a maximum of 10 volts (Table 6). The AE signal was clipped at 10 v, therefore, this was the maximum voltage measured.

Table 6: Average maximum AE by region and test outcome.

	Maximum AE (volts)			
Sensor:	**Frontal**		**Mandible**	
Region	**No Fracture**	**Fracture**	**No Fracture**	**Fracture**
Frontal	7	10	2	2
Nasal	8	10	4	4
Maxilla	4	10	5	8
Mandible	1	1	6	10

A threshold voltage of 9 volts was established based on the magnitude of the AE during fracture (Figure 47) and non-fracture (Figure 48) tests. Therefore, the force corresponding to an AE of 9 volts was utilized as the force at the onset of fracture. Acoustic emission above the threshold is termed “high” and is otherwise termed a “low” AE signal.

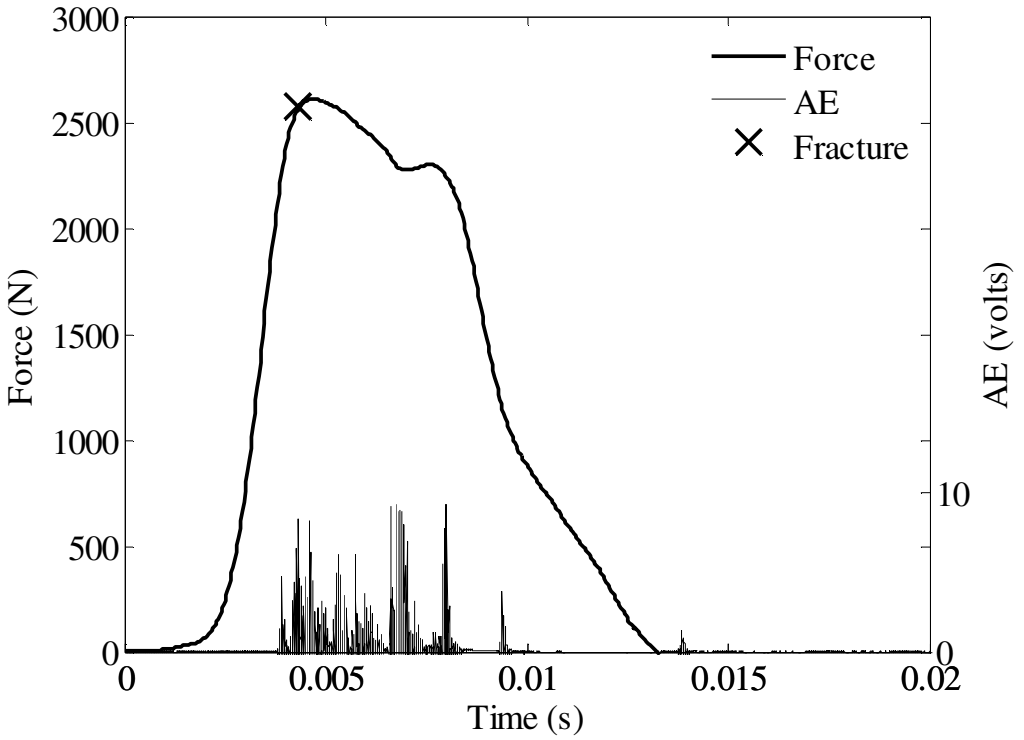

Figure 47. Acoustic emission and force during an impact resulting in a maxilla fracture.

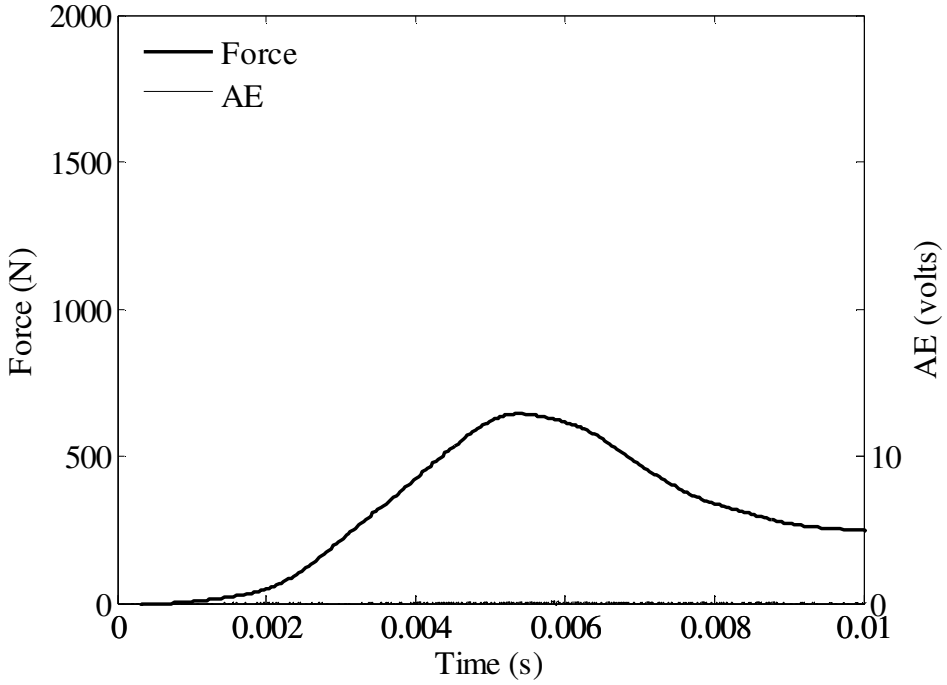

Figure 48. Response for maxilla impact resulting in no fracture (contralateral to Figure 47).

Tests performed on regions with pre-existing fractures revealed that high AE will occur at forces that would not cause fracture in an uncompromised bone (Figure 49, Figure 50).

This provided the validation necessary to rely on the AE data to identify emission patterns that would be consistent with the onset of fracture. In some cases a high AE was recorded during an impact that did not result in fracture. In these cases the counts, or number of times an AE signal was higher than the 9 volt threshold was significantly lower than the counts typically seen during a fracture test (Table 7).

Table 7. Average number of AE counts above threshold by outcome.

	High AE Counts	
	No Fracture	**Fracture**
Frontal	29	76
Nasal	10	20
Maxilla	5	53
Mandible	7	50

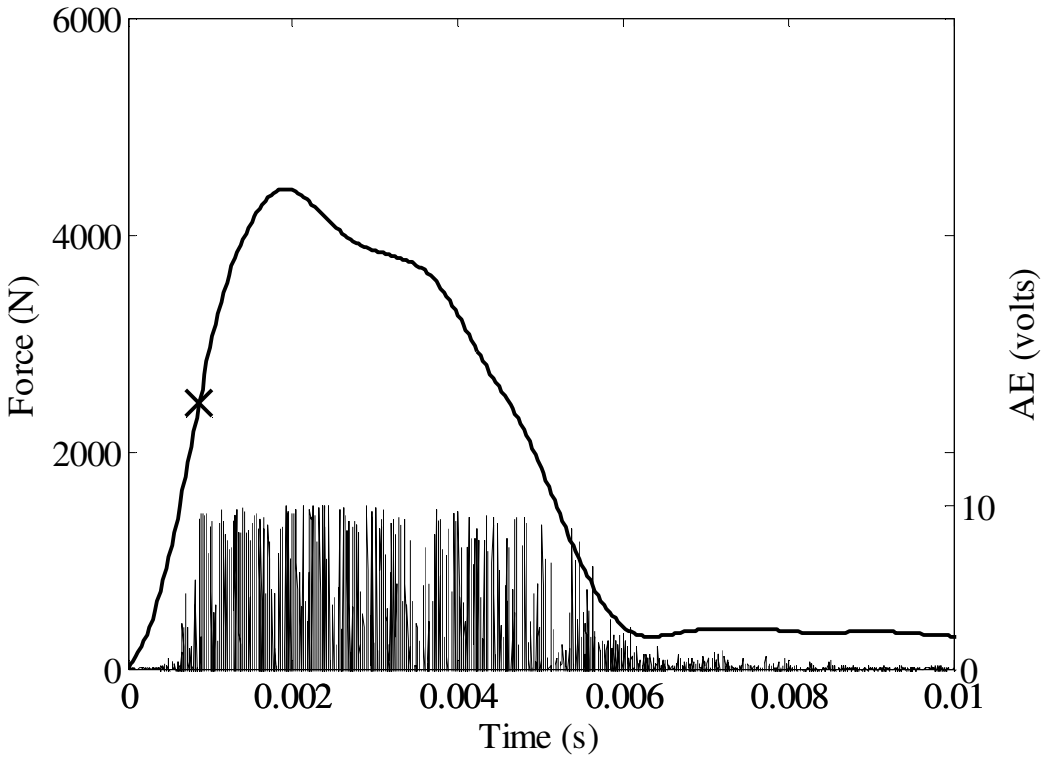

Figure 49. Response from frontal impact resulting in fracture. Positive AE data plotted.

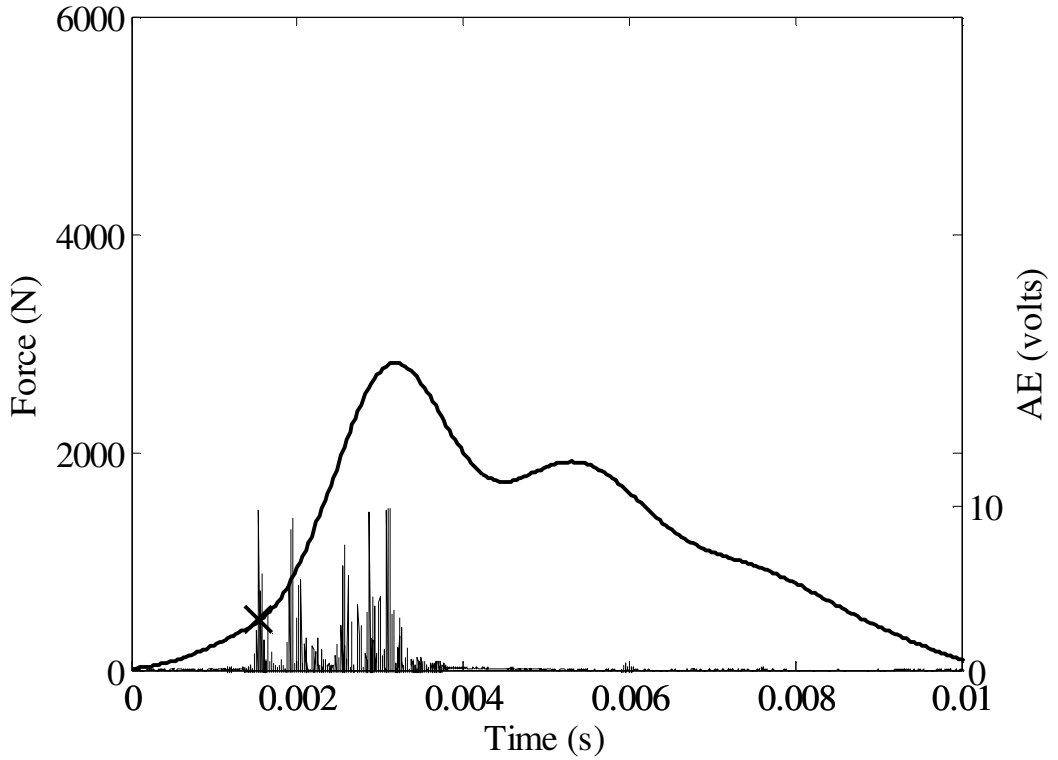

Figure 50. Response due to impact on a pre-existing frontal bone fracture (demonstrated in Figure 49).

Twelve of the eighteen tests performed on a pre-fractured frontal bone resulted in AE above the 9 volt threshold. In one head, tests that did not exceed the threshold were preceded by several tests at the same location; however, the repeated tests exceeded the threshold again if the drop height was slightly increased from 10 to 15 inches. In the second head, high AE was produced if the drop height was increased from 5 to 10 inches.

DISCUSSION

The current study utilized AE sensors to determine the force at which the fracture process initiates due to impact to human facial bones. An AE amplitude threshold was defined which differentiate between AE associated with fracture and non-fracture tests. This approach was validated by comparing the AE obtained during fracture tests (Figure 49) and repeated testing on a previously fracture bone (Figure 50). The repeated tests, performed at low impactor energies confirmed the presence of similar AE amplitude as in the impact producing the original fracture. This is consistent with the idea that the AE is

related to the propagation of fractures and is not necessary related to the applied force. This relationship has not been demonstrated in previous studies due to the lack of AE in non-fracture tests.

The ability of the threshold to distinguish between fracture and non-fracture tests was dependent on the impacted region and sensor location. The AE sensor mounted to the mandible almost never was able to predict a fracture occurring at the frontal bone. Similarly, the frontal bone almost never measured high AE during a mandible impact resulting in fracture.

There were tests that did not result in fracture, but an AE signal above the 9 volt threshold was recorded. In these cases, the number of counts above 9 volts was much lower for the non-fracture tests. The high AE during non-fracture tests were probably the result of a small defect within the bone that did not result in fracture, or the propagation of pre-existing fractures in a different region of the face. The number of AE counts above the threshold occurring during the repeated impacts was more consistent with a fracture producing test, than a non-fracture test. This result reinforces the idea that the higher magnitude signals during fracture are a result of the fracture process and not the higher force of impact.

CONCLUSIONS

This study describes the methods utilized in developing acoustic emission thresholds for facial fracture detection. This method requires the use of fracture and non-fracture tests in order to differentiate the acoustic emission magnitude associated with both outcomes. The association of acoustic emissions with fracture was demonstrated by striking pre-fractured frontal bones at low energy levels. These tests resulted in acoustic emission with the same magnitude as the tests initially causing the fracture at a higher severity. Acoustic emission is a valuable tool in determining the time of fracture, however, in facial fracture analysis it is essential due to the ability of the facial structures to support higher forces after fracture has initiated.

REFERENCES

Allsop D, Warner C, Wille M, Schneider D, Nahum A: Facial Impact Response – A Comparison of the Hybrid 3 Dummy and Human Cadaver, *Society of Automotive Engineers*, SAE No. 881719; 1988a.

Allsop DL, Warner CY, Wille MG, Schneider DC, Nahum AM: Facial Impact Response – A Comparison of the Hybrid 3 Dummy and Human Cadaver, *Society of Automotive Engineers*, SAE No. 881719; 1988b.

Fischer RA, Arms SW, Pope MH, Seligson D: Analysis of the Effect of Using Two Different Strain Rates on the Acoustic Emission in Bone, *J. Biomech.*, 19, 119-27; 1986.

Funk J, Crandall J, Tourret L, MacMahon C, Bass C, Patrie J, Khaewpong N, Eppinger R: The Axial Injury Tolerance of the Human Foot/Ankle Complex and the Effect of Achilles Tension, *Journal of Biomechanical Engineering*, 124; 2002.

Ishimoto M, Iido K: *Bull. Earthq. Res. Inst*, 17, 443-78; 1939.

Kaiser J: Research into Noise Emission in Tensile Tests, *Arch. Eisenhuttenw.*, 24(1-2), 43-5; 1953.

Knets IV, Krauya UE, Vilks YK: Acoustic Emission in Human Bone Tissue Subjected to Longitudinal Extension, *Proceedings of the 1st All-Union Confer. on Eng. And Medicla Biomech.,* October, Riga; 1975.

Kohn DH: Acoustic Emission and Nondestructive Evaluation of Biomaterials and Tissues, *Critical Reviews Biomed. Eng.*, 22(3/4), 221-306; 1995.

Meythaler J, Peduzzi J, Eleftheriou E, Novack T: Current Concepts: Diffuse Axonal Injury - Associated Traumatic Brain Injury, *Arch Phys Med Rehabil*, 82; 2001.

Peters A: Acoustic Emission Technique and Fracture Healing, *Med. Biol. Engng. Comput.*, 20(8); 1982.

Pollock A: Acoustic Emission Amplitude Distribution. International Advances in Nondestructive Testing,. W. McGonnagle**,** 215-39; 1981.

Rajachar RM, Chow DL, Curtis CE, Weissman NA, Kohn DH: Use of Acoustic Emission to Characterize Focal and Diffuse Microdamage in Bone, *Acoustic Emission: Standards and Technology Update*, ASTM STP 1353, Ed. Vahaviolos SJ, ASTM; 1999.

Schwalbe HJ, Bamfaste G, Franke RP: Non-destructive and Non-invasive Observation of Friction and Wear of Human Joints and of Fracture Initiation by Acoustic Emission, *Prc. Instn. Mech. Engrs.*, 213(H), 41-8; 1999.

Wells J, Rawlings R: Acoustic emission and mechanical properties of trabecular bone, *Biomaterials*, 6(4), 218-24; 1985.

Wright TM, Vosburgh F, Burstein AH: Permanent Deformation of Compact Bone Monitored by Acoustic Emission, *J. Biomech.*, 14(6), 405-9; 1981.

CHAPTER 5:
THE TOLERANCE AND RESPONSE OF THE FRONTAL BONE TO BLUNT IMPACT

INTRODUCTION

Fracture of the frontal bone can be a devastating injury, with the potential for associated brain injury. The four most common sources of facial trauma are Motor Vehicle Collision (MVC), assault, sports and falls (Gassner 2003, Jayamanne 1996, Lim 1993, Muraoka 1995, Shapiro 2001). With respect to MVCs, as shown in Chapter 1 frontal bone fractures are more common among occupants involved in impacts with an oblique impact direction. Impact to the frontal bone can also result in fracture of the sinus which is most commonly associated with MVCs (Strong 2006). Due to the importance of the frontal bone in protecting the brain, there has been a lot of attention placed on understanding its tolerance to impact.

Several studies have been performed on the frontal bone of the skull in an attempt to determine its tolerance to various types of impacts. The methods of previous studies include different impactor shapes and sizes, impact location and direction and the use of padding. The large variation between and within previous studies limits the capacity for statistical methods to produce accurate estimates of fracture risk. The previous work can be divided into two main categories by the type of impactor used to strike the face. In one, a cylindrical impactor strikes the subject with the end, consisting of a flat face (Nahum 1968, 1975, Schneider 1972) in the other, a cylindrical impactor strikes the subject side-on (Allsop 1988, Bermond 1999, Bruyere 2000, Cesari 1989, Hodgson 1965, Nyquist 1986, Welbourne 1989, Yoganandan 1988, 1993) meant to represent a steering wheel impact. Cylindrical impactors, meant to represent steering wheel impact, were frequently used to strike horizontally across the entire face. This applies force to multiple regions of the face and, therefore, head position is critical and fewer tests can be performed on a single subject. The tolerance of an individual area cannot be assessed using a broad impactor.

Conversely, a more focal load is applied to the face when utilizing the end of a cylindrical impactor. This impactor was used by Nahum *et al.* (1968, 1975) and Schneider *et al.* (1972). Impacts were performed using a free-falling impactor with a contact area of 6.45 cm^2 (1 in^2). A crushable nickel pad added to the impactor distributed the load more evenly over the contact area and provided a secondary measure of force. Based on their results, minimal force tolerance levels were established for the frontal bone (3560-7117 N), maxilla (667-1334 N), mandible (2447-4000 N) and zygoma (890-2890 N). Varying both the drop height and weight of the impactor allowed for the rate of onset of peak force to be regulated. Pulse duration was changed by adding an adapter to the impactor and did not result in a noticeable effect on fracture tolerance. Further development in fracture tolerances was provided by Schneider *et al.* in 1972 by testing additional impact directions and locations (Schneider, 1972). The tests performed included anterior-posterior and lateral loading of the mandible, impacts to the maxilla, and lateral loading of the zygomatic arch. From 106 impacts the minimal force tolerances described by the authors were 1780 N for the mandible in the anterior-posterior loading direction, 890 N for the mandible in the lateral loading direction, 668 N for the maxilla, and 890 N for the zygomatic arch. Trends between six female subjects and 11 male subjects indicated that females have a lower load tolerance for all impact locations than the males.

Experiments have also been done to investigate fracture patterns as a result of impact with various impactor shapes (Hodgson 1970, Hodgson 1973). In these studies each subject was secured to a table which pivoted such that the aspect of the frontal bone with the smallest radius struck the reaction surface first. Multiple impacts were performed on each specimen until fracture occurred. With respect to impact surface, a flat rigid surface produced fractures at impacts speeds near 2.2 m/s. By comparison, fractures were produced at impact speeds of 3, 4 m/s and 5.5 m/s for the flat 90 and 60 durometer rubber surfaces, respectively. Peak forces and Head Injury Criterion (HIC) values associated with the fracture-producing impacts were reported.

A more recent study utilizing a pendulum as the impact device determined displacement and absorbed energy at fracture (Delye 2007). The impactor had a flat surface with a diameter of 7 cm. Repeated testing was performed until fracture occurred. The force at which fracture occurred was determined by the peak force measured during the impact. The use of peak force is inconsistent with the findings of the previous discussed in which fracture was found to occur prior to peak force. The energy of impact was between 214 J and 706 J, which is well over the energy used in the studies by Nahum *et al.* (1968, 1975) and Hodgson *et al.* (1973). On average, the energy absorbed at fracture (peak force) was only 4% of the original impact energy. The authors concluded that impacts with an energy of 22 to 24 J would be expected to cause a frontal bone fracture. Despite the use of peak force as a fracture force the authors claim that the force-deflection relationship is consistent with sequential failure of the inner and outer cortex. This seems contrary to defining peak force as the force at fracture. Nevertheless, the use of repeated testing until fracture results in data that are inappropriate for the development of a statistical estimate of fracture risk.

Testing by Allsop *et al.* demonstrated that facial bones are capable of supporting load after fracture has initiated (Allsop 2002, Allsop 1988). This is an important concept, as it requires that the fracture force be determined separate from a force-time or force-deflection response. In their studies, Acoustic Emission (AE) was monitored and when a signal burst was detected, fracture was assumed to have occurred. When comparing the time of an AE burst, to the force-time relationship, the authors found that the facial bones would often fracture prior to peak force.

Acoustic Emission (AE) data have also been used to evaluate fatigue fracture and the fracture properties of bone (Fischer 1986, Knets 1975, Peters 1982, Wright 1981). These studies have demonstrated that significant AE is only generated during plastic deformation or fracture. Previous studies have also shown that AE is correlated with changes in bone material properties (Rajachar 1999). Fatigue studies have also demonstrated the occurrence of an AE burst due to fracture which differs from the lower-level AE usually associated with fatigue fracture (Kohn 1995). Studies using cortical

bone have found that the onset of AE begins just prior to maximum force or specimen failure (Allsop 1988, Fischer 1986). Additional studies using bovine femoral bone in torsion and tension found that significant AE signal was only created during plastic deformation and fracture (Netz 1979, Peters 1982, Wright 1981). In contrast, a study using metal pins embedded in cancellous bone found that AE began at low forces with the number of counts increasing exponentially as maximum force was reached. This finding is similar to that of Wright *et al.* (1981) who found that AE during yield occurred at a lower amplitude than AE during fracture. Similarly, Schwalalbe *et al.* (199) found AE to occur at low load levels when performing torsional tests on human femur; however, the amplitude or frequency of the signal was not described. An explanation for the lack of AE during yielding of human bone was offered by Knets *et al.* (1974). They attributed the lack of AE to the Kaiser effect which was discovered in 1953 (Kaiser 1953). The Kaiser effect is similar to the response of a plastically deformed specimen. Once the specimen is reloaded, plastic deformation will not begin until the force at which plasticity was initiated in the previous loading cycle. In the same manner, the Kaiser effect states that AE will not be produced in a specimen during a secondary loading cycle until the force experienced during the previous cycle is exceeded. Knets *et al.* hypothesis was that no AE signal is produced at low forces because the human bone is loaded constantly and, therefore, AE signal is only produced when the forces of daily activity are exceeded. In their study of cortical bone from human femurs, no AE occurred until 94% of the failure strain was reached. The authors also determined that the number of AE counts is directly related to the number of microcracks within the bone and the number of pulses generated by the surface of a crack.

Knowing the precise time of fracture provides a non-censored measure of bone tolerance and, therefore, a more powerful data point for statistical analysis. Other studies have also used acoustic sensors to determine the fracture time of facial bones (Allsop 1988, Cormier 2008) and other bones (Funk 2002a, Kent 2008a, Rudd 2004, Wells 1985). The studies published by Cormier *et al.* (2008) and Rudd *et al.* (2004) discuss the use of a threshold voltage, over which fracture is denoted to have occurred. This threshold was established by comparing AE measured during fracture and non-fracture tests. In the

study by Cormier *et al.* additional validation was obtained by demonstrating that high magnitude AE occurred when striking bones with pre-existing fractures at low energy levels. This suggests that the high magnitude AE was due to the propagation of pre-existing fractures and not the result of the impact itself. The lack of acoustic sensors in the Nahum *et al.* (1968, 1975) and Delye *et al.* (2007) studies suggest that their data are censored and that fracture is most likely occurring at a force less than the peak forces reported. The variable methods and lack of data prohibits the use of statistical analyses to estimate the risk of fracture as a function of impact severity.

The current knowledge is also lacking in an understanding of the mechanical response of the frontal bone to impact. The development of finite element models or Anthropomorphic Test Devices (ATD) for fracture prediction is limited by the lack of a quantitative measure of frontal bone response to impact. One such ATD is the Facial and Ocular CountermeasUre Safety (FOCUS) headform. The FOCUS headform has the ability to measure forces applied to the facial and orbital structures. It has been developed by Virginia Tech and validated for eye injury prediction (Kennedy 2007). There are eight separate sensing regions within the facial structures that overlie embedded load cells (Figure 51). These regions correspond to the frontal bone, nasal bone, zygoma, maxilla and mandible. Each load cell is capable of measuring forces along all three axes.

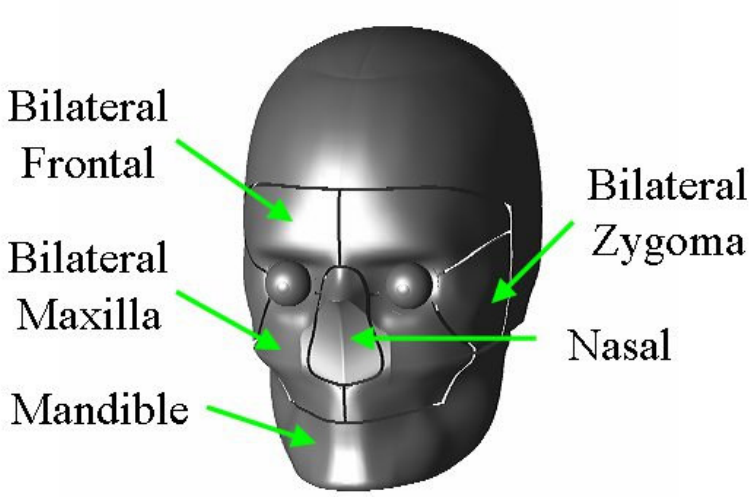

Figure 51: Load cell locations in FOCUS headform.

Defining force-deflection corridors for frontal bone impacts in cadavers will provide a basis for the implementation of the FOCUS headform in injury risk assessment.

The first goal of this study is to generate additional data in order to determine risk functions for the prediction of frontal bone fracture as a result of blunt impact. The second goal of this study is to develop an understanding of the cadaveric response to blunt impact and compare this response to the FOCUS headform.

METHODOLOGY

The data for this study were obtained by performing facial impacts on male cadaveric subjects. The methods of this study consist of striking the frontal bone with the flat face of an unpadded, cylindrical impactor, along with the use of acoustic emission sensors to determine the time of fracture onset. All heads were frozen and thawed prior to testing. A total of 28 male subjects ranging in age from 43 to 76 years were included in the study. Pre-test CT imaging was performed on twelve subjects and post-test CT imaging was performed on three specimens.

Anthropometry

Prior to testing, CT imaging was performed on 22 of the subjects. The CT images were used to measure the thickness of the frontal bone at the horizontal level of the impact location. Skin thickness was also measured at the same vertical level (Figure 52). In some subjects the frontal sinus was more prominent than others; therefore, measurements of the outer table were taken as well. A regression analysis was performed to evaluate the potential relationship between the CT measurements and the fracture tolerance for these specimens as well as their mechanical response.

Figure 52: Facial measurements taken using pre-test CT images.

Specimen Preparation

The specimens were removed from the body and prepared by removing the scalp overlying the occipital region. Metal screws were inserted into the occiput to provide additional structure for the casting material to adhere to. Each head was then rigidly mounted to a semi-circular, polycarbonate support using Bondo (Figure 53). Consistent orientation between subjects was obtained by vertically aligning the Frankfort plane prior to mounting. Specific anatomical landmarks were used to determine impact location. For frontal bone impacts, the impactor was positioned such that its lower edge was

centered to and just superior to the supraorbital ridge. Each impact was performed using a cylindrical, free-falling rigid aluminum impactor (3.2 kg) with a steel tip. The flat impacting surface had an area of 6.45 cm^2 (1 in^2) and was machined with a slight bevel to reduce edge effects.

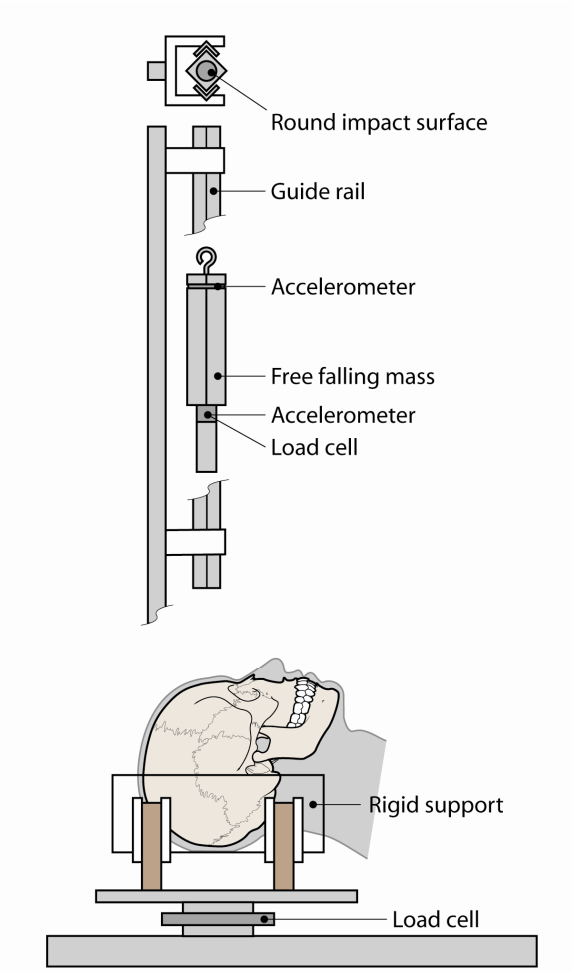

Figure 53: Schematic of test apparatus to be used in the current study.

Instrumentation

The specimens utilized in this study were tested in three separate series that consisted of slightly different instrumentation and data acquisition methods. In all cases an AE sensor (Micro30S, Physical Instruments, New Jersey) was mounted to the frontal bone, just posterior to the apex of the forehead. The AE sensor was mounted directly to the bone by removing the soft tissue and periosteum and gluing the sensor in place with cyanoacrylate adhesive. This method has been used successfully in previous testing during this study

and by others (Funk 2002a, Kent 2008a, Rudd 2004). In all tests, the rigid impactor was instrumented with two single-axis accelerometers (Endevco 7264B-2000, Endevco Corp., San Juan Capistrano CA). All data except AE data were filtered to CFC 300. Previous studies have utilized CFC 180; however the use of CFC 300 did not significantly alter the measured peak forces and was chosen to increase the likelihood of capturing small changes in impactor force during fracture (Bermond 1989, Bruyere 2000, Nyquist 1986). Impactor displacement was calculated by double-integrating the acceleration data. Contact between the impactor and subject was defined based on an impactor force of 10 N. Once the impactor force reached a level above 10 N, the displacement with respect to the frontal bone was set to zero and further motion was calculated by double integration. These aspects remained constant throughout the test series; however there were slight differences between the three testing series that created the entire study.

Series 1, Subjects 1-6: The AE sensors were sampled at a rate of 2 MHz and all other instrumentation at 30 kHz. The acoustic emission data were acquired using a PC card supplied by the sensor manufacturer (PCI-2, Physical Instruments, New Jersey). Each AE sensor was attached to a preamplifier set to a gain of 40 dB. Impact force was obtained by multiplying the impactor acceleration by its mass. Impactor acceleration was determined by the average of the two attached accelerometers. As part of this test series, one to two low-energy impacts were performed contralateral to the fractured side of the frontal bone, prior to the fracture-producing imapct. These tests provided AE data during an impact that did not result in fracture. These data were used to establish a voltage threshold to identify AE consistent with fracture onset.

Series 2, Subjects 7-28: The AE sensors were sampled at a rate of 5 MHz and all other instrumentation at 20 kHz. The acoustic emission data were acquired using an oscilloscope (TDS3000B Tektronix, Oregon). Each AE sensor was attached to a preamplifier set to a gain of 40 dB. A load cell (Denton, 8617JTF, Rochester Hills, MI) was attached to the tip of the impactor which was also instrumented with a single axis accelerometer (Endevco 7264B-2000, Endevco Corp., San Juan Capistrano CA) (Figure 53). A load cell (Denton 1968, Rochester Hills, MI) was mounted to the head support to

measure reaction forces. Impact force was obtained using the impactor load cell along with the inertially compensated tip mass.

Series 3, Subjects 17-28: All parameters described in series two remained the same, with the exception of the AE preamplifier gain which was set to 20 dB in this series. Additionally, high-speed video was also recorded at a frame rate of approximately 4,000 fps. Impactor displacement calculated by double integrating impactor acceleration was verified using high-speed video analysis. This was performed by creating a second-order polynomial fit of the displacement obtained by video analysis.

To define the average force-displacement response of the nasal bone, a corridor was created to encompass the overall force-displacement response of the frontal bone. The response corridor was determined by the mean and standard deviation of the characteristic average (Lessley 2004). The characteristic average was created using the force-displacement response up to 90% of the peak force of each test. This ensured that only the linear portion of the response was included in the characteristic average calculation. The values for the corridor where determined using a custom Matlab program that implemented the algorithm described by Lessley *et al.* (2004). The corridor was fit using 2^{nd} order polynomials so that there values could be reported here. Stiffness of the frontal bone was also calculated up to 20% and between 20% and 80% of the peak force for each test. Student t-tests were performed to test for statistical between the stiffness of the cadaver and FOCUS response.

Acoustic Emission

AE data were used to determine the force at which fracture initiated. Previous Studies using AE data have denoted the onset of AE signal as the onset of fracture (Allsop 1988, Funk 2002a, Funk 2002b). Recently, studies have utilized a threshold to differentiate AE consistent with fracture from a baseline AE signal (Cormier 2008, Kent 2008b, Rudd 2004). Kent *et al.* (2008b) demonstrated that an AE burst corresponded with a sharp decline in force during phalange fracture.

To utilize AE data as a method of estimating the time at which fracture begins, a threshold must be established that differentiates normal background emissions from those associated with the fracture event. This was established after the test series was completed by examining the maximum voltage of the AE signal as well as the number of counts above a given threshold. Due to the use of different data acquisition devices the threshold utilized was not equal for all tests, but the method used to determine the fracture threshold was the same. To establish a relationship between AE and fracture rather than the presence of an impact event, low-severity impacts were performed on specimens with pre-existing fractures. Due to the compromised integrity of these specimens, fracture propagation will occur at forces much lower than that required to initiate fracture. If high levels of AE are a result of fracture then high AE should be observed when the pre-fractured specimens are struck at lower levels of force. Once the threshold was established, the force corresponding to the occurrence of above-threshold AE was treated as the force required to initiate fracture.

Risk Function Analysis

Survival analyses were performed utilizing parametric and non-parametric techniques. For the parametric analysis, a Weibull model was assumed and fit to the data which contained fracture and non-fracture observations. The advantage of using a Weibull model is that the method used to determine the model parameters accounts for the fact that the non-fracture tests are right censored. The LIFEREG procedure within SAS (SAS Institute, Cary N.C) accounts for left and right censoring as well as non-censored data and was used to determine the parameter estimates for the Weibull model (Allison 1995, Cantor 2003). The Weibull distribution is advantageous because it is not forced to be symmetric, so it can accommodate risks that do not increase in the same way throughout the set of input variables. The Weibull CDF is given by,

$$CDF = 1 - \exp -(\lambda \cdot F)^{\gamma} \qquad \text{(Equation 1)}$$

where, λ and γ are the scale and shape parameters, respectively, and F is the applied force. This function provided an estimate of risk of injury using the maximum likelihood estimates of the scale and shape parameters. A non-parametric model was also created using the Kaplan-Meier method. The Kaplan-Meir method assumes the data are only right or non-censored and determines the risk of fracture based on the number of subjects at risk which sustain a fracture for a given force (Kleinbaum 2005). Measurements obtained using CT imaging as well as subject age were also included as covariates to assess their potential for predicting the risk of fracture.

FOCUS Headform Biofidelity

A series of impacts were performed on the frontal bone region of the FOCUS headform in order to characterize its response to blunt impact. Impact severity was chosen to facilitate comparison with cadaver results and to minimize risk of damaging the headform. The impact was applied using the same apparatus used for the cadaver impacts (Figure 54). The impactor was instrumented with a single-axis accelerometer (Endevco 7264B-2000, Endevco Corp., San Juan Capistrano CA). A load cell (Denton, 8617JTF, Rochester Hills, MI) was attached to the tip of the impactor which was also

instrumented with a single axis accelerometer (Endevco 7264B-2000, Endevco Corp., San Juan Capistrano CA) (Figure 53). All instrumentation was sampled at a rate of 20 kHz. Forces measured by the FOCUS internal load cells were recorded and compared to impactor forces and examined for load-sharing between facial regions. The stiffness of the FOCUS response was determined up to 20% and between 20% and 80% of the peak force for comparison to the cadaveric response.

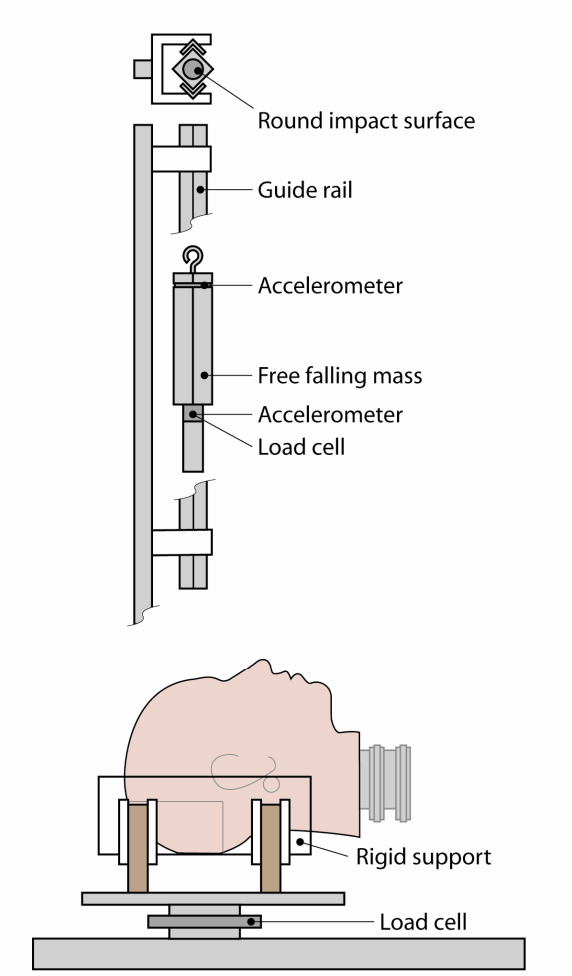

Figure 54: Apparatus used for FOCUS impacts.

RESULTS

A total of 46 tests were performed to determine the tolerance of the frontal bone to blunt impact (Table 8). The peak force during each impact ranged from 520 to 6400 N. Pulse duration of each impact ranged from 5 to 10 ms. A facial fracture was produced in 19 tests subjects and 11 tests were performed on regions with pre-existing fractures. An Acoustic Emission (AE) signal was measured in every test using a sensor mounted on the frontal bone. A threshold voltage of 9 volts was established for series one, 5 volts for series two and 2 volts for the third series. These thresholds were based on the magnitude of AE during fracture (Figure 47) and non-fracture (Figure 48) tests. Therefore, the force corresponding to an AE above the threshold was utilized as the force to initiate fracture in the statistical analysis. Repeated tests on fractured specimens demonstrated the occurrence of AE at low impact forces.

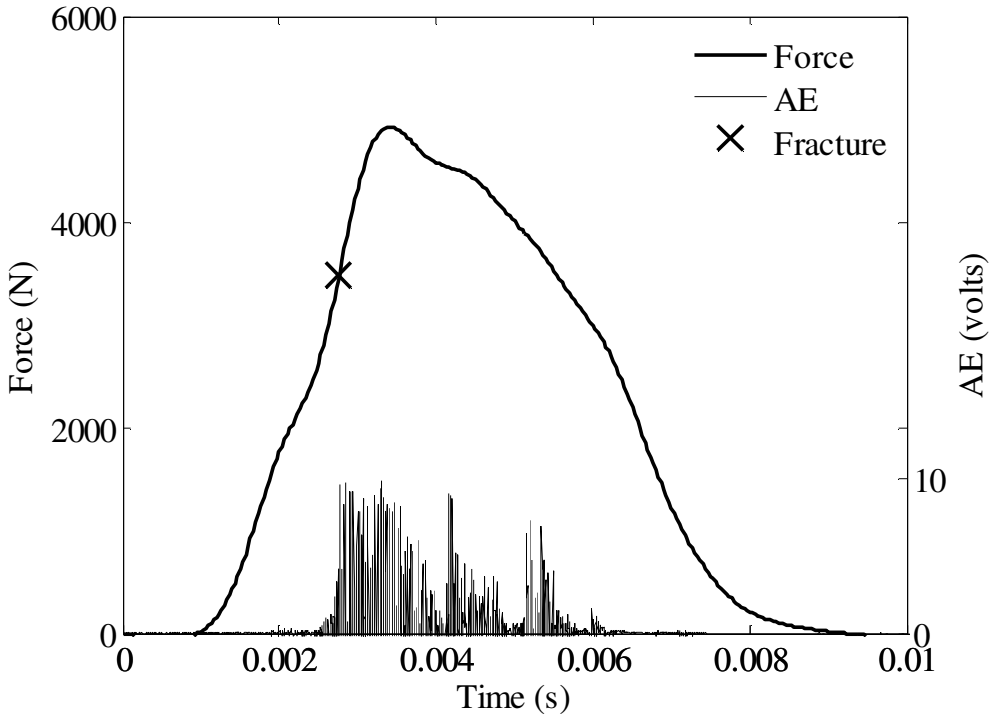

Figure 55: Acoustic emission and force during an impact resulting in a frontal fracture.

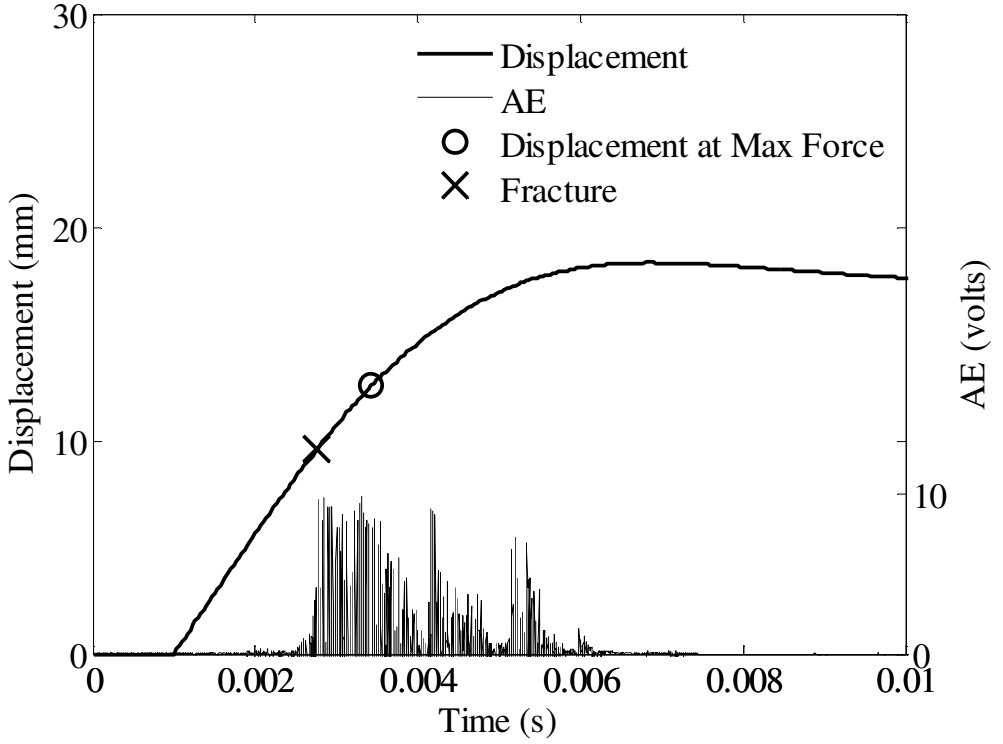

Figure 56: Impactor displacement response from frontal impact (same test as Figure 47).

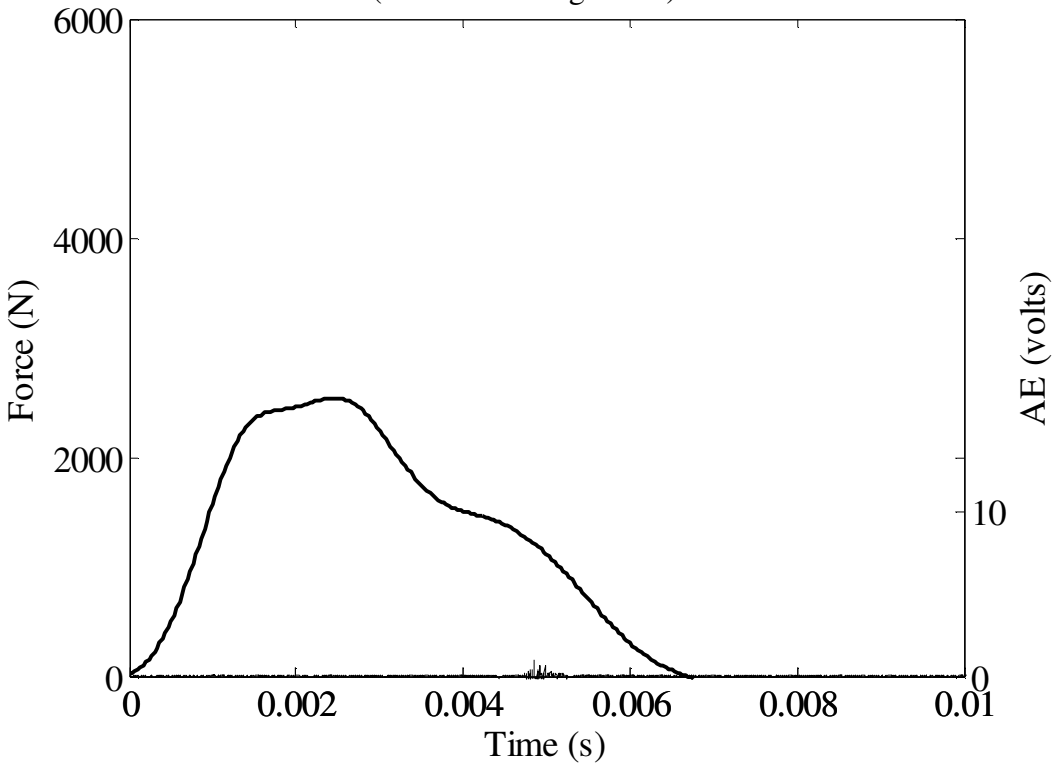

Figure 57: Response for frontal impact resulting in no fracture (contralateral to test in Figure 47).

Tests performed on regions with pre-existing fractures revealed that high AE will occur at forces that would not cause fracture in an uncompromised bone (Figure 49, Figure 50). This provided additional validation that AE is associated with the fracture processes In some cases a high AE was recorded during an impact that did not result in fracture a fracture that was identified during dissection. In these cases the counts, or number of times an AE signal was higher than the threshold was significantly lower than the counts observed during a fracture test. The high AE during non-fracture tests may be the result of a small defect within the bone that did not result in fracture.

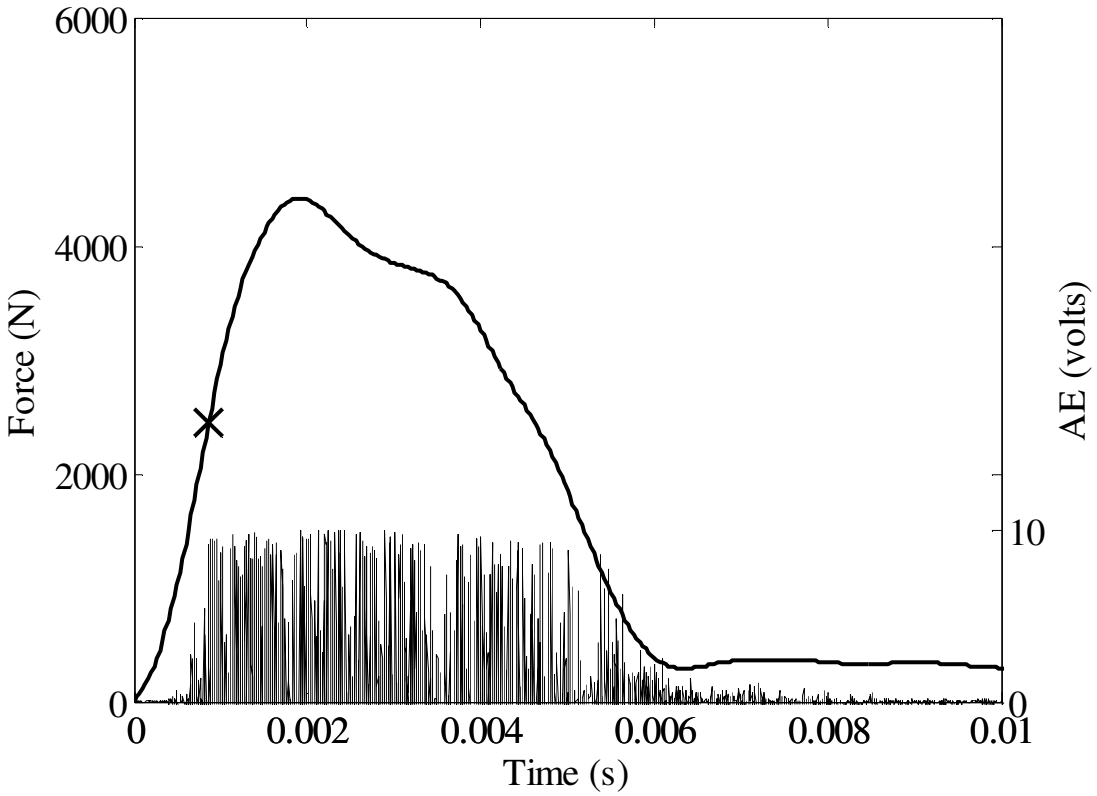

Figure 58: Response from frontal impact resulting in fracture.

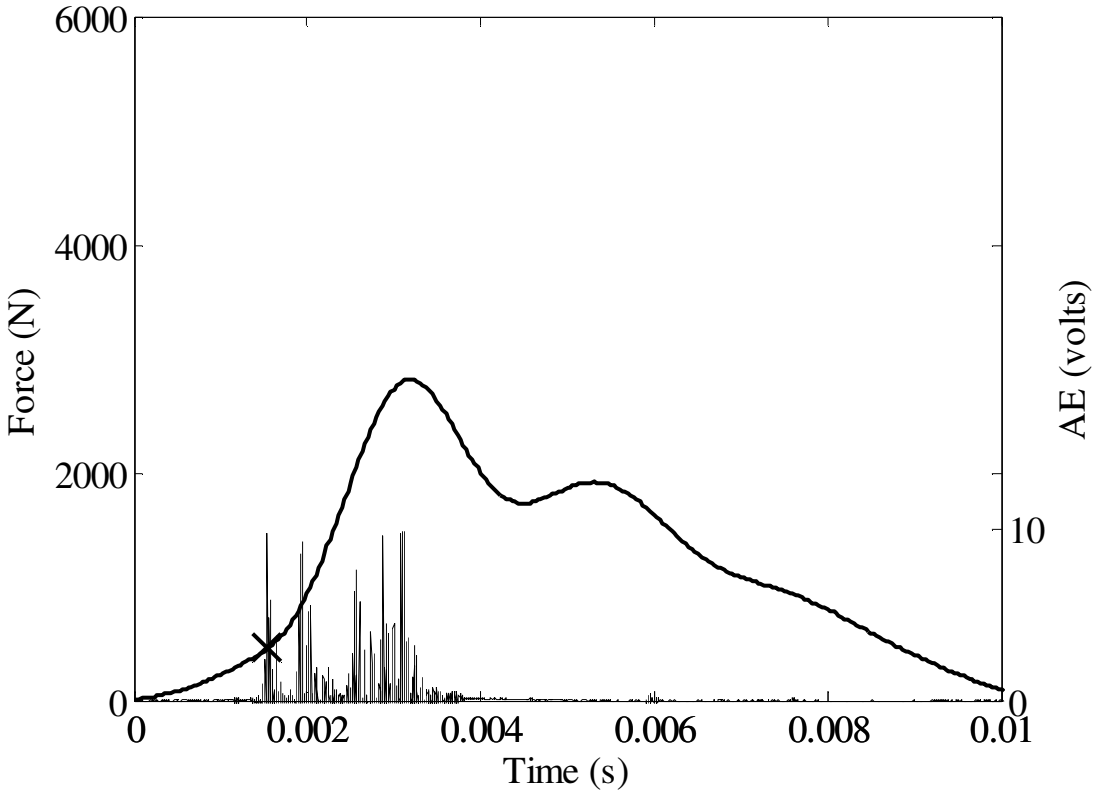

Figure 59: Response due to impact on a pre-existing frontal bone fracture

Table 8: Summary of subject characteristics and results of frontal bone impacts. na = not available

Subject	ID	Age	Height (cm)	Weight (kg)	Aspect	Impactor Energy (J)	Peak Force (N)	Fracture Force (N)
2	SM60	41	170	64.3	Right	11	756	
					Right	17	1296	
					Left	36	2266	
3	SM56	57	170	84	Right	10	1549	
					Right	13	2278	
					Left	44	5934	
4	SM57	75	165	65	Left	8	1382	
					Left	12	2217	
					Right	44	7613	
5	SM61	76	170	44	Right	4	945	
					Right	12	2713	
					Left	48	5535	2405
6	SM62	43	183	112	Left	11	2539	
					Left	17	5246	
					Right	52	4928	3490
14	5758	83	175	73	Right	5	3118	3118
15	5791	94	163	64	Right	5	1685	
					Left	47	6391	1910
16	5556	59	175	82	Left	47	2131	1946
17	5735	67	180	82	Right	5	521	
					Left	47	2965	1321
18	5763	47	183	89	Left	5	1438	
					Right	47	4203	1179
19	5757	84	183	109	Right	5	1097	
					Left	47	3768	1831
20	5642	80	160	71	Left	5	1366	
					Right	47	4025	3424
21	5675	76	152	91	Right	5	1431	
					Left	32	3163	891
22	5664	83	180	73	Left	5	1808	
					Right	32	5402	
23	5760	87	163	75	Right	5	1591	
					Left	47	5458	1734
24	5850	94	165	54	Right	8	1716	
					Left	49	5051	2629
25	5863	78	170	38	Right	39	2485	1016
26	5840	85	150	79	Right	39	3147	1885
27	5821	72	163	59	Right	47	3354	1499
28	5807	85	180	65	Right	47	2686	1055
29	5818	81	175	88	Right	47	5236	
30	SM64	62	178	59	Right	47	6152	1628
31	437	67	na	na	Right	47	4148	1515
32	459	71	na	na	Left	47	5841	2726

33	5805	81	177	79	Right	47	4042	1670
34	5837	68	175	71	Right	47	3879	3185
35	5869	74	191	86	Right	47	4087	2684

Once fracture force was determined, its relationship with various impact and subject descriptors was investigated. The majority of tests were performed with an impactor energy of 47 J which corresponded to an initial velocity of 5.3 m/s. At this level of severity, fracture force ranged from 1055 to 3500 N (Figure 60). The force at fracture was not related to impactor energy ($p = 0.26$). Consequently, the initial impactor velocity had no relationship with fracture force ($p = 0.26$) (Figure 61).

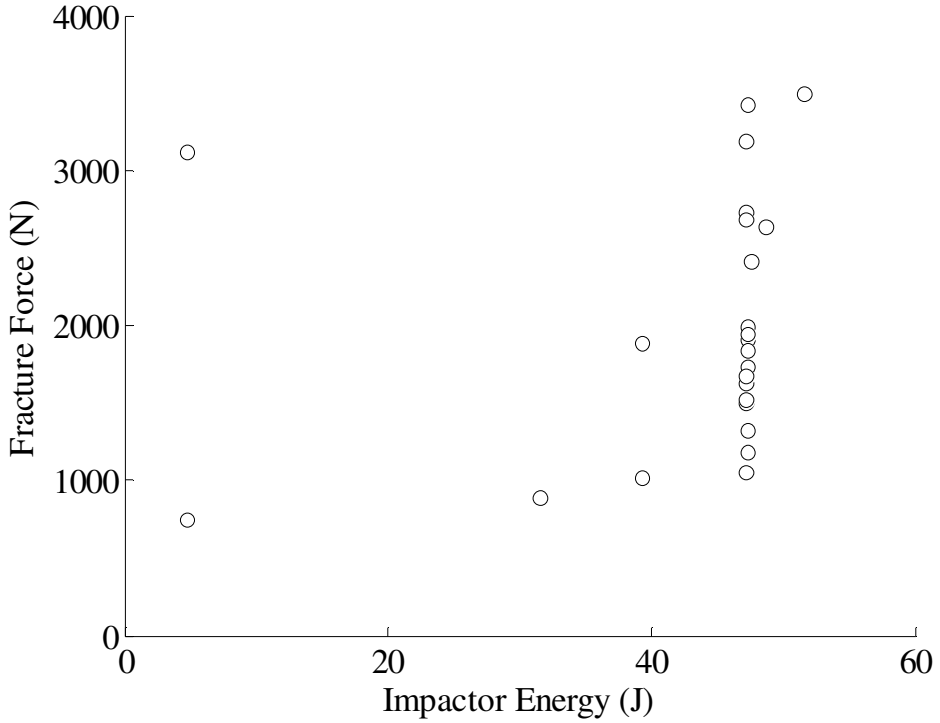

Figure 60: Frontal bone fracture force as a function of impactor energy.

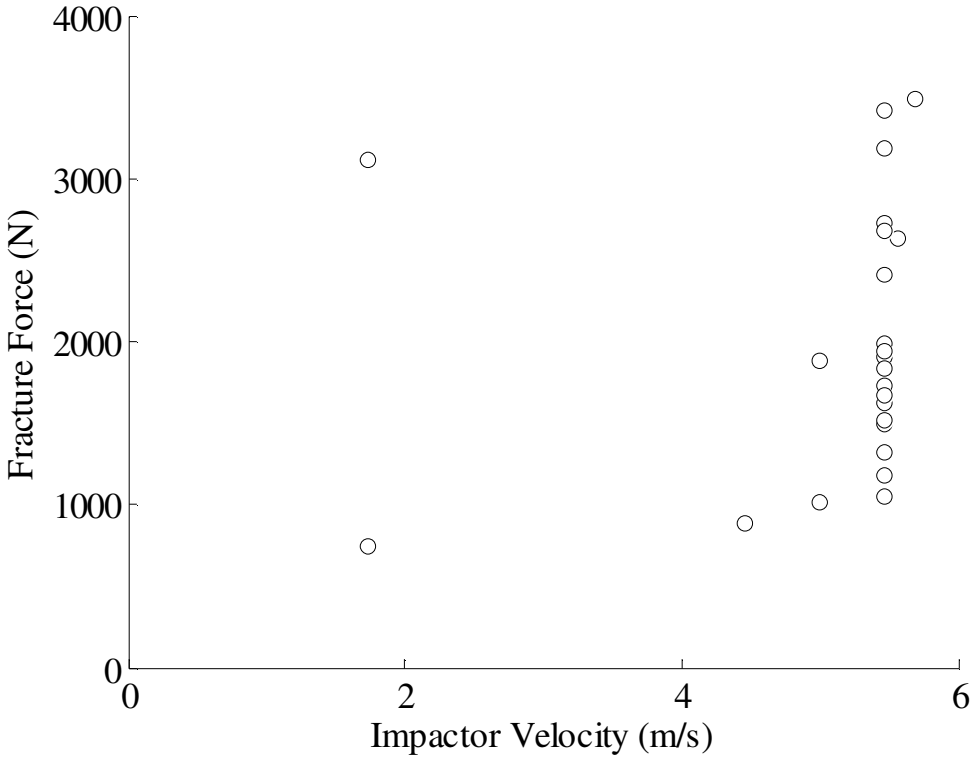

Figure 61: Frontal bone fracture force and initial impactor velocity.

The contact area estimated using Fuji Film on the impactor was utilized to estimate peak pressure. The peak pressure did not demonstrate an increase with impactor energy ($p = 0.91$) (Figure 62). The average contact area in all tests was 2.4cm^2 (std. dev.=1.4) or 37% of the available impactor area. In tests not resulting in fracture the average area was 1.9 cm^2 (std. dev.=1) and in fracture tests the average area was 2.9 cm^2 (std. dev.=1.5). The estimated pressure also showed no trends with respect to fracture force (Figure 63).

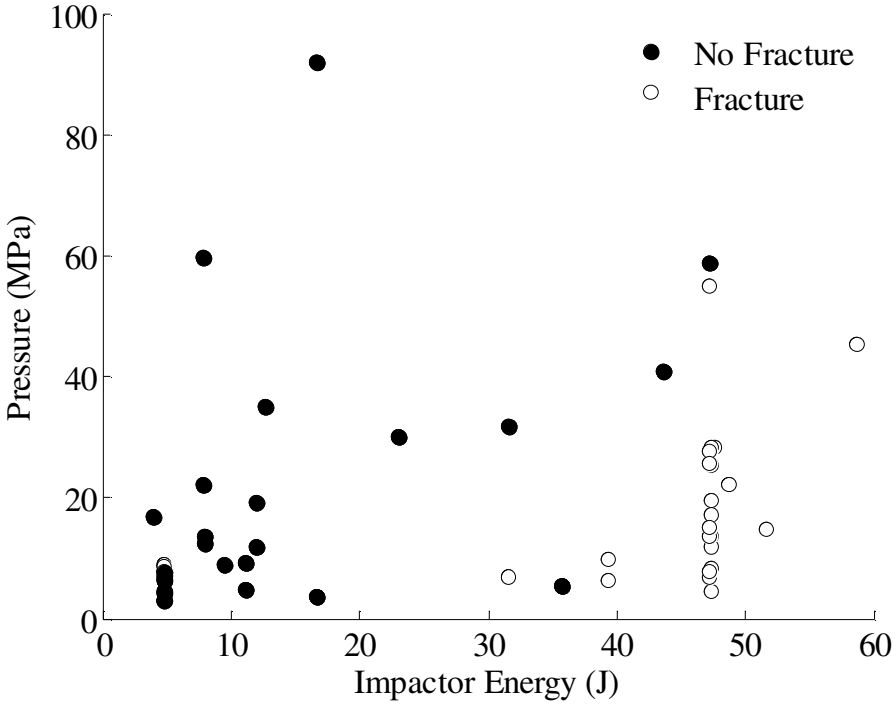

Figure 62: Estimated frontal bone contact pressure as a function of impactor energy.

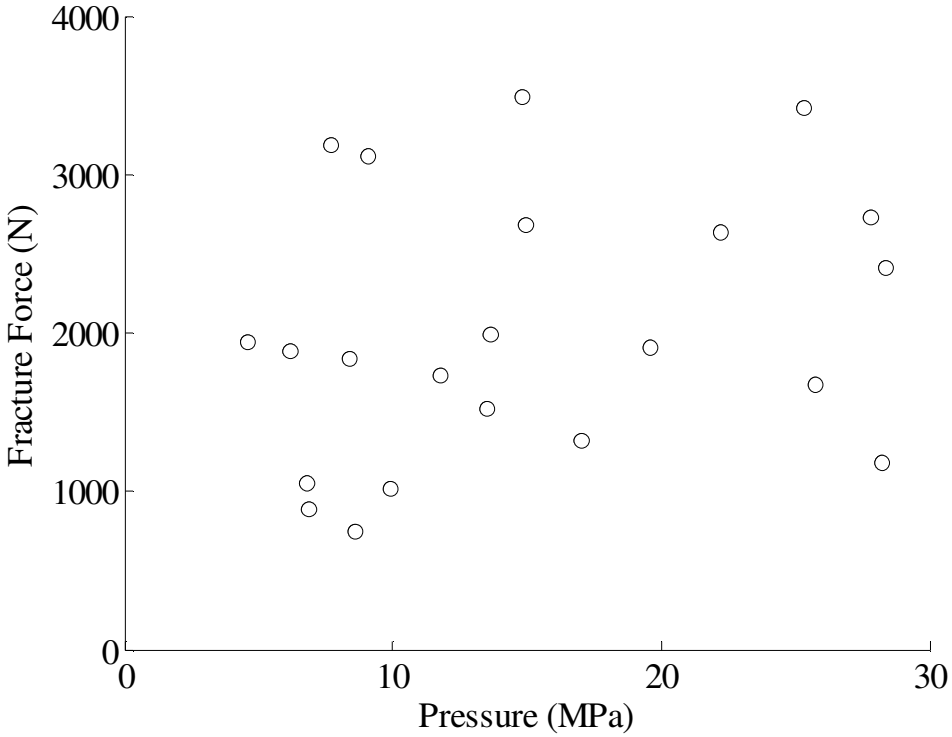

Figure 63: Frontal bone fracture force and estimated pressure.

Anthropometry

Measurements of the frontal bone thickness, overlying skin thickness and head size were taken to evaluate the potential relationship with the mechanical response of the frontal bone. The average frontal bone thickness was 0.5 cm (Std. Dev. = 3 mm) and the average skin thickness was 0.5 cm (SD = 1 mm). Frontal bone thickness was statistically related to head depth (r^2=0.81, $p < 0.0001$) and head width (r^2=0.80, $p < 0.0001$). No correlation was observed between skull and skin thickness and fracture force (Figure 64) or any stiffness measure (toe region length, initial and secondary stiffness). With respect to overall head size, neither head depth nor head width was significantly correlated with any of the mechanical responses. Head size did not exhibit a correlation with fracture force ($p = 0.21$) (Figure 65). Subject age did not have a statistically significant influence on the force at fracture onset ($p = 0.96$) (Figure 66).

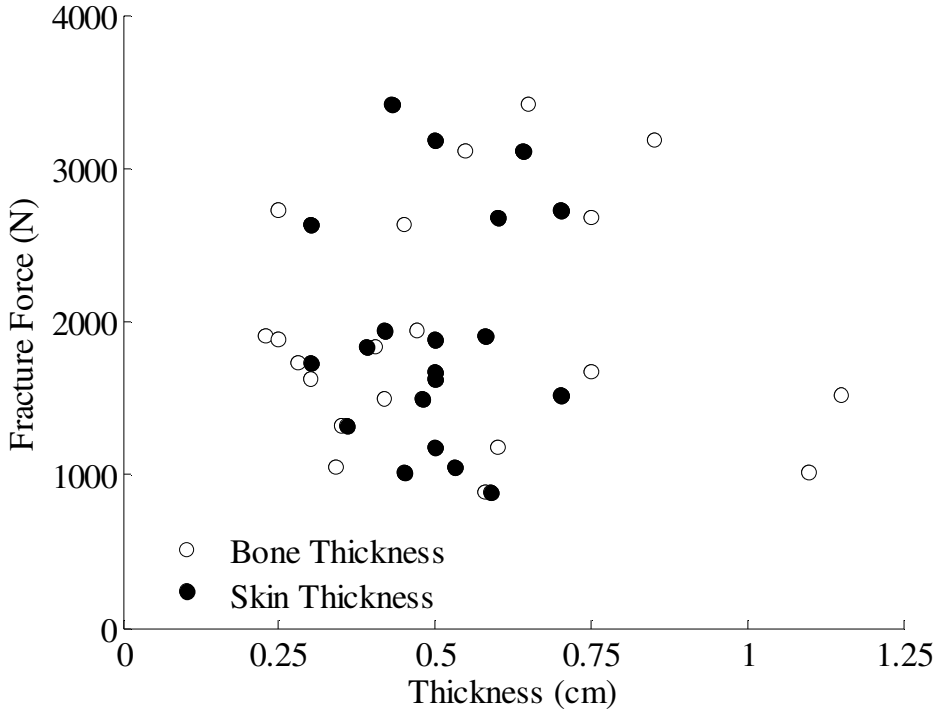

Figure 64: Frontal bone fracture force and corresponding frontal bone thickness and skin depth.

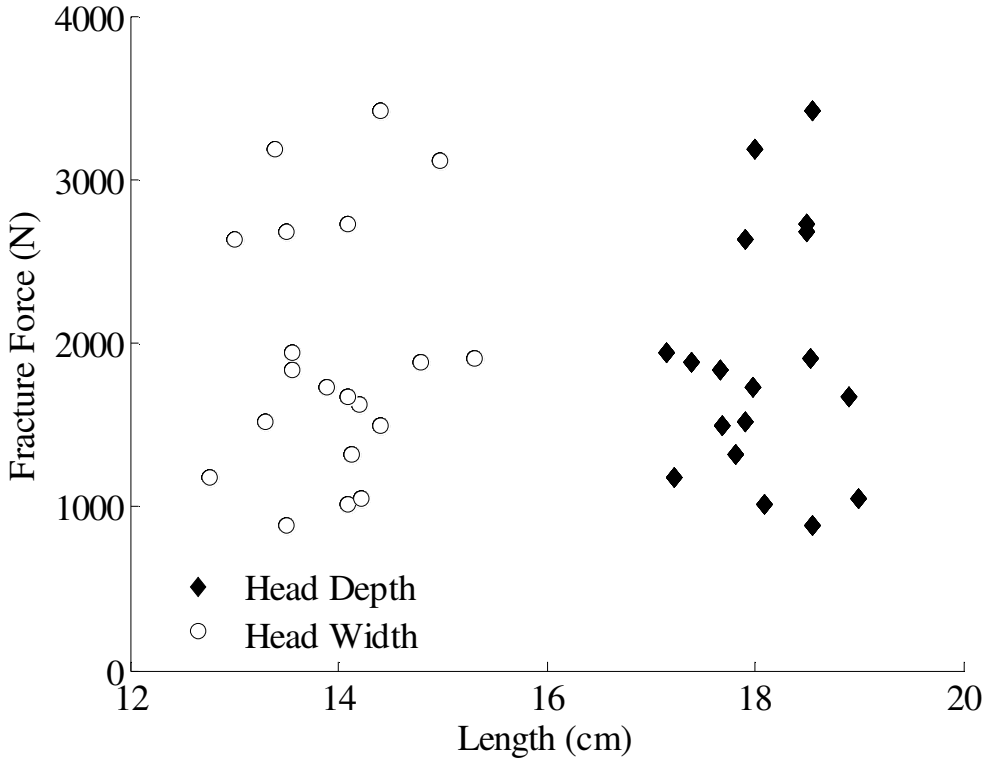

Figure 65: Frontal bone fracture force and head depth and width measured using CT imaging.

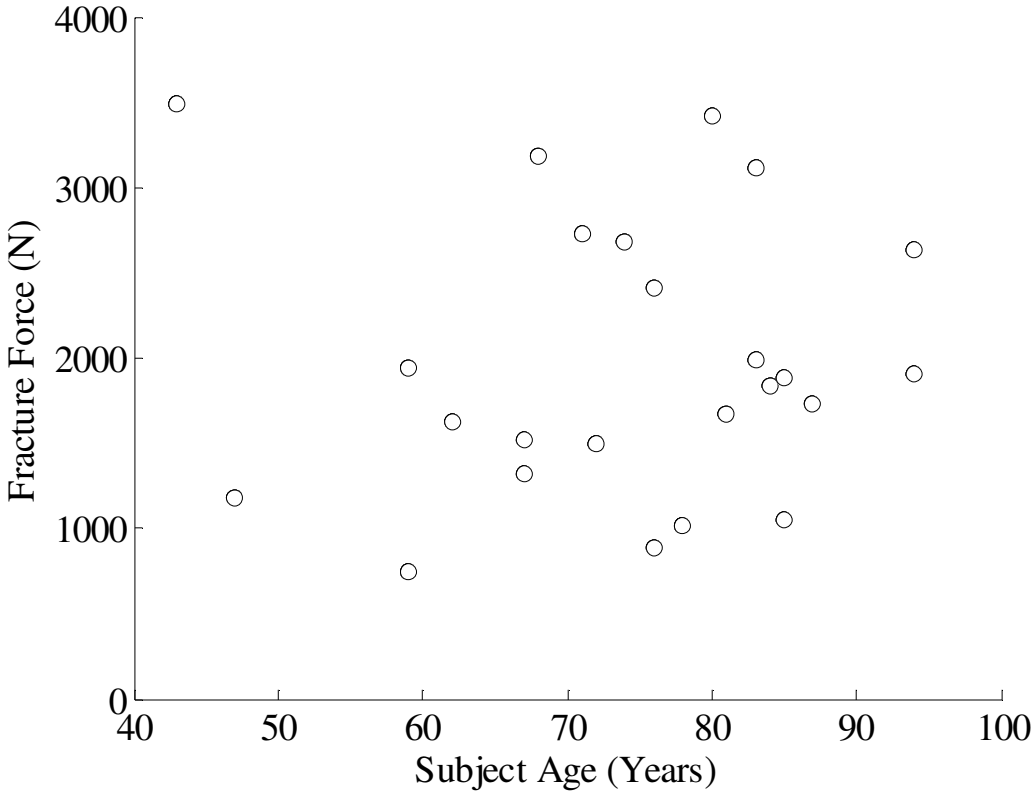

Figure 66: Frontal bone fracture force and subject age.

Risk of Frontal Bone Fracture

Parametric and non-parametric models were used to estimate the risk of fracture as a function of impactor force. Only one test per subject was used and no repeated tests resulting in fracture were used in the risk estimate. Two sets of data were used to develop the current risk functions. In one set, both fracture and non-fracture tests were used (Figure 67) and only fracture tests were used in the second (Figure 68). Using the Kaplan-Meir estimates, the 50% risk of fracture was 1950 N and 1830 N respectively. When included in the survival model, age did not statistically ($p = 0.55$) improve the fit. The scale and shape parameter estimates can be utilized in Equation 1 to reproduce the developed risk curves (Table 9). The Kaplan-Meier risk does not reach 100% in the dataset with non-fracture data due to the presence of non-fracture tests at 5236, 5402, 5934 and 7613 N.

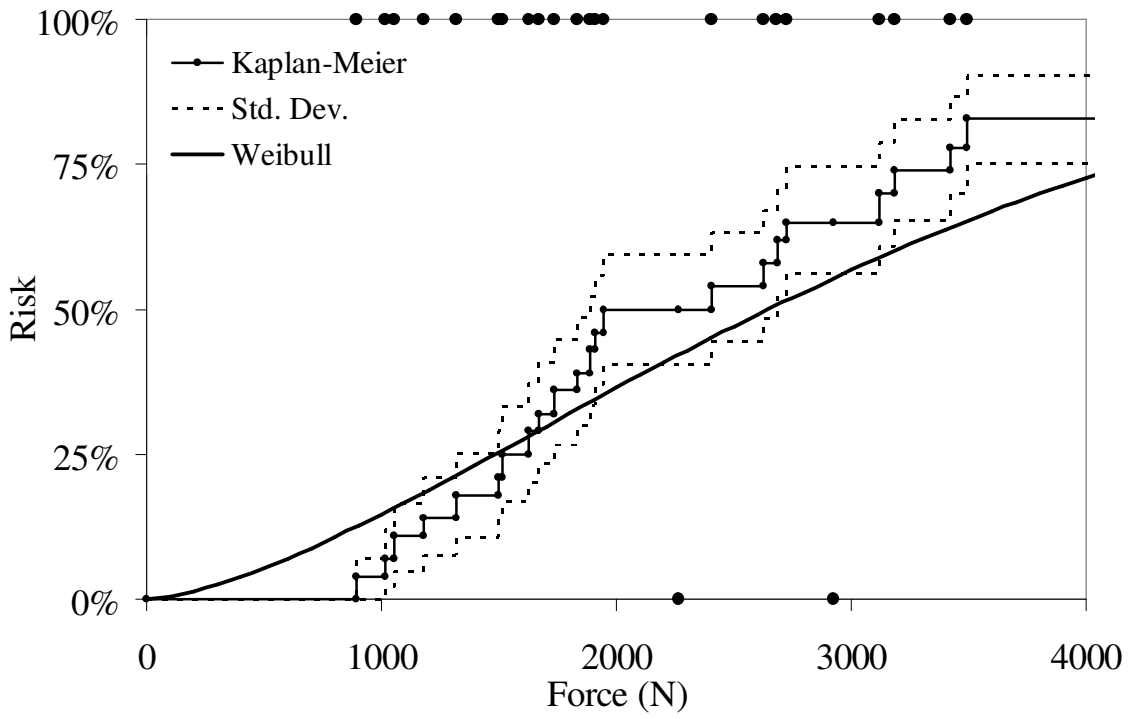

Figure 67: Risk functions for frontal bone fracture using fracture and no-fracture tests.

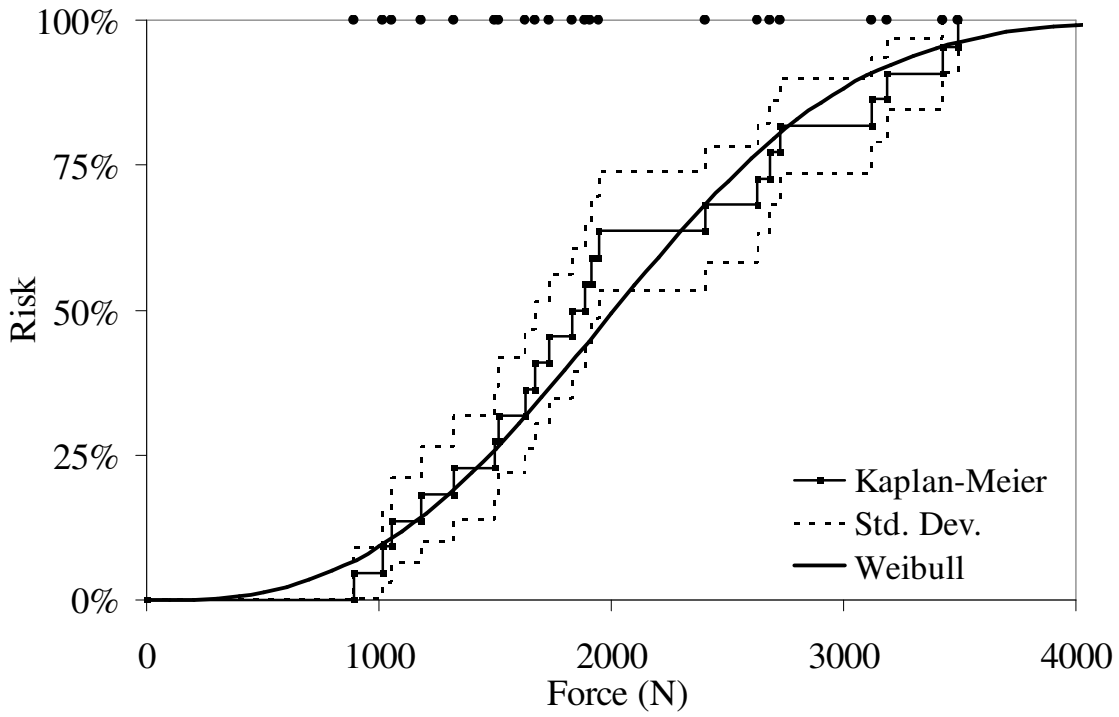

Figure 68: Risk functions for frontal bone fracture using fracture tests only.

Table 9: Frontal bone parameter estimates for Weibull distribution by model.

		95% Confidence Interval		
Model	**Estimate**	**Lower**	**Upper**	**Parameter**
All Data	0.00033	0.00041	0.00026	Scale (λ)
	1.79	1.30	2.47	Shape (γ)
Fracture Only	0.00044	0.00051	0.00037	Scale (λ)
	2.83	2.04	3.92	Shape (γ)

Cadaveric Force-Displacement

Impactor displacement (Figure 72) determined from double integration of accelerometer data was almost identical to that determined from high speed video (mean $r^2 = 0.98$). Due to the nature of the interaction between the frontal bone and the impactor, in some tests the impactor slid along the surface of the bone. Therefore, in these cases the force-displacement response did not reflect the deflection of the bone and soft tissue. These cases were identifiable by a low initial stiffness and excessive displacement (Figure 69). The lack of any rebound and continued displacement after impact was a clear indicator of impactor slip. When available, video analysis confirmed the sliding motion of the impactor. The tests identified as exhibiting a sliding motion prior to peak force where not

included in the development of a force-displacement corridor. If slippage was questionable and video analysis was not available to verify, the test was not utilized for the corridor development. The dataset used to assess the force-displacement response of the cadaveric frontal bone consisted of 25 tests. The stiffness of the frontal bone was calculated at 20% of peak force and between 20% and 80% of peak force (Table 10).

Table 10: Stiffness of frontal bone response at 20% and between 20 to 80% of peak force.

	Stiffness (N/mm)		**Displacement at 20% peak force (mm)**
	20%	**20-80%**	
Mean	331	731	1.7
Standard deviation	180	461	0.9
Min	111	293	0.6
Max	766	1735	5.2

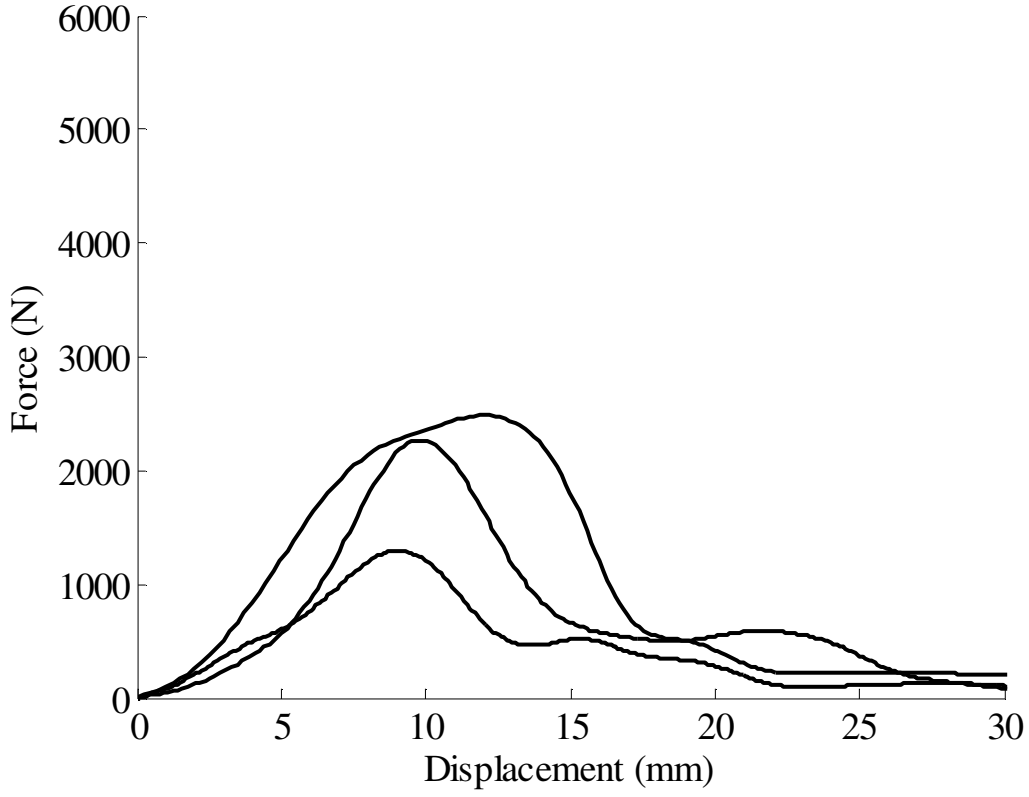

Figure 69: Example of frontal bone force-displacement responses with impactor slip.

The force-displacement response varied depending upon the type of fracture incurred by the specimen. Tests resulting in a depressed fracture tended to have a force-displacement response that reached an initial peak followed by continued displacement with an

oscillating force (Figure 70). In some cases the impactor continued to translate, while others stopped within the depression in the frontal bone. Tests that caused a stellate fracture pattern with little depression demonstrated a force-displacement response that reach a peak and then decreased with little continued impactor motion (Figure 71). This phenomenon occurred in subjects exposed to the same impactor energy.

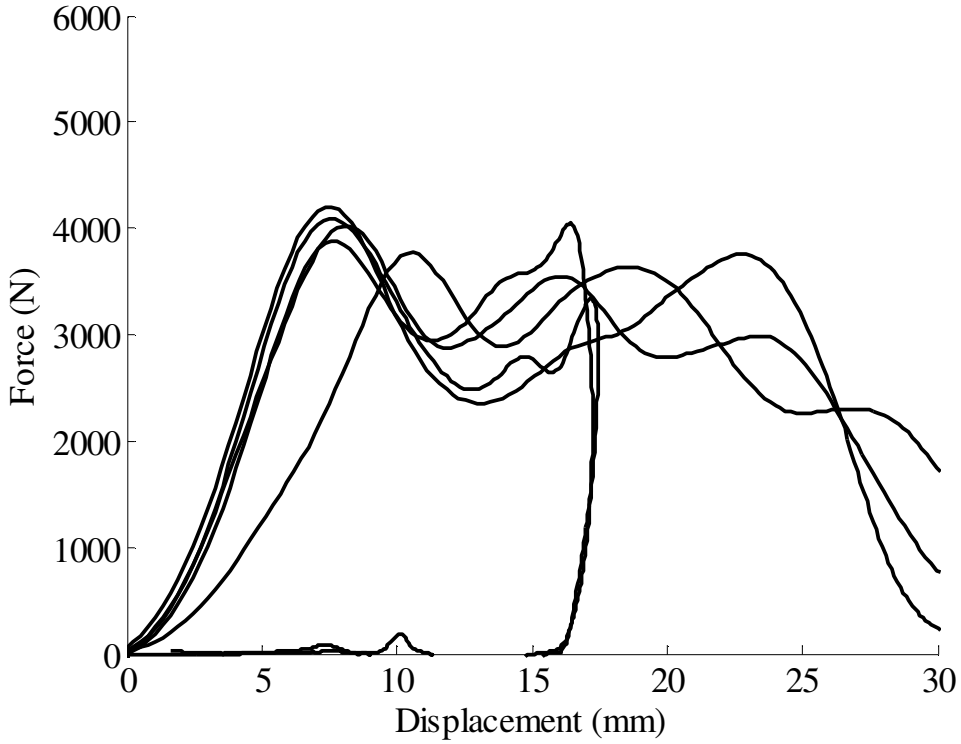

Figure 70: Representative frontal bone force-displacement responses for tests resulting in a depressed frontal bone fracture.

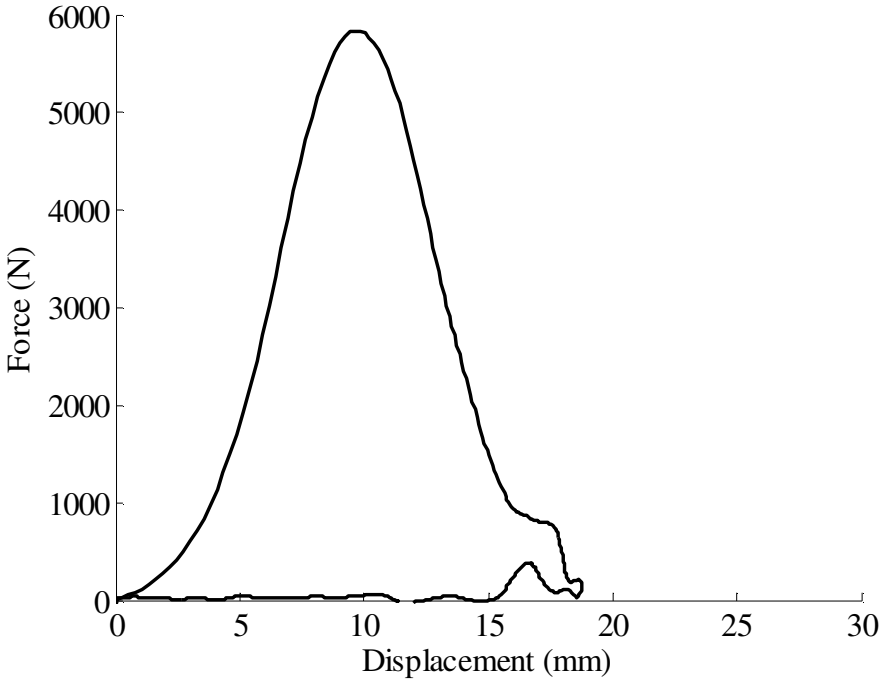

Figure 71: Frontal bone force-displacement response of test resulting in stellate fractures with no depression.

The range of the force-displacement response up to 90% of the peak force was described by calculating the characteristic average (Figure 72) (Lessley 2004). The corridor was only defined for tests in which the impactor did not slide against the frontal bone. The corridor was created by only using the standard deviation of the characteristic average in the y-axis, or force direction. This was done because it generated a tighter fit to the current data, creating a smaller corridor. The majority of tests were within one standard deviation of the mean with some tests exhibiting a stiffer response. The corridors can be accurately recreated using 2nd order polynomials (Figure 73).

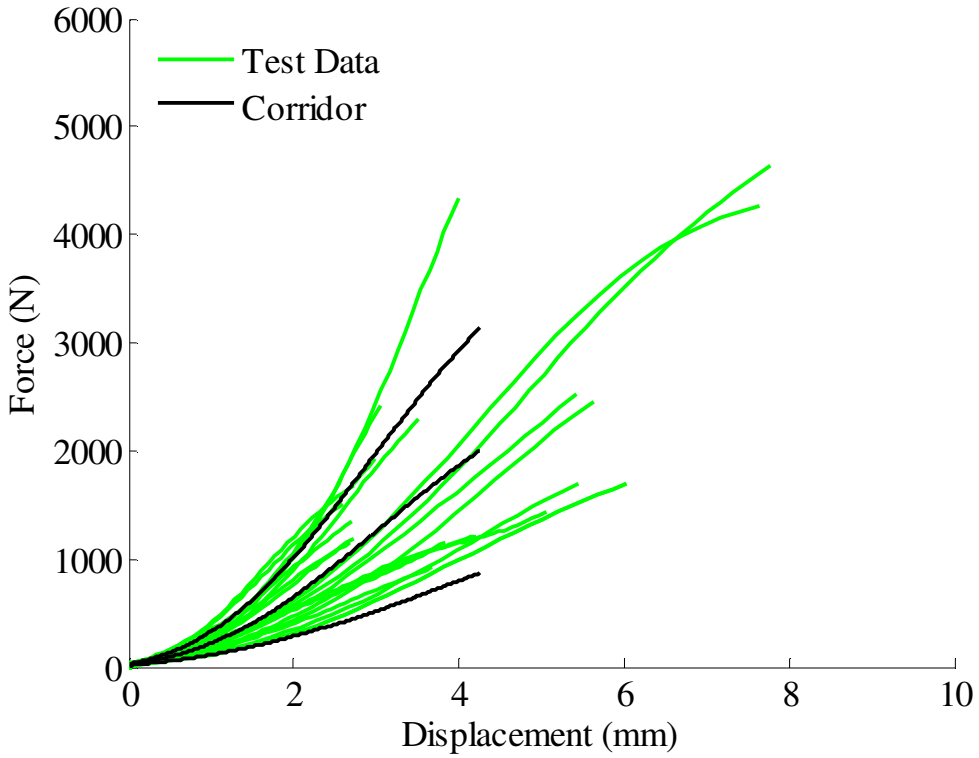

Figure 72: Frontal bone force-displacement relationship of cadaver specimens with corridor.

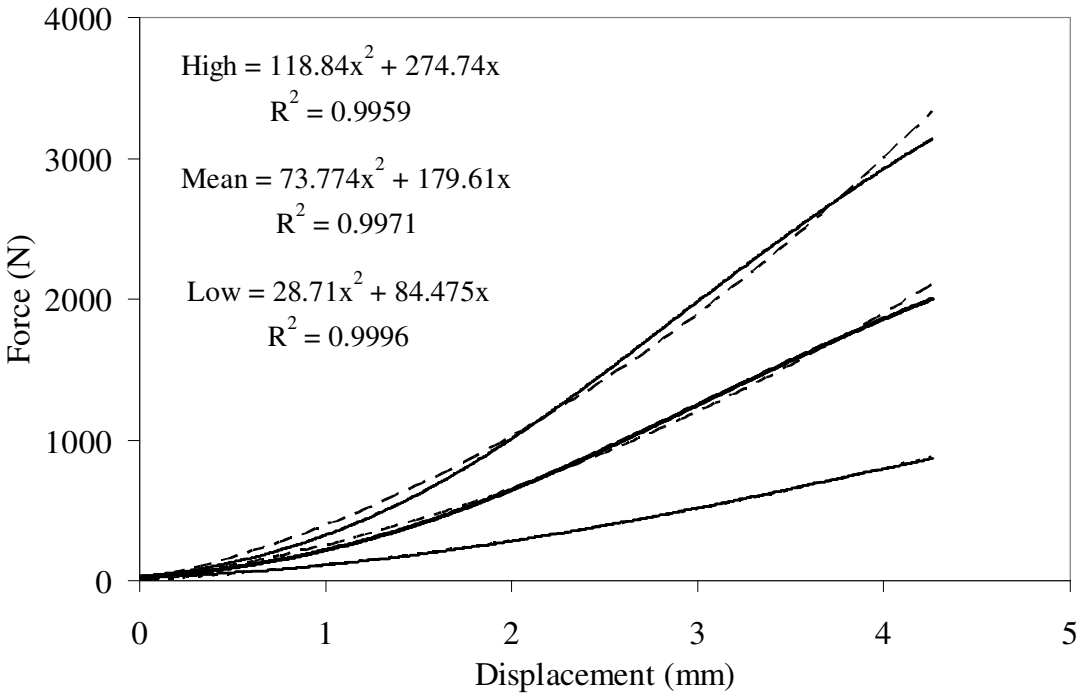

Figure 73: Polynomial fits of frontal bone response corridors.

FOCUS Headform Biofidelity

A total of 6 tests were performed on the frontal bone region of the FOCUS headform. Impactor velocity ranged from 2 to 2.2 m/s resulting corresponding to an impactor energy of 6.3 to 7.9 J. The peak forces measured by the impactor ranged from 2754 to 3260 N. The peak force measured by the internal FOCUS load cells were practically equal (Figure 74) to the impactor force with an average difference of 0.3%. On average 20% of the response occurred at a displacement of 2.7 mm (Std. Dev. = 0.18) with an initial stiffness of 210 N/mm (SD = 19) and a secondary stiffness of 846 N/mm (SD = 68).

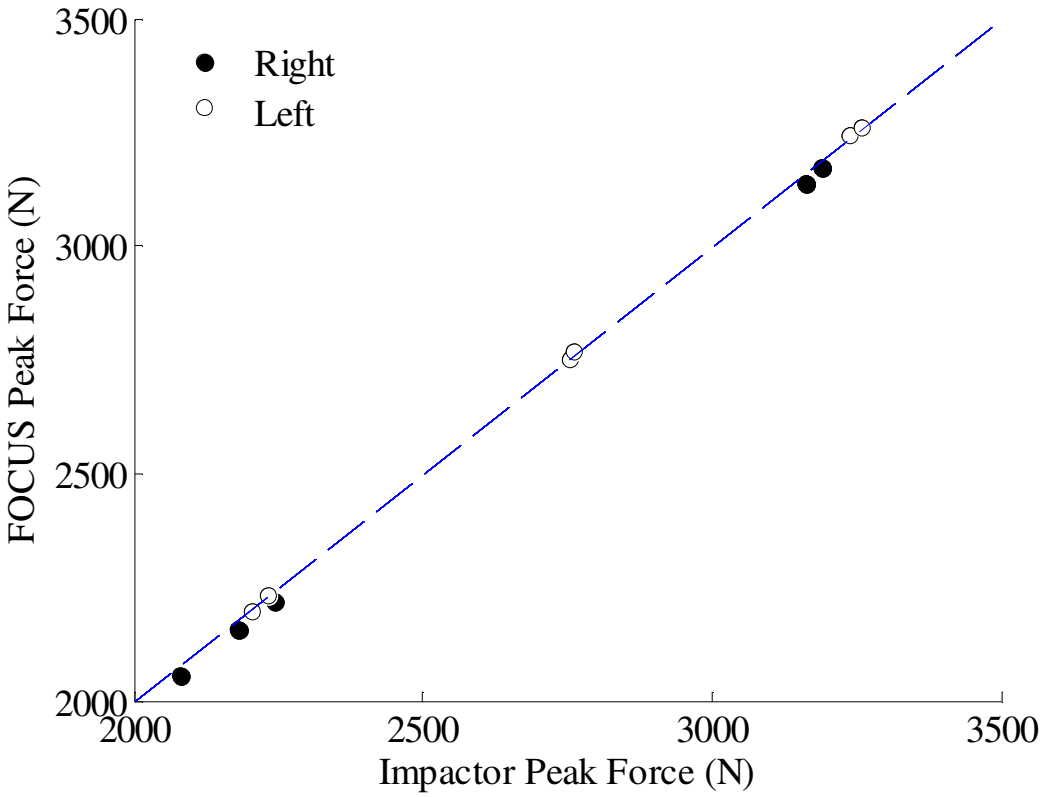

Figure 74: Impactor force and internal FOCUS force due to frontal bone impact.

The force-displacement of the FOCUS headform was repeatable and followed the same upward path at the various impactor energies (Figure 75). The FOCUS response to the impact was elastic and resulted in the impactor bouncing off the headform following the initial impact. The stiffness of the FOCUS response increased with impact velocity over the ranged utilized (Table 11).

Table 11: Stiffness of FOCUS frontal bone response by range in impactor velocity.

	Initial Stiffness (N/mm)		Secondary Stiffness (N/mm)	
Impactor Velocity (m/s)	**Mean**	**Std. Dev.**	**Mean**	**Std. Dev.**
2	197	11	761	2
2.2	217	20	889	889

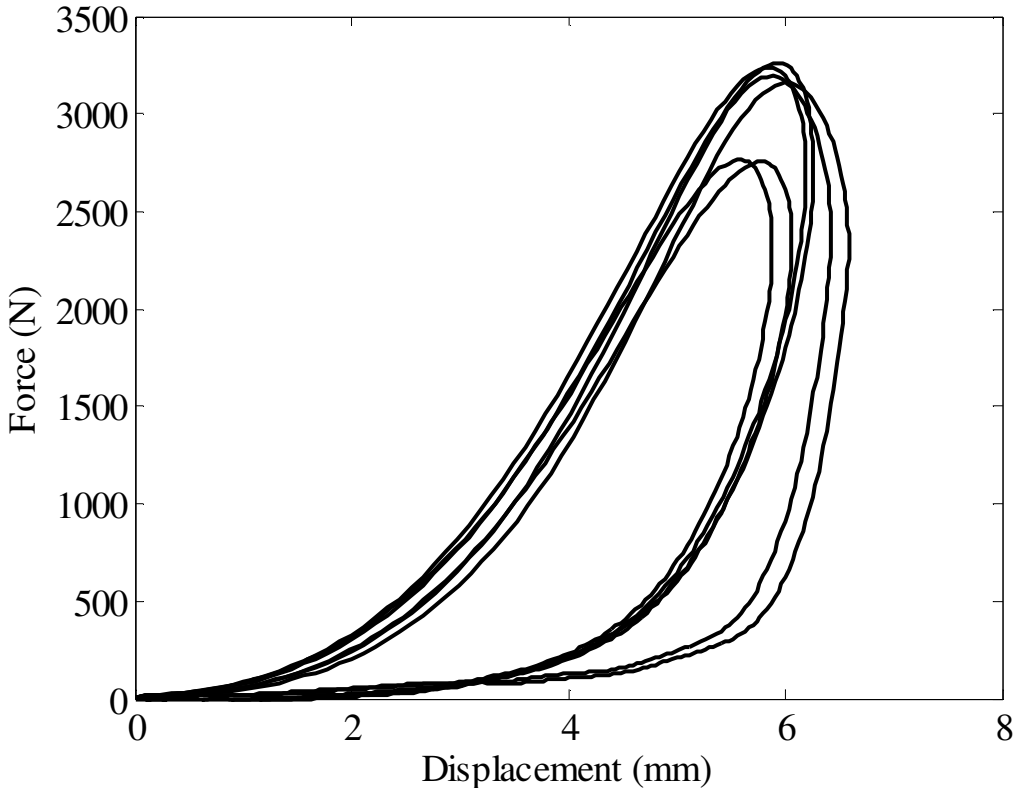

Figure 75: FOCUS headform force-displacement for frontal bone impacts.

The characteristic average of the FOCUS force-deflection response was created using all tests (Figure 76) (Lessley 2004). There was no evidence within high-speed video or impactor displacement to suggest that the impactor slid along the FOCUS headform during any test. The 2nd order polynomials fit the derived corridor well. Therefore, they can be useful in recreating the average response of the FOCUS headform (Figure 77).

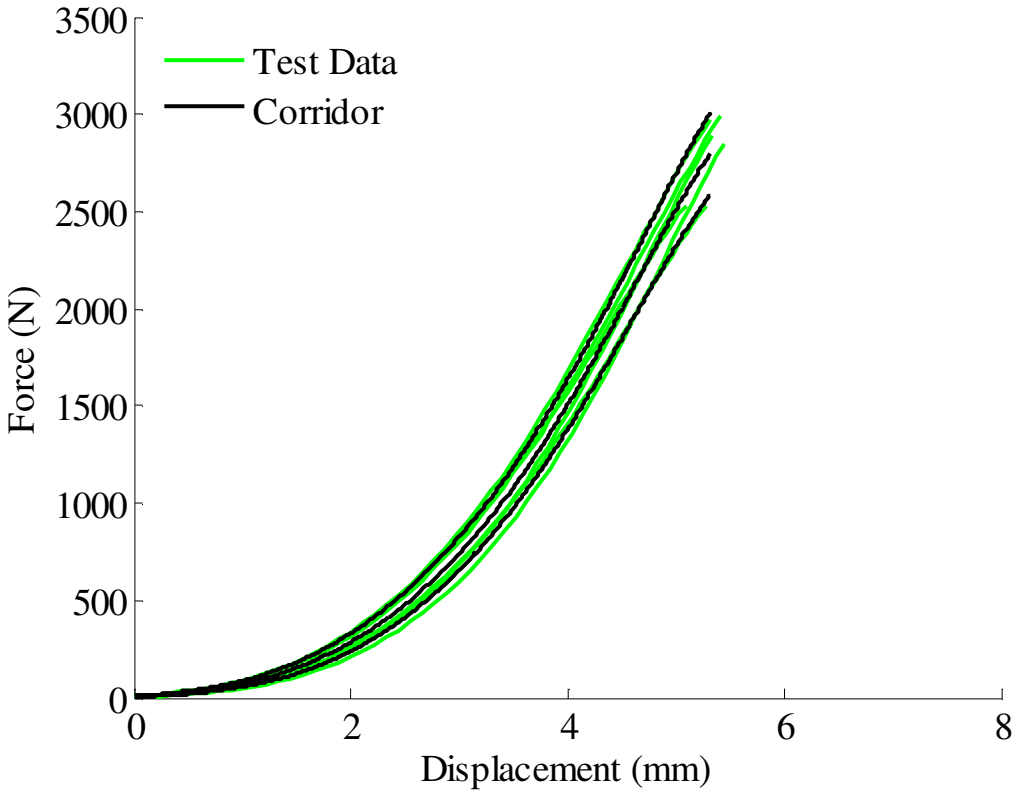

Figure 76: FOCUS headform characteristic average for frontal force-displacement.

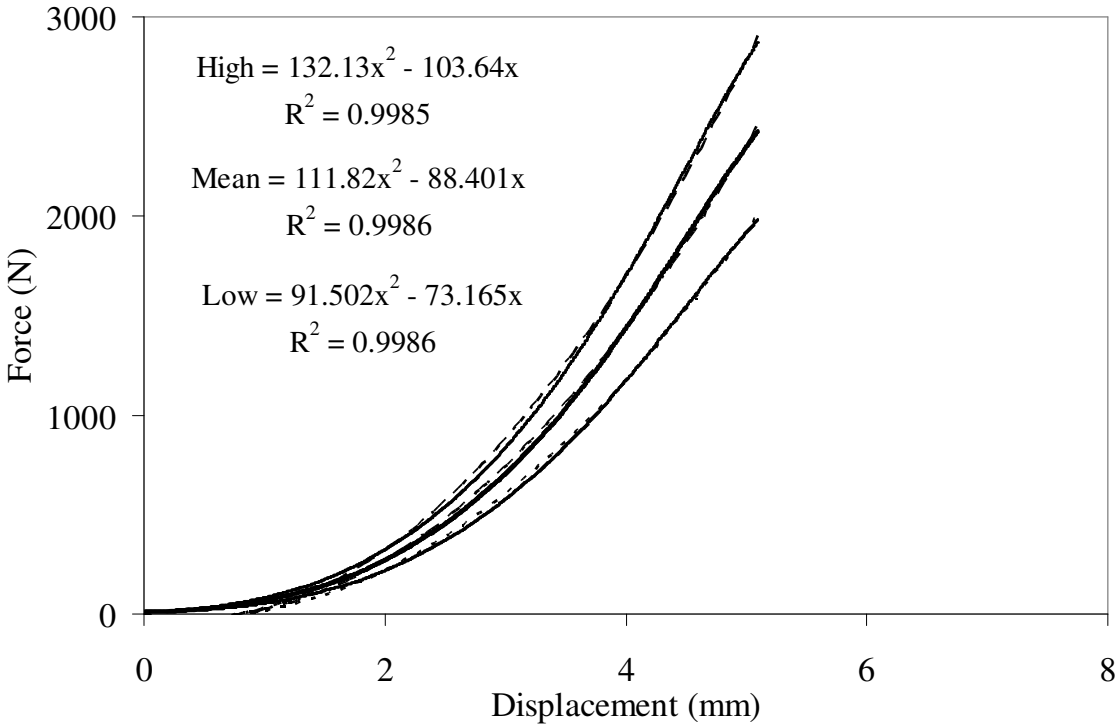

Figure 77: Polynomial fit to FOCUS frontal bone force-displacement corridor.

The corridor determined from the FOCUS force-displacement response was well within the cadaveric corridors for frontal bone impacts (Figure 78). On average, the toe region for the FOCUS test exhibited a less stiff response than the cadaver response. The stiffness of the FOCUS headform increased after approximately 2 mm such that the force achieved was well within the cadaver corridor. The initial stiffness and toe region up to 20% of peak force were statistically different between the cadaver and FOCUS responses (respectively, $p = 0.001$, $p < 0.0001$). The secondary stiffness, between 20 and 80% of peak force was also statistically different ($p = 0.003$).

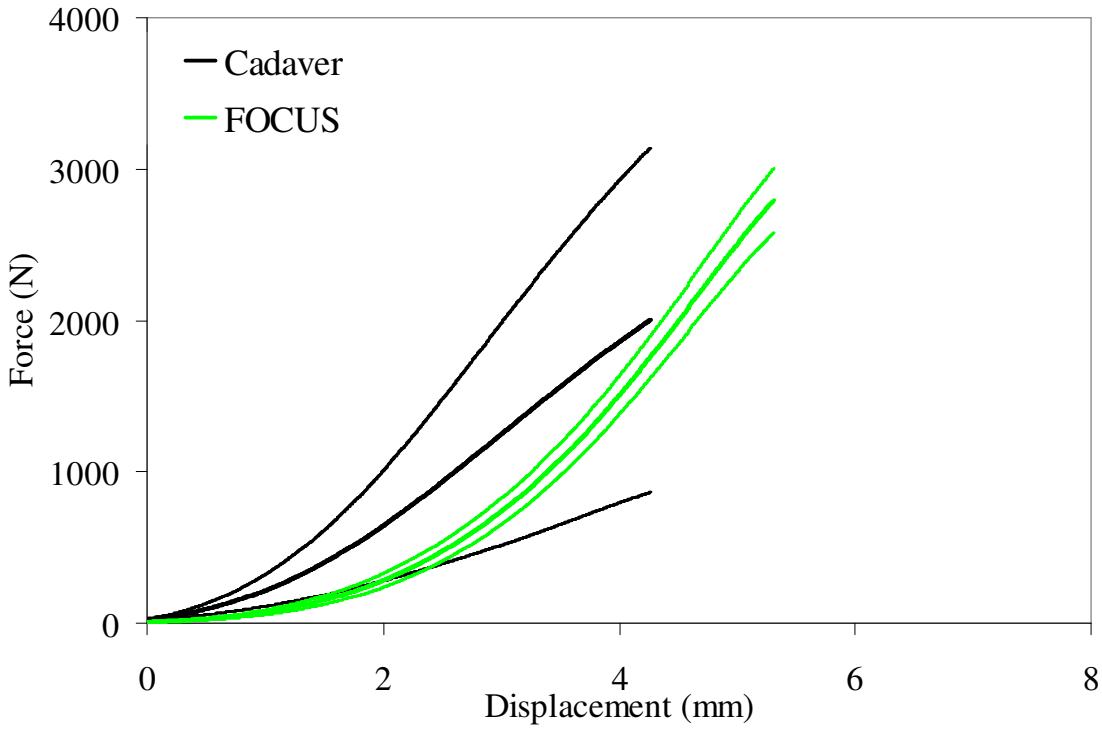

Figure 78: Corridor for cadaveric and FOCUS frontal bone response to blunt impact.

DISCUSSION

The purpose of this study was to provide the information necessary to understand the frontal bone response to blunt impact and determine a relationship for fracture risk. Force-deflection corridors were determined to define this relationship up to peak force. Due to the nature of the impact, force-displacement following peak force varied by subject. In non-fracture tests it was common for the impactor to continue moving along the curvature of the frontal bone after impact. This occurred in fracture tests as well, however, in cases in which the fracture was severe enough, the impactor continued to penetrate into the skull cavity or frontal sinus. Impacts resulting in fracture with little or no depression demonstrated a different force-displacement relationship than those with depression. Fracture without depression still contained multiple fractures radiating from the impact site.

No trends were found between impact severity or fracture force and the contact area estimated using Fuji Film. The fact that pressure is not related to impactor energy prohibits its use as a predictor of fracture since it is not related to the severity of the impact. The lack of trends with respect to area can be partially attributed to the use of Fuji Film to estimate the contact area. This produces a quantitative measure of contact area and may not be the area of contact at the time of peak force or fracture due to compression of the soft tissue and movement of the impactor following the initial contact. The area estimated for fracture tests was higher on average than no fracture tests. The increased contact area is due to the conformation of the flesh onto the impactor at higher forces which results from larger deformation of the tissue and loss of structural integrity.

The current study utilized Acoustic Emission (AE) to determine the force at which the onset of fracture occurred. An AE threshold was defined which would indicate the occurrence of fracture behavior. This approach was validated by comparing the AE obtained during fracture (Figure 49) and non-fracture tests (Figure 48) and additional testing on a previously fractured bone (Figure 50). Repeated tests on fractured bone, performed at low impactor energies confirmed the presence of an AE amplitude similar

to the impact that produced the original fracture. This is consistent with the idea that the AE is related to the propagation of fractures and is not necessarily related to the applied force. In some cases, above threshold AE signal was recorded during a non-fracture test. In these cases the number of counts above the threshold was significantly lower than a fracture test. The occurrence of high AE in tests without fracture may be a result of sub-failure fracture behavior that is not observed during dissection.

Accounting for severity, the peak force generated in each test was not influenced by the occurrence of fracture. This exemplifies the importance of using AE to determine the force at which fracture begins. The peak forces reported by Nahum *et al.* (1965, 1975) suggest that fracture actually occurred at a much lower force and, therefore, incorporation of these data in a statistical analysis should assume that they are left-censored. Despite the use of a lighter impactor and higher impact velocities, the forces reported by Nahum *et al.* correspond well with those in the current study (Figure 79). Seven of the specimens in the Nahum *et al.* studies did not fracture at an average peak force of 6.1 kN, the majority (n=31) fractured with an average force of 5.3 kN. The higher forces achieved in the Nahum *et al*. study without fracture is likely the result of the use of a padded impactor and human variation.

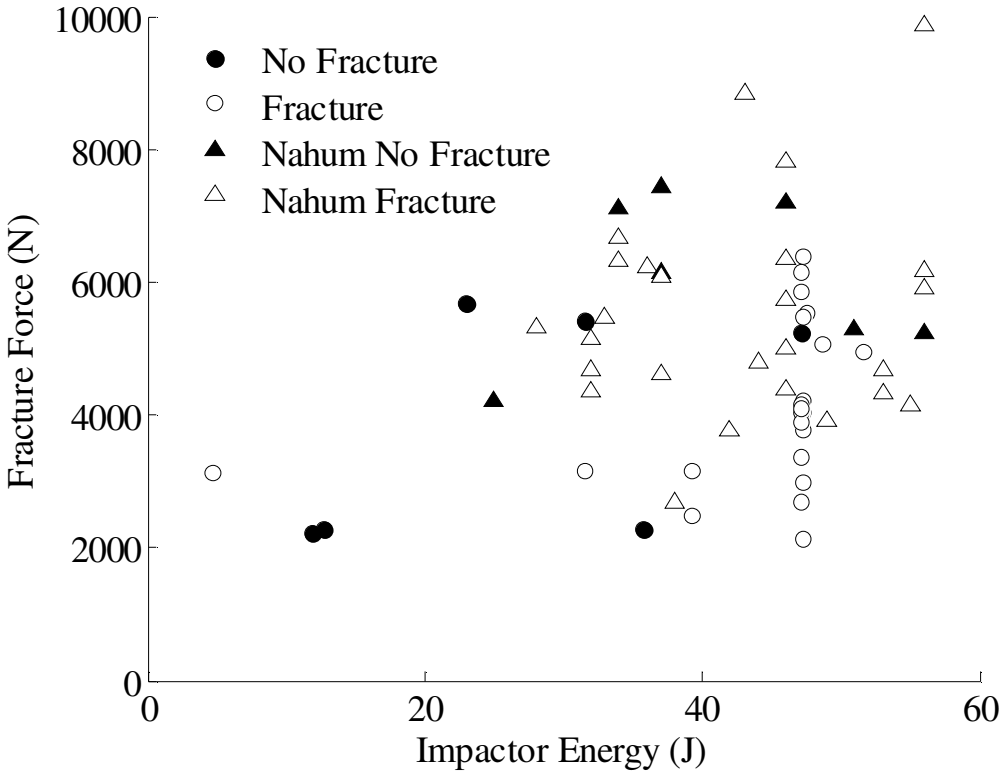

Figure 79: Frontal bone peak force with respect to impactor energy by study.

The risk curves developed represent a conservative criterion for a projectile with an area of 6.45 cm^2 (1 in^2). This is because the actual contact patch between the impactor and the facial bone is always less than the actual impactor area. If the facial bones were flat, the contact area and impactor area would be equal and, therefore, the impactor force divided by the area would be an accurate measure of the pressure applied. The uneven nature of the face prevents an even distribution of pressure from being applied when struck by a flat impactor. This exemplifies the importance of padding that not only absorbs energy, but distributes force over a greater area. In fact, the average area of contact for the current study was 2.4 cm^2. With these ideas in mind, the estimated risk of fracture can be conservatively applied to impacts involving impactors with larger area, but if the area is considerably less than one square inch and controlling for impactor energy, the risk of fracture will be higher. The impactor in the current study was the same as that used by Nahum *et al.* (1965, 1975), except for the addition of 0.5 cm of a nickel foam padding. Quantitatively it appears that this padding allowed their subjects to sustain higher peak forces without fracture than the current study. In this study a pressure of 10 MPa was

approximately a 50% risk of fracture when using the average area to estimate the area at fracture.

Age was found to have no influence on the risk of frontal bone fracture. The average age of the subjects in this study was 71 years (SD = 15). Our results agree with a previous study that found that age does not significantly affect the strength of facial bones. This insensitivity was explained by the fact that facial bones are comprised mostly of cortical bone, which does not degenerate with age to the extent that cancellous bone does (Yoganandan 1988).

The skull and skin thicknesses measured during pre-test CT imaging were also not correlated with the response of the frontal bone. This result suggests that the response to impact is a combination of several factors that are not accounted for in a single measure of bone or skin thickness. The CT imaging did allow identification of the frontal sinus and its location with respect to the impacted site. In eleven of the 22 subjects with CT imaging, the fontal sinus was present at the impact location. This presents a fundamentally different structure that consists of a relatively thinner anterior structure compared to the frontal bone (Figure 80). Interestingly, the frontal sinus is not symmetric about the midline of the skull and, therefore, one side of the frontal bone may exhibit a fundamentally different response than the other. In this study, the majority of subjects without a frontal sinus within the impacted region did not sustain a depressed fracture. These subjects typically incurred radiating fractures with little or no depression.

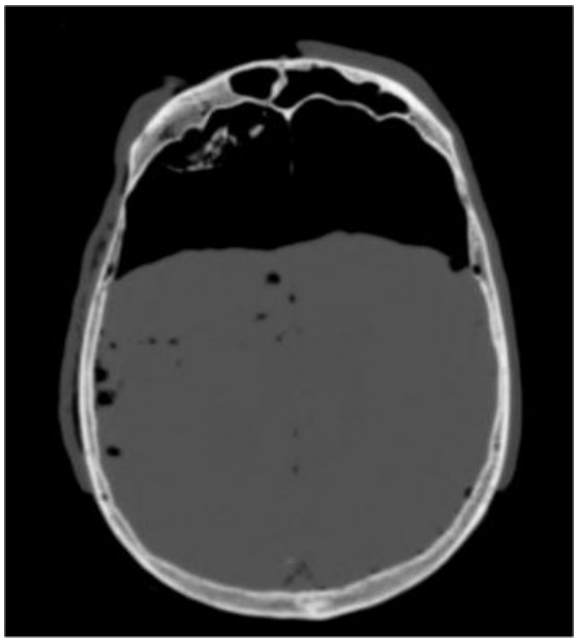

Figure 80: CT image demonstrating frontal sinus of one subject used in current study.

CT data were available for 22 of the 28 subjects used to create the risk estimates. A separate estimate of risk was created using the 22 subjects and it was found that the presence of the frontal sinus within the impacted region was a statistically significant parameter in the model (p=0.0422). The risk estimate generated with the reduced dataset does not incorporate all the data available, therefore it does not represent the distribution of all data collected. However, it does demonstrate the influence of the frontal sinus on fracture risk (Figure 81).

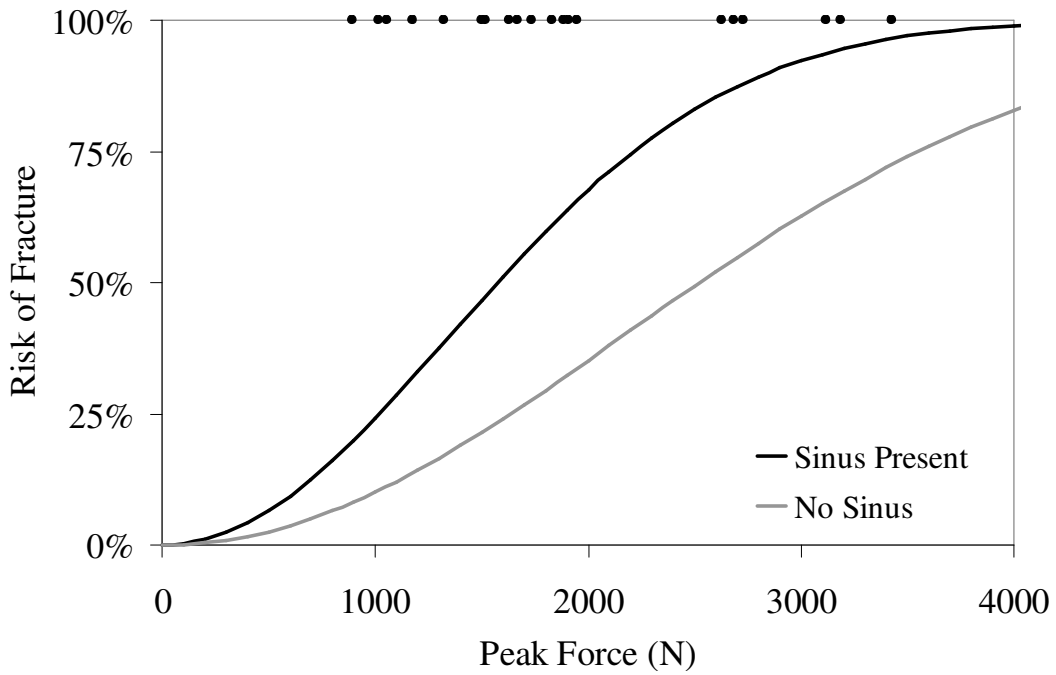

Figure 81: Risk of frontal bone fracture using reduced dataset with CT data indicating presence of frontal sinus.

Tests were performed on the FOCUS headform to determine the force-displacement response when struck with the same impactor used in the cadaver testing. Its response was within the lower segment of the corridor using the mean and standard deviation of the cadaver response as defined by the characteristic average. This suggests that for impacts of similar severity to those utilized here, the FOCUS headform will produce forces similar to those of a cadaver. For impacts performed at the severities chosen in this study, the peak force estimated by the FOCUS headform will be approximately 30% higher than the actual force. The forces measured by the internal FOCUS sensors were equal to the impactor force. This agreement is based on impacts that were central to the internal load cells and, therefore, caution should be used when performing off-centered impacts due to possible load-sharing with other reaction surfaces with the headform. Several impacts were performed at a constant impactor energy and, for the number of tests performed in the current study, the peak forces were repeatable.

Limitations

This study is limited to a single impactor type. Size and shape of the striking object was not assessed in this study and, therefore, estimation of fracture risk for other impactor

types is limited. The area of contact measured in this study suggests that the total area of our 6.45 cm^2 impactor is not being utilized in the majority of impacts. Therefore, for objects slightly smaller than the current impactor, the risk of fracture should be a fair approximation. Impact direction was not assessed in this study which, due to the facial geometry, could play a role in fracture risk.

The force-displacement relationship of the FOCUS headform is limited to impacts performed at a location centered on the load cells. Addition testing will elucidate any effects of off-centered impacts to this region. Higher severity impacts should also be performed to evaluate potential changes in the force-deflection response of the FOCUS exterior.

CONCLUSIONS

The current study presents data describing the response and tolerance of the frontal bone to blunt impact. A force-displacement corridor was defined by excluding tests in which the impactor moved with respect to the frontal bone. Comparison with previous studies using similar results showed good agreement with peak force at a given impactor energy. Similar to other studies as well, fracture force was not related to subject age.

To achieve non-censored fracture force data, acoustic emission sensors were used to identify the time of fracture initiation. These data were then used to create parametric and non-parametric risk curves. A 50% risk of fracture was found to occur at forces between 2,000 and 2,500 N.

The frontal bone thickness and overlying skin thickness measured using CT images were not correlated with fracture force. However, the presence of the frontal sinus was a significant factor in predicting the risk of fracture. The frontal sinus was observed to be an asymmetric structure and its presence was associated with the occurrence of depressed, comminuted fractures and a higher risk of fracture. This fracture pattern produced a unique force-displacement response.

Impactor size and shape is an important aspect of the frontal bone response as it influences the nature of the interaction. As observed in the current study, the impactor can slide along the surface of the bone, reducing the severity of the impact. This is a function of the impactor, impact direction and the frontal bone geometry. Using a single impactor and impact direction the current study demonstrates that, due to human variation, subjects exposed to the same impact can incur vastly different injuries. This was demonstrated in fracture patterns and the force-displacement response of the impactor.

A series of tests were performed to assess the response of the FOCUS headform to frontal bone impacts. The force-displacement response of the FOCUS was within the cadaver corridors defined by the characteristic average, however, there were statistically significant differences between the stiffness values of the cadaver and FOCUS headform. This study provides the data necessary to improve the biofidelity of the frontal bone region of the FOCUS headform to improve its utility in predicting facial fractures.

REFERENCES

Allsop D, Kennett K: Skull and Facial Bone Trauma. Accidental Injury: Biomechanics and Prevention. A. Nahum and J. Melvin. New York, Springer-Verlag. 2nd Edition**,** 254-76; 2002.

Allsop D, Warner C, Wille M, Schneider D, Nahum A: Facial Impact Response – A Comparison of the Hybrid 3 Dummy and Human Cadaver, *Society of Automotive Engineers*, SAE No. 881719; 1988.

Bermond F, Kallieris D, Mattern R, Ramet M, Bouquet R, Caire Y, Voiglio E: Human Face Response at an Angle to the Fore-aft Vertical Plane Impact, *Proceedings of the IRCOBI*; 1989.

Bruyere K, Bermond F, Bouguet R, Caire Y, Ramet M, Voiglio E: Human Maxilla Bone Response to 30 degree Oriented Impacts and Comparison with Frontal Bone Impacts, *Proceedings of the 44th Association for the Advancement of Automotive Medicine Conference*, 219-34; 2000.

Cormier J, Manoogian S, Bisplnghoff J, McNally C, Duma S: The Use of Acoustic Emission in Facial Fracture Detection, *Biomed. Sci. Instrum.*, 44, 147-52; 2008.

Delye H, Verschueren P, Depreitere B, Verpoest I, Berckmans D, Sloten J, Van Der Perre G, Goffin J: Biomechanics of Frontal Skull Fracture, *J Neurotrauma*, 24, 1576-86; 2007.

Fischer RA, Arms SW, Pope MH, Seligson D: Analysis of the Effect of Using Two Different Strain Rates on the Acoustic Emission in Bone, *J. Biomech.*, 19, 119-27; 1986.

Funk J, Crandall J, Tourret L, MacMahon C, Bass C, Patrie J, Khaewpong N, Eppinger R: The Axial Injury Tolerance of the Human Foot/Ankle Complex and the Effect of Achilles Tension, *Journal of Biomechanical Engineering*, 124; 2002a.

Funk J, Srinivasan S, Crandall J, Khaewpong N, Eppinger R, Jaffredo A, Potier P, Petit P: The Effects of Axial Preload and Dorsiflexion on the Tolerance of the Ankle/Subtalar Joint to Dynamic Inversion and Eversion, *Stapp Car Crash Journal*, 46(0S2-34); 2002b.

Gassner R, Tuli T, Hächl O, Rudisch A, Ulmer H: Cranio-Maxillofacial Trauma: A 10 Year Review of 9543 cases with 21067 Injuries, *Cranial and Maxillofacial Surgery*, 31, 51-61; 2003.

Hodgson VR, Brinn J, Thomas LM, Greenberg SW: Fracture Behavior of the Skull Frontal Bone Against Cylindrical Surfaces, *Proceedings of the 14th Stapp Car Crash Conference,* SAE No. 700909; 1970.

Hodgson VR, Thomas LM: Breaking Strength of the Human Skull Versus Impact Surface Curvature, *Wayne State University Report* DOT-HS-146-2-230; 1973.

Jayamanne DGR, Gillie RF: Do Patients with Facial Trauma to the Orbito-Zygomatic Region also Sustain Significant Ocular Injuries?, *Coll. Surg. Eding.*, 41, 200-3; 1996.

Kennedy EA: The Development and Validation of a Biofidelic Sythetic Eye for the Facial and Ocular Countermeasure Safety (FOCUS) Headform, PhD Biomedical Eng., Virginia Tech; 2007.

Kent R, Stacey S, Parenteau C: Dynamic Pinch Tolerance of the Phalanges and Interphalangeal Joints, *Traffic Inj Prev*, 9(1), 83-8; 2008a.

Kent R, Stacey S, Parenteau C: Dynamic Pinch Tolerance of the Phalanges and Interphalangeal Joints, *Traffic Injury Prevention*, 9, 83-8; 2008b.

Kleinbaum D, Klein M: Survival Analysis: A Self-Learning Text, 2nd, New York, Springer Science; 2005.

Knets IV, Krauya UE, Vilks YK: Acoustic Emission in Human Bone Tissue Subjected to Longitudinal Extension, *Proceedings of the 1st All-Union Confer. on Eng. And Medicla Biomech.,* October, Riga; 1975.

Kohn DH: Acoustic Emission and Nondestructive Evaluation of Biomaterials and Tissues, *Critical Reviews Biomed. Eng.*, 22(3/4), 221-306; 1995.

Lessley D, Crandall J, Shaw G, Kent R, Funk J: A Normalization Technique for Developing Corridors from Individual Subject Responses, *Society of Automotive Engineers*, 2004-01-0288; 2004.

Lim LH, Lam LK, Moore MH, Trott JA, David DJ: Associated Injuries in Facial Fractures: A Review of 839 Patients, *British J. Plast. Surg.*, 46, 365-38; 1993.

Muraoka M, Nakai Y, Nakagawa K, Yoshioka N, Nakaki Y, Yabe T, Hyodo T, Kamo R, Wakami S: Fifteen – Year Statistics and Observation of Facial Bone Fracture, *Osaka City Med. J.*, 41(2), 49-61; 1995.

Nyquist GW, Cavanaugh JM, Goldberg SJ, King AI: Impact Tolerance and Response of the Face, *Proceedings of the Advances in Bioengineering Conference*, Anaheim, CA; 1986.

Peters A: Acoustic Emission Technique and Fracture Healing, *Med. Biol. Engng. Comput.*, 20(8); 1982.

Rajachar RM, Chow DL, Curtis CE, Weissman NA, Kohn DH: Use of Acoustic Emission to Characterize Focal and Diffuse Microdamage in Bone, *Acoustic Emission: Standards and Technology Update*, ASTM STP 1353, Ed. Vahaviolos SJ, ASTM; 1999.

Rudd R, Crandall J, Millington S, Hurwitz S, Hoglund N: Injury Tolerance and Response of the Ankle Joint in Dynamic Dorsiflexion, *Proceedings of teh 48th Stapp Car Crash Conference*, SAE No. 2004-22-0001; 2004.

Shapiro AJ, Johnson RM, Miller SF, McCarthy MC: Facial Fractures in a Level I Trauma Centre: The Importance of Protective Devices and Alcohol Abuse, *Injury Int. J. Care Injured*, 32, 353-56; 2001.

Strong B, Pahlavan N, Saito D: Frontal Sinus Fractures: A 28-Year Retrospective Review, *Otolar. H. N. Surgery*, 135, 774-9; 2006.

Wells J, Rawlings R: Acoustic emission and mechanical properties of trabecular bone, *Biomaterials*, Volume 6(July); 1985.

Wright TM, Vosburgh F, Burstein AH: Permanent Deformation of Compact Bone Monitored by Acoustic Emission, *J. Biomech.*, 14(6), 405-9; 1981.

CHAPTER 6:
THE TOLERANCE AND RESPONSE OF THE NASAL BONE TO BLUNT IMPACT

INTRODUCTION

The nasal bone has received little attention in studies investigating facial tolerance. It is relatively weaker and was shown in the NASS study of Chapter 1, to be the more frequent facial bone fractured in frontal collisions for both drivers and right-front passengers. Fractures of the nasal bone have been shown to be the most frequent among other forms of trauma such as violence, sports and falls (Muraoka 1995). Previous studies investigating the tolerance of the nasal bone have used cylindrical impactors by striking the nose with the flat end as well as with the rounded surface of the cylinder. Striking the nasal bone with the end of the cylinder applies a more focal load on the face without involving other structures. This method was utilized in a undocumented number of tests by Nahum *et al.* (1975). The area of the impact surface was 6.45 cm^2 and was covered with a thin piece of nickel foam padding. The impact severity of the nasal impacts was not documented; however, a minimal tolerance of 111-334 N was determined. A cylindrical impactor, representing a steering wheel rim was utilized in a separate study on the nasal bone (Nyquist 1986). A rigid, 25 mm diameter cylinder was oriented in the horizontal plane with the longitudinal axis aligned with the inferior orbital ridge. The cylinder was attached to an impactor weighing 32 or 64 kg and rode freely on bearings at the time of impact. The impacted head was held in an upright position with weak tape tethers. Impactor energy ranged from 241 to 815 J and resulted in peak forces of 2010 to 3890 N. All tests resulted in a nasal bone fracture at a minimum. Four of the eleven tests resulted in more extensive fractures involving the maxilla, frontal bone, zygoma and orbit. The average impactor penetration into the nose was 21 mm. The authors concluded that a 3 kN force appeared to be a threshold for generating fractures not limited to the nasal bones. The need for a deformable face for an Anthropomorphic Test Device (ATD) in order to produce realistic head acceleration was also discussed. Nasal impacts meant to represent a steering wheel rim have been performed in a separate study as well (Cesari 1989). In this study a horizontal bar impactor was used to strike the

nasal bone at speeds of 2.3 to 4.8 m/s. The higher impact severities were significantly higher than that necessary to cause a nasal fracture. In fact, Le Fort Type III fractures were generated at impact speeds of 3.86 and 3.67 m/s. Peak forces in this study ranged from 1790 to 3760 N. Combined, the previous work consists of 19 tests performed on the nasal bone.

Using a different approach to facial tolerance investigation, Allsop *et al.* demonstrated that facial bones are capable of supporting load after fracture has occurred (Allsop 2002, Allsop 1988). This is an important concept as it requires that the fracture force is determined separate from a force-time or force-deflection response. In their studies, Acoustic Emission (AE) was monitored and when a signal burst was detected, fracture was assumed to have occurred. When comparing the time of an AE burst, to the force-time relationship, the authors found that the facial bones would often fracture prior to peak force. This is an important consideration for nasal bone impacts due to the presence of posterior skeletal structures such as the frontal bone and maxilla which can continue to support impact forces after nasal bone fracture.

Knowing the precise time of fracture provides a non-censored measure of bone tolerance and therefore a more powerful data point for statistical analysis. Other studies have also used acoustic sensors to determine the fracture time of facial bones (Allsop 1988, Cormier 2008) and other bones (Funk 2002a, Kent 2008a, Rudd 2004, Wells 1985). The studies published by Cormier *et al.* (2008) and Rudd *et al.* (2004) discuss the use of a threshold voltage, over which fracture is denoted to have occurred. These studies established the fracture threshold by comparing the resulting AE between fracture and non-fracture tests. In the study by Cormier *et al.* (2008) additional validation was obtained by demonstrating that high magnitude AE occurred when striking bones with pre-existing fractures at low energy levels. This suggests that the high magnitude AE was due to the propagation of pre-existing fractures and not the result of the impact itself. The lack of acoustic sensors in the Nahum *et al.* studies suggest that their data are censored and that fracture is most likely occurring at a force less than the peak forces reported (Nahum 1968; Nahum 1975). The use of high impactor energies in the studies

by Cesari *et al.* (1989) and Nyquist *et al.* (1975), along with the occurrence of maxilla and frontal bone fractures demonstrate the continued structural support after nasal bone fracture.

Fracture of the nasal bone is expected to cause a change in the force-displacement response; however, the bony structures surrounding the nasal bones (i.e., frontal bone, maxilla) will continue to support the applied impact force. Therefore, peak forces in nasal bone impacts do not represent the tolerance of the nasal bone, but the strength of supporting structures as well. The statistical power of the censored data in previous studies limits their use in survival analyses. The data from previous studies are also limited in number and are derived from a variety of test methods. As a result, statistical analyses to estimate the risk of fracture as a function of impact severity are unavailable in the current literature. Additionally, force-displacement relationships characterizing the response of the nasal bones are not available. These data can be used in the development of finite element models or Anthropomorphic Test Devices (ATD) which can predict the occurrence of fracture. One such ATD is the FOCUS headform which has previously been validated for the prediction of ocular injuries (Kennedy 2007) and it is capable of measuring forces applied to the face through internal load cells.

The FOCUS headform consists of eight separate sensing regions supported by embedded load cells (Figure 51). These regions correspond to the frontal bone, nasal bone, zygoma, maxilla and mandible. Each load cell is capable of measuring forces in all three directions.

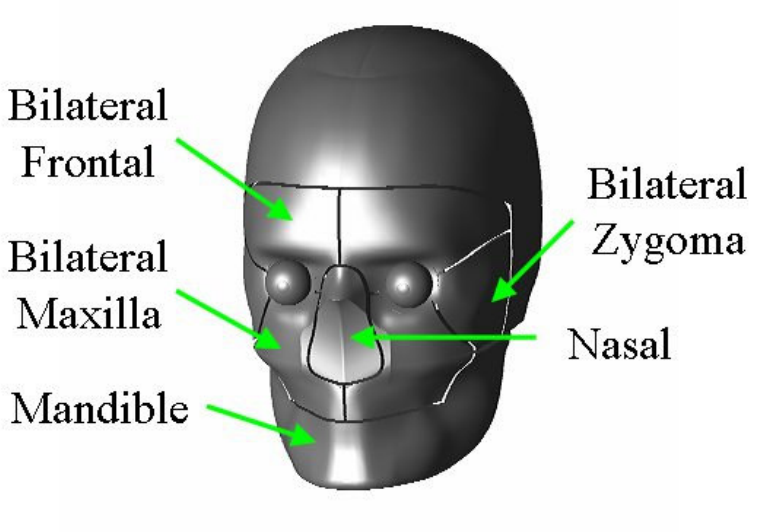

Figure 82: Load cell locations in FOCUS headform.

Defining force-deflection corridors for nasal bone impacts in cadavers will provide a basis for the implementation of the FOCUS headform in injury risk assessment.

The first goal of this study is to generate additional data in order to determine risk functions for the prediction of nasal bone fracture as a result of blunt impact. The second goal of this study is to develop an understanding of the cadaveric response to blunt impact and compare this response to the FOCUS headform.

METHODOLOGY

The data for this study were obtained by performing facial impacts on male cadaveric subjects. The methods of this study consist of striking the nasal bone with the flat face of an unpadded, cylindrical impactor, along with the use of acoustic emission sensors to determine the time of fracture onset. All heads were frozen and thawed prior to testing. A total of 25 male subjects ranging in age from 43 to 76 years were included in the study. Pre-test CT imaging was performed on 13 subjects and post-test CT imaging was performed on two specimens.

Anthropometry

Prior to testing CT imaging was performed on 13 of the subjects. From these images, the length and width of the nasal bone was measured along with the thickness of the nasal bone (Figure 83). An additional measurement was taken to determine the maximum length of the nose in the horizontal plane. A regression analysis was performed to evaluate the potential relationship between bone thickness and fracture tolerance for these specimens. Pearson correlation coefficients were determined to evaluate relationships between the anthropometric measurements taken from CT images and the mechanical response of the nasal bone.

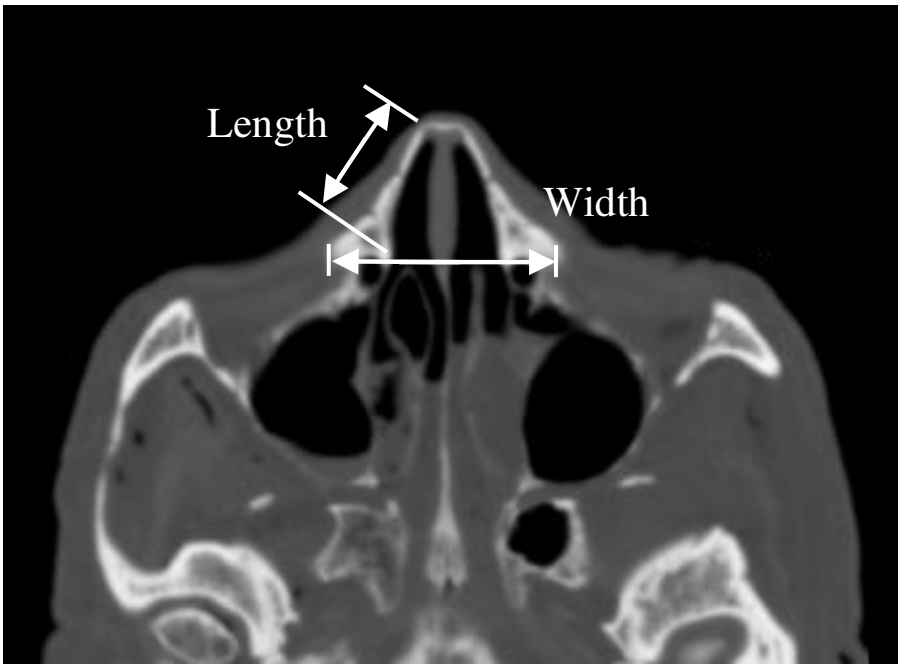

Figure 83: Measurements of nasal bone taken using pre-test CT images.

Specimen Preparation

The specimens were removed from the body and prepared by removing the scalp overlying the occipital region. This provided a rigid support at the posterior skull. Metal screws were inserted into the occiput to provide additional structure for the casting material to adhere to. Each head was then rigidly mounted to a semi-circular, polycarbonate support using Bondo. Consistent orientation between subjects was

obtained by vertically aligning the Frankfort plane prior to mounting. Specific anatomical landmarks were used to determine impact location. For nasal bone impacts, the impactor was centered over the palpated inferior surface of the nasal bone. Each impact was performed using a cylindrical, free-falling rigid aluminum impactor (3.2 kg) with a steel tip (Figure 53). The flat impacting surface had an area of 6.45 cm^2 (1 in^2) and was machined with a slight bevel to reduce edge effects.

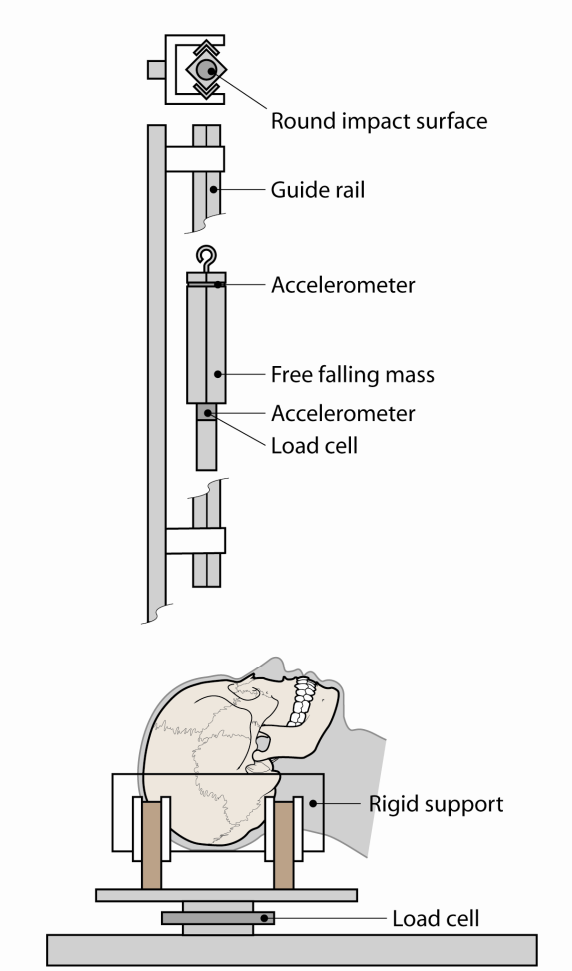

Figure 84: Schematic of test apparatus to be used in the current study.

Instrumentation

The specimens utilized in this study were tested in three separate series that consisted of slightly different instrumentation and data acquisition methods. In all cases an AE sensor (Micro30S, Physical Instruments, New Jersey) was mounted to the frontal bone, just

posterior to the apex of the forehead. The AE sensor was mounted directly to the bone by removing the soft tissue and periosteum and gluing the sensor in place with cyanoacrylate adhesive. This method has been used successfully in previous testing during this study and by others (Funk 2002a, Kent 2008a, Rudd 2004). In all tests, the rigid impactor was instrumented with two single-axis accelerometers (Endevco 7264B-2000, Endevco Corp., San Juan Capistrano CA). All data except AE data were filtered to CFC 300. Previous studies have utilized CFC 180; however the use of CFC 300 did not significantly alter the measured peak forces and was chosen to increase the likelihood of capturing small changes in impactor force during fracture (Bermond 1989, Bruyere 2000, Nyquist 1986). Impactor displacement was calculated by double-integrating the acceleration data. Contact between the impactor and subject was defined based on an impactor force of 10 N. Once the impactor force reached a level above 10 N, the displacement with respect to the nasal bone was set to zero and further motion was calculated by double integration. These aspects remained constant throughout the test series.

Series 1, subjects 1-14: The AE sensors were sampled at a rate of 2 MHz and all other instrumentation at 30 kHz. The acoustic emission data were acquired using a PC card supplied by the sensor manufacturer (PCI-2, Physical Instruments, New Jersey). Each AE sensor was attached to a preamplifier set to a gain of 40 dB. Impact force was obtained by multiplying the impactor acceleration by its mass. Impactor acceleration was determined by the average of the two attached accelerometers.

Series 2, subjects 15-24: The AE sensors were sampled at a rate of 5 MHz and all other instrumentation at 20 kHz. The acoustic emission data were acquired using an oscilloscope (TDS3000B Tektronix, Oregon). Each AE sensor was attached to a preamplifier set to a gain of 40 dB. A load cell (Denton, 8617JTF, Rochester Hills, MI) was attached to the tip of the impactor which was also instrumented with a single axis accelerometer (Endevco 7264B-2000, Endevco Corp., San Juan Capistrano CA). A load cell (Denton 1968, Rochester Hills, MI) was mounted to the head support to measure reaction forces. Impact force was obtained using the impactor load cell along with the inertially compensated tip mass.

Series 3, subjects 25-36: All parameters described in series two remained the same, with the exception of the AE preamplifier gain which was set to 20 dB in this series. Additionally, high-speed video was also recorded at a frame rate of approximately 4,000 fps. Impactor displacement calculated by double integrating impactor acceleration was verified using high-speed video analysis. This was performed by creating a second-order polynomial fit of the displacement obtained by video analysis.

To define the average force-displacement response of the nasal bone, a corridor was created to encompass the overall force-displacement response of the nasal bone. The response corridor was determined by the mean and standard deviation of the characteristic average (Lessley 2004). The characteristic average was created using the force-displacement response up to 90% of the peak force of each test. This ensured that only the linear portion of the response was included in the characteristic average calculation. The values for the corridor where determined using a custom Matlab program that implemented the algorithm described by Lessley *et al.* (2004). Stiffness of the nasal bone was also calculated up to 20% and between 20% and 80% of the peak force for each test.

Acoustic Emission

AE data were used to determine the force at which fracture initiated. Previous studies using AE data have denoted the onset of AE signal as the onset of fracture (Allsop 1988, Funk 2002a). Recently, studies have utilized a threshold to differentiate AE consistent with fracture from a baseline AE signal (Cormier 2008, Kent 2008b, Rudd 2004). Kent *et al.* (2008b) demonstrated that an AE burst corresponded with a sharp decline in force during phalange fracture.

To utilize AE data as a method of estimating the time at which fracture begins, a threshold must be established that differentiates normal background emissions from those associated with the fracture event. The methods used to establish the AE threshold was described in a previous publication (Cormier 2008: Chapter 4). To establish a

relationship between AE and fracture rather than the presence of an impact event, low-severity impacts were performed on specimens with pre-existing fractures. Due to the compromised integrity of these specimens, fracture propagation will occur at forces much lower than that required to initiate fracture. If high levels of AE are a result of fracture then high AE should be observed when the pre-fractured specimens are struck at lower levels of force. Once the threshold was established, the force corresponding to the occurrence of above-threshold AE was treated as the force required to initiate fracture.

Risk Function Analysis

Survival analyses were performed utilizing parametric and non-parametric techniques. For the parametric analysis, a Weibull model was assumed and fit to the data which contained fracture and non-fracture observations. The advantage of using a Weibull model is that the method used to determine the model parameters accounts for the fact that the non-fracture tests are right censored. The LIFEREG procedure within SAS (SAS Institute, Cary N.C) accounts for left and right censoring as well as non-censored data and was used to determine the parameter estimates for the Weibull model (Allison 1995, Cantor 2003). The Weibull distribution is advantageous because it is not forced to be symmetric, so it can accommodate risks that do not increase in the same way throughout the set of input variables. The Weibull CDF is given by,

$$CDF = 1 - \exp -(\lambda \cdot F)^{\gamma} \qquad \text{(Equation 2)}$$

Where, λ and γ are the scale and shape parameters, respectively, and F is the applied force. This function will provide an estimate of risk of injury using the maximum likelihood estimates of the scale and shape parameters. A non-parametric model was also created using the Kaplan-Meier method. The Kaplan-Meir method assumes the data are only right or non-censored and determines the risk of fracture based on the number of subjects at risk which sustain a fracture for a given force (Kleinbaum 2005). Measurements obtained using CT imaging as well as subject age were also included as covariates to assess their potential for predicting the risk of fracture.

FOCUS Headform Biofidelity

A series of nasal impacts were performed on the FOCUS headform in order to characterize its response to blunt impact. Impact severity was chosen to facilitate the development of risk functions for facial fracture based on results of the cadaver tests and the capability of the FOCUS headform. The impact was applied using the same apparatus used for the cadaver impacts (Figure 54). The impactor was instrumented with a single-axis accelerometer (Endevco 7264B-2000, Endevco Corp., San Juan Capistrano CA). A load cell (Denton, 8617JTF, Rochester Hills, MI) was attached to the tip of the impactor which was also instrumented with a single axis accelerometer (Endevco 7264B-2000, Endevco Corp., San Juan Capistrano CA) (Figure 53). All instrumentation was samples at a rate of 20 kHz. Forces measured by the internal load cells were recorded and compared to impactor forces and examined for load-sharing between facial regions. The stiffness of the FOCUS response was determined up to 20% and between 20% and 80% of the peak force for comparison to the cadaveric response.

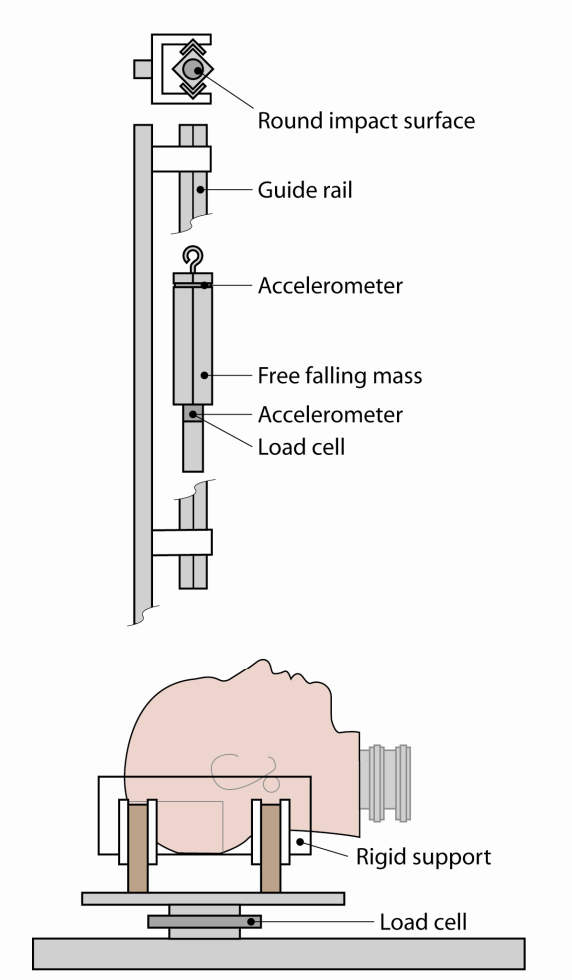

Figure 85: Apparatus used for FOCUS impacts.

RESULTS

A total of 25 tests were performed to determine the tolerance of nasal bone to blunt impact (Table 12). The peak force during each impact ranged from 715 to 2260 N. A nasal fracture was produced in 23 tests. An Acoustic Emission (AE) signal was measured in every test using a sensor mounted on the frontal bone. A threshold voltage of 9 volts was established for series one, 5 volts for series two and 2 volts for the third series. These thresholds were based on the magnitude of AE during fracture (Figure 47) and non-fracture (Figure 48) tests. Therefore, the force corresponding to an AE above the threshold was utilized as the force to initiate fracture in the statistical analysis.

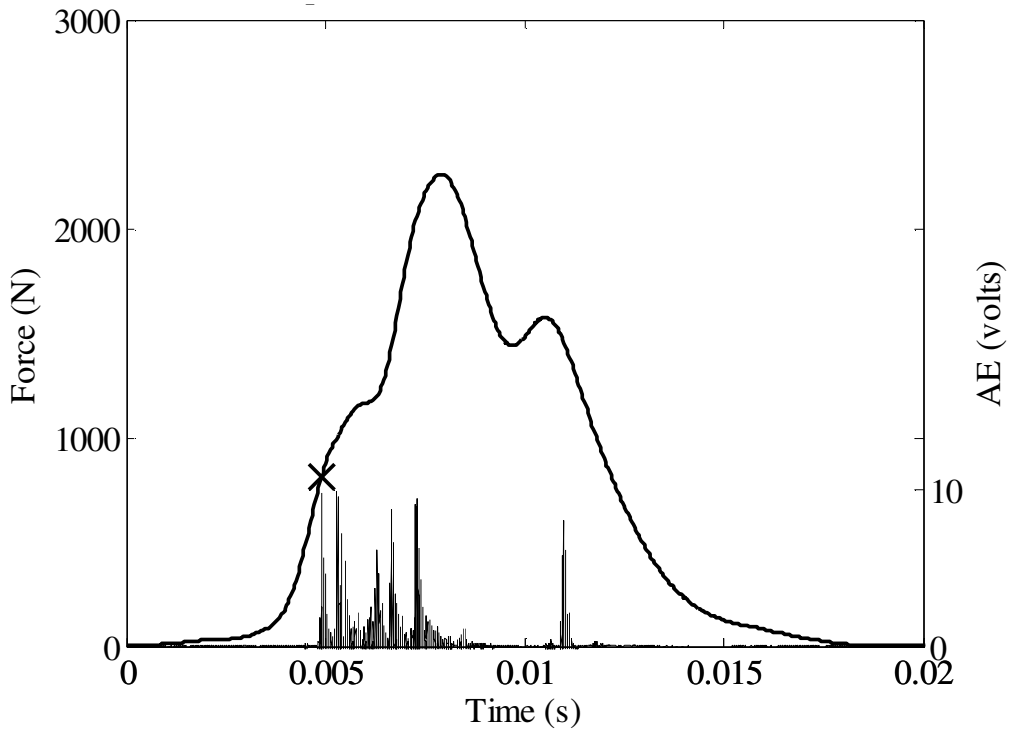

Figure 86: Acoustic emission and force during an impact resulting in a nasal fracture.

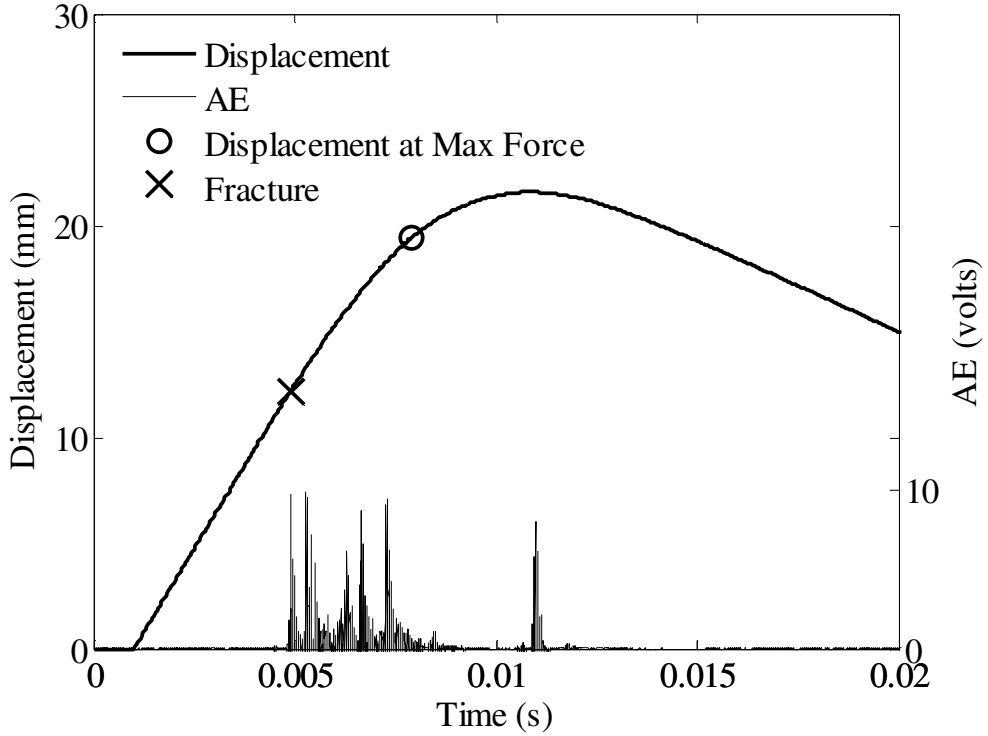

Figure 87: Force-displacement response from nasal impact shown in Figure 47.

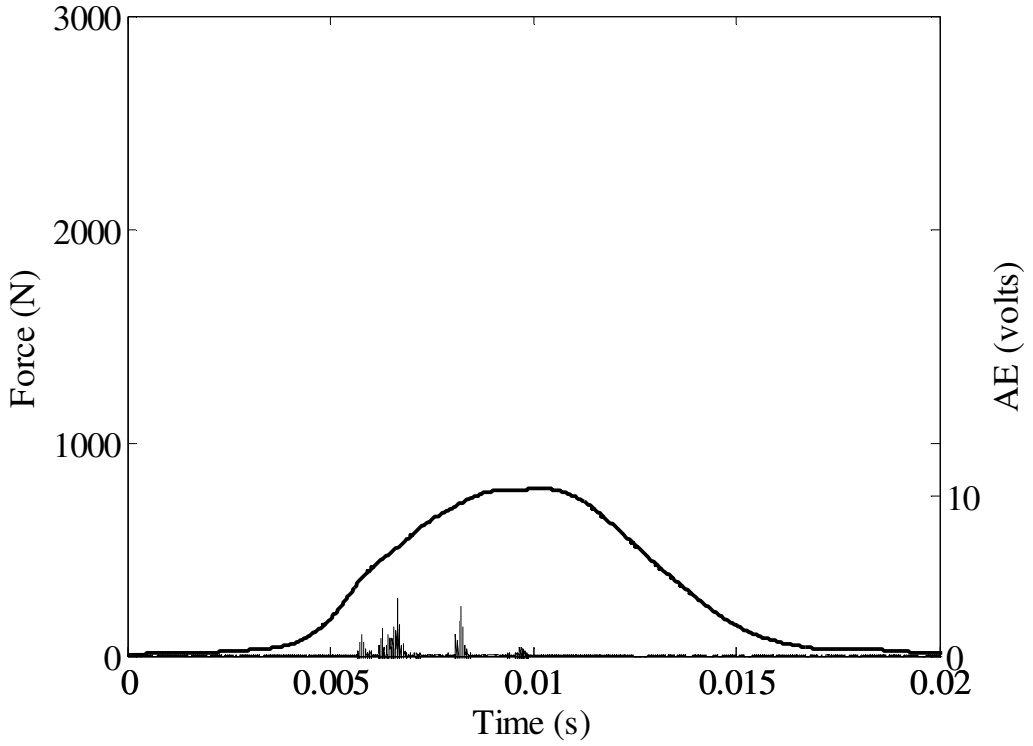

Figure 88: Impact force and AE during nasal impact resulting in no fracture.

Table 12: Summary cadaver characteristics and test results for nasal bone impacts. na = not available

Subject	ID	Age	Height (cm)	Weight (kg)	Impactor Energy (J)	Peak Force (N)	Fracture Force (N)
1	SM58	61	168	69	8	1774	1767
2	SM60	41	170	64	16	1764	1402
3	SM56	57	170	84	4	784	
4	SM57	75	165	65	16	2260	810
5	SM61	76	170	44	4	828	605
6	SM62	43	183	112	8	1355	598
7	34237	66	na	na	8	1406	1000
8	34236	54	na	na	8	1924	1426
10	34249	72	na	na	12	2081	752
12	33995	49	na	na	10	1429	228
13	34403	79	na	na	10	1734	781
14	SM56	57	170	84	4	715	
14	5758	83	175	73	8	1804	152
15	5791	94	163	64	8	1378	214
17	5735	67	180	82	8	1581	533
19	5757	84	183	109	8	1431	106
21	5675	76	152	91	8	1088	375
23	5760	87	163	75	8	1438	428
24	5850	94	165	54	8	1045	305
26	5840	85	150	79	16	1490	182
27	5821	72	163	59	16	1110	502
29	5818	81	175	88	16	1927	845
31	437	67	na	na	16	1167	813
33	5805	81	177	79	16	1424	903
35	5869	74	191	86	16	2185	542

Once fracture force was determined, its relationship with various impact and subject descriptors was investigated. The range in fracture force was consistent among the various energy levels utilized (Figure 89). Fracture force had no statistical correlation between impactor energy and, consequently impactor velocity ($p = 0.59$) (Figure 90).

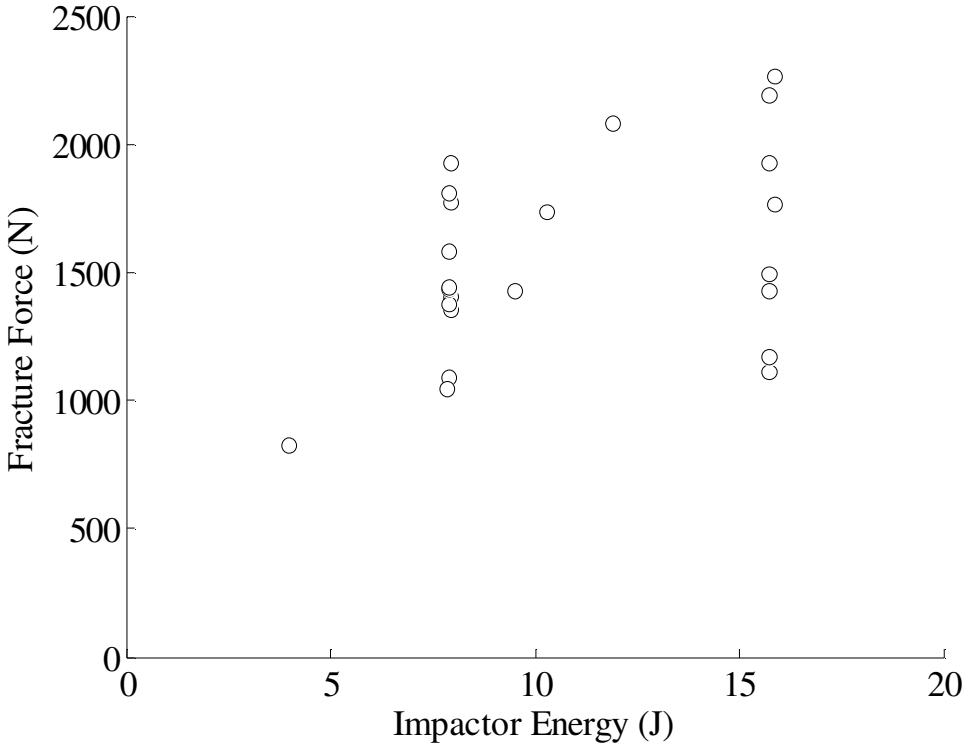

Figure 89: Impactor energy and nasal bone fracture force.

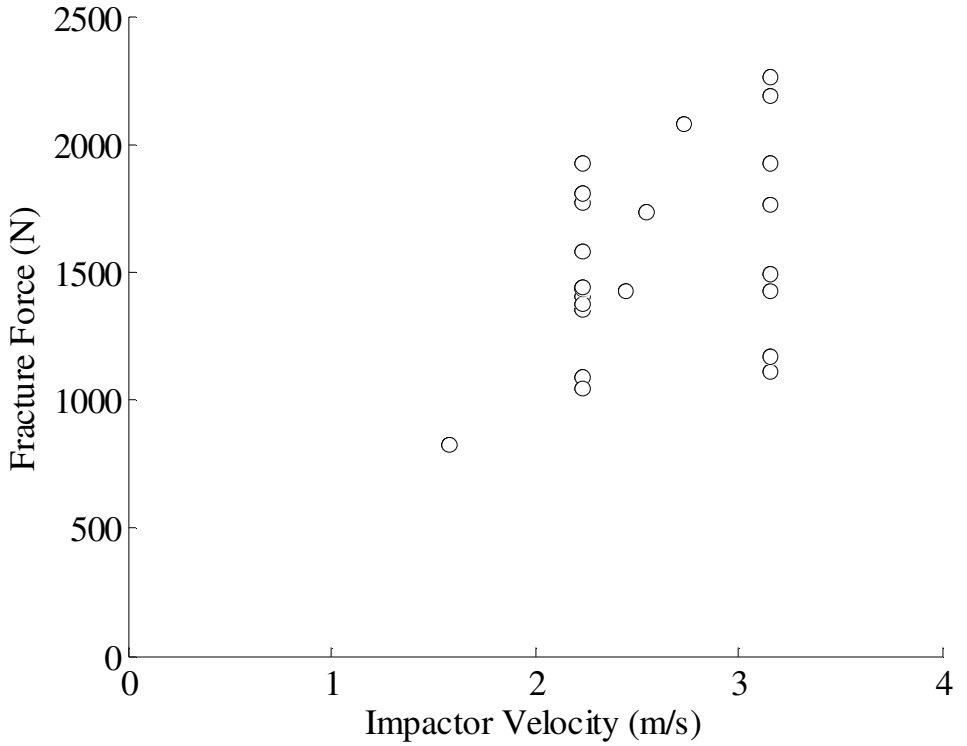

Figure 90: Initial impactor velocity and nasal bone fracture force.

Fuji film placed on the impactor surface prior to impact was used to estimate contact area during the event. The area obtained through this analysis represents the maximum area of contact and not necessarily the area at fracture. The average contact area was 1.8 cm^2 (std. dev.=1.6) and had a weak correlation with peak force (R^2 = 0.53, p = 0.007) (Figure 91). This area is less than half of the available contact area of 6.45 cm^2. Peak pressure calculated using the estimated area was not related to impactor energy (p = 0.66) (Figure 92).

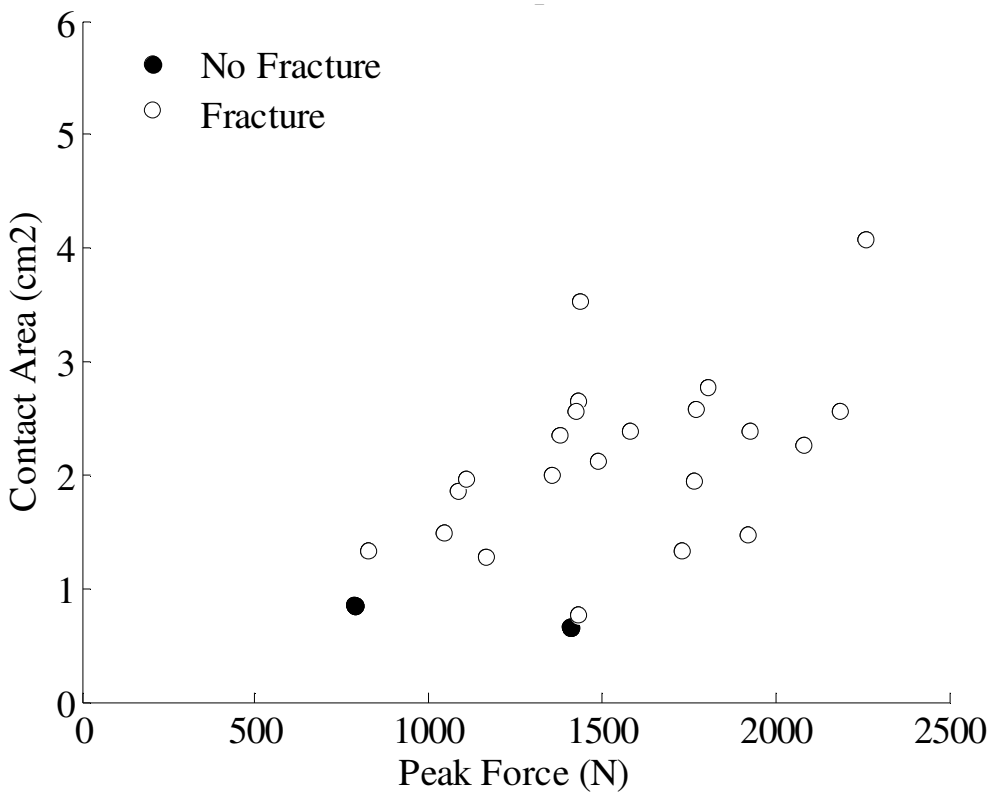

Figure 91: Relationship between contact area and peak force during nasal bone impact.

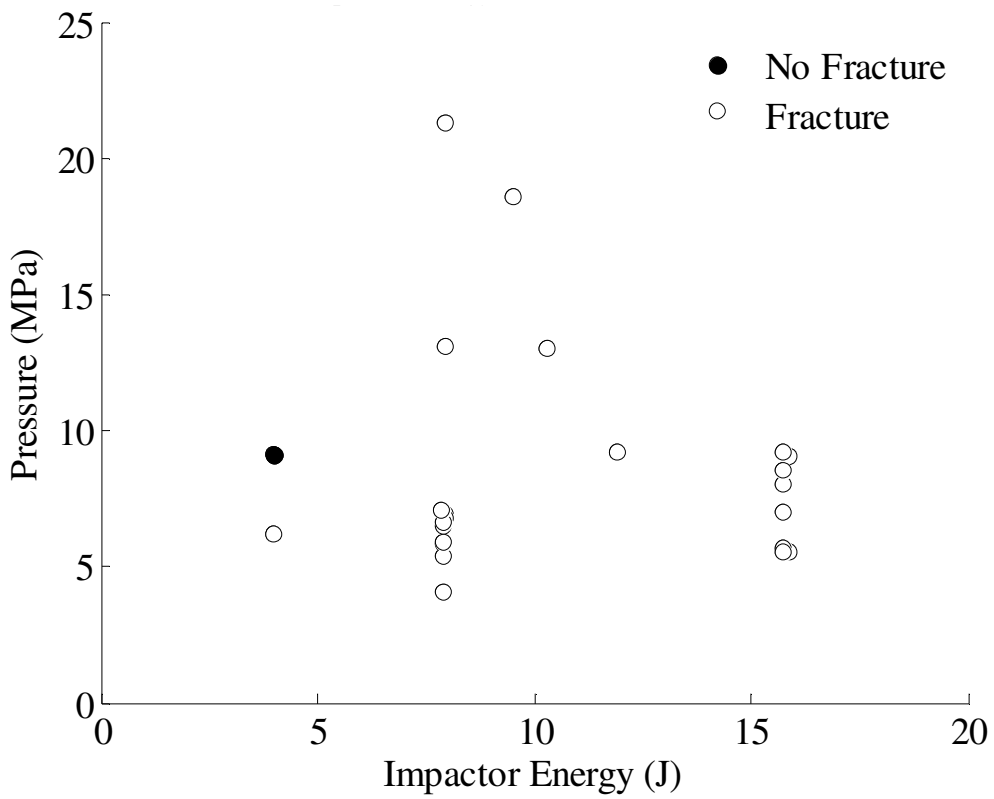

Figure 92: Nasal bone contact pressure as a function of impactor energy.

Anthropometry

Pre-test CT imaging was used to measure head width and depth, nasal bone width, length and nose length in 13 of the tested subjects (Figure 83). The average nasal bone length in the axial plane was 2.3 cm (SD = 0.31) with a maximum of 2.9 cm and a minimum of 2.0 cm. The distance between the base of the two nasal bones was 2 cm on average (SD = 0.44) with a maximum of 2.8 cm and a minimum of 1.3 cm. The maximum length of the nose in the axial plane was 3.4 cm on average (SD = 0.38) with a maximum of 4.2 cm and a minimum of 2.65 cm. The length of the nose measured in the axial plane was statistically correlated with head width ($p = 0.023$). There was a weak positive correlation between the maximum force in each test and the width of the nasal bone ($p = 0.05$). No correlation was found between the nasal dimensions and the stiffness of the nasal bone (all $p > 0.45$). With respect to fracture force, none of the nasal measurements were statistically correlated to fracture force, including nasal bone length ($p = 0.45$) and width ($p = 0.24$) (Figure 93) and head depth and width. Head width had the strongest correlation, although not statistically significant ($p = 0.18$) which demonstrated a

negative correlation between head width and fracture force (Figure 94). There was a negative, statistically significant ($p = 0.006$) correlation between age and fracture force (Figure 95) which was illustrated further in the risk of nasal bone fracture. The correlation coefficient between age and fracture force was -0.53.

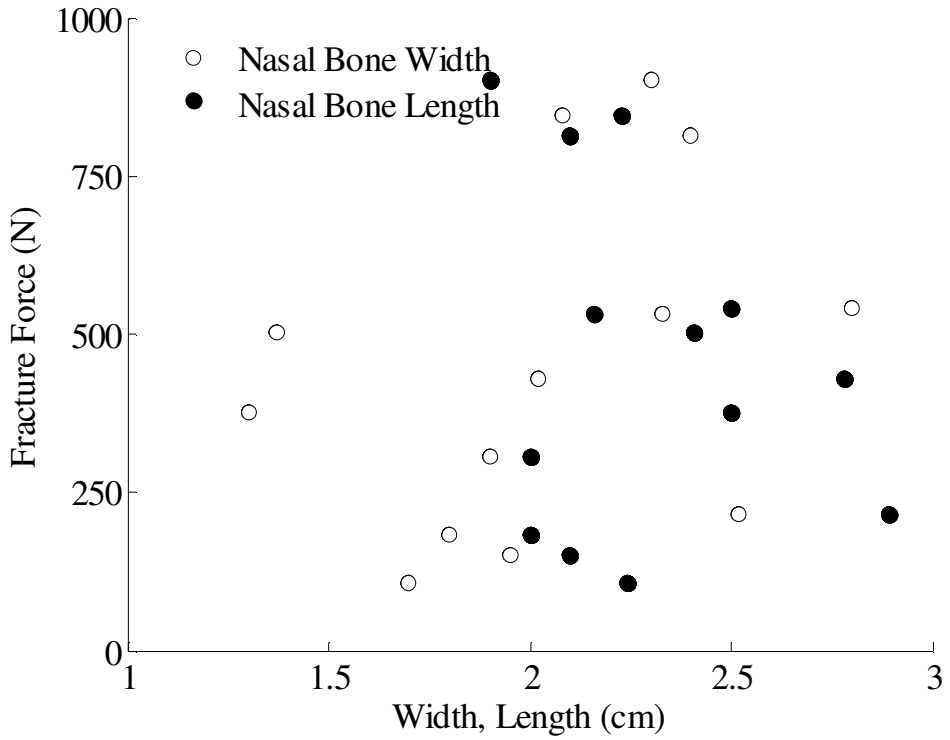

Figure 93: Nasal bone fracture force with respect to nasal bone width and length measured using CT images.

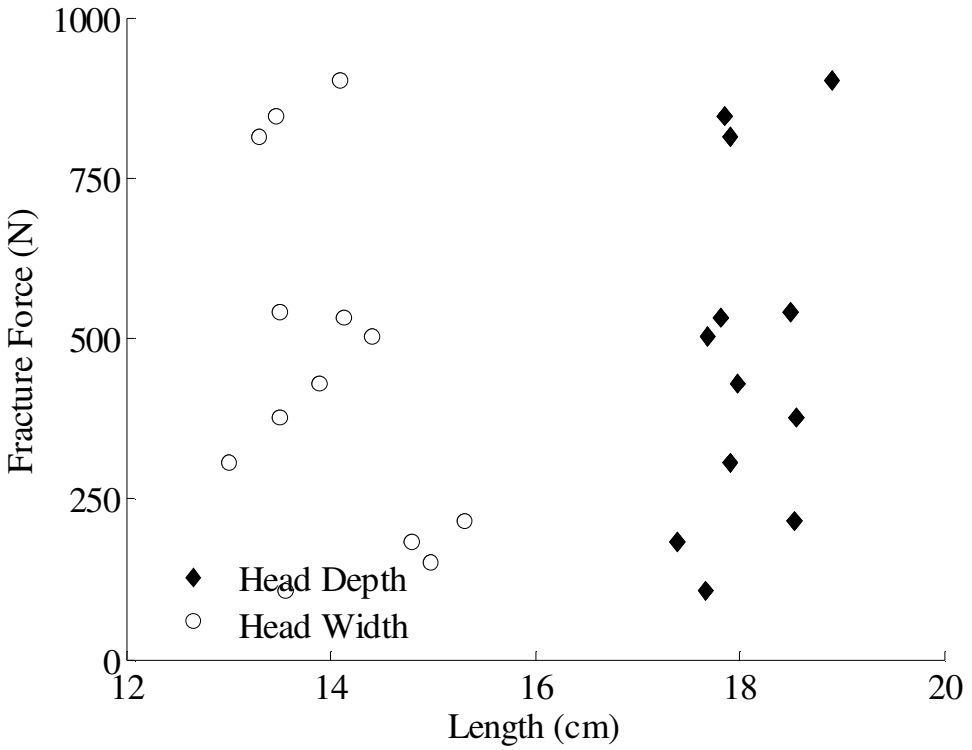

Figure 94: Nasal bone fracture force with respect to head depth and width measured using CT images.

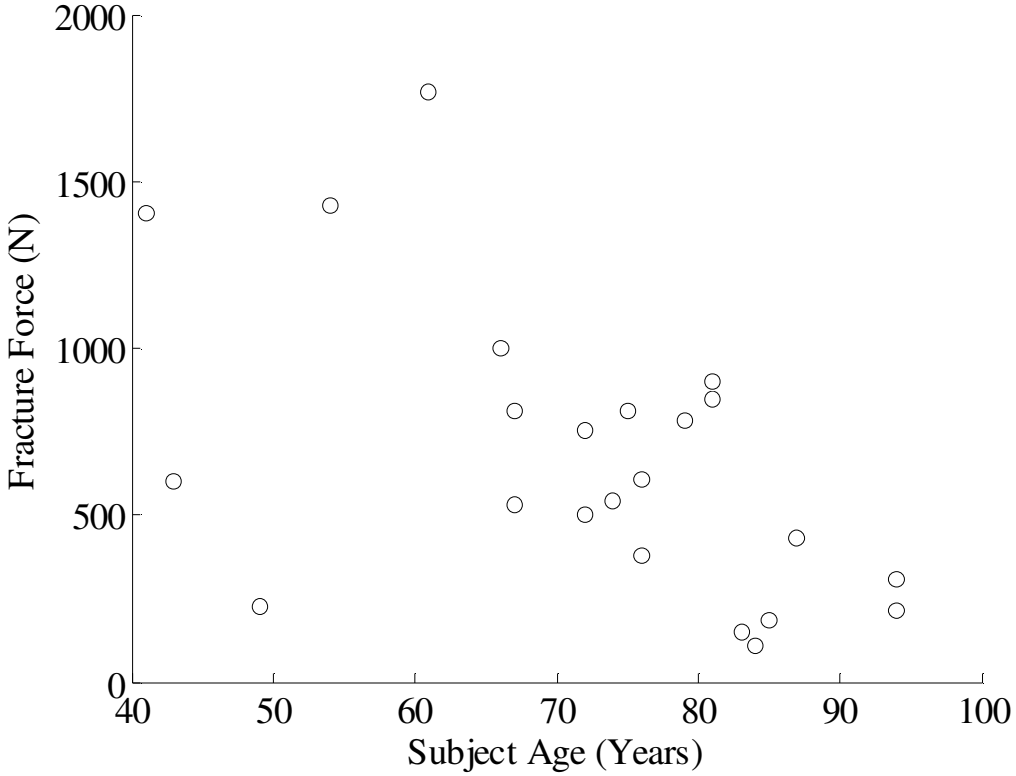

Figure 95: Relationship between subject age and nasal bone fracture force.

Risk of Nasal Bone Fracture

The risk of fracture was estimated using a Kaplan-Meir non-parametric estimate and a two-parameter Weibull distribution (Figure 67). Risk estimates were generated using all data and using only tests resulting in a fracture. The 50% risk of fracture was 600 and 540 N respectively. The anthropometric measures were included in the model to evaluate there utility in predicting nasal bone fracture. None of the measures were found to be a statistically significant parameter in predicting fracture within the reduced dataset (n=13). The model parameters between the two models were relatively equal (Table 13).

Table 13: Parameters for Weibull models of nasal bone fracture risk.

		95% Confidence Interval		
Model	**Estimate**	**Lower**	**Upper**	**Parameter**
All Data	0.0013	0.0016	0.0010	Scale
	1.66	1.21	2.29	Shape
Fracture Only	0.0013	0.0018	0.0010	Scale
	1.63	2.39	1.24	Shape

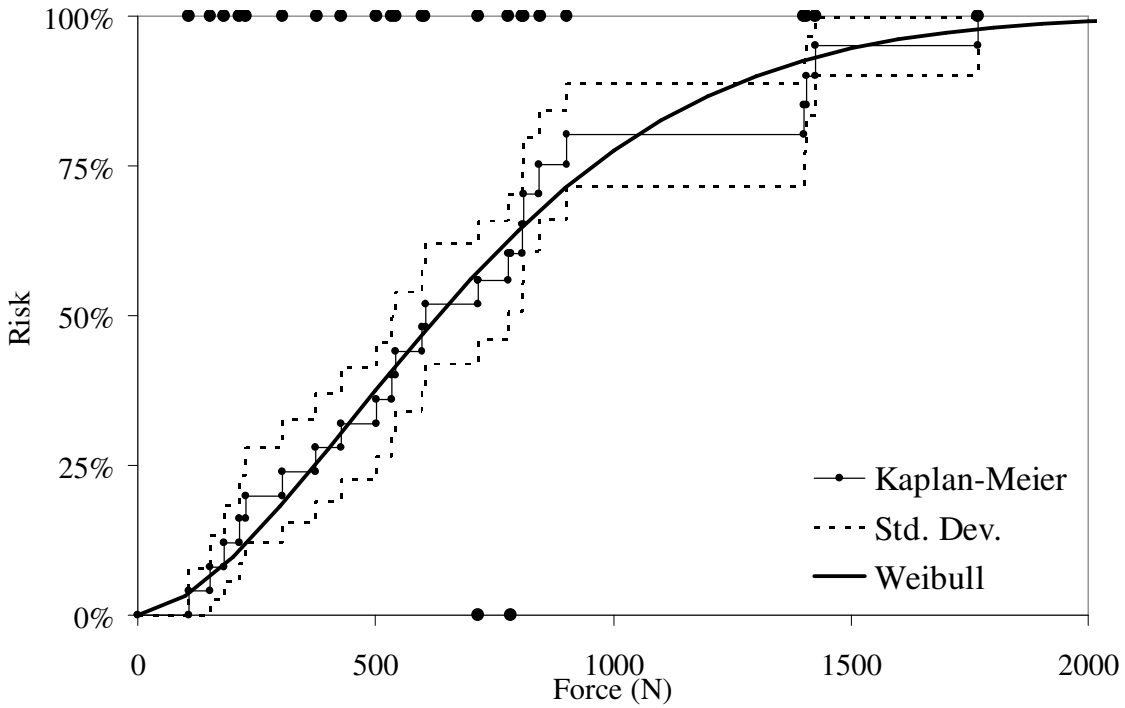

Figure 96: Risk of nasal bone fracture based on fracture and non-fracture data.

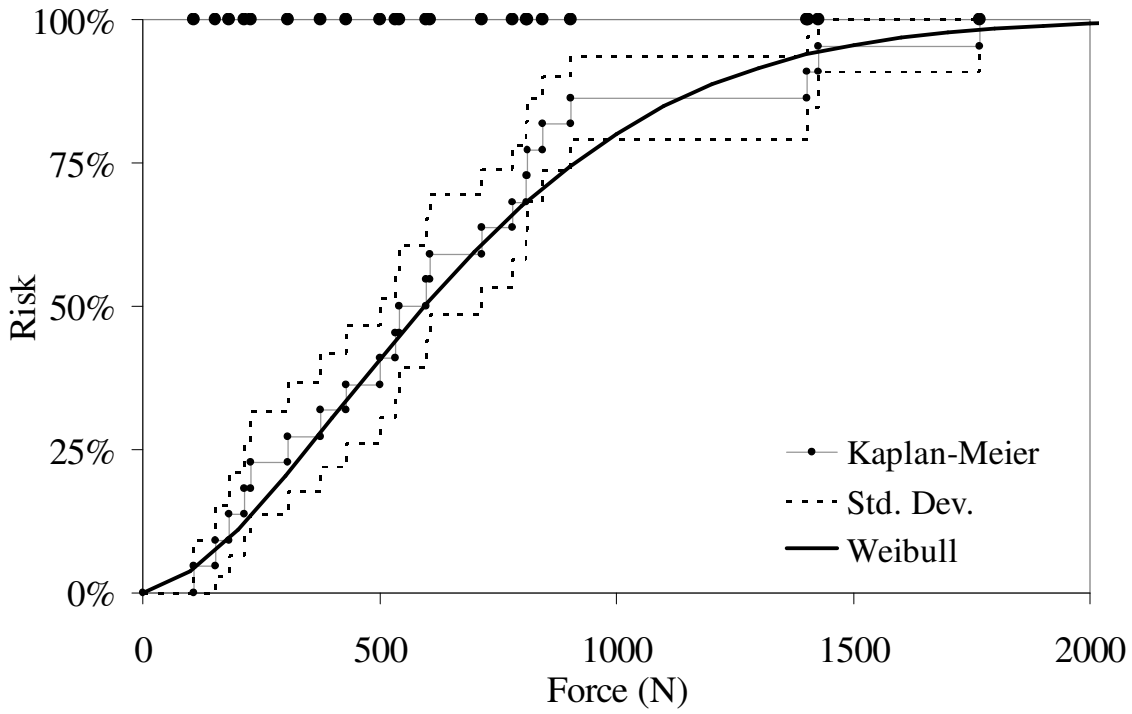

Figure 97: Risk of nasal bone fracture based on fracture data only.

Age was available for the entire dataset and when added to the Weibull model as a covariate, it was found to be a statistically significant ($p = 0.0003$) parameter. The model with age as a covariate produced similar results to the overall model at an age of 70 years, which is the mean age for the subjects included in this study (Figure 98). Non-fracture tests were included in the model with age as a covariate. Use of these curves should be limited to a qualitative sense until additional data can be added to improve the confidence in the estimates.

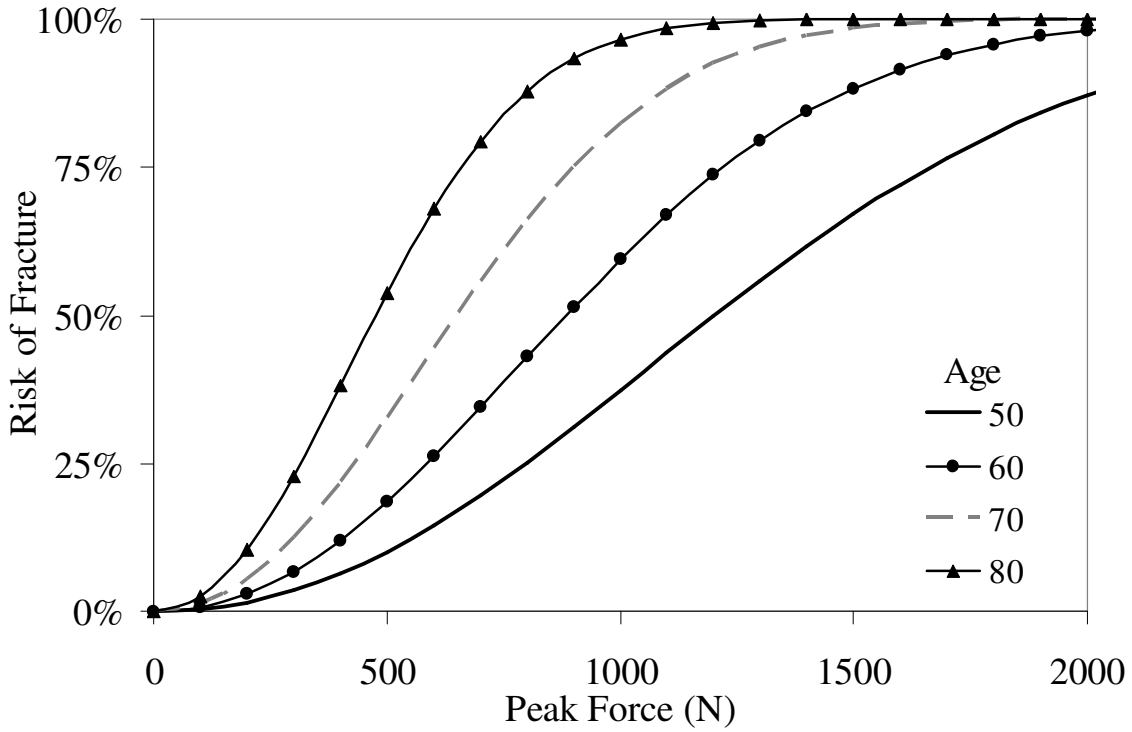

Figure 98: Risk of nasal bone fracture with age as a covariate.

Force-Displacement

In all cases force-deflection relationships were determined using double integration of impactor acceleration data. Impactor displacement determined from double integration of accelerometer data was almost identical to that determined from high speed video (mean $r^2 = 0.98$). As a result of the wide variation in subject anthropometry, the displacement at which engagement of the actual nasal bone differed greatly between subjects. This created a wide variation in the displacement achieved during the toe region of the force-displacement response (Table 14).

Table 14: Nasal bone stiffness determined at 20% and between 20 and 80% of peak force.

	Initial Stiffness (N/mm)	**Secondary Stiffness (N/mm)**	**Toe Length (mm)**
Mean	55	201	6
Standard Deviation	56	118	4

The majority of the tests exhibited an initial low stiffness for approximately the first 5 mm of displacement (Figure 99). Within this group all tests resulting in fracture

exhibited some degree of variation in stiffness with increasing displacement. In the majority, an initial peak in force was followed by a stiffer response to a higher force before coming to a stop. The test not resulting in fracture did not exhibit a change in stiffness. The five tests that did not fit the category above demonstrated a relative lack of a toe region and reached higher peak forces (Figure 100). All but one of these tests exhibited an initial peak in force with a subsequent higher peak at the end of impactor travel.

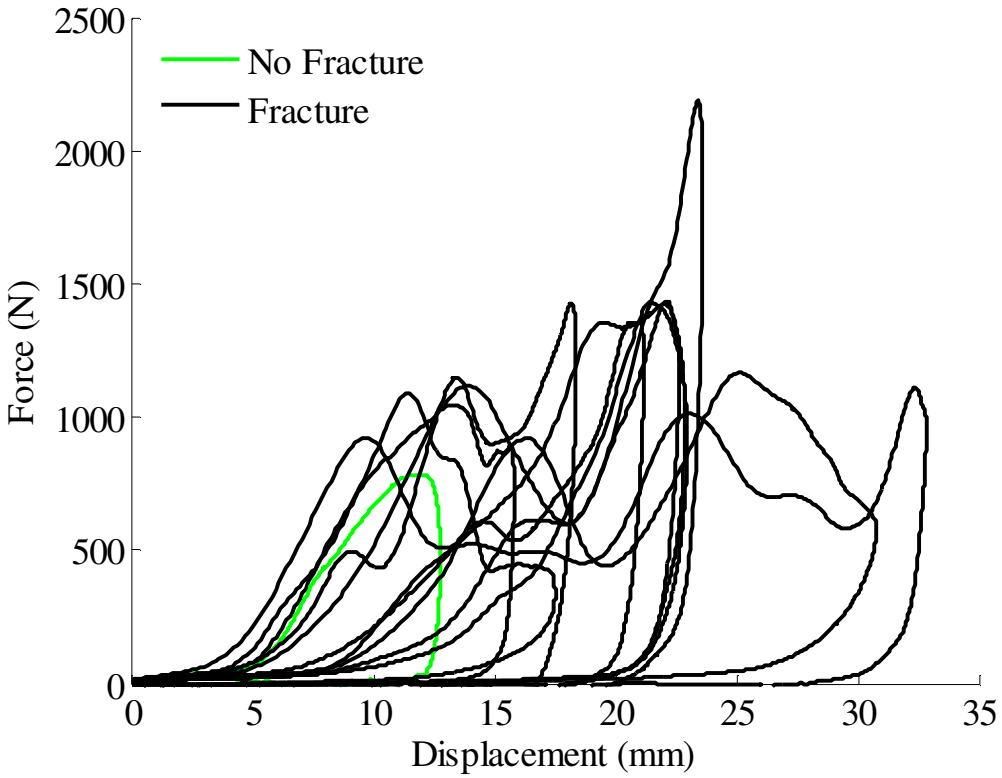

Figure 99: Force-displacement response during cadaveric tests with lower initial stiffness.

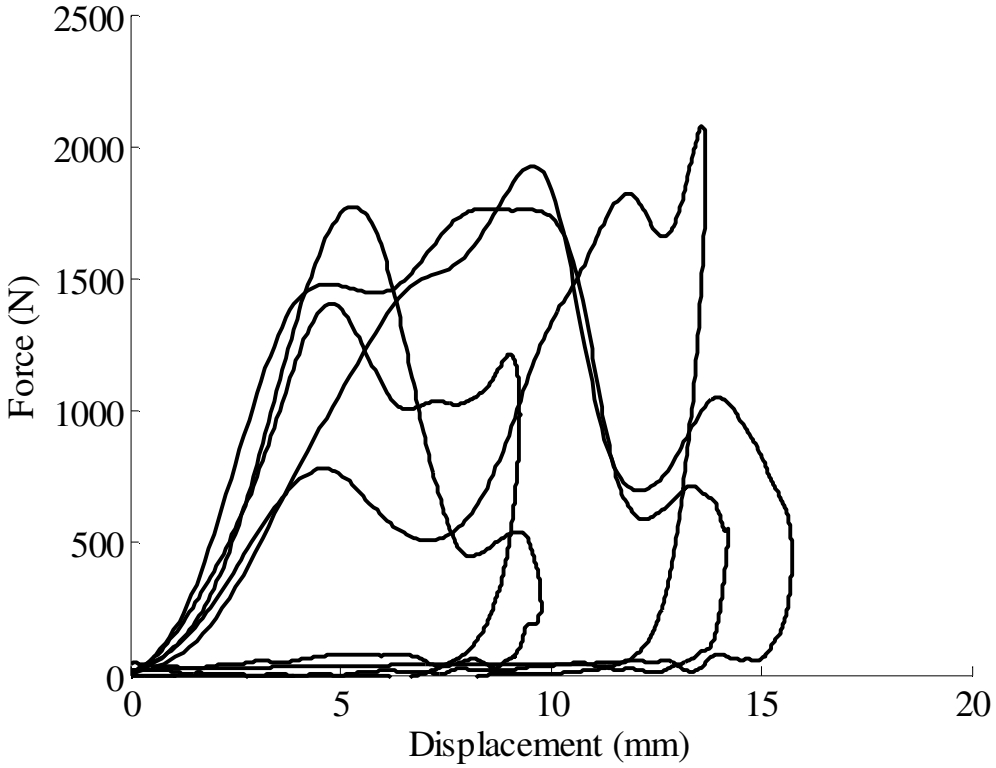

Figure 100: Nasal bone force-displacement response in cadaveric tests with a short toe region.

The corridor of the force-displacement response of the nasal bone was described by calculating the characteristic average (Figure 101). All nasal bone impacts were included in the characteristic average calculation. The upper and lower bounds of the corridor were defined by the standard deviation of the force and displacement data. The upper bound of the corridor does not pass through zero due to the presence of subjects exhibiting stiffer responses with little impactor motion,

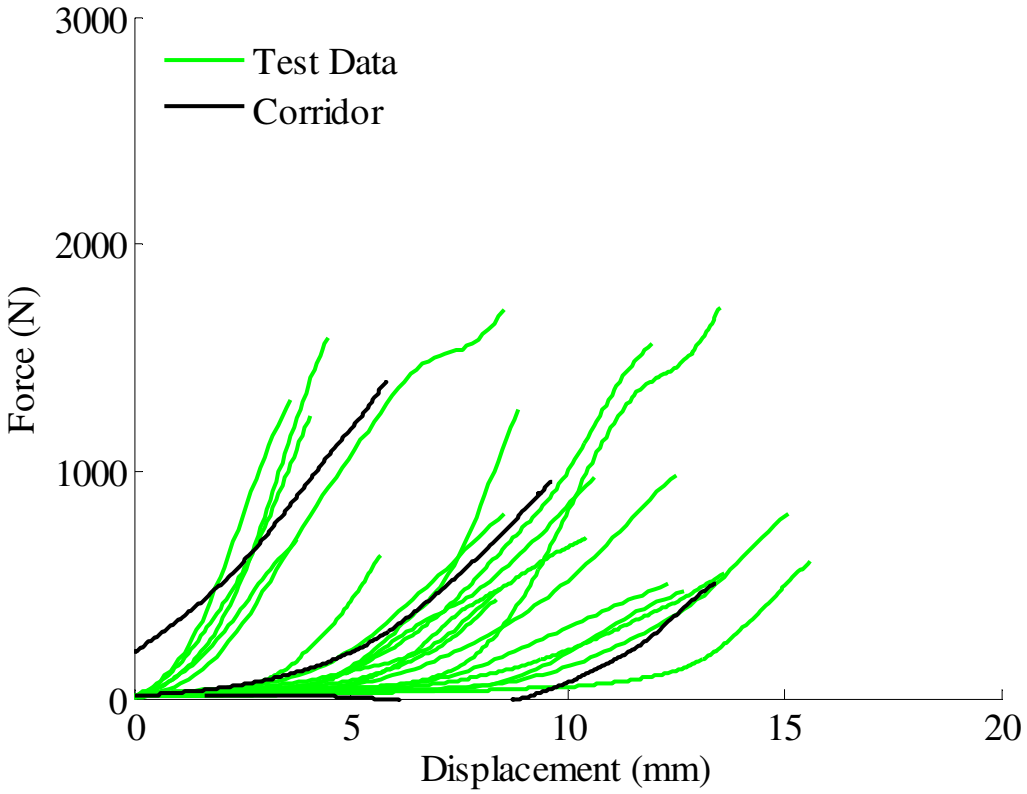

Figure 101: Force-displacement response of cadaver nasal impacts.

FOCUS Headform Biofidelity

In order to evaluate the biofidelity of the nasal region of the FOCUS headform, a series of four tests were performed at a location which matched that used in the cadaver tests. The severity of all nasal impacts was equal. The impactor velocity was 2.2 m/s, which corresponded to an impactor energy of 8 J. In all of tests the internal load cell measures were monitored and found to be very similar to the forces measured by the impactor. On average, the internal and impactor peak forces differed by 2%.

The four impacts performed at the matched position demonstrated a repeatable force-displacement response (Figure 102). These tests produced an average peak force of 4110 N (SD = 37). The response of the FOCUS was elastic and resulted in the impactor rebounding off the dummy after initial impact.

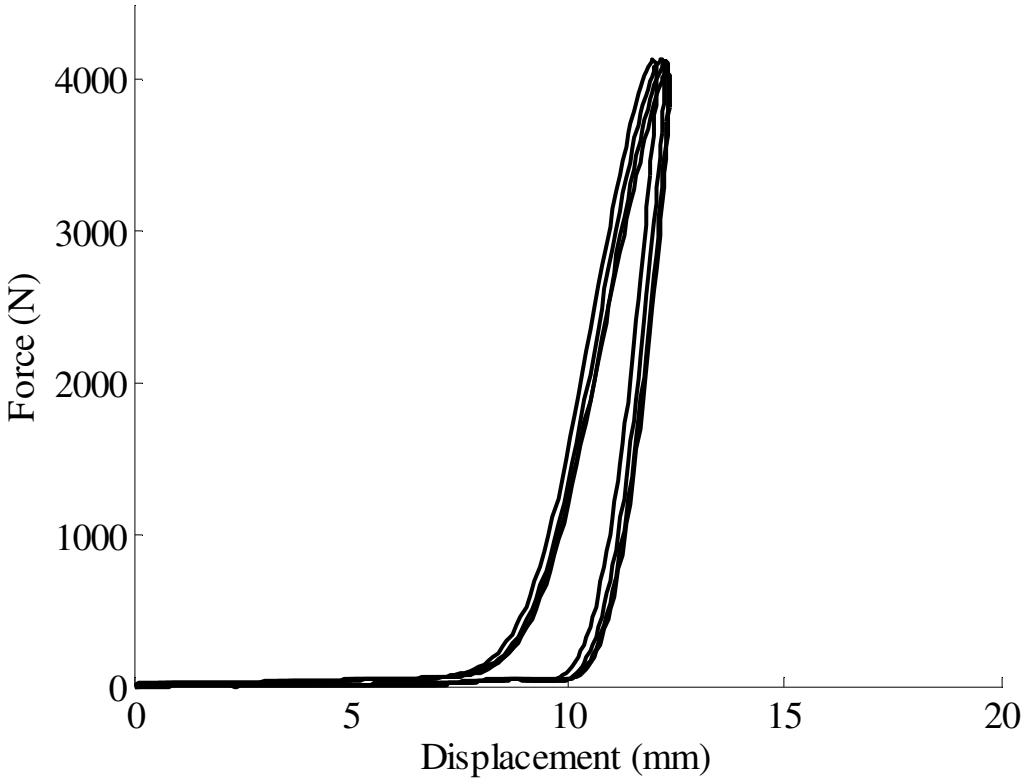

Figure 102: FOCUS force-dispalcement response for nasal impacts.

The extended toe region of the FOCUS nasal response is a result of the soft nature of the nasal insert used between the reaction surface for the nasal bone and the FOCUS skin. The characteristic average was used to describe the response corridor of the FOCUS nasal region at position 2 (Figure 103) and this was compared to the cadaveric response (Figure 104). The soft nasal structure of the FOCUS headform resulted in a longer toe region than exhibited in the cadaver response. Due to the delayed stiff response, the peak forces achieved in the FOCUS tests were significantly higher than the nasal corridor. The average stiffness of the FOCUS due to impact at this position was 1365 N/mm (SD = 51).

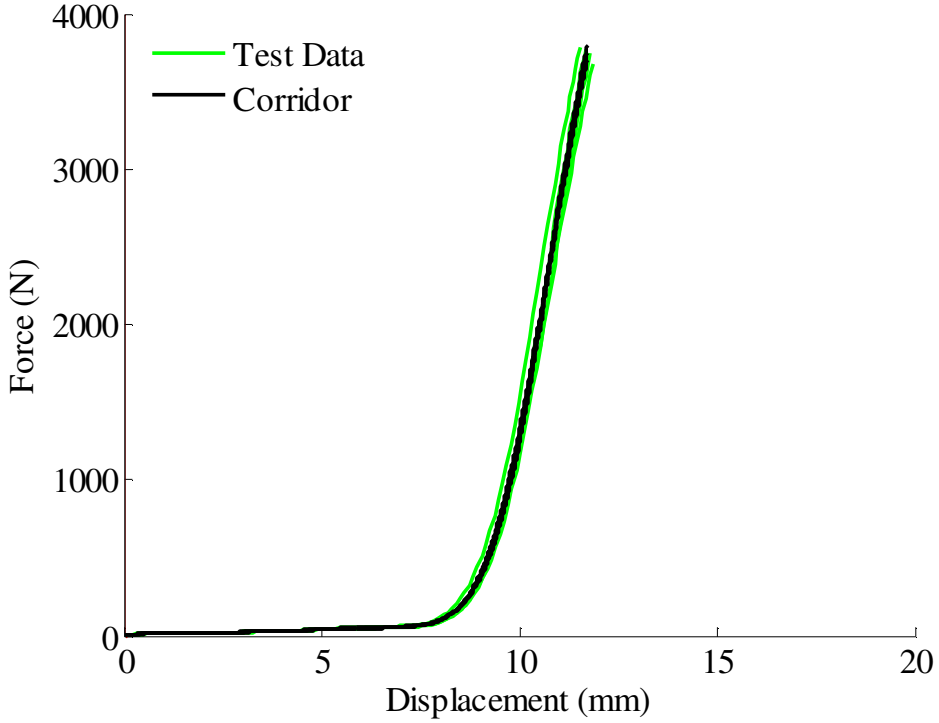

Figure 103: Characteristic average of FOCUS nasal impacts at Position 2.

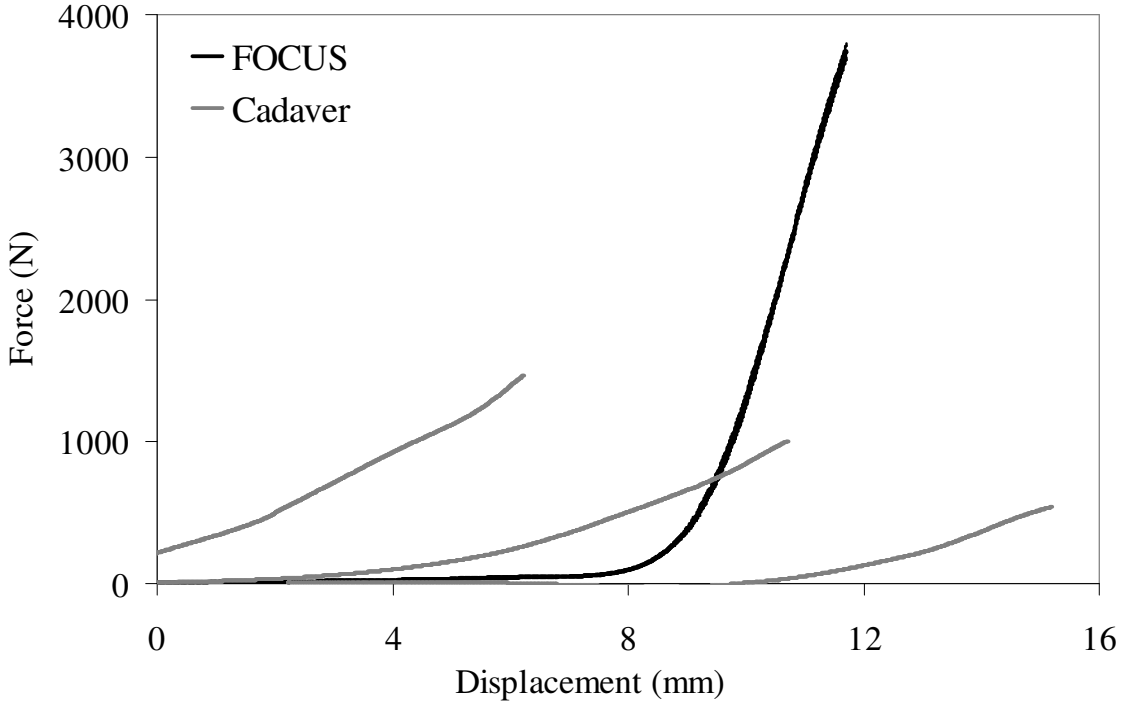

Figure 104: Response corridors for cadaver and FOCUS nasal bone impacts.

To demonstrate the sensitivity of the FOCUS nasal response, a series of tests were performed at four additional locations along the nose (Figure 105). Impacts performed at

the top of the nose do not interact with the nasal insert and, therefore, there was a relative lack of a toe region in these impacts. As the impact location progressed downward, the effects of the insert resulted in a longer toe region as well as a lower peak force.

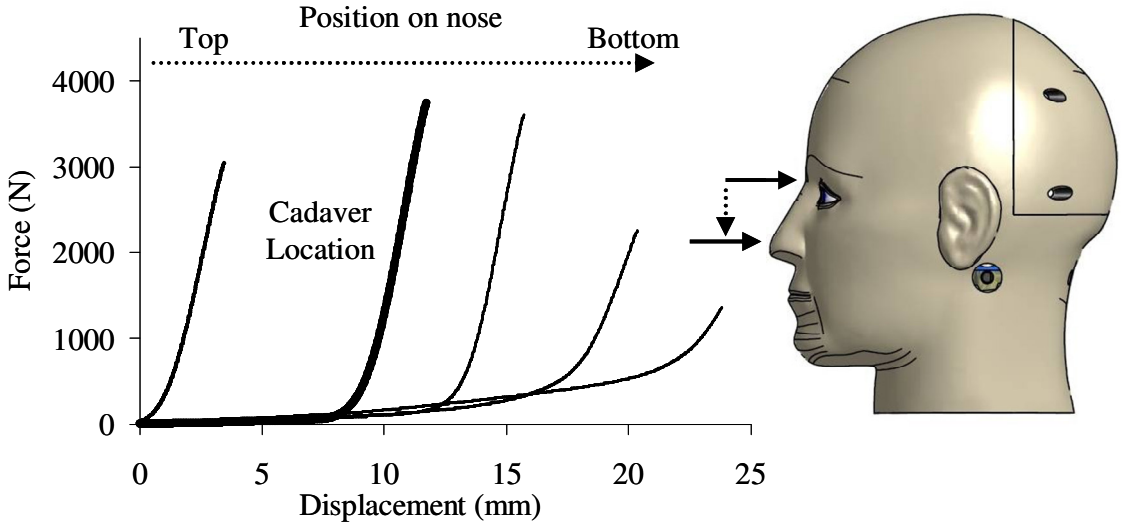

Figure 105: Relative change in FOCUS force-displacement response by nasal impact location.

DISCUSSION

The purpose of this study was to define the response of the nasal bone to blunt impact and to determine a relationship between applied force and risk of fracture. Using a total of twenty-five impacts, force-displacement corridors were defined for the nasal response to blunt impact. Due to the variation in nasal geometry, the toe region of the response varied significantly between subjects. The length of the nasal bone and nasal geometry will influence the depth at which the impactor will interact with the nasal bone after initial contact with the nose (Figure 106). In this study, five subjects exhibited a higher initial stiffness than the remaining subjects. The variation in the toe region between subjects was related to the shape of the nose. In the five tests with a relative lack of a toe region, the angle of the nose was relatively vertical. This allowed early contact with the nasal bones rather than deforming the nose first. In tests with a relatively longer toe region, the angle of the nose resulted in more impactor interaction, creating a bi-linear response.

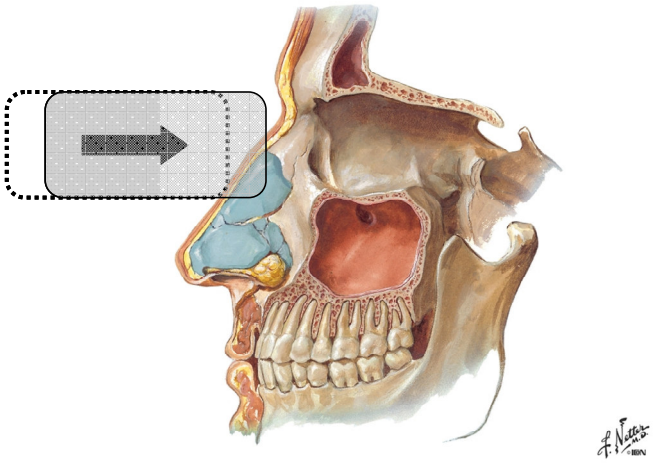

Figure 106: Penetration of impactor to nasal bone following initial contact with nose.

One common aspect among the force-deflection response was the presence of a pronounced initial peak, followed by a secondary higher peak occurring as the impactor motion was arrested. Using acoustic emission sensors to detect that onset of fracture, it was found that fracture occurred prior to the initial peak in force. This is consistent with the idea that following nasal bone fracture, the impactor continues to translate toward the face and begins to interact with additional facial structures. These structures can include the frontal process of the maxilla and the frontal bone. Interestingly, fractures of the nasal bone were usually isolated to the nasal bone by the sutures with the maxilla and frontal bones. This phenomenon illustrates the importance of acoustic emission sensors in determining fracture onset rather than relying on peak forces, since additional structures (the frontal bone and maxilla) can support higher loads after the nasal bone has fractured and become structurally unstable. These structures are stronger and therefore capable of generating higher reaction forces following nasal bone fracture.

Two previous studies have reported peak forces resulting from nasal impacts (Cesari 1989, Nyquist 1986). These studies struck the nasal region using the side of a cylindrical impactor to represent steering wheel impact. Peak forces measured during the studies by Cesari *et al.* (1989) (Figure 79) and Nyquist *et al.* (1986) (Figure 108) were significantly higher than those of the current study. This is consistent with the higher range of impactor energies utilized in their tests as well as the relative size of the contact area available. The impactor energy utilized by Nyquist *et al* (1986) was over an order of

magnitude greater than that in the current study and over twice that used in the Cesari *et al.* (1989) study. Despite the larger impactor energy, the peak forces achieved in their study were less than twice those achieved in the current study and approximately equal to those obtained in the Cesari *et al.* (1989) study.

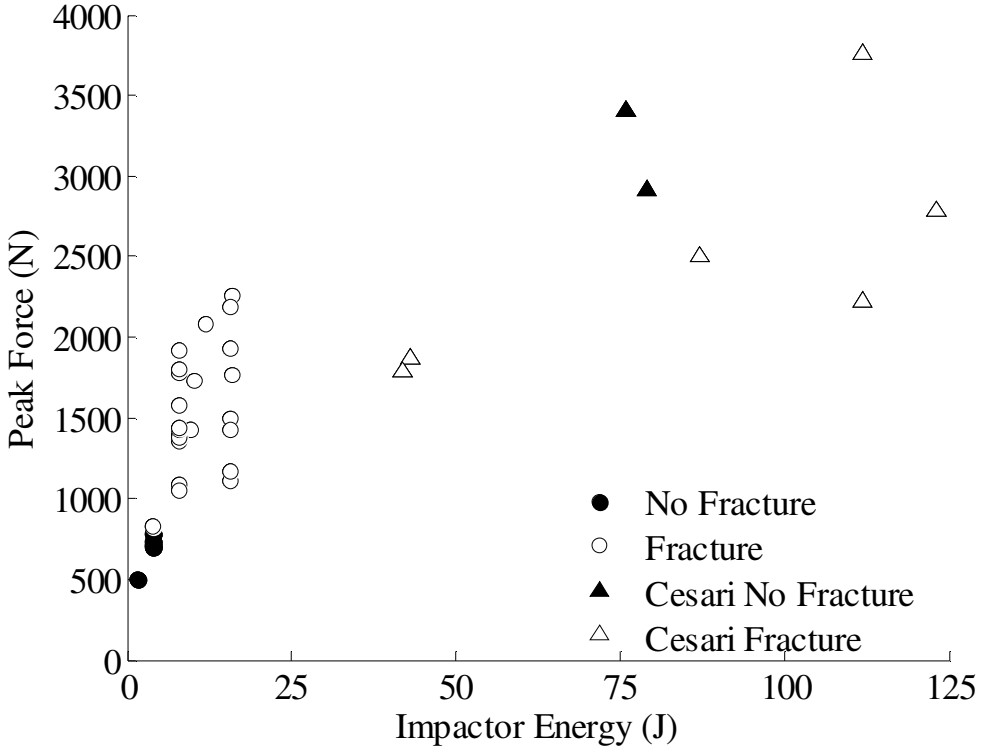

Figure 107: Nasal bone peak force with respect to impactor energy by study.

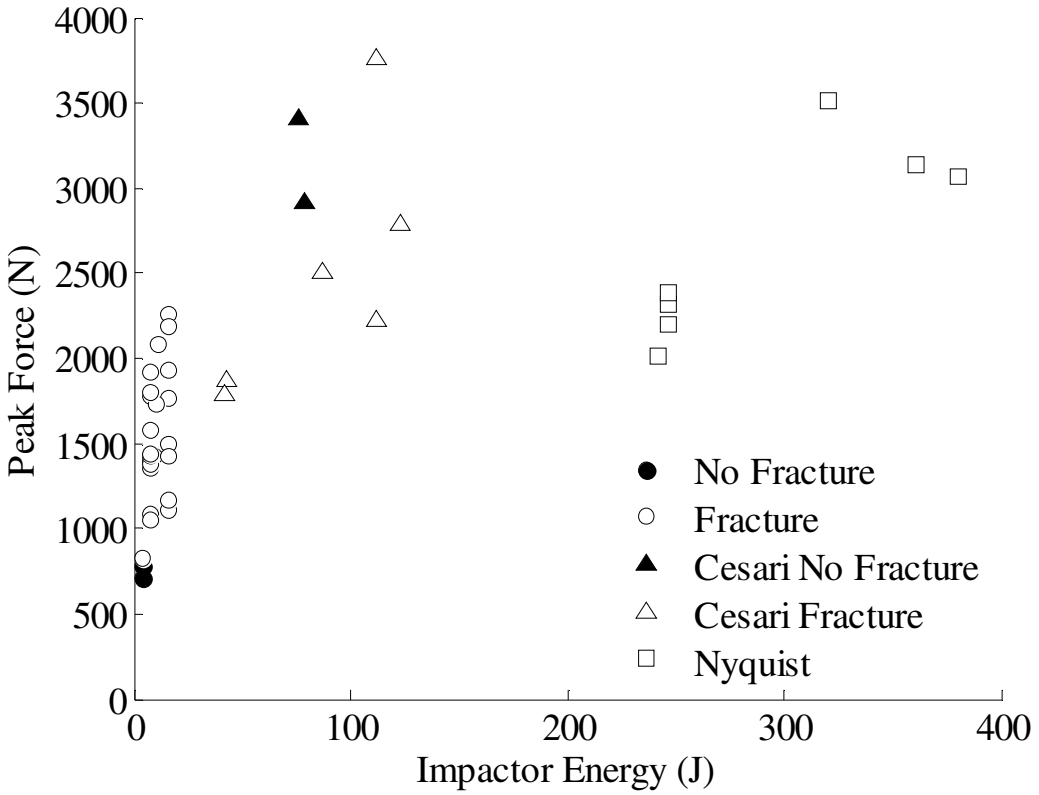

Figure 108: Nasal bone peak force with respect to imapctor energy by study.

The current study utilized Acoustic Emission (AE) to determine the force at which the onset of fracture occurred. An AE threshold was defined which would indicate the occurrence of fracture. This approach was validated by comparing the AE obtained during fracture (Figure 47) and non-fracture tests (Figure 48). Additional validation was demonstrated in a previous study (Cormier 2008: Chapter 4). The force at which the AE threshold was exceeded represents the force necessary to initiate fracture. The onset of AE occurred prior to the initial peak in the force-displacement response, indicating that the fracture process began before structural integrity was altered. The force corresponding to the onset of AE was used as a non-censored measure of the nasal bone tolerance.

Parametric and non-parametric models were used to estimate the risk of fracture as a function of impactor force. The 50% risk of nasal bone fracture corresponded to a force of 530 to 780 N. None of the anthropometric measures were found to be a statistically significant parameter in fracture prediction. These measures were available for thirteen

of the 25 subjects; therefore, the lack of trends may be due to the lack of data. Age however, was available for each subject and was found to have a statistically significant influence on the risk of nasal bone fracture. The average age of the specimens in the current study was 71 (SD = 15). Using age as a covariate, the force corresponding to a 50% risk of fracture decreased approximately 250 N for a 10 year increase in age. The mechanism for the change in tolerance with age is unknown.

The risk curves were developed based on the current study which utilized an impactor with an available area of 6.45 cm^2 (1 in^2). On average the actual contact area was approximately 28% of the available impactor surface. This suggests that the risk curves can be applied to flat impactors with a smaller area as long as the nasal bones are allowed to interact with the impacting surface. The impactor in the current study is not padded and focal enough to apply loading directly to the nasal bone, making a more aggressive surface. Previous studies have shown the importance of padding and surface area on the tolerance of the face. In a study evaluating instrument panel interaction a cadaver was subjected to padded instrument panel strikes at head velocities up to 40 kph resulting in head accelerations up to 60 G without sustaining a facial fracture (Daniel 1965). Larger, flat impactors will distribute forces across the entire face, whereas the impactor in the current study places focal loading to the nasal bone. In this aspect, the risk curves produced in this study are conservative due to the aggressive nature of the impact surface.

Limitations

The force-displacement relationship of the FOCUS headform is limited to impacts performed at a location centered on the load cells. Addition testing will elucidate any effects of off-centered impacts to this region. Higher severity impacts should also be performed to evaluate potential changes in the force-deflection response of the FOCUS exterior.

CONCLUSIONS

This study presents force-displacement corridors for nasal impacts using a blunt, rigid impactor. The overall response of the nasal bone was biphasic, consisting of two peaks in impactor force as a result nasal bone fracture followed by loading of posterior structures, namely the maxilla and frontal bone. Using acoustic emission sensors, non-censored fracture data were used to determine risk curves for nasal bone fracture. The 50% risk of nasal bone fracture corresponded to a force of 530 to 780 N. Age was found to have a statistically significant influence on fracture risk ($p = 0.0003$). Using CT imaging, the width of the nasal bone was measured and found to have a statistically significant relationship with the maximum force achieved during impact. The energy dissipated at the time of fracture was small compared to the initial kinetic energy of the impactor; therefore, the remaining energy was dissipated due to compression of the nasal structures and loading of the surrounding facial region. In the majority of cases, fracture was isolated to the nasal bone by its adjoining sutures. In some cases, the frontal process of the maxilla also sustained fractures.

The response of the FOCUS headform to nasal impacts was assessed to determine its biofidelity. The results of the tests performed in this study suggest that the FOCUS nose should be made stiffer in order to produce a more biofidelic force-displacement response. As is, the FOCUS nose produces little resistance to deformation, causing a stiff response once the nose reaches maximum compression. The results of this study provide the data necessary to improve the biofidelity of the FOCUS headform and improve its utility in facial fracture prediction.

REFERENCES

Allsop D, Kennett K: Skull and Facial Bone Trauma. Accidental Injury: Biomechanics and Prevention. A. Nahum and J. Melvin. New York, Springer-Verlag. 2nd Edition**,** 254-76; 2002.

Allsop D, Warner C, Wille M, Schneider D, Nahum A: Facial Impact Response – A Comparison of the Hybrid 3 Dummy and Human Cadaver, *Society of Automotive Engineers*, SAE No. 881719; 1988.

Bermond F, Kallieris D, Mattern R, Ramet M, Bouquet R, Caire Y, Voiglio E: Human Face Response at an Angle to the Fore-aft Vertical Plane Impact, *Proceedings of the IRCOBI*; 1989.

Bruyere K, Bermond F, Bouguet R, Caire Y, Ramet M, Voiglio E: Human Maxilla Bone Response to 30 degree Oriented Impacts and Comparison with Frontal Bone Impacts, *Proceedings of the 44th Association for the Advancement of Automotive Medicine Conference*, 219-34; 2000.

Cesari D, Ramet M, Welbourne E: Experimental Evaluation of Human Facial Tolerance to Injuries, *Proceedings of the IRCOBI*, Stockholm, Sweden; 1989.

Cormier J, Manoogian S, Bisplnghoff J, McNally C, Duma S: The Use of Acoustic Emission in Facial Fracture Detection, *Biomed. Sci. Instrum.*, 44, 147-52; 2008.

Daniel R, Patrick L: Instrument Panel Impact Study, *Procedings of the 9th Stapp Car Crash Conference*; 1965.

Funk J, Crandall J, Tourret L, MacMahon C, Bass C, Patrie J, Khaewpong N, Eppinger R: The Axial Injury Tolerance of the Human Foot/Ankle Complex and the Effect of Achilles Tension, *Journal of Biomechanical Engineering*, 124; 2002a.

Funk J, Srinivasan S, Crandall J, Khaewpong N, Eppinger R, Jaffredo A, Potier P, Petit P: The Effects of Axial Preload and Dorsiflexion on the Tolerance of the Ankle/Subtalar Joint to Dynamic Inversion and Eversion, *Stapp Car Crash Journal*, 46(0S2-34); 2002b.

Kennedy EA: The Development and Validation of a Biofidelic Sythetic Eye for the Facial and Ocular Countermeasure Safety (FOCUS) Headform, PhD Biomedical Eng., Virginia Tech; 2007.

Kent R, Stacey S, Parenteau C: Dynamic Pinch Tolerance of the Phalanges and Interphalangeal Joints, *Traffic Inj Prev*, 9(1), 83-8; 2008a.

Kent R, Stacey S, Parenteau C: Dynamic Pinch Tolerance of the Phalanges and Interphalangeal Joints, *Traffic Injury Prevention*, 9, 83-8; 2008b.

Kleinbaum D, Klein M: Survival Analysis: A Self-Learning Text, 2nd, New York, Springer Science; 2005.

Lessley D, Crandall J, Shaw G, Kent R, Funk J: A Normalization Technique for Developing Corridors from Individual Subject Responses, *Society of Automotive Engineers*, 2004-01-0288; 2004.

Muraoka M, Nakai Y, Nakagawa K, Yoshioka N, Nakaki Y, Yabe T, Hyodo T, Kamo R, Wakami S: Fifteen – Year Statistics and Observation of Facial Bone Fracture, *Osaka City Med. J.*, 41(2), 49-61; 1995.

Nyquist GW, Cavanaugh JM, Goldberg SJ, King AI: Impact Tolerance and Response of the Face, *Proceedings of the Advances in Bioengineering Conference*, Anaheim, CA; 1986.

Rudd R, Crandall J, Millington S, Hurwitz S, Hoglund N: Injury Tolerance and Response of the Ankle Joint in Dynamic Dorsiflexion, *Proceedings of teh 48th Stapp Car Crash Conference*, SAE No. 2004-22-0001; 2004.

Wells J, Rawlings R: Acoustic emission and mechanical properties of trabecular bone, *Biomaterials*, Volume 6(July); 1985.

CHAPTER 7:
THE TOLERANCE AND RESPONSE OF THE MAXILLA TO BLUNT IMPACT

INTRODUCTION

As observed in Chapter 1, the maxilla represents about one-quarter of the facial fractures sustained by drivers and right front passengers in frontal impacts. The maxilla is an important structure for mastication and supplies the majority of support to the orbital floor; therefore, fractures to this structure can have significant repercussions. As a result of its importance, the tolerance of the maxilla has been assessed by studies utilizing various impactor types and impact locations. Two main categories of methods include those using the flat end of a rigid cylinder to strike the face (Nahum 1975, Nahum 1968, Schneider 1972) and those utilizing a horizontal bar (Allsop 1988, Bermond 1989, Bruyere 2000, Cesari 1989, Hodgson 1965, Nyquist 1986, Welbourne 1989, Yoganandan 1988, Yoganandan 1993) meant to represent steering wheel impact horizontally across the entire face. This applies force to multiple regions of the face and, therefore, head position is critical. Also, fewer tests can be performed on a single subject. Cesari *et al*. (1989) performed impacts to the sub-nasal maxilla region with impactor energies between 15 and 90 J. The most extensive fracture produced by the impacts was limited to the nasal spine. Peak forces ranged from 516 to 1254 N. Addition steering-wheel type impacts were performed by Bruyere *et al* (2000) using a cylindrical impactor which struck the maxilla at an angle of 30 degrees. The sub-nasal region of the maxilla was struck in this study and peak forces of 2010 to 3890 N were generated. A total of eleven tests were performed and five resulted in fracture.

Using the flat end of a cylindrical impactor applies a more focal load on the face and was used by Nahum *et al.* (1968, 1975) and Schneider *et al.* (1972). Based on their results, minimal force tolerance levels were established for the frontal bone (3560-7117 N), maxilla (667-1334 N), mandible (2447-4000 N) and zygoma (890-2890 N). A flat, circular impactor tip with a contact area of 6.45 cm^2 (1 in^2) was used for all impacts. A crushable nickel pad added to the impactor distributed the load more evenly over the

contact area and provided a secondary measure of force. The location of the impact was the suborbital region of the maxilla. This region is particularly vulnerable due to the presence of the maxillary sinus. Varying both the drop height and weight of the impactor allowed for the rate of onset of peak force to be regulated. Pulse duration was changed by adding an adapter to the impactor. Altering the rate of onset or pulse duration did not have a noticeable affect on the fracture tolerance.

Further development in fracture tolerances was provided by Schneider in 1972 by testing additional impact directions and locations (Schneider 1972). The tests performed included anterior-posterior and lateral loading of the mandible, impacts to the maxilla, and lateral loading of the zygomatic arch. A free falling weight impacted the subject which had the soft tissue intact. From 106 impacts the minimal force tolerances described by the authors was 668 N for the maxilla. Trends between 6 six female subjects and 11 male subjects, indicated that females have a lower load tolerance for all impact locations than the males. The authors observed that the bone at the anterior surface of the maxillary sinus was thin and the thickness of the overlying skin ranged from 6.35 to 25.4 mm. All tests resulting in maxilla fracture were comminuted and depressed.

Testing by Allsop *et al.* demonstrated that facial bones are capable of supporting load after fracture has occurred (Allsop 2002, Allsop 1988). This is an important concept as it requires that the fracture force is determined separate from a force-time or force-deflection response. In their studies, Acoustic Emission (AE) was monitored and when a signal burst was detected, fracture was assumed to have occurred. When comparing the time of an AE burst, to the force-time relationship, the authors found that the facial bones would often fracture prior to peak force.

Knowing the precise time of fracture provides a non-censored measure of bone tolerance and, therefore, a more powerful data point for statistical analysis. Other studies have also used acoustic sensors to determine the fracture time of facial bones (Allsop 1988, Cormier 2008) and other bones (Funk 2002a, Kent 2008a, Rudd 2004, Wells 1985). The

studies published by Cormier *et al.* (2008) and Rudd *et al.* (2004) discuss the use of a threshold voltage, over which fracture is denoted to have occurred. These studies established the fracture threshold by comparing the resulting AE between fracture and non-fracture tests. In the study by Cormier *et al.* (2008) additional validation was obtained by demonstrating that high magnitude AE occurred when striking bones with pre-existing fractures at low energy levels. This suggests that the high magnitude AE was due to the propagation of pre-existing fractures and not the result of the impact itself. The lack of acoustic sensors in the Nahum *et al.* studies suggest that their data are censored and that fracture is most likely occurring at a force less than the peak forces reported (Nahum 1968; Nahum 1975). The limitations of the previous studies prohibit the use of statistical analyses to determine the risk of maxilla fracture as a function of impact force.

The current knowledge is also lacking in an understanding of the mechanical response of the maxilla to impact. The development of finite element models or Anthropomorphic Test Devices (ATD) for fracture prediction is limited by the lack of a quantitative measure of the maxilla response to impact. One such ATD is the Facial and Ocular CountermeasUre Safety (FOCUS) headform. The FOCUS headform has the ability to measure forces applied to the facial and orbital structures. It has been developed by Virginia Tech and validated for eye injury prediction (Kennedy 2007). There are eight separate sensing regions within the facial structures that overlie embedded load cells (Figure 51). These regions correspond to the frontal bone, nasal bone, zygoma, maxilla and mandible. Each load cell is capable of measuring forces along all three axes.

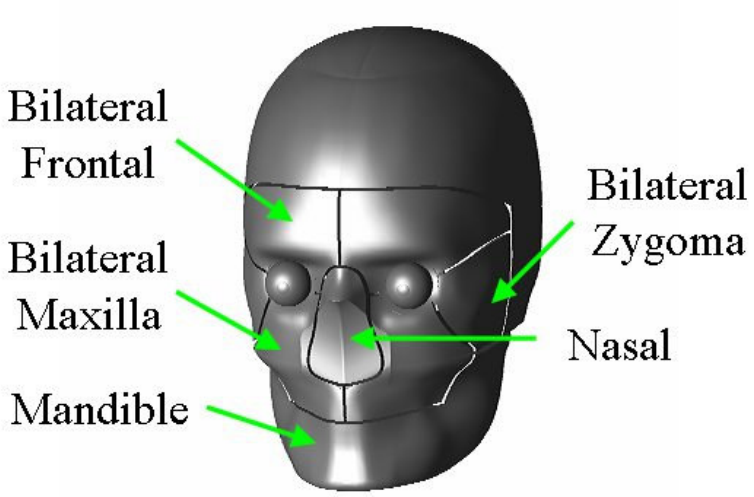

Figure 109: Load cell locations in FOCUS headform.

Defining force-deflection corridors for maxilla impacts in cadavers will provide a basis for the implementation of the FOCUS headform in injury risk assessment.

The first goal of this study is to generate additional data in order to determine risk functions for the prediction of maxilla fracture as a result of blunt impact. The second goal of this study is to develop an understanding of the cadaveric response to blunt impact and compare this response to the FOCUS headform.

METHODOLOGY

The data for this study were obtained by performing facial impacts on male cadaveric subjects. The methods of this study consist of striking the sub-nasal region of the maixlla with the flat face of an unpadded, cylindrical impactor, along with the use of acoustic emission sensors to determine the time of fracture onset. A total of 24 male subjects ranging in age from 43 to 76 years were included in the study. All heads were frozen and thawed prior to testing. Pre-test CT imaging was performed on eleven subjects and post-test CT imaging was performed on three specimens.

Anthropometry

Prior to testing, CT imaging was performed on eleven of the subjects in the current study. The CT images were used to measure the thickness of the bone at the anterior surface of the maxillary sinus as well as the skin thickness overlying this bone. The width of the section of bone at the maxillary sinus along the medial-lateral direction in the horizontal plane was also measured (denoted as sinus width). The wider this region the more likely an object will cause fracture due to a large area of weaker bone. Measurements were taken at the level of the zygomatic arch for consistency (Figure 52). Pearson correlation coefficients were determined to evaluate the correlation between anthropometric measures and the mechanical response of the nasal bone.

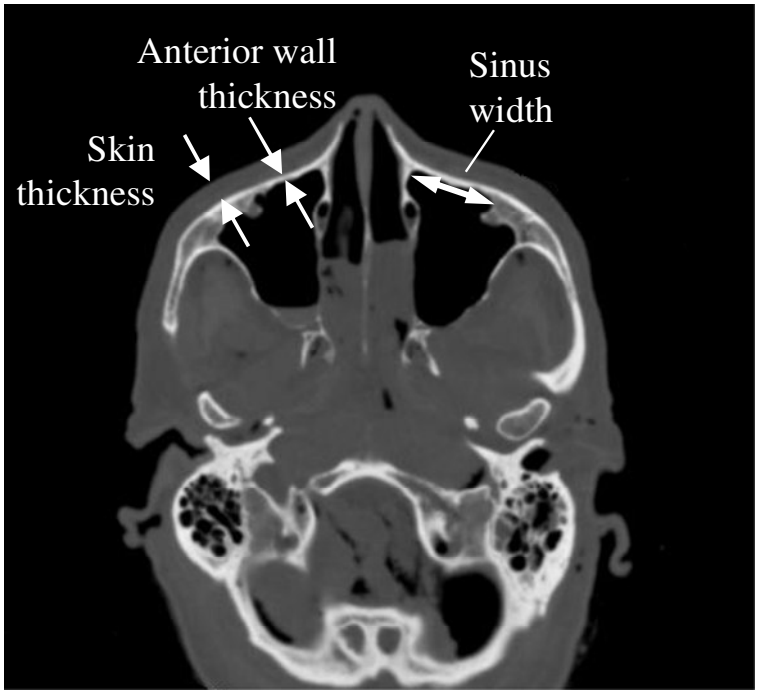

Figure 110: Facial measurements taken using pre-test CT images.

Specimen Preparation

The specimens were removed from the body and prepared by removing the scalp overlying the occipital region. This provided a rigid support at the posterior skull. Metal screws were inserted into the occiput to provide additional structure for the casting material to adhere to. Each head was then rigidly mounted to a semi-circular,

polycarbonate support using Bondo. Consistent orientation between subjects was obtained by vertically aligning the Frankfort plane prior to mounting. Specific anatomical landmarks were used to determine impact location. For the maxilla impacts in this study, the impactor was aligned vertically below the center of the orbit at a level such that the top of the impactor was just below the inferior orbital rim (Figure 111). Each impact was performed using a cylindrical, free-falling rigid aluminum impactor (3.2 kg) with a steel tip (Figure 53). The flat impacting surface had an area of 6.45 cm^2 (1 in^2) and was machined with a slight bevel to reduce edge effects.

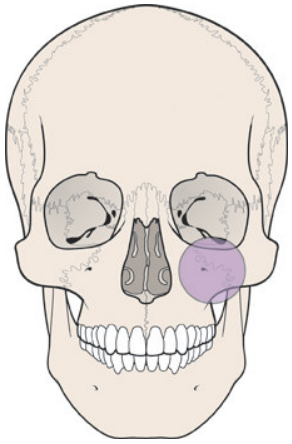

Figure 111: Impact location used in the current study.

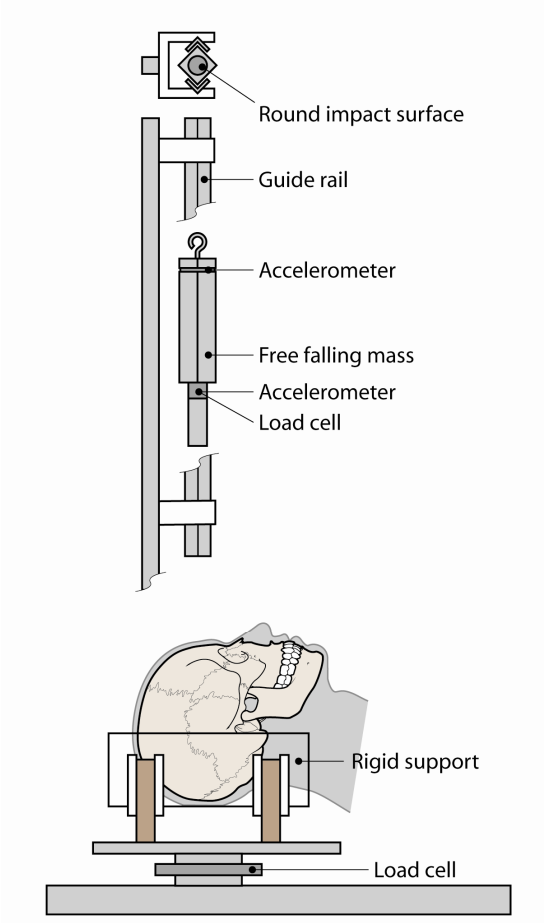

Figure 112: Schematic of test apparatus to be used in the current study.

Instrumentation

The specimens utilized in this study were tested in three separate series that consisted of slightly different instrumentation and data acquisition methods. In all cases an AE sensor (Micro30S, Physical Instruments, New Jersey) was mounted to the frontal bone, just posterior to the apex of the forehead. The AE sensor was mounted directly to the bone by removing the soft tissue and periosteum and gluing the sensor in place with cyanoacrylate adhesive. This method has been used successfully in previous testing during this study and by others (Funk 2002a, Kent 2008a, Rudd 2004). In all tests, the rigid impactor was instrumented with two single-axis accelerometers (Endevco 7264B-2000, Endevco Corp., San Juan Capistrano CA). All data except AE data were filtered to CFC 300. Previous studies have utilized CFC 180; however the use of CFC 300 did not significantly alter the measured peak forces and was chosen to increase the likelihood of capturing small

changes in impactor force during fracture (Bermond 1989, Bruyere 2000, Nyquist 1986). Impactor displacement was calculated by double-integrating the acceleration data. Contact between the impactor and subject was defined based on an impactor force of 10 N. Once the impactor force reached a level above 10 N, the displacement with respect to the maxilla was set to zero and further motion was calculated by double integration. These aspects remained constant throughout the test series; however there were slight differences between the three testing series that created the entire study.

Series 1, subjects 1-13: The AE sensors were sampled at a rate of 2 MHz and all other instrumentation at 30 kHz. The acoustic emission data were acquired using a PC card supplied by the sensor manufacturer (PCI-2, Physical Instruments, New Jersey). Each AE sensor was attached to a preamplifier set to a gain of 40 dB. Impact force was obtained by multiplying the impactor acceleration by its mass. Impactor acceleration was determined by the average of the two attached accelerometers.

Series 2, subjects 14-23: The AE sensors were sampled at a rate of 5 MHz and all other instrumentation at 20 kHz. The acoustic emission data were acquired using an oscilloscope (TDS3000B Tektronix, Oregon). Each AE sensor was attached to a preamplifier set to a gain of 40 dB. A load cell (Denton, 8617JTF, Rochester Hills, MI) was attached to the tip of the impactor which was also instrumented with a single axis accelerometer (Endevco 7264B-2000, Endevco Corp., San Juan Capistrano CA). A load cell (Denton 1968, Rochester Hills, MI) was mounted to the head support to measure reaction forces. Impact force was obtained using the impactor load cell along with the inertially compensated tip mass.

Series 3, subjects 26-35: All parameters described in series two remained the same, with the exception of the AE preamplifier gain which was set to 20 dB in this series. Additionally, high-speed video was also recorded at a frame rate of approximately 4,000 fps. Impactor displacement calculated by double integrating impactor acceleration was verified using high-speed video analysis. This was performed by creating a second-order polynomial fit of the displacement obtained by video analysis.

To define the average force-displacement response of the maxilla, a corridor was created to encompass the overall force-displacement response of the frontal bone. The response corridor was determined by the mean and standard deviation of the characteristic average (Lessley 2004). The characteristic average was created using the force-displacement response up to 90% of the peak force of each test. This ensured that only the linear portion of the response was included in the characteristic average calculation. The values for the corridor where determined using a custom Matlab program that implemented the algorithm described by Lessley *et al.* (2004). The corridor was fit using 3rd order polynomials so that there values could be reported here. Stiffness of the maxilla was also calculated up to 20% and between 20% and 80% of the peak force for each test. Student t-tests were performed to test for statistical between the stiffness of the cadaver and FOCUS response.

Acoustic Emission

AE data were used to determine the force at which fracture initiated. Previous studies using AE data have denoted the onset of AE signal as the onset of fracture (Allsop 1988, Funk 2002a). Recently, studies have utilized a threshold to differentiate AE consistent with fracture from a baseline AE signal (Cormier 2008, Kent 2008b, Rudd 2004). Kent *et al.* (2008b) demonstrated that an AE burst corresponded with a sharp decline in force during phalange fracture.

To utilize AE data as a method of estimating the time at which fracture begins, a threshold must be established that differentiates normal background emissions from those associated with the fracture event. The methods used to establish the AE threshold was described in a previous publication (Cormier 2008: Chapter 4). To establish a relationship between AE and fracture rather than the presence of an impact event, low-severity impacts were performed on specimens with pre-existing fractures. Due to the compromised integrity of these specimens, fracture propagation will occur at forces much lower than that required to initiate fracture. If high levels of AE are a result of fracture then high AE should be observed when the pre-fractured specimens are struck at lower

levels of force. Once the threshold was established, the force corresponding to the occurrence of above-threshold AE was treated as the force required to initiate fracture.

Risk Function Analysis

A survival analysis was performed utilizing parametric and non-parametric techniques. For the parametric analysis, a Weibull model was assumed and fitted to the fracture data. The advantage of using a Weibull model is that the method used to determine the model parameters accounts for the fact that the non-fracture tests are right censored. The LIFEREG procedure within SAS (SAS Institute, Cary N.C) accounts for left and right censoring as well as non-censored data and was used to determine the parameter estimates for the Weibull model (Allison 1995, Cantor 2003). The Weibull distribution is advantageous because it is not forced to be symmetric, so it can accommodate risks that do not increase in the same way throughout the set of input variables. The Weibull CDF is given by,

$$CDF = 1 - \exp -(\lambda \cdot F)^{\gamma} \qquad \text{(Equation 3)}$$

Where λ and γ are the scale and shape parameters respectively and F is the applied. This function will provide an estimate of risk of injury using the maximum likelihood estimates of the scale and shape parameters. A non-parametric model was also created using the Kaplan-Meier method. The Kaplan-Meir method assumes the data are only right or non-censored and determines the risk of fracture based on the number of subjects at risk which sustain a fracture for a given force (Kleinbaum 2005). Measurements obtained using CT imaging as well as subject age were also included as covariates to assess their potential for predicting the risk of fracture.

FOCUS Headform Biofidelity

A series of impacts were performed on the FOCUS headform in order to characterize its response to blunt impact. Impact severity was chosen to facilitate the development of risk functions for facial fracture based on results of the cadaver tests and the capability of the FOCUS headform. The impact was applied using the same apparatus used for the cadaver impacts (Figure 54). Impact location was determined the same way as the

cadaveric impacts. The impactor was instrumented with a, single-axis accelerometer (Endevco 7264B-2000, Endevco Corp., San Juan Capistrano CA). A load cell (Denton, 8617JTF, Rochester Hills, MI) was attached to the tip of the impactor which was also instrumented with a single axis accelerometer (Endevco 7264B-2000, Endevco Corp., San Juan Capistrano CA) (Figure 53). All instrumentation was samples at a rate of 20 kHz. Forces measured by the internal load cells were recorded and compared to impactor forces and examined for load-sharing between facial regions. The stiffness of the FOCUS response was determined up to 20% and between 20% and 80% of the peak force for comparison to the cadaveric response.

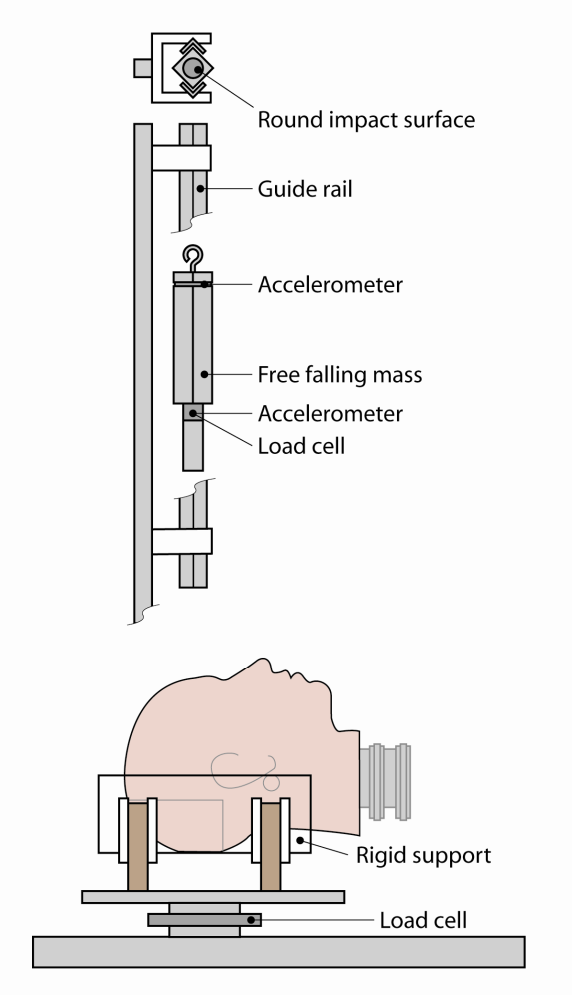

Figure 113: Apparatus used for FOCUS impacts.

RESULTS

A total of 38 tests were performed to determine the response of the maxilla to blunt impact (Table 15). The peak force during each impact ranged from 644 to 2609 N. Pulse duration of each impact ranged from 10 to 15 ms. A facial fracture was produced in 24 tests. An Acoustic Emission (AE) signal was measured in every test using a sensor mounted on the frontal bone. A threshold voltage of 9 volts was established for series one, 5 volts for series two and 2 volts for the third series. These thresholds were based on the magnitude of AE during fracture (Figure 47) and non-fracture (Figure 48) tests. Therefore, the force corresponding to an AE above the threshold was utilized as the force to initiate fracture in the statistical analysis.

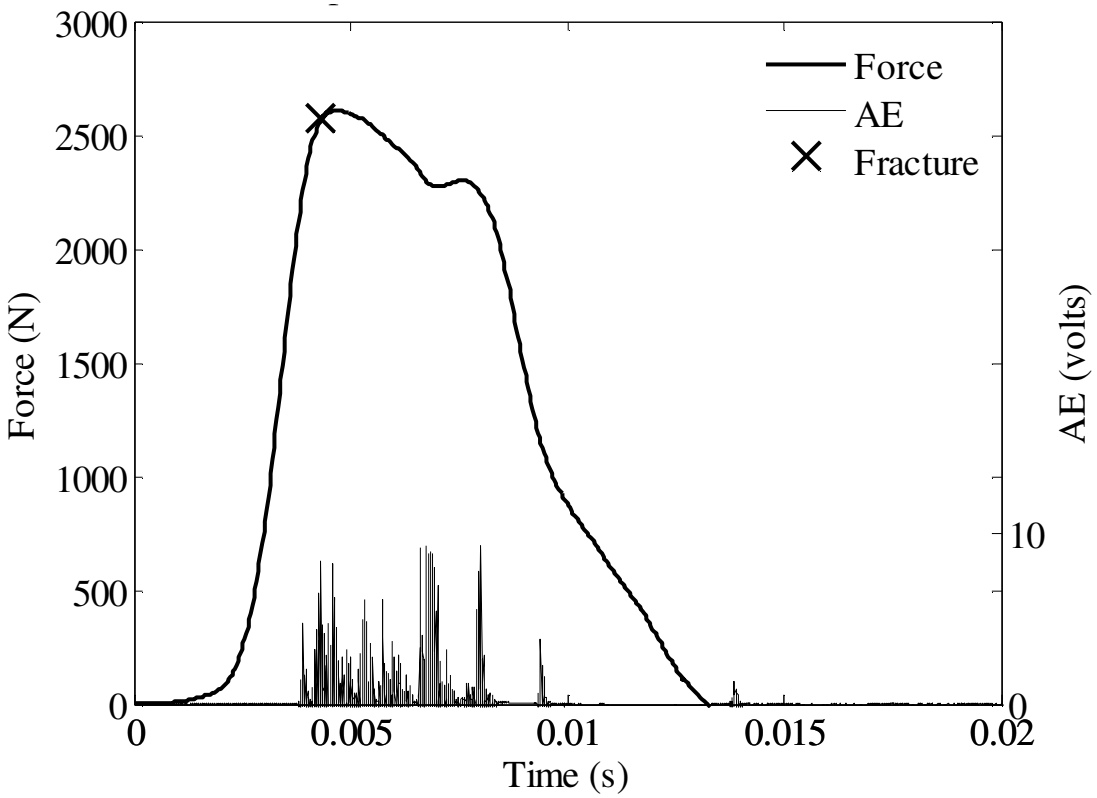

Figure 114: Acoustic emission and force during an impact resulting in a maxilla fracture.

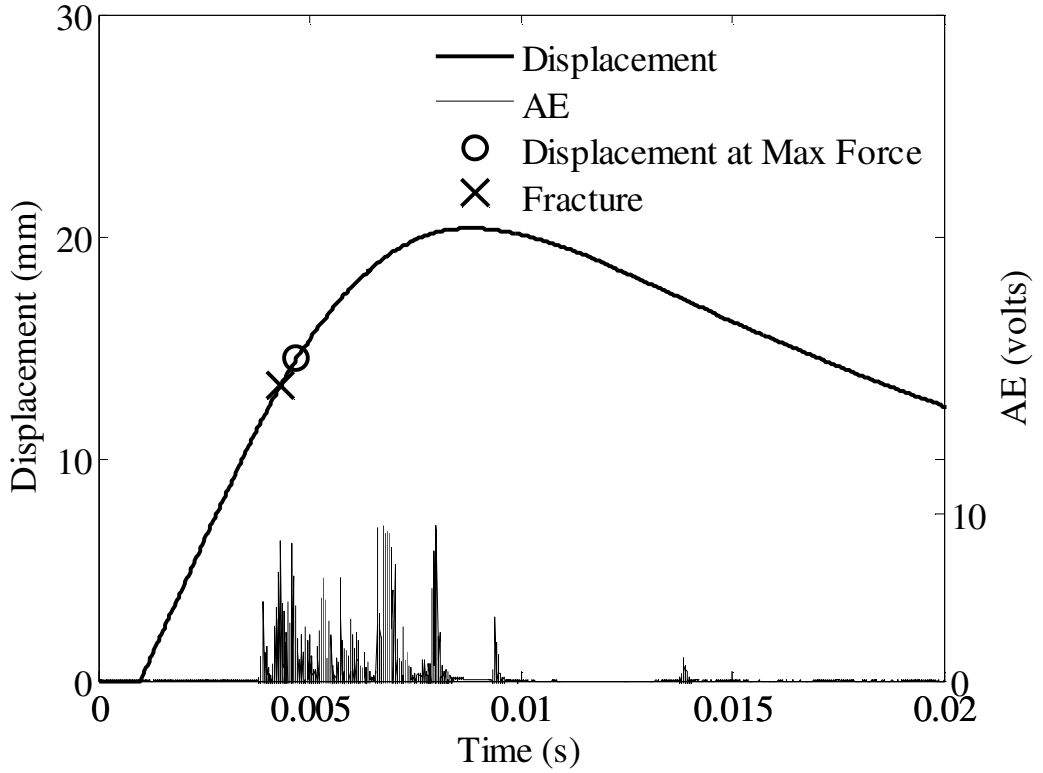

Figure 115: Force-displacement response from maxilla impact shown in Figure 6.

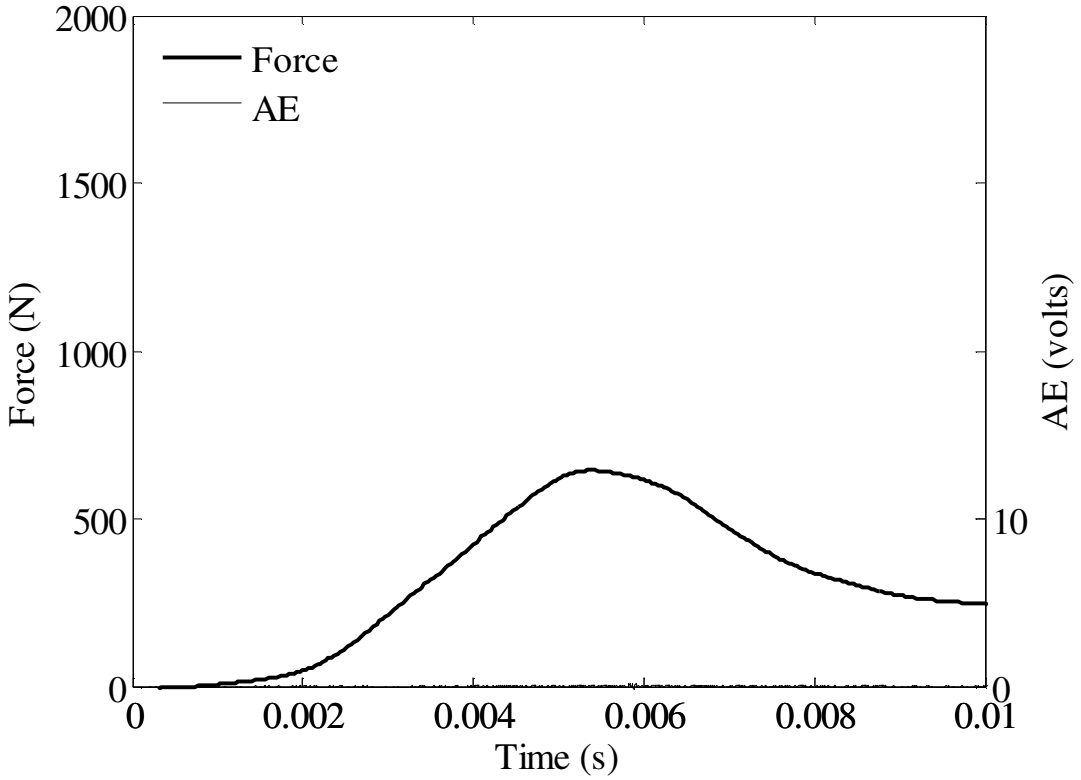

Figure 116: Maxilla impulse response not resulting in fracture.

Table 15: Summary of subject characteristics and test results for maxilla impacts. na=not available

Subject	ID	Age	Height (cm)	Weight (kg)	Aspect	Impactor Energy (J)	Peak Force (N)	Fracture Force (N)
1	SM58	61	168	69	Right	3	644	
2	SM60	41	170	64	Right	4	845	
					Left	8	1019	
3	SM56	57	170	84	Right	6	750	
					Right	10	1224	
					Left	38	1889	1888
4	SM57	75	165	65	Left	4	821	
					Left	6	1225	
					Right	28	2609	2570
5	SM61	76	170	44	Right	6	961	
					Right	10	939	
					Left	24	1103	419
6	SM62	43	183	112	Left	8	1304	
					Right	20	1827	1223
7	34237	66	na	na	Left	6	1591	
					Right	10	1463	1398
8	34236	54	na	na	Right	8	885	
					Left	4	1025	
9	32120	58	na	na	Left	8	1395	1335
					Right	4	722	
10	34249	72	na	na	Right	4	679	
					Left	40	1661	1450
11	33574	57	na	na	Left	4	670	
					Right	44	1202	774
12	33995	49	na	na	Left	6	1009	
					Right	12	1063	1024
13	34403	79	na	na	Left	6	1100	
14	5758	83	175	73	Left	32	1763	1608
15	5791	94	163	64	Left	32	1414	834
16	5556	59	175	82	Left	32	1445	510
18	5763	47	183	89	Left	32	2023	1187
20	5642	80	160	71	Left	32	1591	486
22	5664	83	180	73	Left	32	1279	647
25	5863	78	170	38	Right	24	1414	581
28	5807	85	180	65	Right	24	1277	706
30	SM64	62	178	59	Right	24	2060	1774
32	459	71	na	na	Right	24	1269	1136
34	5837	68	175	71	Right	24	1206	1205

Once fracture force was determined, its relationship with various impact and subject descriptors was investigated. All tests performed with an impactor energy above 20 J resulted in fracture and exhibited peak forces between 1,000 to 2,000 N. Fracture force was not correlated with impactor energy ($p = 0.2$) (Figure 117) and consequently, initial impactor velocity (Figure 118).

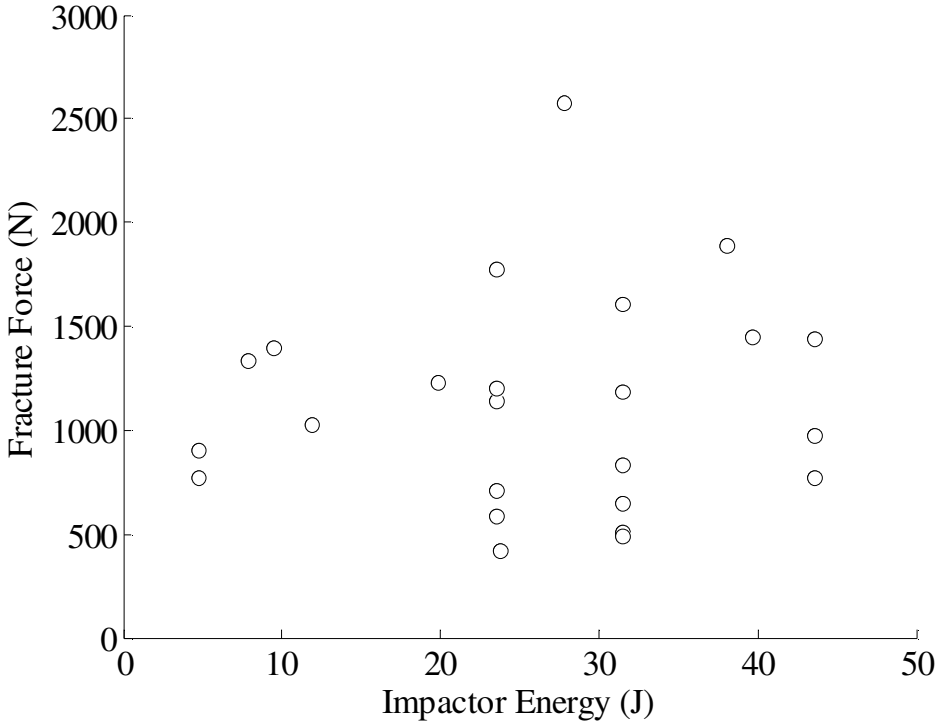

Figure 117: Maxilla fracture force with respect to impactor energy.

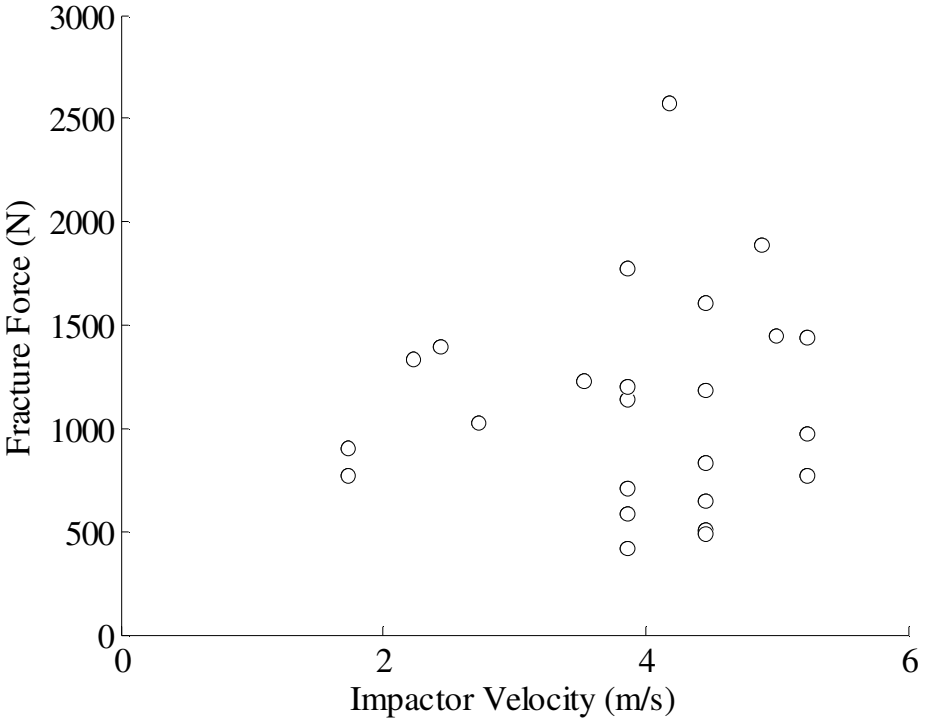

Figure 118: Maxilla fracture force and impactor velocity for maxilla impacts.

With respect to contact area, the higher energy tests resulting in fracture had a greater contact area (1.9 cm^2) than the no fracture (1.0 cm^2) tests (p=0.034) (Figure 119). This is consistent with the higher forces in the fracture tests resulting in increased tissue compliance and the fractured structure conforming to the impactor surface. The force at fracture onset was not correlated with contact area (p = 0.53) or pressure (p = 0.35). There was a decreasing trend in peak pressure with impactor energy (Figure 120). This trend was statistically significant (p = 0.038) but weak as indicated by the correlation coefficient of 0.3301. This resulted from the increase in contact area with impactor energy.

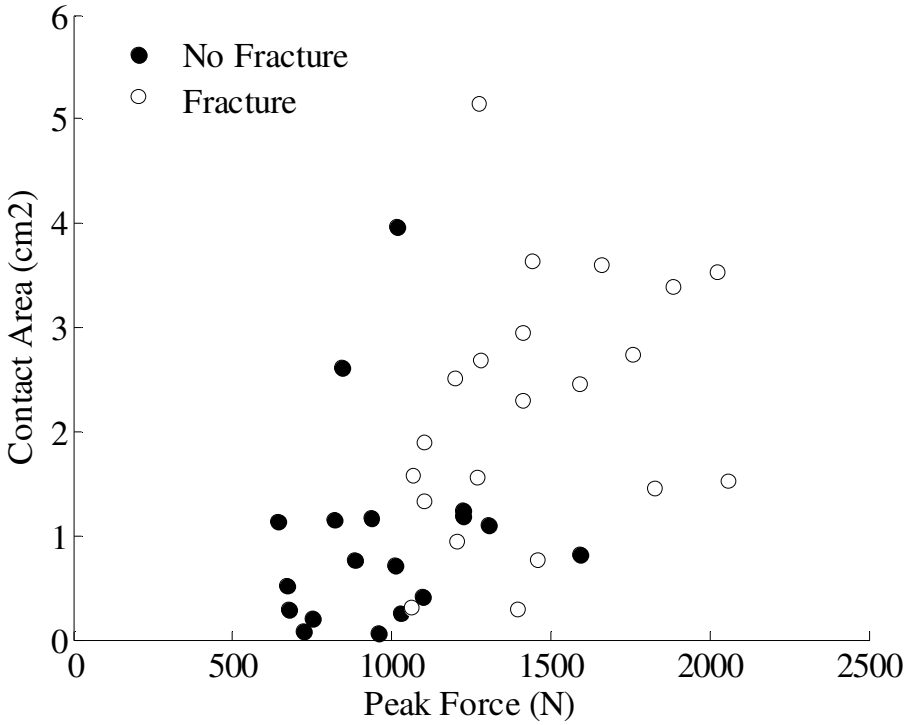

Figure 119: Relationship between maxilla contact pressure and peak force.

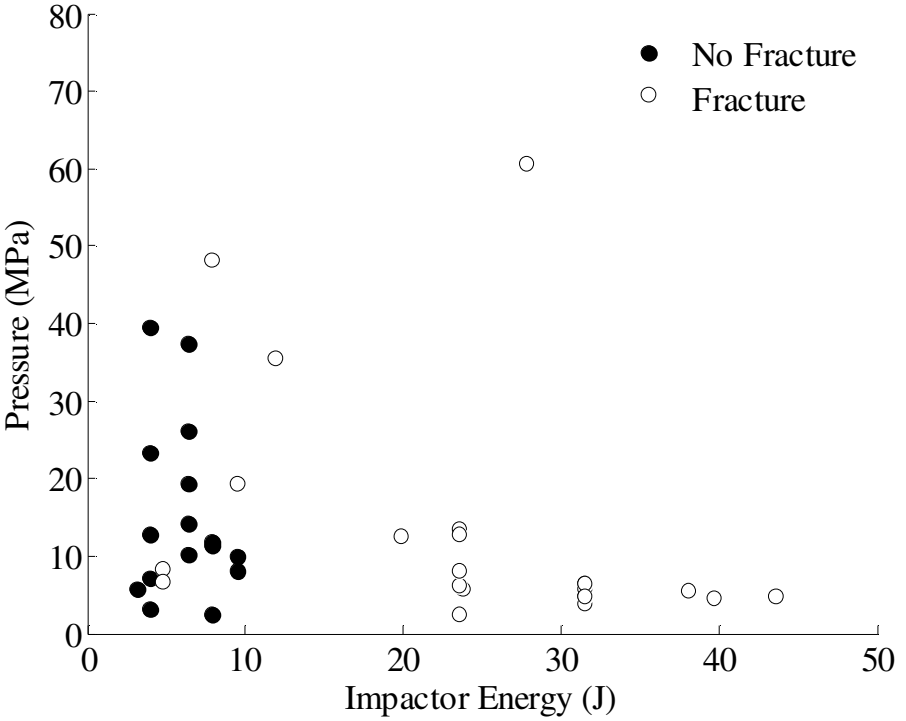

Figure 120: Peak pressure by impactor energy and maxilla fracture status.

Anthropometry

Five different measurements were taken from pre-test CT images to evaluate the relationship between physical descriptors of the maxilla and its mechanical response (Table 16). The CT images were available for eleven subjects all of which incurred maxilla fractures. The thickness of the anterior wall of the maxillary sinus was consistently less than 0.5 mm. The accuracy of the CT images taken was limited to 0.5 mm, therefore, no analysis was performed with these data. The width of the sinus opening ranged from 1.7 to 3.55 cm and skin thickness over the maxilla ranged from 0.4 to 1.18 cm. With respect to the size of the head, head depth and width were not found to be correlated to fracture force (respectively, p = 0.08, 0.91) (Figure 121).

Table 16: Average values from CT measurements of maxilla (cm).

	Sinus Width	**Skin Thickness**	**Head Width**	**Head Depth**
Mean	2.94	0.76	14.09	18.54
Std. Dev.	0.53	0.26	0.70	0.97

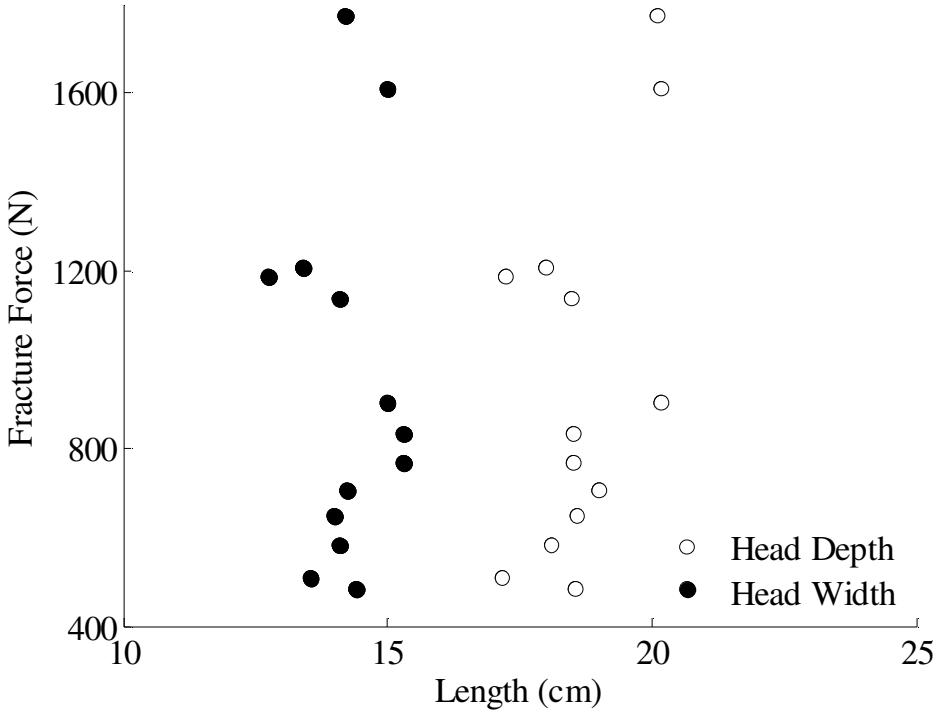

Figure 121: Maxilla fracture force and subject head depth and length.

Within the limited number of subjects with CT data, there were no trends observed between anthropometric measures and the force at which the maxilla fractured or the stiffness of each subject's response. The width of the maxillary sinus and skin thickness were highly correlated ($p < 0.0001$), but did not demonstrate an association with fracture force (respectively, $p = 0.12, 0.38$) (Figure 122). Age also demonstrated no association with fracture force ($p = 0.13$) (Figure 123). Age was correlated with the initial stiffness of the maxilla ($p = 0.002$) with a positive correlation coefficient of 0.46.

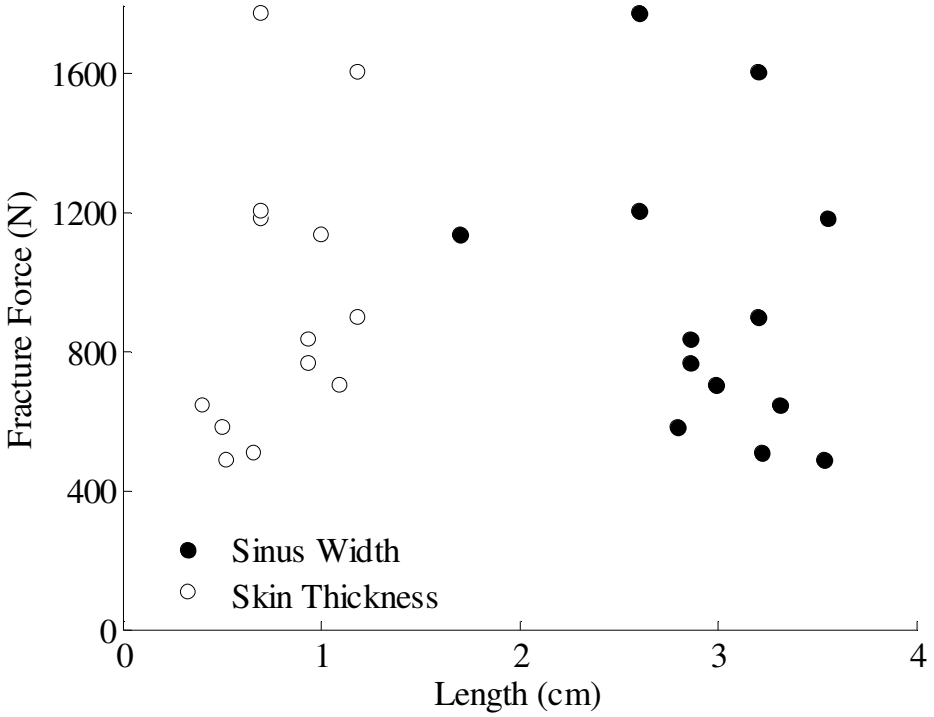

Figure 122: Fracture force and associated maxillary sinus width and skin thickness measured from CT images.

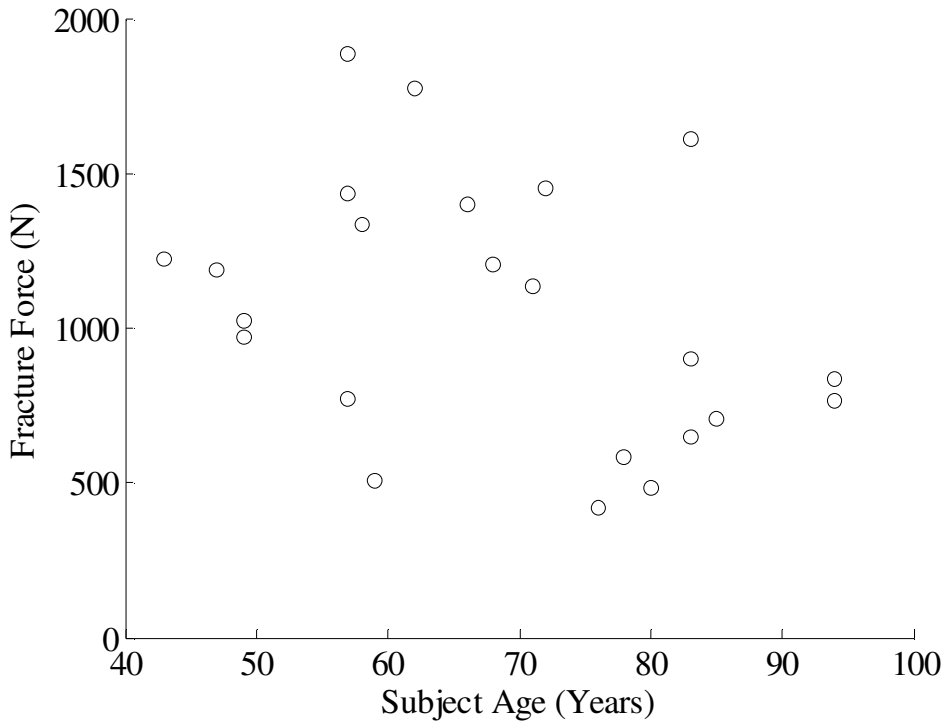

Figure 123: Subject age and corresponding maxilla fracture force.

Risk of Maxilla Fracture

Parametric and non-parametric models were used to estimate the risk of fracture as a function of impactor force. Only one test per subject was used and no repeated tests resulting in fracture were used in the risk estimate. Two sets of data were used to develop the current risk functions. In one set, both fracture and non-fracture tests were used (Figure 124) and only fracture tests were used in the second (Figure 125). In both sets, the 50% risk of maxilla fracture was approximately 1100 N. When included in the model as a covariate, age was found to be an insignificant parameter ($p = 0.52$). There were only small differences in the parameter estimates used to generate the Weibull distribution (Table 17).

Table 17: Parameter estimates of Weibull distribution of maxilla fracture risk.

		95% Confidence Interval		
Model	**Estimate**	**Lower**	**Upper**	**Parameter**
All Data	0.0007	0.0009	0.0006	Scale
	2.39	1.73	3.29	Shape
Fracture Only	0.0008	0.0010	0.0006	Scale
	2.26	1.62	3.14	Shape

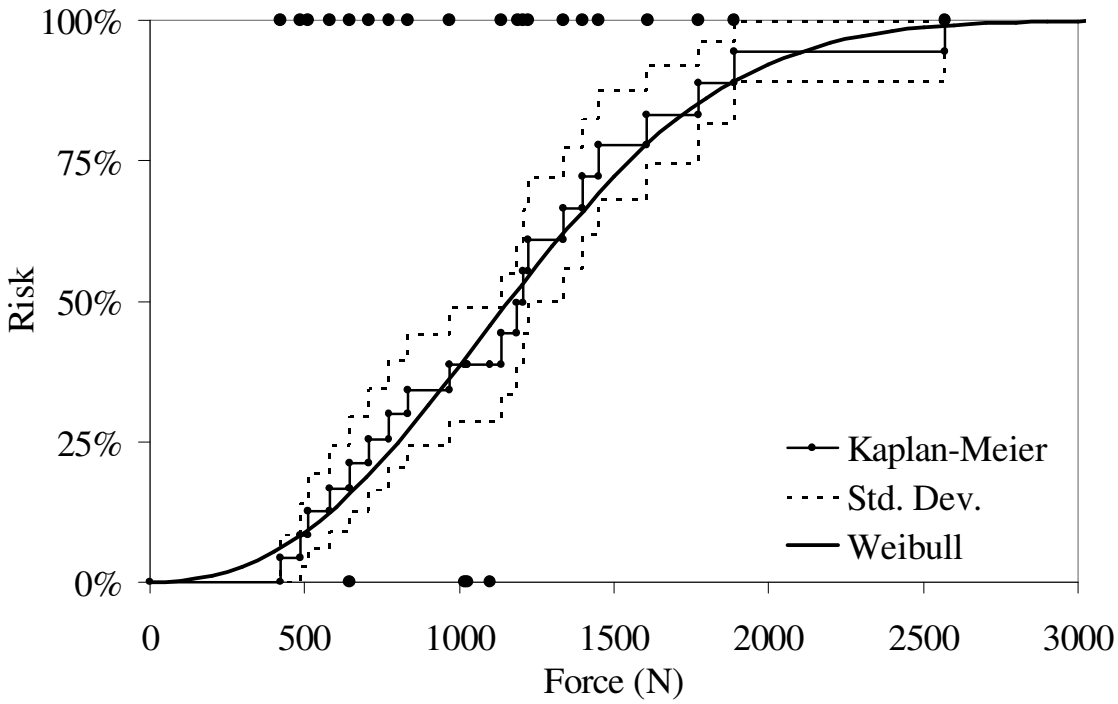

Figure 124: Risk of maxilla fracture estimated using all impacts.

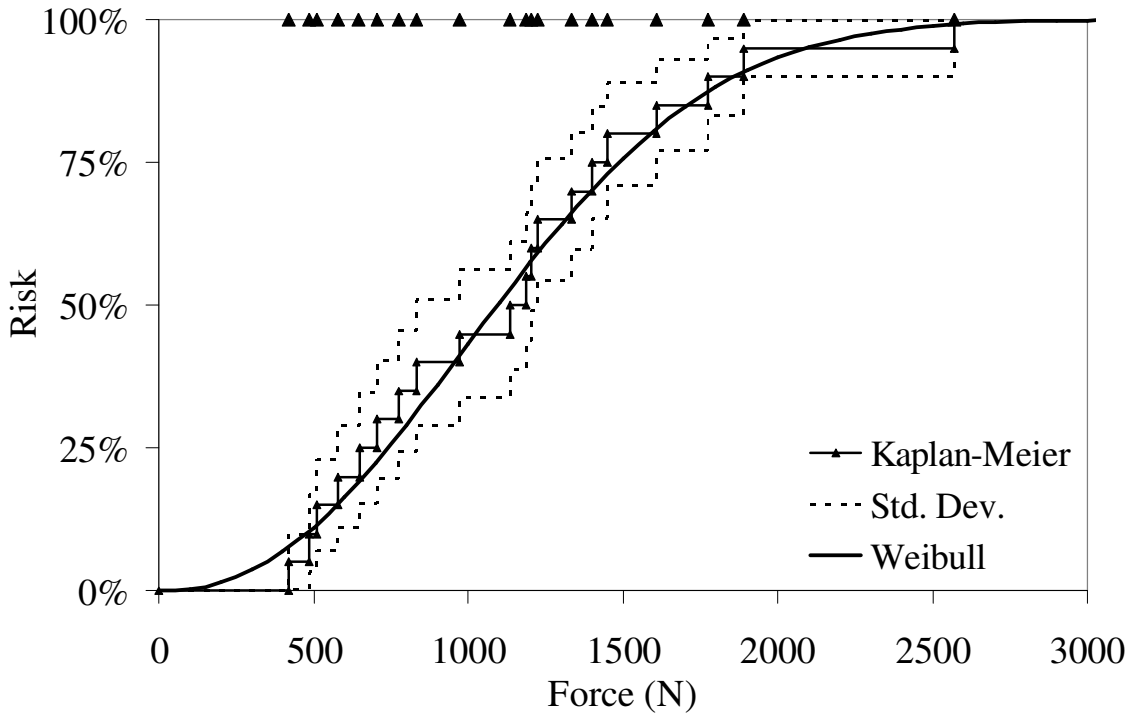

Figure 125: Risk of maxilla fracture determined by fracture data only.

Pre-test CT data were available for a reduced number of subjects (n=11). Head depth was available for these subjects, and when included in the model, it was found to be a statistically significant parameter when predicting fracture force (p=0.03). Head depth did have a positive correlation, indicating a higher tolerance with a greater head depth. The resulting risk of fracture within this reduced dataset was not similar to that obtained when using the full dataset. Contact area was found to be a statistically significant parameter (p = 0.015) in the Weibull model of fracture risk. However, the model predicted that an increase in area would increase the risk of fracture. This a result of the association between higher impact forces and increased contact area previously described.

Cadaveric Force-Displacement

The force-displacement response of the maxilla was determined from double-integration of accelerometer data and verified using high-speed video. Video data were available for five maxilla impacts and a total of 37 tests within the entire investigation (including other bones) and was compared to the displacement obtained from the accelerometers. Overall,

the displacement determined by video analysis and the accelerometer data were similar (r = 0.976). Not all tests were used to determine the force-displacement response of the maxilla. In some tests interaction with the nose occurred prior to interaction with the maxilla which resulted in impactor force initiating prior to contact with the maxilla. As a result of using a force threshold of 10 N to determine contact, the displacement of the impactor was determined form the time of nasal contact and not maxilla interaction. The time of maxilla contact could not be reliably estimated and therefore these tests were excluded from the corridor calculation.

Within tests resulting in fracture, the force-displacement response exhibited two different patterns. In one pattern, a maximum force was reached, followed by continued displacement with a fairly constant or decreasing force (Figure 126). The maximum force achieved in these tests was higher than tests exhibiting the second pattern in force-displacement. The second pattern in the force-displacement response was characterized by an initial peak in force, followed by continued impactor displacement at a lower, fairly constant load (Figure 127). Impact force then rose toward the end of impactor travel. In both cases fracture onset occurred just prior to the first peak in the force-displacement response.

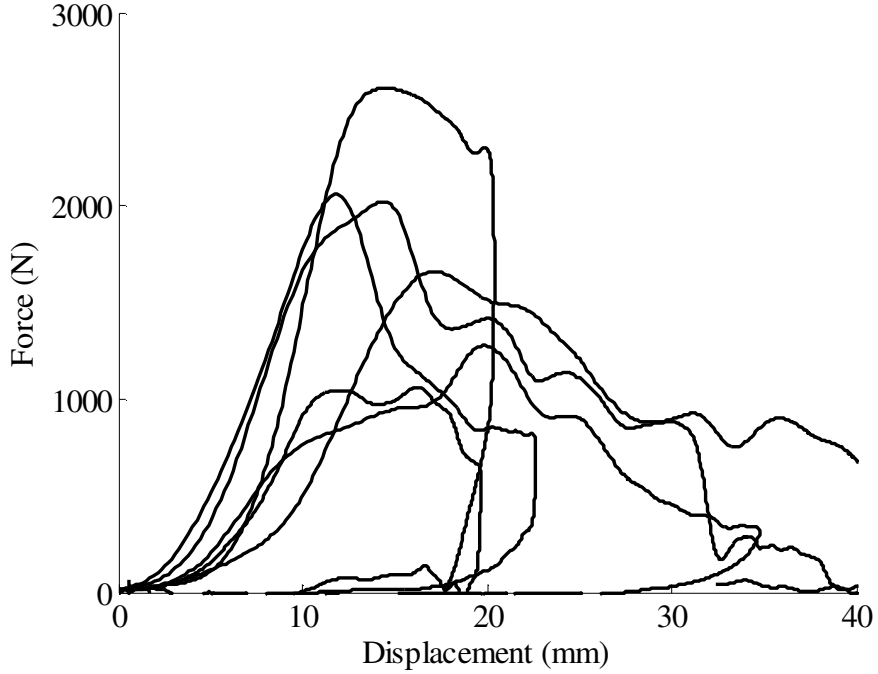

Figure 126: Example of maxilla force-displacement response resulting in fracture.

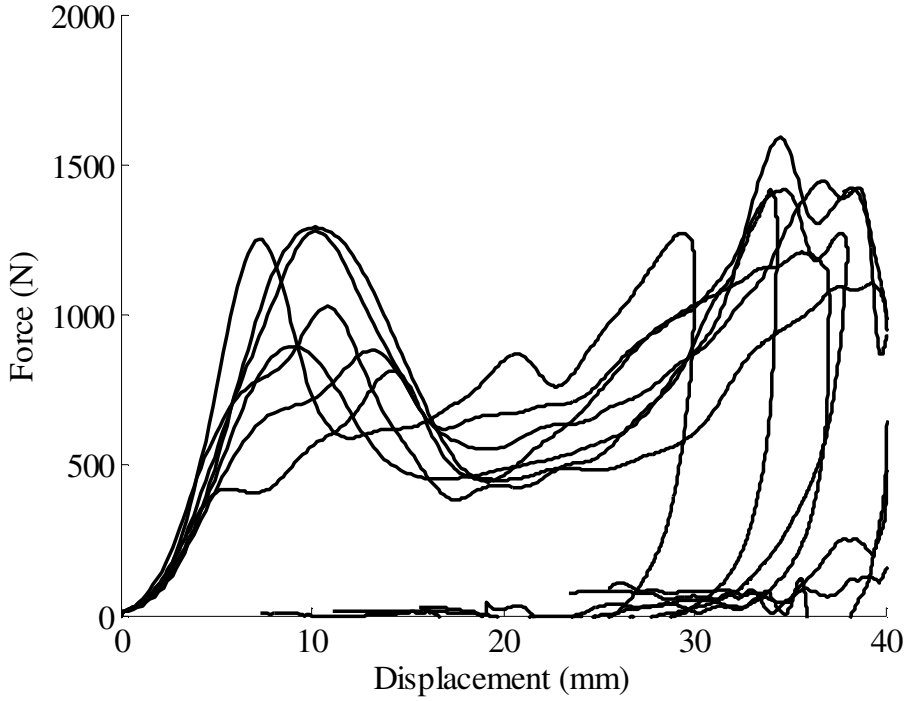

Figure 127: Example of maxilla force-displacement response exhibiting two peaks during a fracture test.

Tests not resulting in fracture demonstrated similar toe regions and stiffness up to peak force as tests with fracture (Figure 128). Changes in the force-displacement response of the fracture tests typically occurred near the first peak in force. Tests not resulting in

fracture demonstrated an inelastic response, with the unloading phase being characterized by a decrease in force with little impactor motion (Figure 129).

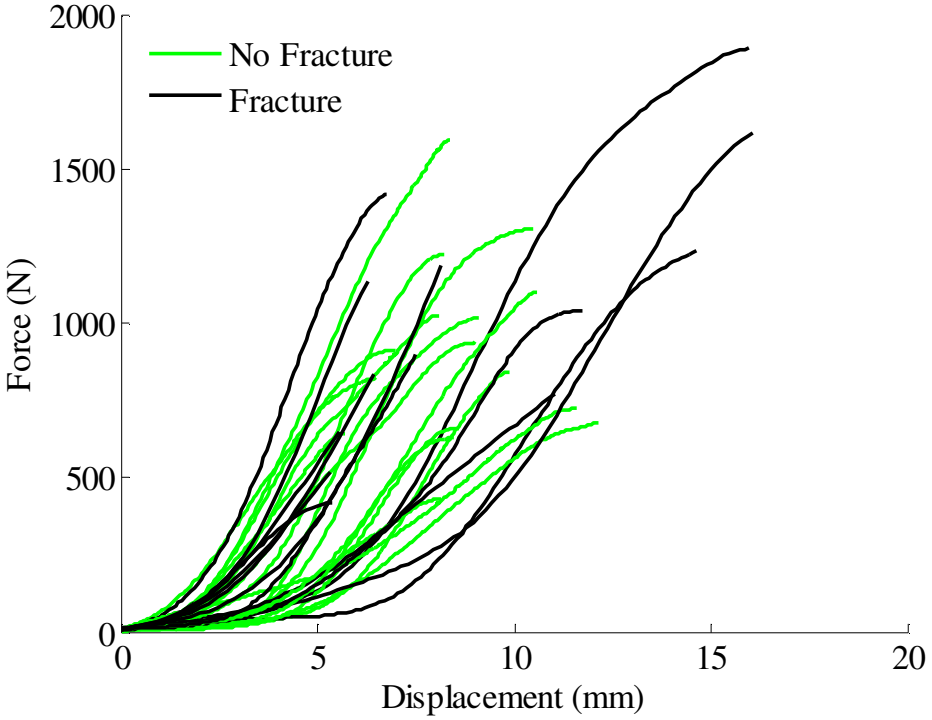

Figure 128: Cadaveric maxilla force-displacement response up to peak force by fracture status.

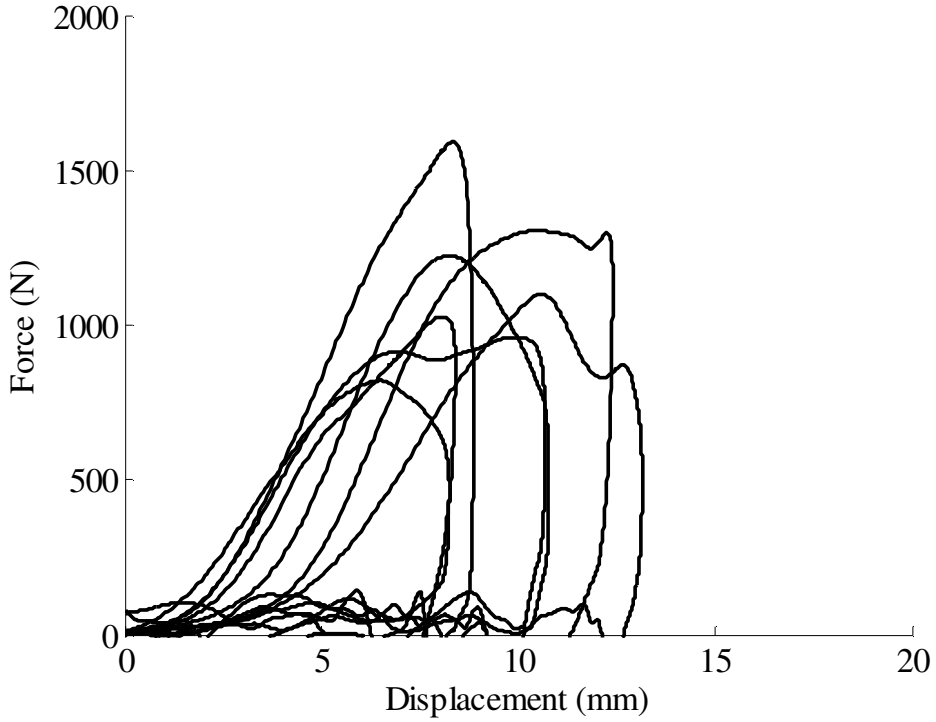

Figure 129: Typical maxilla force-displacement traces for tests not resulting in fracture.

The corridor of the force-displacement response was defined by the characteristic average and its standard deviation in both the x and y directions (Figure 130). The upper and lower bounds of the corridor fit the data well.

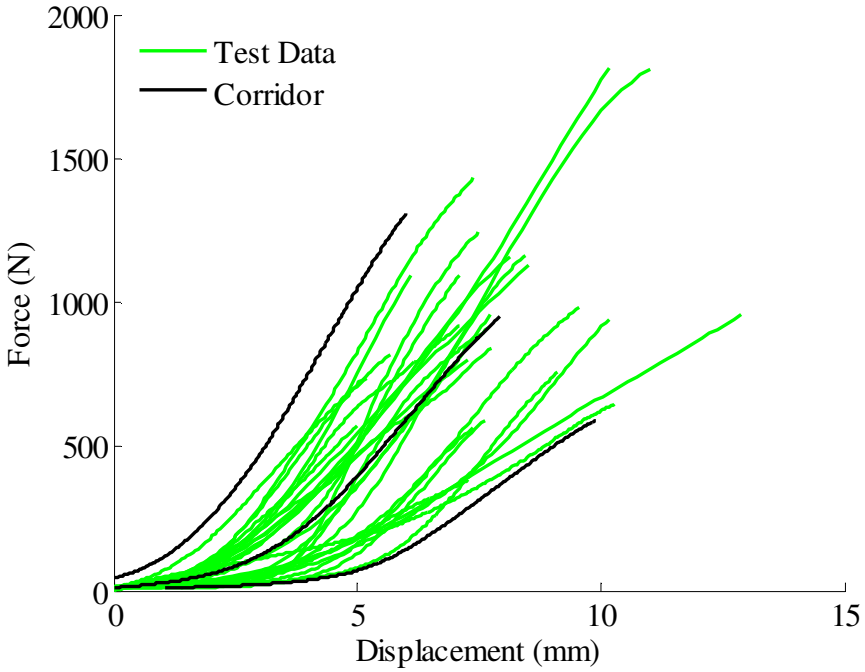

Figure 130: Cadaveric force-deflection response with corridor for maxilla impacts.

FOCUS Headform Biofidelity

A total of 9 tests were performed on the maxilla bone region of the FOCUS headform. Impactor velocity ranged from 2.4 to 2.8 m/s and resulted in corresponding impactor energies of 9.4 to 12.6 J. The peak forces measured by the impactor ranged from 1485 to 1769 N. The peak force measured by the internal FOCUS load cells differed from the impactor forces by 14% on average (Figure 131). On average 20% of the peak force was reached at a displacement of 5.3 mm (Std. Dev. = 0.42) with an initial stiffness of 59 N/mm (SD = 3) and a secondary stiffness (after toe region) of 222 N/mm (SD = 13).

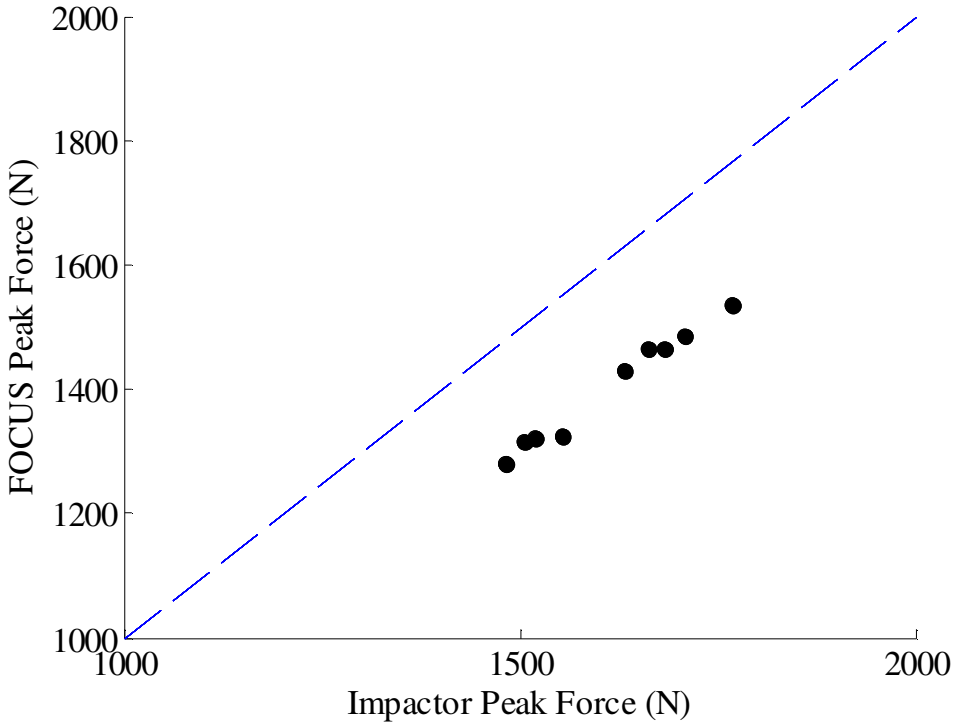

Figure 131: Impactor force and internal maxilla force measured by FOCUS headform.

The characteristic average of the force-displacement response enclosed the response for all tests (Figure 132). The focus force-displacement corridors for maxilla impact were fit using 2nd order polynomials to facilitate recreation (Figure 133).

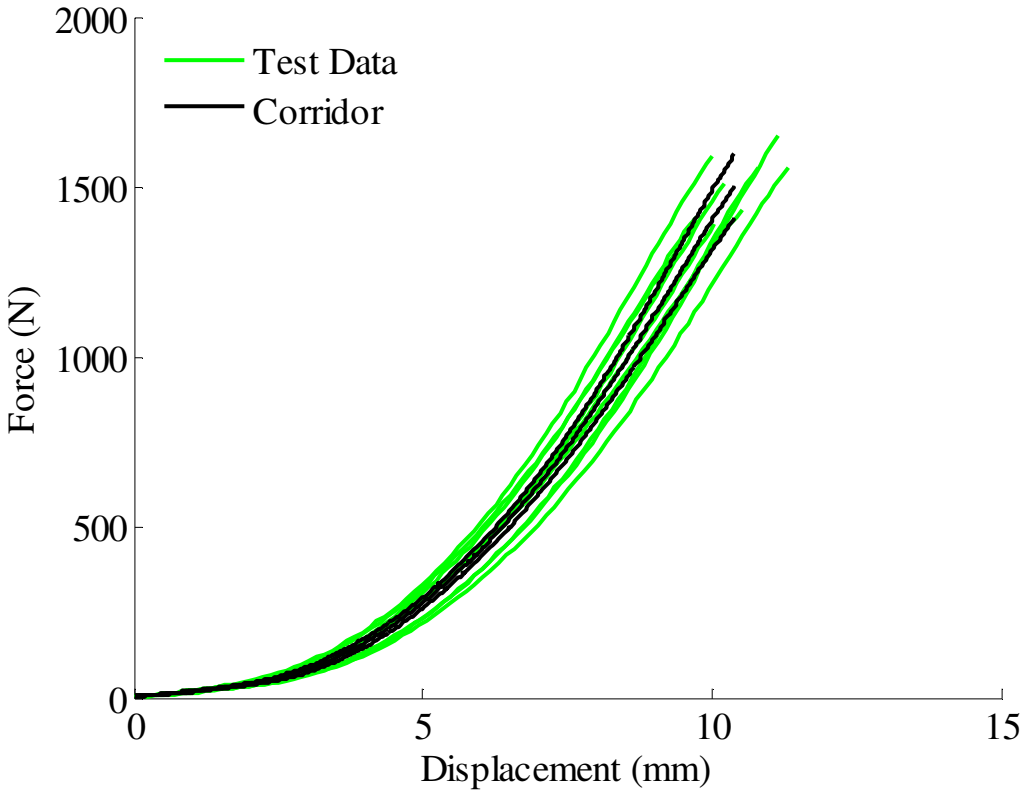

Figure 132: Force-displacement corridors for FOCUS maxilla impacts.

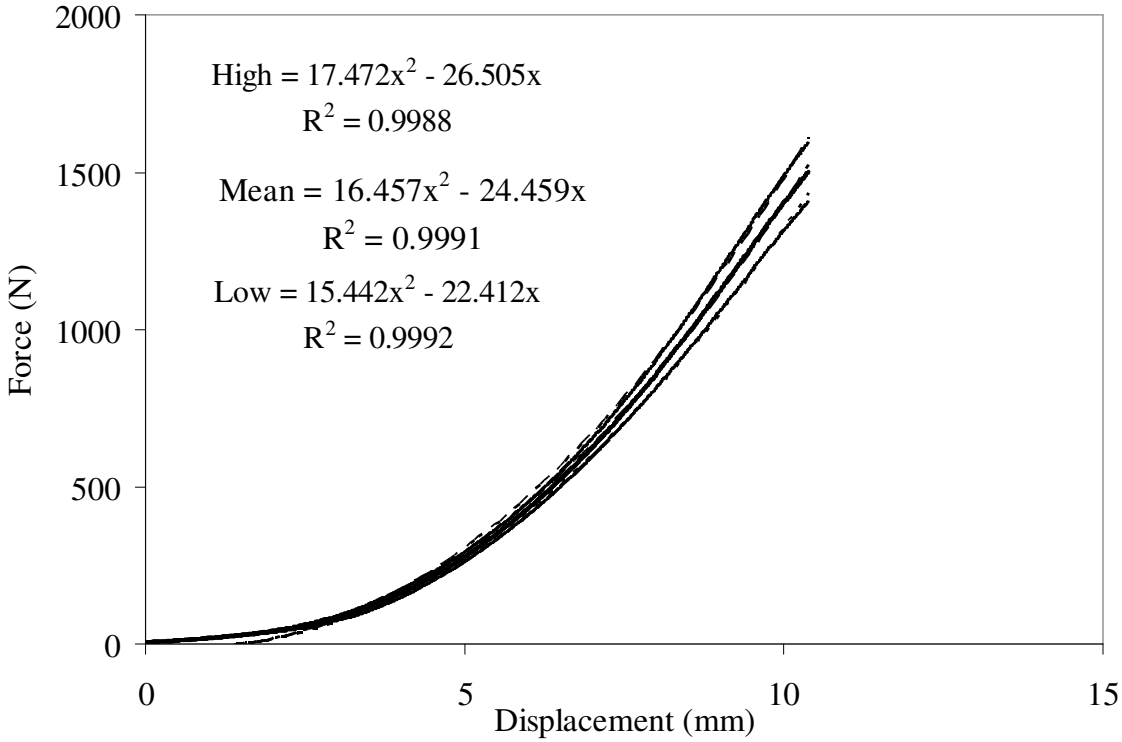

Figure 133: Polynomial fit to FOCUS maxilla force-displacement corridor.

The cadaveric and FOCUS headform corridors were fairly similar throughout the response (Figure 134). The FOCUS exhibited a slightly softer toe region, with a higher stiffness therefore, however, its mean response was well within the cadaver corridor. There was no statistical difference between the stiffness of the FOCUS and cadaver response up to 20% of peak force ($p = 0.5$). The stiffness between 20 and 80% of the peak force was statistically different between the FOCUS and cadaver responses ($p = 0.003$). Similarly, the displacement at 20% of the peak force was statistically different between the FOCUS and cadaver responses ($p = 0.02$).

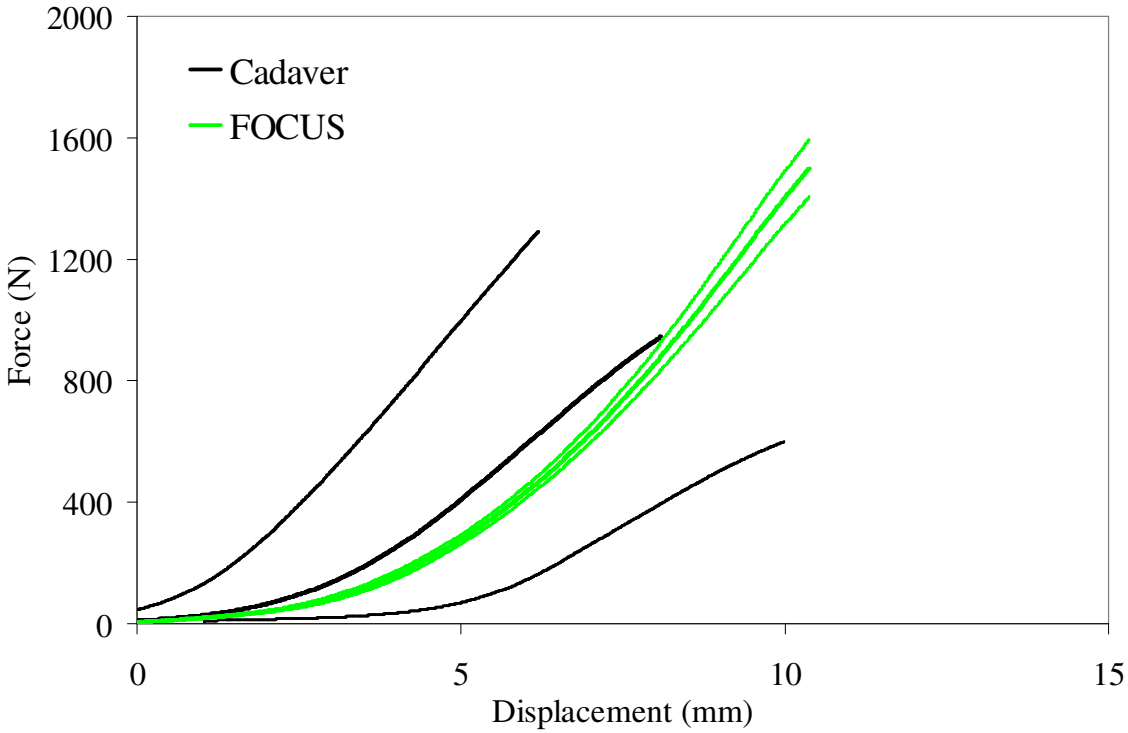

Figure 134: Force-displacement corridor for cadaver and FOCUS maxilla impacts.

DISCUSSION

The purpose of this study was to investigate the response of the maxilla to blunt impact and determine the risk of fracture as a function of impact force. Through the 42 tests performed for this study, force-displacement corridors were defined and functions to predict maxilla fracture were developed. The force-displacement response of the maxilla was found to differ by fracture status. The occurrence of fracture resulted in an increased deflection of the impactor and an attenuation of impactor force. Within the fracture tests,

there was no appreciable increase in peak force with an increase in impactor energy. The lack of an increase in peak force with impactor energy is attributed to the loss of structural integrity due to fracture. Nahum *et al.* (1968, 1975) performed a similar study using the same sized impactor as the current study and found the same trends between impactor energy and peak force (Figure 135).

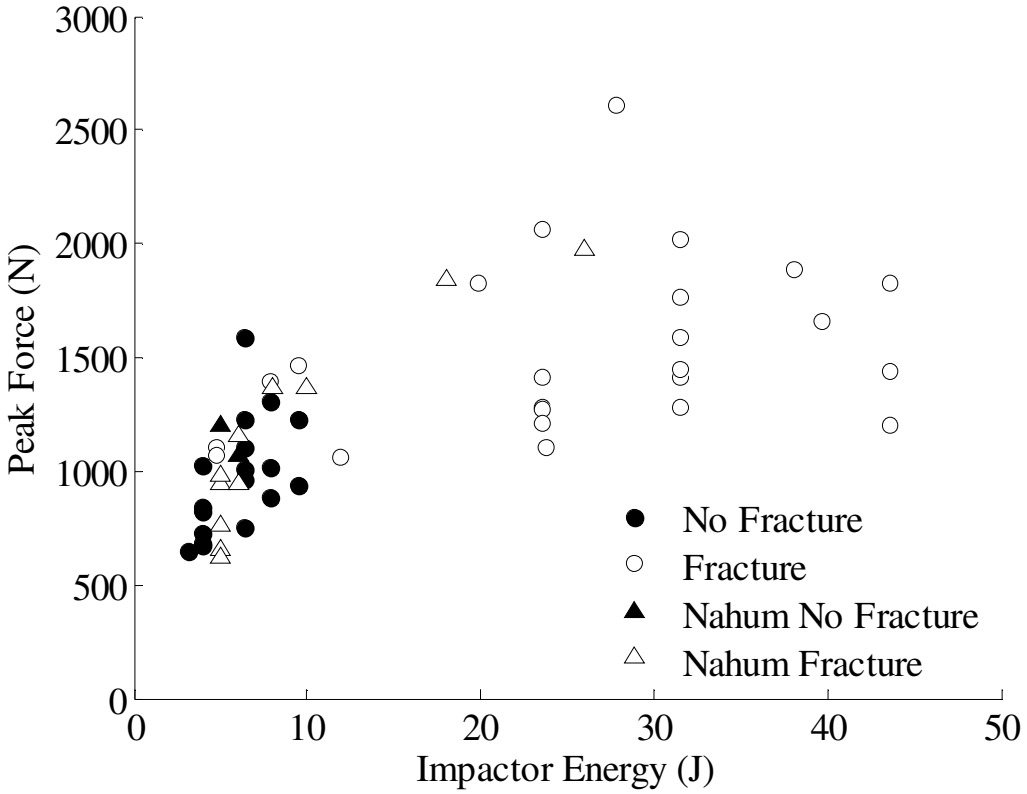

Figure 135: Maxilla peak force with respect to impactor energy by study.

Additional studies by Cesari *et al.* (1989) and Bruyere *et al.* (2000) utilized the side of a cylindrical impactor to represent steering wheel impacts. Impactor energy in their studies was considerably higher than the current study (Figure 136). Despite the use of higher energies, the resulting peak forces were not considerably higher than those of the current study. This is likely a result of the lack of a head restraint in their studies and the load-limited effects of fracture. In general, the tests by Bruyere *et al.* (2000) that resulted in fracture had a lower peak force than those with fracture.

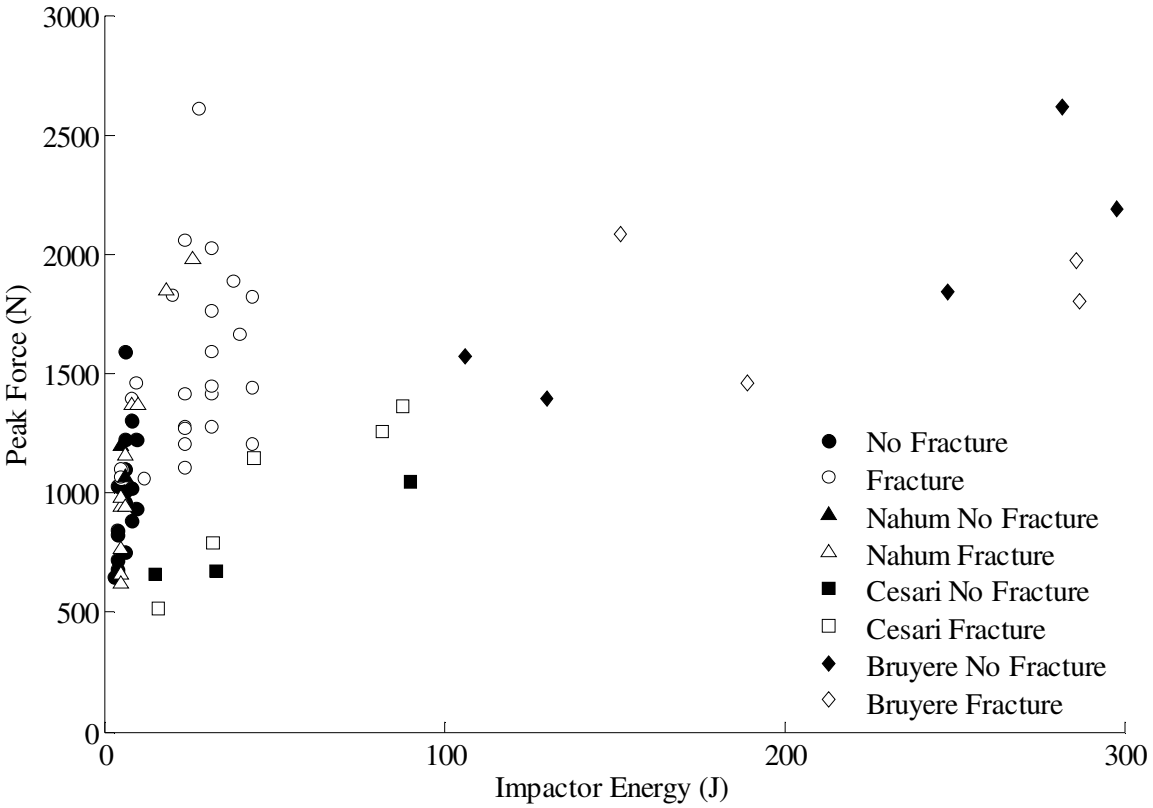

Figure 136: Peak force resulting from maxilla impact by study.

In this study, the impact was delivered to the sub-orbital region of the maxilla, which is a comparatively weak structure due to the thin wall of bone on its anterior surface (Figure 137). As in the Schneider *et al.* (1972) study, it is among the weakest regions in the face. Therefore, it is important to consider impact location and impactor size when utilizing the fracture thresholds obtained in the current study.

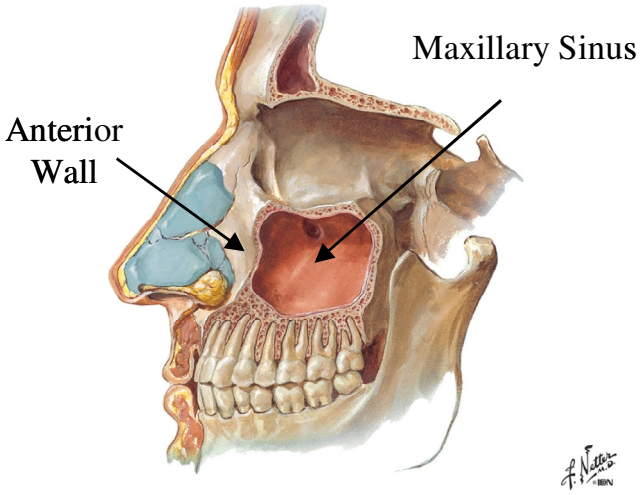

Figure 137: Lateral view of maxillary sinus.

The risk curves developed represent a conservative criterion for a projectile with an area of 6.45 cm^2 (1 in^2). This is because the actual contact patch between the impactor and the facial bone was always less than the actual impactor area. If the facial bones were flat, the contact area and impactor area would be equal and, therefore, the impactor force divided by the area would be an accurate measure of the pressure applied. The uneven nature of the face prevents an even distribution of pressure from being applied when struck by a flat impactor. This exemplifies the importance of padding that not only absorbs energy, but distributes force over a greater area. In fact, the average area of contact for the current test series was 1.9 cm^2. With these ideas in mind, the developed risk curves can be conservatively applied to impacts involving impactors with larger area, but if the area is considerably less controlling for impactor energy, the risk of injury will be proportionally higher.

Age was not found to be a significant factor in fracture force, but was found to be correlated with the initial stiffness of the maxilla response. The fact that age was not related to fracture force is supported in previous research (Yoganandan 1988). In their study the insensitivity to age was explained by the fact that facial bones are comprised mostly of cortical bone, which does not degenerate with age to the extent that cancellous bone does. Within the region of the maxilla that was struck in the current study, the maxilla consists mostly of cortical bone which may explain the lack of an age effect.

Limitations

The current study is limited by the use of a single impact direction and impactor type. This limitation was chosen so that a large sample size of consistent data could be obtained, however, due to the geometry of the maxilla it is reasonable to assume that impact direction will play a role in fracture risk. Due to the exclusive use of male subjects, gender effects could not be addressed.

Similar limitations exist for the evaluation of the FOCUS headform. In this study, a limited number of tests were performed to evaluate the FOCUS response to impact at one location at severities known not to cause any risk of damage to the headform. Additional testing at higher severities and various directions will elucidate its response and broaden its utility in fracture prediction.

CONCLUSIONS

The current study presents data describing the response of the maxilla to blunt impact and its tolerance to fracture. Acoustic emission sensors were utilized to generate non-censored fracture forces. In this test series fracture force generally occurred just prior to a change in the force-displacement response. This suggests that the load carrying capability of the maxilla is altered significantly following fracture onset. This response differs from the frontal bone which generally did not exhibit a change in stiffness until much larger changes in force were created after fracture onset. The non-censored forces values were utilized in parametric and non-parametric analyses to estimate risk functions for fracture risk. The 50% risk of maxilla fracture was determined to be between 1000 and 1200 N. Age was not found to be related with the risk of sustaining a maxilla fracture which is consistent with previous work. Impactor contact area was found to be a statistically significant variable when predicting the risk facial fracture.

The force-displacement response of the maxilla was defined by creating a corridor based on the characteristic average of the data. The force-displacement response often consisted of a biphasic response. Using acoustic emission sensors to determine the force

at which fracture occurred, it was observed that fracture always occurred prior to the initial peak.

The force-displacement corridors defined in this study can be used to improve finite element models and ATDs used in facial injury prediction. The FOCUS headform was evaluated and found to exhibit similar force-displacement relationships to the cadaver tests. Further evaluation and development of the FOCUS headform, through application of the current data, will improve its utility as a tool to evaluate facial fracture countermeasures.

REFERENCES

Allsop D, Kennett K: Skull and Facial Bone Trauma. Accidental Injury: Biomechanics and Prevention. A. Nahum and J. Melvin. New York, Springer-Verlag. 2nd Edition**,** 254-76; 2002.

Allsop D, Warner C, Wille M, Schneider D, Nahum A: Facial Impact Response – A Comparison of the Hybrid 3 Dummy and Human Cadaver, *Society of Automotive Engineers*, SAE No. 881719; 1988.

Bermond F, Kallieris D, Mattern R, Ramet M, Bouquet R, Caire Y, Voiglio E: Human Face Response at an Angle to the Fore-aft Vertical Plane Impact, *Proceedings of the IRCOBI*; 1989.

Bruyere K, Bermond F, Bouguet R, Caire Y, Ramet M, Voiglio E: Human Maxilla Bone Response to 30 degree Oriented Impacts and Comparison with Frontal Bone Impacts, *Proceedings of the 44th Association for the Advancement of Automotive Medicine Conference*, 219-34; 2000.

Cesari D, Ramet M, Welbourne E: Experimental Evaluation of Human Facial Tolerance to Injuries, *Proceedings of the IRCOBI*, Stockholm, Sweden; 1989.

Cormier J, Manoogian S, Bisplnghoff J, McNally C, Duma S: The Use of Acoustic Emission in Facial Fracture Detection, *Biomed. Sci. Instrum.*, 44, 147-52; 2008.

Funk J, Crandall J, Tourret L, MacMahon C, Bass C, Patrie J, Khaewpong N, Eppinger R: The Axial Injury Tolerance of the Human Foot/Ankle Complex and the Effect of Achilles Tension, *Journal of Biomechanical Engineering*, 124; 2002a.

Funk J, Srinivasan S, Crandall J, Khaewpong N, Eppinger R, Jaffredo A, Potier P, Petit P: The Effects of Axial Preload and Dorsiflexion on the Tolerance of the Ankle/Subtalar Joint to Dynamic Inversion and Eversion, *Stapp Car Crash Journal*, 46(0S2-34); 2002b.

Hodgson VR, Lange WA, Talwalker RK: Injury to the Facial Bones, *Proceedings of the 9th Stapp Car Crash Conference*, SAE No. 650957; 1965.

Kennedy EA: The Development and Validation of a Biofidelic Sythetic Eye for the Facial and Ocular Countermeasure Safety (FOCUS) Headform, PhD Biomedical Eng., Virginia Tech; 2007.

Kent R, Stacey S, Parenteau C: Dynamic Pinch Tolerance of the Phalanges and Interphalangeal Joints, *Traffic Inj Prev*, 9(1), 83-8; 2008a.

Kent R, Stacey S, Parenteau C: Dynamic Pinch Tolerance of the Phalanges and Interphalangeal Joints, *Traffic Injury Prevention*, 9, 83-8; 2008b.

Kleinbaum D, Klein M: Survival Analysis: A Self-Learning Text, 2nd, New York, Springer Science; 2005.

Lessley D, Crandall J, Shaw G, Kent R, Funk J: A Normalization Technique for Developing Corridors from Individual Subject Responses, *Society of Automotive Engineers*, 2004-01-0288; 2004.

Nahum AM: The Biomechanics of Facial Bone Fracture, *Laryngoscope*, 85(1), 140-56; 1975.

Nahum AM, Gatts JD, Gadd CW, Danforth J: Impact Tolerance of the Skull and Face, *Proceedings of the 12th Stapp Car Crash Conference,* October 22-23, New York; 1968.

Nyquist GW, Cavanaugh JM, Goldberg SJ, King AI: Impact Tolerance and Response of the Face, *Proceedings of the Advances in Bioengineering Conference*, Anaheim, CA; 1986.

Rudd R, Crandall J, Millington S, Hurwitz S, Hoglund N: Injury Tolerance and Response of the Ankle Joint in Dynamic Dorsiflexion, *Proceedings of teh 48th Stapp Car Crash Conference*, SAE No. 2004-22-0001; 2004.

Schneider DC, Nahum AM: Impact Studies of Facial Bones and Skull, *Proceedings of the 16th Stapp Car Crash Conference,* SAE No. 720965; 1972.

Welbourne ER, Ramet M, Zarebski M: A Comparison of Human Facial Fracture Tolerance with the Performance of a Surrogate Test Device, *Proceedings of the 12th ESV,* 89-4A-0-004, Gothenberg, Sweden; 1989.

Wells J, Rawlings R: Acoustic emission and mechanical properties of trabecular bone, *Biomaterials*, Volume 6(July); 1985.

Yoganandan N, Fintar F, Sances A, Myklebust J, Schmaltz D: Steering Wheel Induced Facial Trauma, *Proceedings of the 32nd Stapp Car Crash Conference,* SAE No. 881712; 1988.

Yoganandan N, Pintar FA, Reinartz J, Sances A: Human facial tolerance to steering wheel impact: A biomechanical study., *Journal of Safety Research*, 24(2), 77-85; 1993.

CHAPTER 8:
THE BIOMECHANICAL RESPONSE OF THE MANDIBLE TO BLUNT IMPACT

INTRODUCTION

The results of the National Automotive Sampling System (NASS) study performed in chapter one demonstrated that in frontal impacts, the mandible is the second most common site of a facial fracture, after the nose. Mandible fractures were found to be more common among unbelted occupants with no airbag. In side impacts, mandible fractures were more common the nasal bone fractures. Studies performing surveys on hospital data have also observed that the mandible is one of the more common sites of a facial fracture due to a MVC (Beck 1989, Zargar 2004). Mandible fractures occurring as a result of motor vehicle collisions (MVC) are often associated with more severe injuries (Fischer 2001). Fischer *et al.* (2001) found that 65% of patients with a mandible fracture due to a MVC also sustained a closed head injury. Facial fractures and lacerations were the most common injury associated with mandible fractures. Early studies examining the tolerance of the mandible were aimed at understanding its response to steering wheel impact. Based on the injury sources identified in chapter 1, steering wheel impact still plays a role in facial fractures.

Previous studies examining the tolerance of facial bones to impact have utilized a variety of experimental methods. These included differing impactor shapes and sizes, impact location, impact direction, and the use of padding. These variations limit the number of tests that can be pooled together in a statistical analysis to produce accurate estimates of fracture risk. Two main categories of methods include those using the flat surface of a cylindrical impactor (Nahum 1968, 1975, Schneider 1972) and those utilizing horizontal bars (Allsop 1988, Bermond 1999, Bruyere 2000, Cesari 1989, Hodgson 1965, Nyquist 1986, Welbourne 1989, Yoganandan 1988, 1993) meant to represent a steering wheel impact. Cylindrical impactors, meant to represent steering wheel impact, were utilized in the study by Cesari *et al*. (1989) to strike mandible at a upward angle of 45 degrees and in the horizontal plane. In there study peak forces ranged from 315 and 1860 N. A

horizontal impact, performed after an initial impact at 45 degrees resulted in a condylar fracture with a peak force of 683 N. The previous test on the same mandible had a peak force of 1860 N with a wound incurred to the mandible.

Flat, round impactors apply a more focal load on the face and were used by Nahum *et al.* (1968, 1975) and Schneider *et al.* (1972). Based on their results, minimal force tolerance levels were established for the mandible of 2447-4000 N. A flat, circular impactor tip with a contact area of 1 in^2 was used for all impacts. A crushable nickel pad added to the impactor distributed the load more evenly over the contact area and provided a secondary measure of force. Varying both the drop height and weight of the impactor allowed for the rate of onset of peak force to be regulated. Pulse duration was changed by adding an adapter to the impactor. Altering the rate of onset or pulse duration did not have a noticeable affect on the fracture tolerance. During the test by Nahum *et al.* (1975) they observed an instability when striking the mandible in the A-P direction and, therefore, impacts where performed with the force vector aligned through the condylar processes. The peak forces in their study ranged from 1890 to 4000 N. Seven of the ten tests resulted in a fracture.

Testing by Allsop *et al.* demonstrated that facial bones are capable of supporting load after fracture has occurred (Allsop 2002, Allsop 1988). This is an important concept as it requires that the fracture force is determined separate from a force-time or force-deflection response. In their studies, Acoustic Emission (AE) was monitored and when a signal burst was detected, fracture was assumed to have occurred. When comparing the time of an AE burst, to the force-time relationship, the authors found that the facial bones would fracture prior to peak force.

Knowing the precise time of fracture provides a non-censored measure of bone tolerance and, therefore, a more powerful data point for statistical analysis. The lack of acoustic sensors in the Nahum *et al.* studies suggest that their data are censored and that fracture is most likely occurring at a force less than the peak forces reported (Nahum 1968; Nahum

1975). These data can still provide useful information when assumed to be left censored and accounted for in a statistical analysis.

The current knowledge is also lacking in an understanding of the sub-failure mechanical response of the mandible to impact. The development of finite element models or Anthropomorphic Test Devices (ATD) for fracture prediction is limited by the lack of a quantitative measure of the maxilla response to impact. One such ATD is the Facial and Ocular CountermeasUre Safety (FOCUS) headform. The FOCUS headform has the ability to measure forces applied to the facial and orbital structures. It has been developed by Virginia Tech and validated for eye injury prediction (Kennedy 2007). There are eight separate sensing regions within the facial structures that overlie embedded load cells (Figure 51). These regions correspond to the frontal bone, nasal bone, zygoma, maxilla and mandible. Each load cell is capable of measuring forces along all three axes.

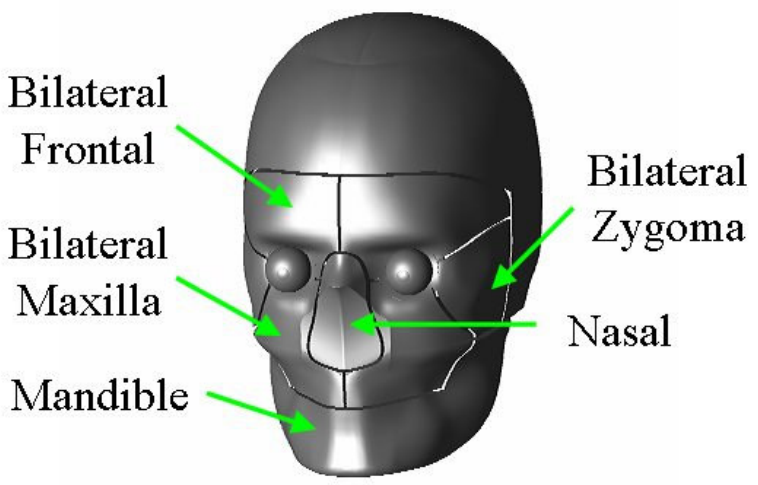

Figure 138: Load cell locations in FOCUS headform.

Defining force-deflection corridors for mandible impacts in cadavers will provide a basis for the implementation of the FOCUS headform in injury risk assessment.

The first goal of this study is to develop an estimate of the fracture tolerance of the mandible. The second goal of this study is to develop an understanding of the cadaveric response to blunt impact and compare this response to the FOCUS headform.

METHODOLOGY

A total of 29 male subjects ranging in age from 43 to 76 years were included in the study. All heads were frozen and thawed prior to testing. Pre-test CT imaging was performed on twelve subjects and post-test CT imaging was performed on three specimens.

Anthropometry

Prior to testing, CT imaging was performed on 17 of the subjects in the current study. The CT images were used to measure the thickness of the bone at the mandible symphysis, the skin thickness overlying the chin and the width of the mandible at the angle (Figure 139). Pearson correlation coefficients were determined to evaluate the correlation between anthropometric measures and the mechanical response of the nasal bone. These measures were also included in the survival analysis to determine their utility in predicting maxilla fracture.

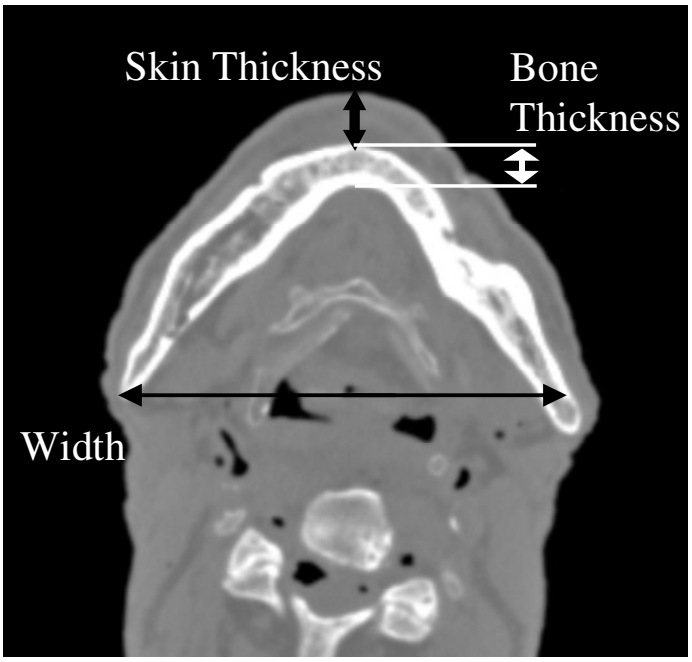

Figure 139: Measurements taken using pre-test CT imaging.

Specimen Preparation

The specimens were removed from the body and prepared by removing the scalp overlying the occipital region to provide a rigid support at the posterior skull. Metal screws were inserted into the occiput to provide additional structure for the casting material to adhere to. Each head was then rigidly mounted to a semi-circular, polycarbonate support using Bondo. Consistent orientation between subjects was obtained by vertically aligning the Frankfort plane prior to mounting. Specific anatomical landmarks were used to determine impact location of impact. For the mandible impacts in this study, the impactor was aligned with the midline of the chin and vertically such that the superior edge of the impactor was below the alveolar processes. Each impact was performed using a cylindrical, free-falling rigid aluminum impactor (3.2 kg) with a steel tip (Figure 53). The flat impacting surface had an area of 6.45 cm^2 (1 in^2) and was machined with a slight bevel to reduce edge effects. Prior to testing, the mandible was held in a closed position with tape. The tape was pre-torn such that it would tear easily once mandible motion began.

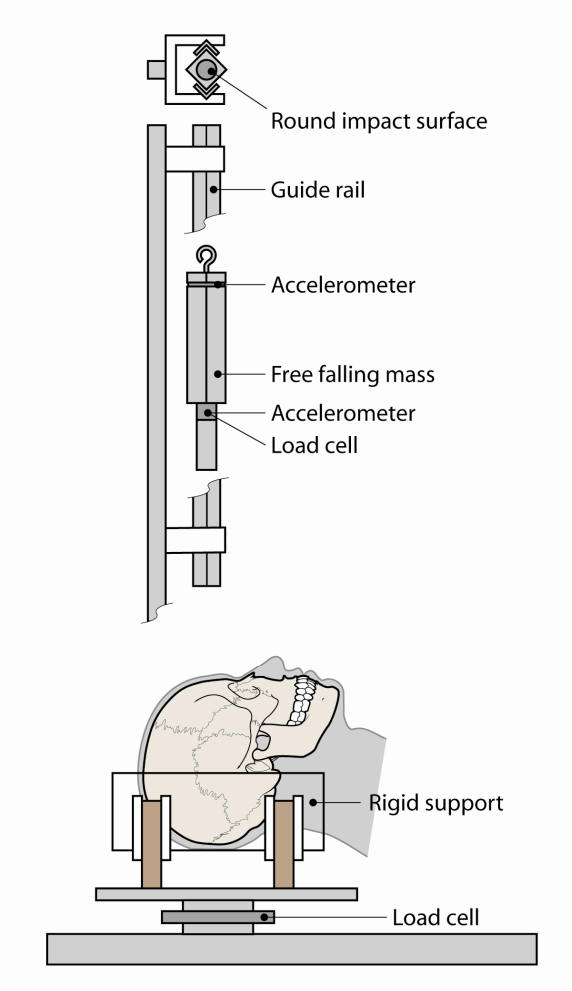

Figure 140: Schematic of test apparatus to be used in the current study.

Instrumentation

The specimens utilized in this study were tested in three separate series that consisted of slightly different instrumentation and data acquisition methods. In all cases an AE sensor (Micro30S, Physical Instruments, New Jersey) was mounted to the mandible, anterior to the angle at a location with a flat surface to facilitate mounting the sensor. The AE sensor was mounted directly to the bone by removing the soft tissue and periosteum and gluing the sensor in place with cyanoacrylate adhesive. This method has been used successfully in previous testing during this study and by others (Funk 2002, Kent 2008a, Rudd 2004). In all tests, the rigid impactor was instrumented with two single-axis accelerometers (Endevco 7264B-2000, Endevco Corp., San Juan Capistrano CA). All data except AE data were filtered to CFC 300. Previous studies have utilized CFC 180;

however the use of CFC 300 did not significantly alter the measured peak forces and was chosen to increase the likelihood of capturing small changes in impactor force during fracture (Bermond 1989, Bruyere 2000, Nyquist 1986). Impactor displacement was calculated by double-integrating the acceleration data. Contact between the impactor and subject was defined based on an impactor force of 10 N. Once the impactor force reached a level above 10 N, the displacement with respect to the mandible was set to zero and further motion was calculated by double integration. These aspects remained constant throughout the test series.

Series 1, subjects 1-13: The AE sensors were sampled at a rate of 2 MHz and all other instrumentation at 30 kHz. The acoustic emission data were acquired using a PC card supplied by the sensor manufacturer (PCI-2, Physical Instruments, New Jersey). Each AE sensor was attached to a preamplifier set to a gain of 40 dB. Impact force was obtained by multiplying the impactor acceleration by its mass. Impactor acceleration was determined by the average of the two attached accelerometers.

Series 2, subjects 14-23: The AE sensors were sampled at a rate of 5 MHz and all other instrumentation at 20 kHz. The acoustic emission data were acquired using an oscilloscope (TDS3000B Tektronix, Oregon). Each AE sensor was attached to a preamplifier set to a gain of 40 dB. A load cell (Denton, 8617JTF, Rochester Hills, MI) was attached to the tip of the impactor which was also instrumented with a single axis accelerometer (Endevco 7264B-2000, Endevco Corp., San Juan Capistrano CA). A load cell (Denton 1968, Rochester Hills, MI) was mounted to the head support to measure reaction forces. Impact force was obtained using the impactor load cell along with the inertially compensated tip mass.

Series 3, subjects 26-35: All parameters described in series two remained the same, with the exception of the AE preamplifier gain which was set to 20 dB in this series. Additionally, high-speed video was also recorded at a frame rate of approximately 4,000 fps. Impactor displacement calculated by double integrating impactor acceleration was

verified using high-speed video analysis. This was performed by creating a second-order polynomial fit of the displacement obtained by video analysis.

To define the average force-displacement response of the mandible, a corridor was created up to 90% of the peak force. The response corridor was determined by the mean and standard deviation of the characteristic average (Lessley 2004). The characteristic average was created using the force-displacement response up to 90% of the peak force of each test. This ensured that only the linear portion of the response was included in the characteristic average calculation. The values for the corridor where determined using a custom Matlab program that implemented the algorithm described by Lessley *et al.* (2004). The corridor was fit using 3rd order polynomials so that there values could be reported here.

Acoustic Emission

AE data were used to determine the force at which fracture is initiated. Previous Studies using AE data have denoted the onset of AE signal as the onset of fracture. Recently, studies have utilized a threshold to differentiate AE consistent with fracture from a baseline AE signal (Cormier 2008, Funk 2002, Kent 2008b, Rudd 2004). Kent *et al.* (2008b) demonstrated that an AE burst corresponded with a sharp decline in force during phalange fracture.

To utilize AE data as a method of estimating the time at which fracture begins, a threshold must be established that differentiates normal background emissions from those associated with the fracture event. The methods used to establish the AE threshold was described in a previous publication (Cormier 2008: Chapter 4). To establish a relationship between AE and fracture rather than the presence of an impact event, low-severity impacts were performed on specimens with pre-existing fractures. Due to the compromised integrity of these specimens, fracture propagation will occur at forces much lower than that required to initiate fracture. If high levels of AE are a result of fracture then high AE should be observed when the pre-fractured specimens are struck at lower

levels of force. Once the threshold was established, the force corresponding to the occurrence of above-threshold AE was treated as the force required to initiate fracture.

Risk Function Analysis

A survival analysis was performed utilizing parametric and non-parametric techniques. For the parametric analysis, a Weibull model was assumed and fit to the fracture data. The advantage of using a Weibull model is that the method used to determine the model parameters accounts for the fact that the non-fracture tests are right censored. The LIFEREG procedure within SAS (SAS Institute, Cary N.C) accounts for left and right censoring as well as non-censored data and was used to determine the parameter estimates for the Weibull model (Allison 1995, Cantor 2003). The Weibull distribution is advantageous because it is not forced to be symmetric, so it can accommodate risks that do not increase in the same way throughout the set of input variables. The Weibull CDF is given by,

$$CDF = 1 - \exp -(\lambda \cdot F)^{\gamma} \qquad \text{(Equation 4)}$$

Where λ and γ are the scale and shape parameters respectively and F is the applied. This function will provide an estimate of risk of injury using the maximum likelihood estimates of the scale and shape parameters. A non-parametric model was also created using the Kaplan-Meier method. The Kaplan-Meir method assumes the data are only right or non-censored and determines the risk of fracture based on the number of subjects at risk which sustain a fracture for a given force (Kleinbaum 2005).

FOCUS Headform Biofidelity

A series of impacts were performed on the FOCUS headform in order to characterize its response to blunt impact. Impact severity was chosen to facilitate the development of risk functions for mandible fracture based on results of the cadaver tests and the capability of the FOCUS headform. The impact was applied using the same apparatus used for the cadaver impacts (Figure 54). Impact location was determined the same way as the cadaveric impacts. The impactor was instrumented with a, single-axis accelerometer (Endevco 7264B-2000, Endevco Corp., San Juan Capistrano CA). A load

cell (Denton, 8617JTF, Rochester Hills, MI) was attached to the tip of the impactor which was also instrumented with a single axis accelerometer (Endevco 7264B-2000, Endevco Corp., San Juan Capistrano CA) (Figure 53). All instrumentation was samples at a rate of 20 kHz. Forces measured by the internal load cells were recorded and compared to impactor forces and examined for load-sharing between facial regions. The stiffness of the FOCUS response was determined up to 20% and between 20% and 80% of the peak force for comparison to the cadaveric response.

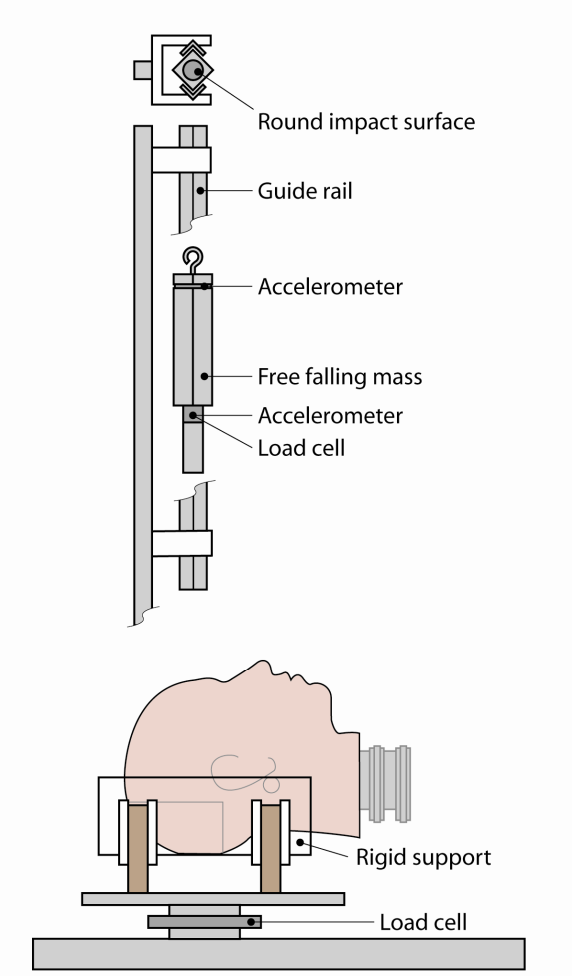

Figure 141: Apparatus used for FOCUS impacts.

RESULTS

A total of 41 tests were performed to determine the response of the mandible to blunt impact (Table 18). The lack of mandible constraint resulted in mandible motion after

initial impact. As a result, impact force generally reached an initial peak, and then decreased with a secondary peak occurring later due to interaction with other anatomy or being deflected off the subject. The data presented here will be limited to the initial response and not the subsequent events occurring after mandible motion.

The maximum force during the initial peak ranged from 402 to 1607 N. A mandible fracture was produced in four tests and an additional six incurred fractures of the alveolar processes. The voltage measured by the AE sensor ranged from 0 to 10 volts, with the majority of fracture tests reaching a maximum of 10 volts. A threshold voltage of 9 volts was established for heads 1 through 14 and 5 volts for the remaining heads. These thresholds were based on the magnitude of AE during fracture (Figure 142) and non-fracture (Figure 144) tests. Therefore, the force corresponding to an AE above the threshold was utilized as the force to initiate fracture in the statistical analysis.

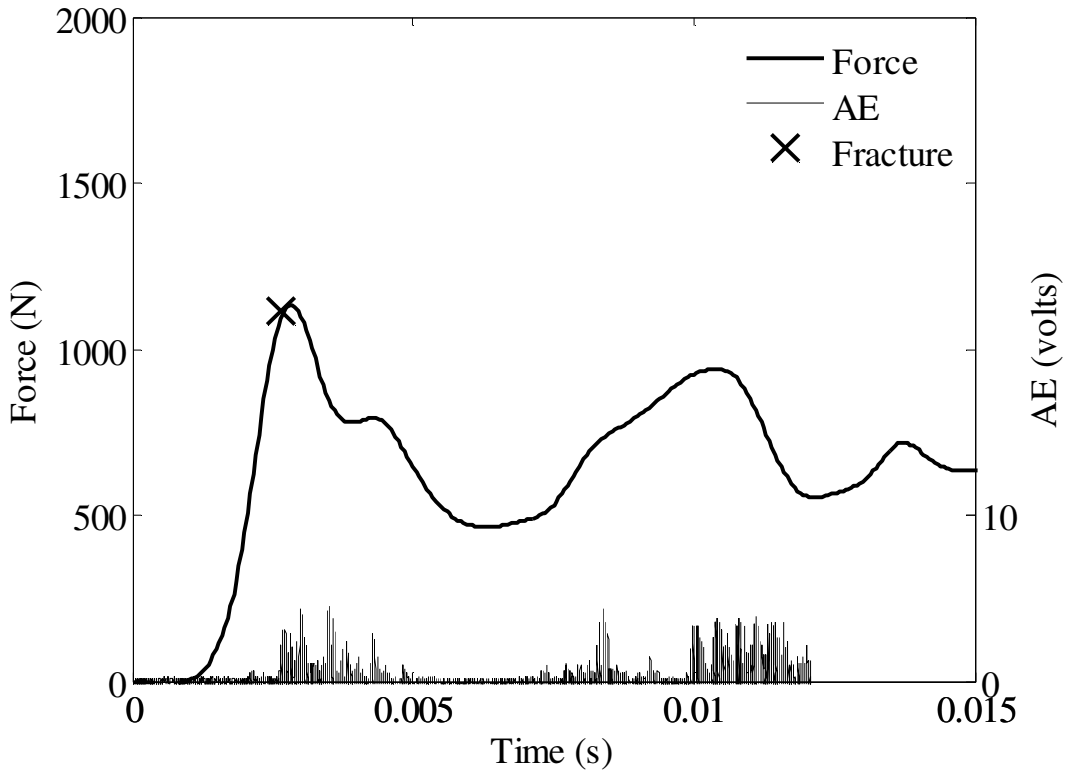

Figure 142: Impact force and acoustic emission during a mandible impact resulting in fracture.

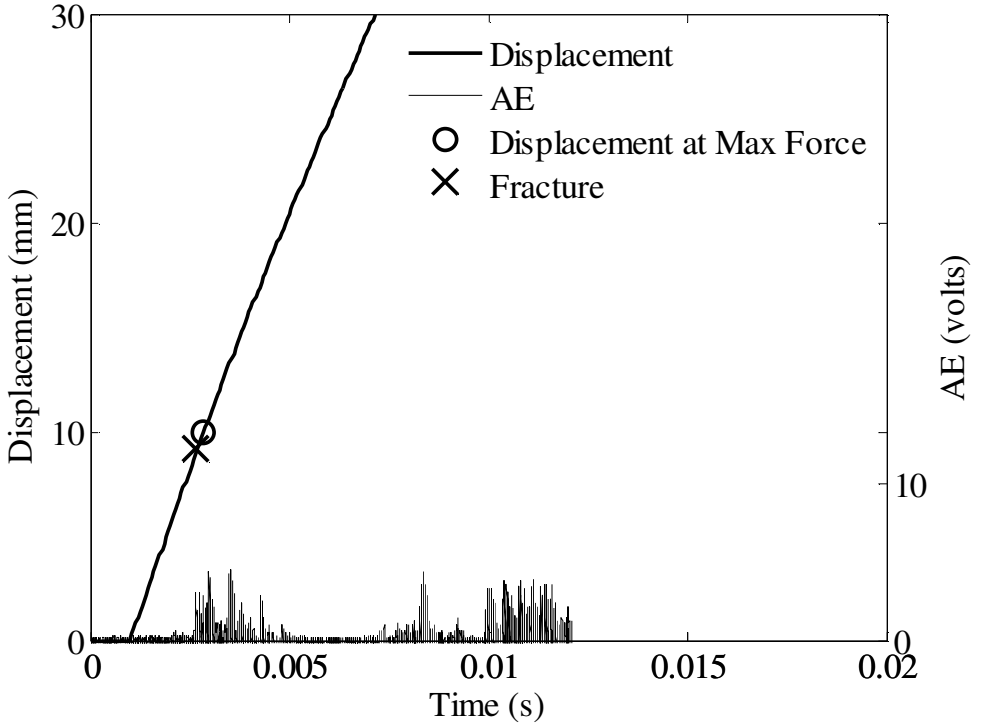

Figure 143: Impactor displacement and acoustic emission during a mandible impact resulting in fracture.

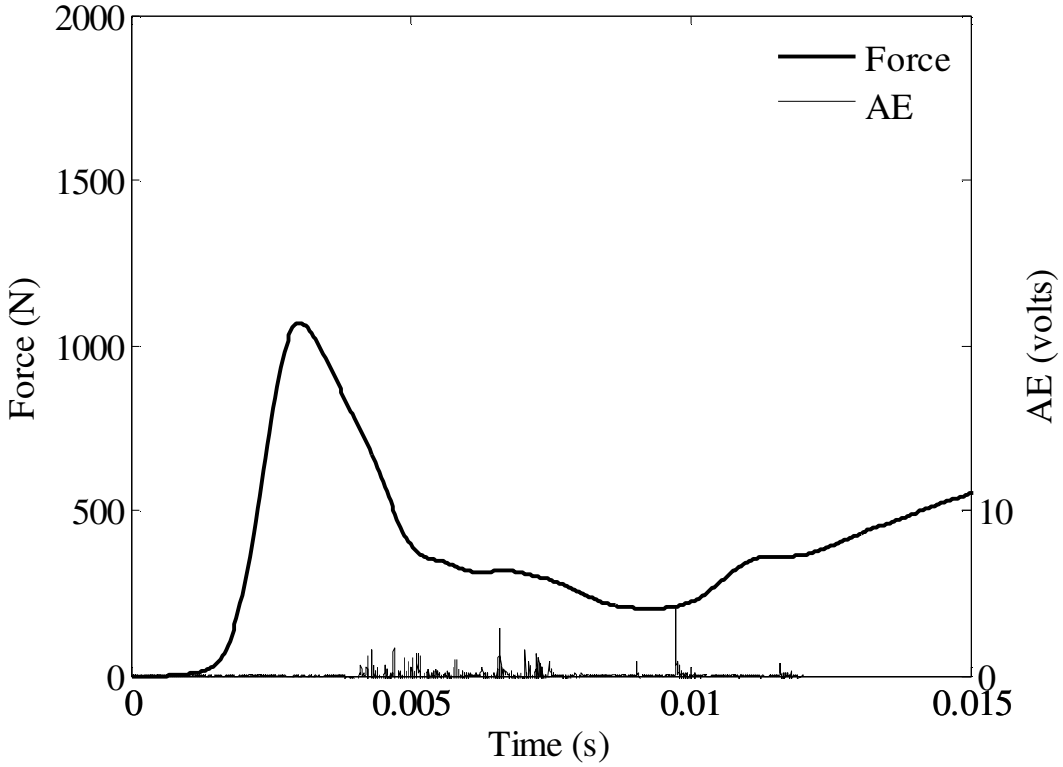

Figure 144: Impact force and acoustic emission during mandible impact without fracture.

Table 18: Summary of subject characteristics and results of mandible impacts. n.a. = not available

Subject	ID	Age	Height (cm)	Weight (kg)	Impactor Energy (J)	Peak Force (N)	Fracture Force (N)
1	SM58	61	168	69	34	1069	
2	SM60	41	170	64	48	1607	
3	SM56	57	170	84	8	658	
					44	1245	
4	SM57	75	165	65	8	402	
5	SM61	76	170	44	59	876	
5	SM61	76	170	44	59	1257	
6	SM62	43	183	112	58	1162	601
7	34237	66	na	na	12	602	
					58	1284	
8	34236	54	na	na	58	1106	
9	32120	58	na	na	48	1153	
11	33574	57	na	na	58	1015	
12	33995	49	na	na	59	1047	
13	34403	79	na	na	58	772	
14	5758	83	175	73	54	763	
15	5791	94	163	64	54	784	
16	5556	59	175	82	55	713	
17	5735	67	180	82	55	793	
18	5763	47	183	89	54	1302	
19	5757	84	183	109	53	1008	769
21	5675	76	152	91	54	749	750
22	5664	83	180	73	54	999	
23	5760	87	163	75	54	1075	
25	5863	78	170	38	47	788	
27	5821	72	163	59	47	1300	
28	5807	85	180	65	47	1132	1098
29	5818	81	175	88	47	615	
31	437	67	na	na	47	660	
32	459	71	na	na	47	614	
33	5805	81	177	79	47	747	
34	5837	68	175	71	47	1328	

The majority of impacts were performed at an impactor energy between 45 and 60 J. Peak force did not show an increasing trend within this range of impactor energy (Figure 79).

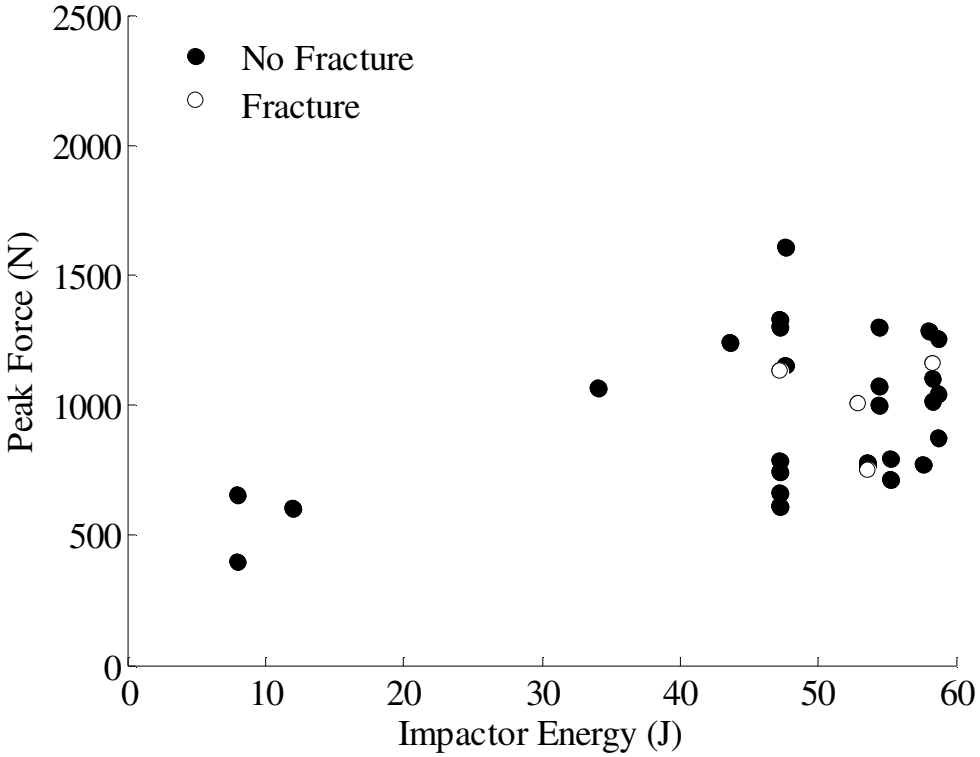

Figure 145: Peak impactor force with respect to impactor energy for mandible impacts.

The average contact area estimated using Fuji Film during the mandible impacts was 2.8 cm^2 (SD = 1.6). This value was less than half of the available 6.45 cm^2 impactor area. There was no correlation between peak force and contact area ($p = 0.09$).

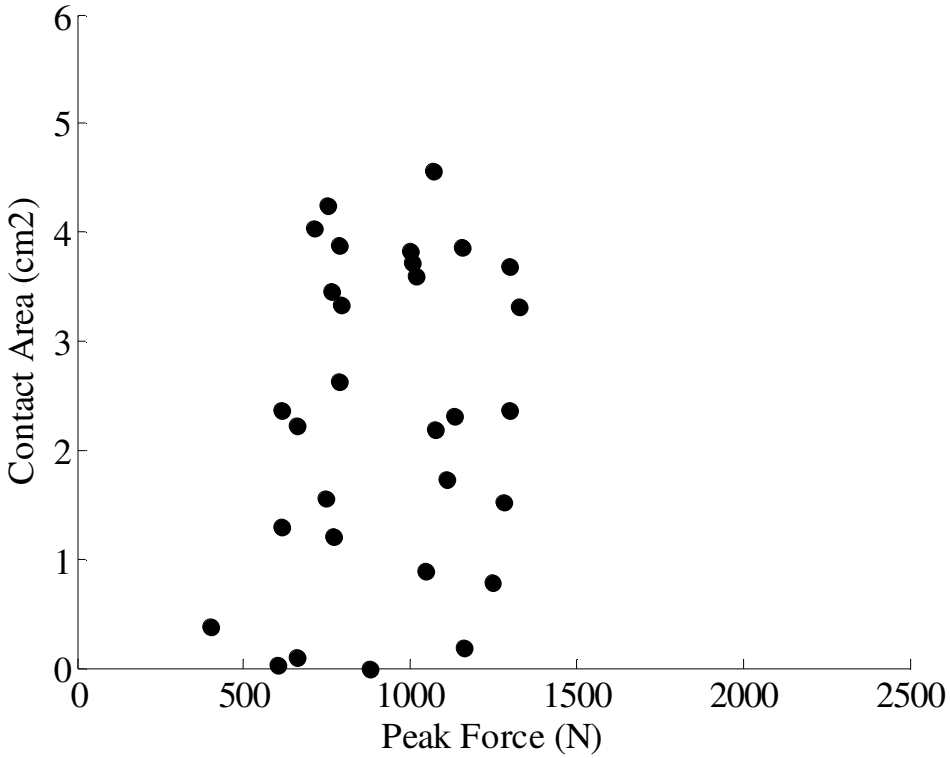

Figure 146: Relationship between contact pressure and peak mandible force.

Anthropometry

Measurements describing the size of the mandible were correlated with subject head size. Head depth was correlated with the thickness of the mandible ($p = 0.01$) and its width at the angle ($p = 0.006$). The thickness of the skin overlying the mandible demonstrated a negative correlation with the initial stiffness of the mandible response ($p = 0.047$). The correlation coefficient was -0.49, indicating a weak trend. Subject age demonstrated no correlation with the stiffness of the mandible response.

Risk of Mandible Fracture

A total of 29 tests were used in the development of risk functions for mandible fracture. Only one test for each subject was used and no repeated tests resulting in fracture were included in the survival analysis. Only four of the tests performed in this study resulted in a fracture of the mandible. As a result, the risk estimates based on the Kaplan-Meier method do not reach 100% (Figure 147). The risk estimated by the Weibull distribution (Table 19) pass through the average risks generated by the Kaplan-Meier non-parametric method.

Table 19: Parameter estimates of Weibull distribution of mandible fracture risk.

		95% Confidence Interval	
Parameter	**Estimate**	**Lower**	**Upper**
Scale	0.0005	0.0009	0.0003
Shape	2.77	1.23	6.24

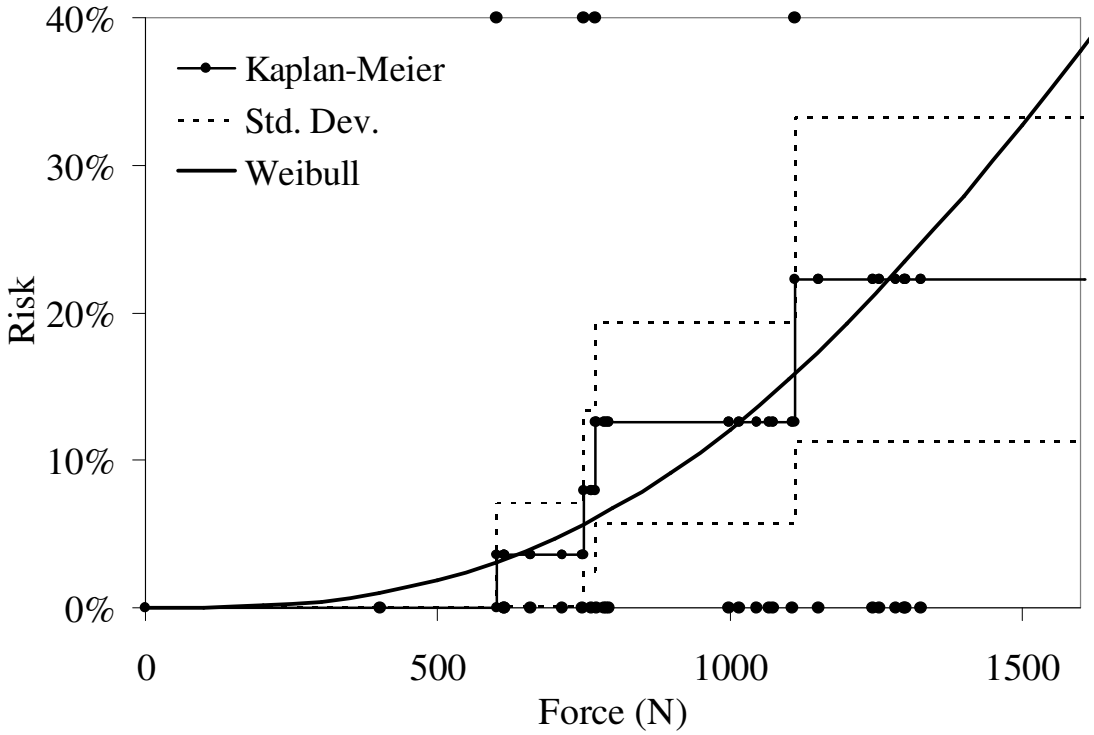

Figure 147: Risk of mandible fracture using Kaplan-Meier and Weibull models.

Cadaveric Force-Displacement

The force-displacement response of the cadaver was defined just beyond the initial peak in force. The response secondary to this was a result of the impactor sliding off of the mandible and therefore, did not reflect the response of the mandible. The majority of tests were confined to the standard deviation of the characteristic average (Figure 148). In two cases, the subjects exhibited a longer toe region that reached beyond the corridor.

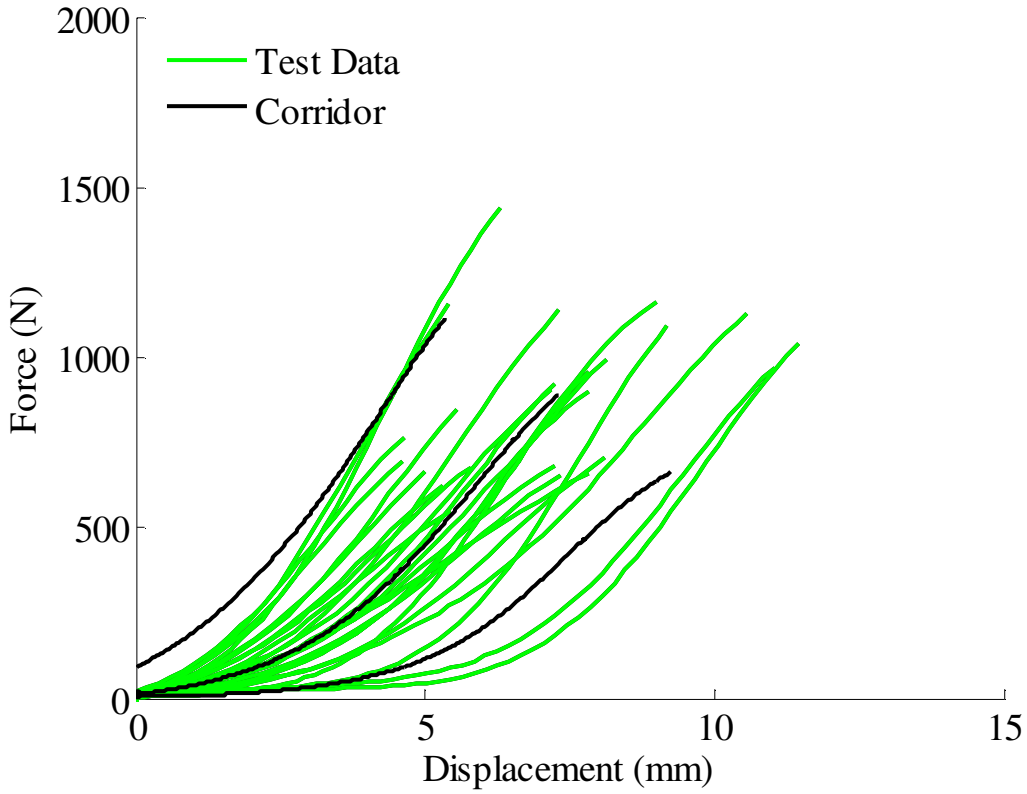

Figure 148: Cadaveric mandibular force-displacement response with corridor.

FOCUS Headform Biofidelity

A total of 5 tests were performed on the mandible region of the FOCUS headform. Impactor velocity ranged from 2.8 to 3.2 m/s resulting corresponding to an impactor energy of 12.7 to 15.7 J. The peak forces measured by the impactor ranged from 1874 to 2032 N. On average 20% of the response occurred at a displacement of 3.3 mm (Std. Dev. = 0.3) with an initial stiffness of 115 N/mm (SD = 9) and a secondary stiffness of 181 N/mm (SD = 42). The peak force measured by the internal FOCUS load cells were practically equal (Figure 149) to the impactor force with an average difference of 0.8%. The forces measured by the internal mandible load cell in the vertical (z) and transverse (y) directions were low, with the vertical forces being the higher at values of approximately 13% of the impactor peak force.

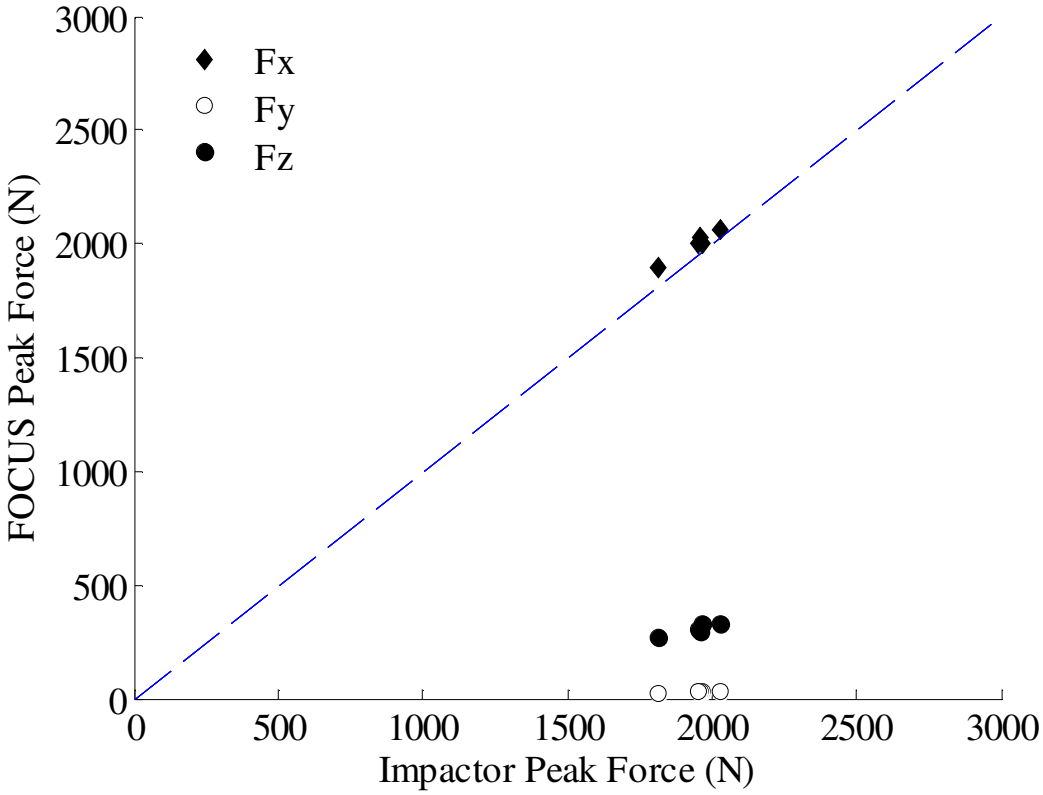

Figure 149: Internal FOCUS mandible force by direction and impactor force.

The force-displacement of the FOCUS headform was repeatable and followed a similar force-displacement response at the various impactor energies (Figure 150). The FOCUS response to the impact was elastic and resulted in the impactor bouncing off the headform following the initial impact. The polynomials used to fit the FOCUS corridor can be used to recreate the overall force-displacement response (Figure 151).

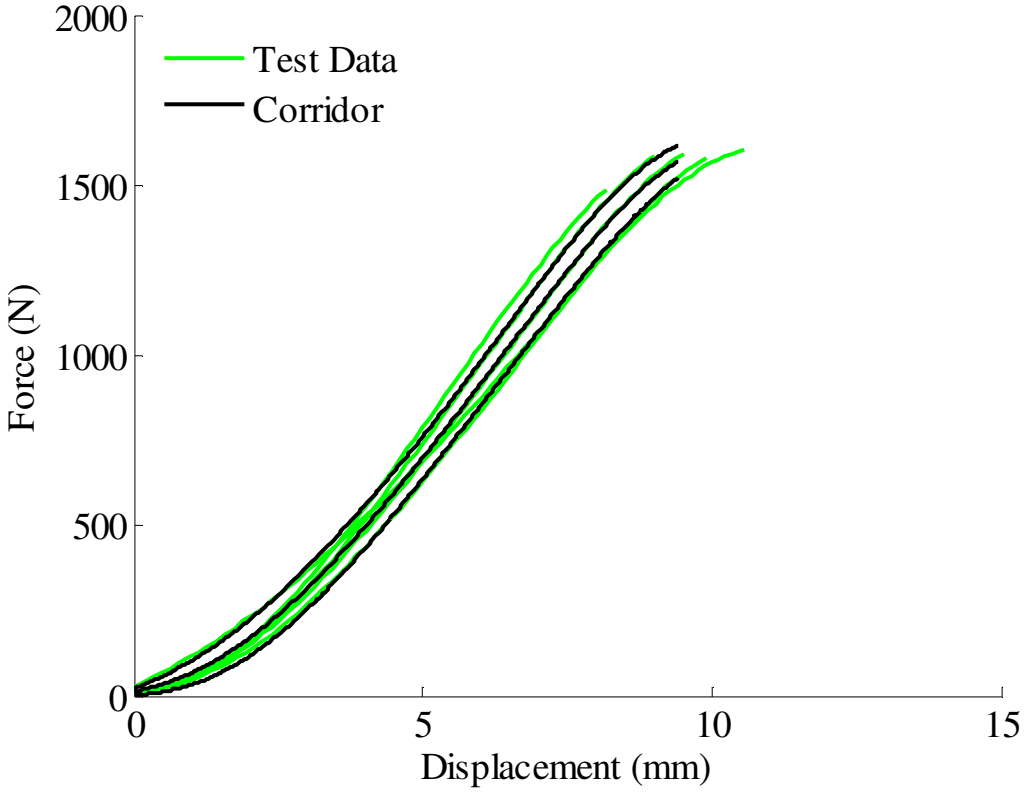

Figure 150: Mandible force- displacement response of FOCUS with corridor.

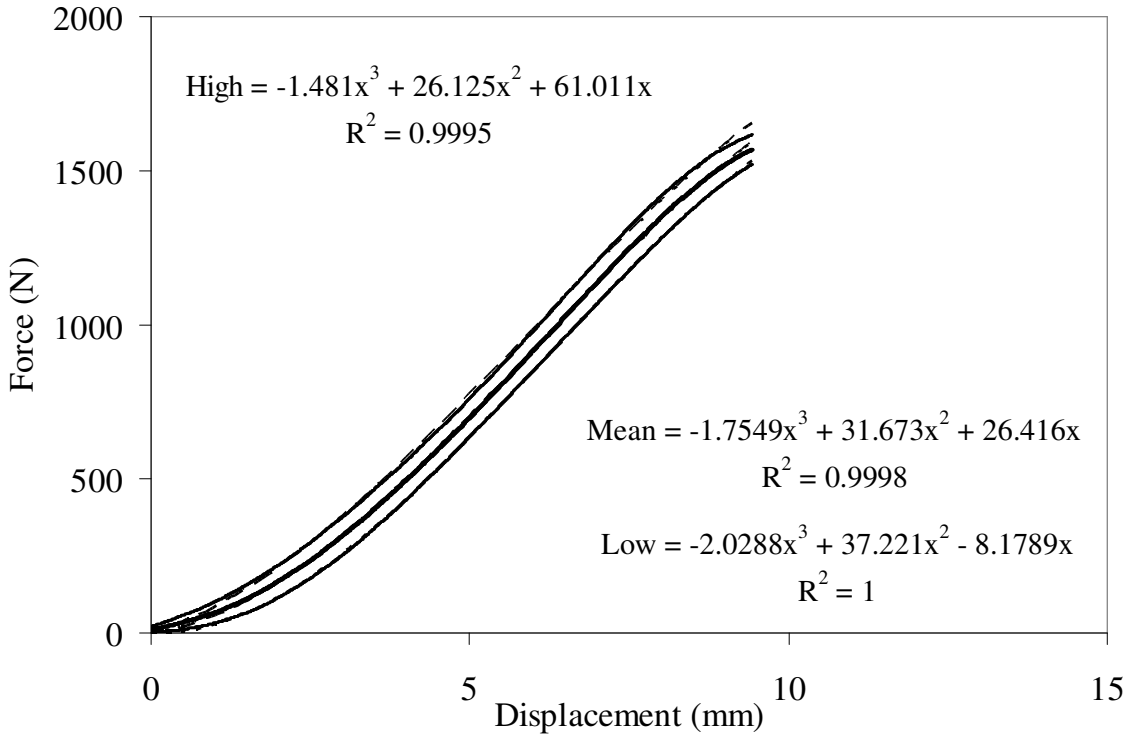

Figure 151: Polynomial fit to mandible force-displacement FOCUS response.

The response of the FOCUS headform was within the upper standard deviation of the FOCUS response (Figure 152). The secondary stiffness of the cadaver and FOCUS were not statistically different ($p = 0.65$). The stiffness up to 20% of peak force between the cadaver and the FOCUS were statistically different ($p < 0.0001$), but the displacement at this force was not ($p = 0.58$).

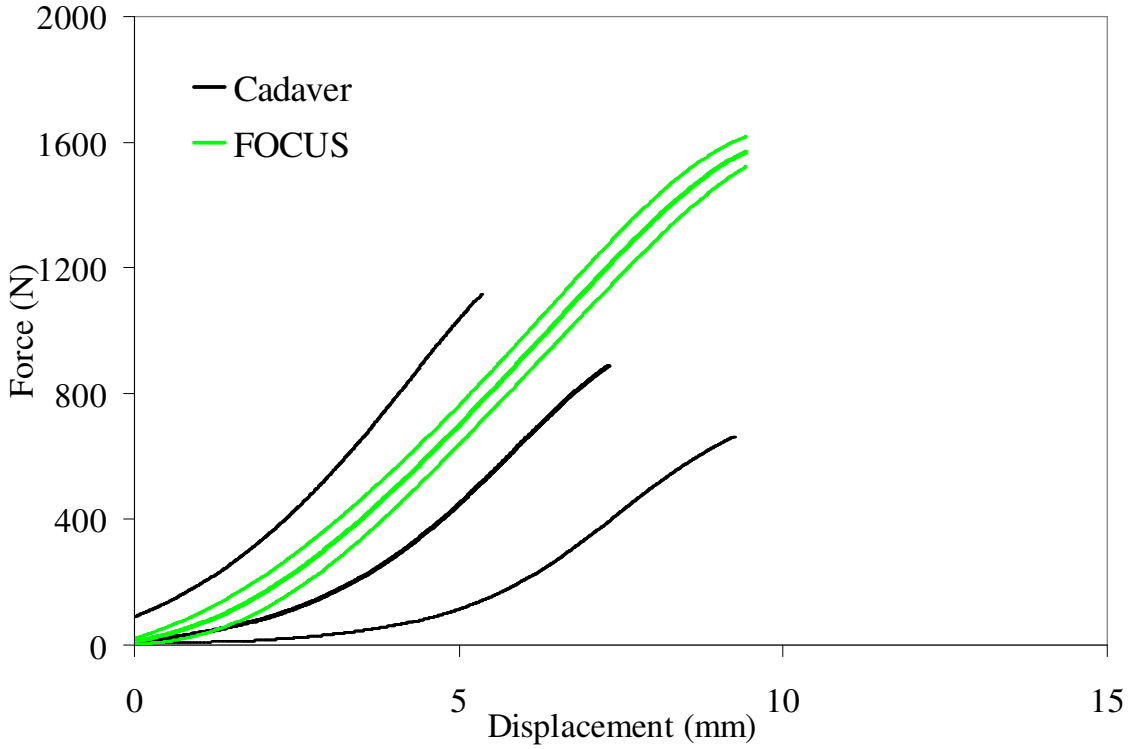

Figure 152: Cadver and FOCUS corridors for mandible impact.

DISCUSSION

This study presents an estimate of the risk for mandible fracture as a result of blunt impact and the resulting force-displacement response. The impact in the study was applied in the anterior-posterior (AP) direction to an unconstrained mandible. This resulted in motion of the mandible following impact and, therefore, the force-displacement responses reported here reflect the global response of the mandible and not deformation of the mandible. The influence of impact direction can be illustrated by comparing the current study to the results of Nahum *et al.* (1975) (Figure 153). In their

study, the mandible was struck such that the line of force was aligned with the condylar processes. This prohibited the mandible from opening as occurred in the current study, which has a force limiting effect.

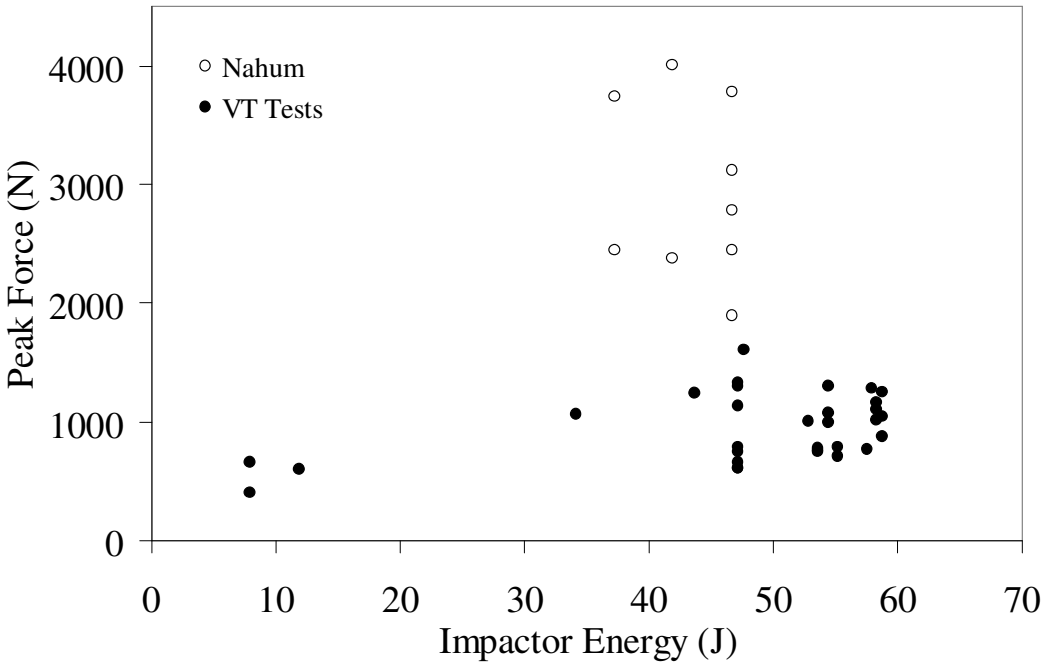

Figure 153: Mandible peak forces in current study and Nahum *et al.* (1975) by impactor energy.

The average contact area of 2.8 cm^2 measured using Fuji Film is less than half of the available (6.45 cm^2) impactor area. On average, the area measured by the Fuji Film is likely an overestimate of the actual contact area. This is due to the interaction between the impacting surface and other regions of the subject or test mount following the initial interaction with the mandible.

The mandible of the FOCUS headform is a rigid structure and, therefore, the reaction forces it can provide will exceed those of a human. This is especially true when loaded in the AP direction as in the current study. The results of this study suggest that without muscle tone the inertia of the mandible will support approximately 1600 N. This force was capable of causing fracture in a small percentage of the tests performed in this study. Considering that these subjects were mostly edentulous, it appears that peak forces measured in this study represent a relatively low risk of mandible fracture. Only one of

the subjects that sustained a fracture in this study was not edentulous. This was subject 28, which had the highest fracture force of the other three subjects sustaining a mandible fracture.

The response of the FOCUS headform was within the corridor created based on the cadaver responses. As a result of the higher stiffness of the FOCUS headform, the peak forces were higher than those expected from a cadaver impact at the same severity. The current study does demonstrate statistically significant differences between the FOCUS and cadaver stiffness. However, it also provides the data necessary to improve the biofidelity of the FOCUS headform.

Limitations

The current study is limited in the direction at which the impact was applied. Previous work by Nahum *et al.* (1975) has demonstrated influence of impact direction on the fracture tolerance of the mandible. Additional testing should be performed to expand the biofidelity of the FOCUS headform to lateral impacts. The low number of mandible fracture incurred in the current study limits the capacity to develop risk curves for fracture, however it is clear that at this impact severity and direction, the mandible will generally move out from under the impactor before injurious loading can be applied.

CONCLUSIONS

This study presents the results of 31 tests performed by impacting the mandible with a blunt impactor in the anterior-posterior direction. Do to the horizontal impact angle at the mandible, impact caused the mandible to open freely. This reduced the peak forces exerted on the mandible as demonstrated by comparison to a previous study using a similar impactor and a 45 degree upward impact angle. The motion of the mandible in this study reduced the likelihood of fracture, and thusly, only four of the subjects incurred a mandible fracture. One of these four was not edentulous and, using acoustic emission sensors the fracture force for this subject was higher than the others. Based on the limited number of fractures, the risk of fracture was estimated by parametric and non-

parametric techniques. The estimated 10% risk of fracture corresponded to a force between 770 and 1112 N.

Force-deflection corridors of the cadaver response were generated to facilitate evaluation of the FOCUS headform. The response of the FOCUS headform was within the cadaver corridor, however, the resulting peak forces were higher than those expected from the cadaver response at similar impact severities. The data provided in the current study can be utilized to improve the biofidelity of the FOCUS headform so that it can become a useful tool in assessing facial fracture countermeasures.

REFERENCES

Allsop D, Kennett K: Skull and Facial Bone Trauma. Accidental Injury: Biomechanics and Prevention. A. Nahum and J. Melvin. New York, Springer-Verlag. 2nd Edition**,** 254-76; 2002.

Allsop D, Warner C, Wille M, Schneider D, Nahum A: Facial Impact Response – A Comparison of the Hybrid 3 Dummy and Human Cadaver, *Society of Automotive Engineers*, SAE No. 881719; 1988.

Beck RA, Blakeslee DB: The changing picture of facial fractures. 5-Year review, *Arch Otolaryngol Head Neck Surg*, 115(7), 826-9; 1989.

Bermond F, Kallieris D, Mattern R, Ramet M, Bouquet R, Caire Y, Voiglio E: Human Face Response at an Angle to the Fore-aft Vertical Plane Impact, *Proceedings of the IRCOBI*; 1989.

Bruyere K, Bermond F, Bouguet R, Caire Y, Ramet M, Voiglio E: Human Maxilla Bone Response to 30 degree Oriented Impacts and Comparison with Frontal Bone Impacts, *Proceedings of the 44th Association for the Advancement of Automotive Medicine Conference*, 219-34; 2000.

Cormier J, Manoogian S, Bisplnghoff J, McNally C, Duma S: The Use of Acoustic Emission in Facial Fracture Detection, *Biomed. Sci. Instrum.*, 44, 147-52; 2008.

Fischer K, Zhang F, Angel MF, Lineaweaver WC: Injuries associated with mandible fractures sustained in motor vehicle collisions, *Plast Reconstr Surg*, 108(2), 328-31; 2001.

Funk J, Crandall J, Tourret L, MacMahon C, Bass C, Patrie J, Khaewpong N, Eppinger R: The Axial Injury Tolerance of the Human Foot/Ankle Complex and the Effect of Achilles Tension, *Journal of Biomechanical Engineering*, 124; 2002.

Kennedy EA: The Development and Validation of a Biofidelic Sythetic Eye for the Facial and Ocular Countermeasure Safety (FOCUS) Headform, PhD Biomedical Eng., Virginia Tech; 2007.

Kent R, Stacey S, Parenteau C: Dynamic Pinch Tolerance of the Phalanges and Interphalangeal Joints, *Traffic Inj Prev*, 9(1), 83-8; 2008a.

Kent R, Stacey S, Parenteau C: Dynamic Pinch Tolerance of the Phalanges and Interphalangeal Joints, *Traffic Injury Prevention*, 9, 83-8; 2008b.

Kleinbaum D, Klein M: Survival Analysis: A Self-Learning Text, 2nd, New York, Springer Science; 2005.

Lessley D, Crandall J, Shaw G, Kent R, Funk J: A Normalization Technique for Developing Corridors from Individual Subject Responses, *Society of Automotive Engineers*, 2004-01-0288; 2004.

Nyquist GW, Cavanaugh JM, Goldberg SJ, King AI: Impact Tolerance and Response of the Face, *Proceedings of the Advances in Bioengineering Conference*, Anaheim, CA; 1986.

Rudd R, Crandall J, Millington S, Hurwitz S, Hoglund N: Injury Tolerance and Response of the Ankle Joint in Dynamic Dorsiflexion, *Proceedings of teh 48th Stapp Car Crash Conference*, SAE No. 2004-22-0001; 2004.

Zargar M, Khaji A, Karbakhsh M, Zarei MR: Epidemiology study of facial injuries during a 13 month of trauma registry in Tehran, *Indian J Med Sci*, 58(3), 109-14; 2004.

CHAPTER 9:
MATHEMATICAL MODELING OF FACIAL IMPACTS

INTRODUCTION

The previous chapters describe the sub-failure mechanical response of the facial bone to blunt impact. The information provided can be utilized to improve finite element models and Anthropometric Test Device (ATD) biofidelity, such as the Facial and Ocular CountermeasUre Safety (FOCUS) headform described previously. Additional utility can be gained from these data by developing mathematical models which are optimized to reproduce the facial response to impact. Mathematical models can be utilized to estimate the expected response of the facial bones as a function of impactor mass and velocity. Since the current study utilized the same impactor and impact direction, the only input parameter is the initial impactor velocity. The resulting cadaver response is a function of human variability consisting of geometry and material properties. The influence of these variables on the facial bone response can be approximated by optimizing the model parameters. The purpose of this study is to develop mathematical models of the frontal bone, nasal bone and maxilla based on their response to blunt impact.

METHODOLOGY

The response of the frontal bone, nasal bone and maxilla were characterized by creating a Maxwell material model consisting of a spring and dashpot in series (Figure 154). The spring stiffness was estimated using a bilinear fit due to the presence of an initial toe region in the force-deflection response. The magnitude of the linear stiffness (k) and damping factor (c) were initially optimized for each test.

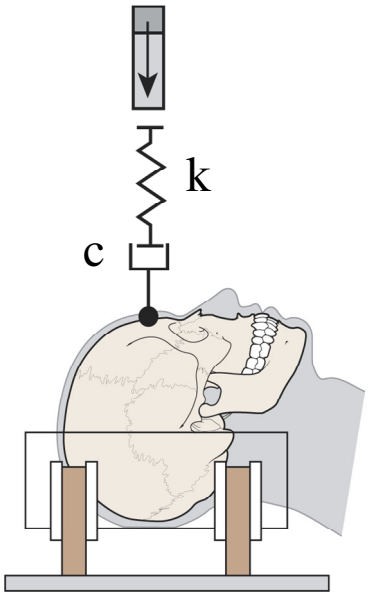

Figure 154: Representation of Maxwell model developed in the current study.

The magnitude of the linear stiffness (k) and damping factor (c) were optimized such that the model peak force was within 100 N of the reference test and such that it occurred within 0.2 ms of the reference test. Displacement at peak force was optimized to within 0.5 mm. The model and optimization was performed using custom algorithms written in Matlab (Mathworks, Natick, MA). An overall model of each bone response was then generated using the average values for the spring and dashpot parameters used to create the Maxwell model of each test. For all three bones, only tests included in the corridor calculation were modeled. Tests that did not represent a typical response were excluded because including them in the optimized model would skew the general model creating by averaging the optimized model parameters.

In the case of the frontal bone, the general model was then used to generate peak force values based on impactor mass and velocity in the previous testing performed by Nahum *et al.* (1968, 1975). For the nasal bone the general model was used to generate peak force values based on impactor mass and velocity in the previous testing performed by Cesari *et al.* (1989) and Nyquist *et al.* (1986). The general maxilla model was used to generate peak force values based on impactor mass and velocity in the previous testing performed by Bruyere *et al.* (2000), Cesari *et al.* (1989) and Nahum *et al.* (1975).

Additional analyses were performed by applying the model to an unsupported head (Figure 155). This allowed the modeled head to translate freely when struck by the impactor. To achieve an average response, the mass of the head was assumed to be 4.55 kg (10 lb) which is the head mass of the 50th percentile male Hybrid III dummy. The results of this model were then used to evaluate the effects of using a rigid constraint in the current study.

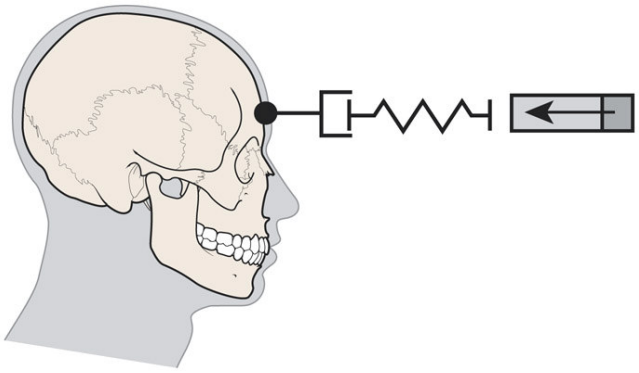

Figure 155: Representation of Maxwell model utilizing an unsupported head assumption.

RESULTS

Frontal Bone

A numerical model of the frontal bone impacts was created using a Maxwell material model. This model consists of a spring and damper in series. One end of the model is attached to the impactor mass with an initial velocity and the other end is rigidly constrained. The model was initially optimized to produce the maximum force achieved in each test (Figure 156). The bilinear force-deflection response fit the actual test response up to the peak with an average correlation coefficient of 0.93. The peak force obtained from the model was within 4% (std. dev. = 3%) of the peak force in all tests. The model deflection at peak force was within 4% (std. dev. = 3%) of each test on average (Figure 157).

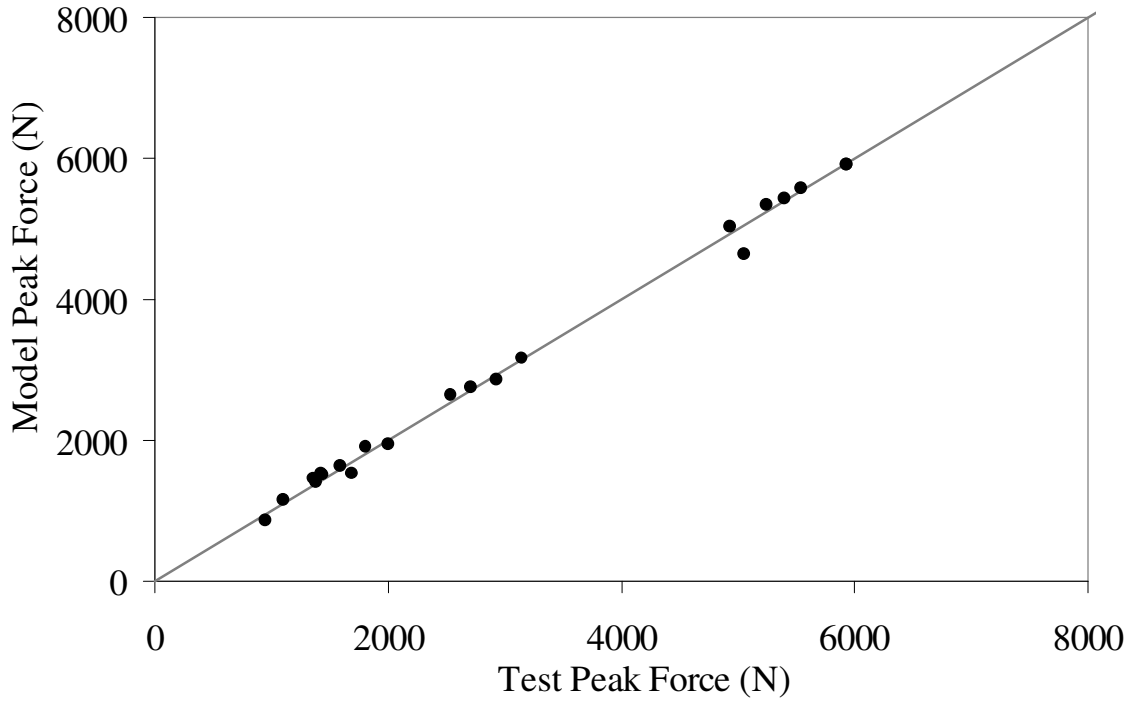

Figure 156: Peak force in optimized model with respect to experimental peak force.

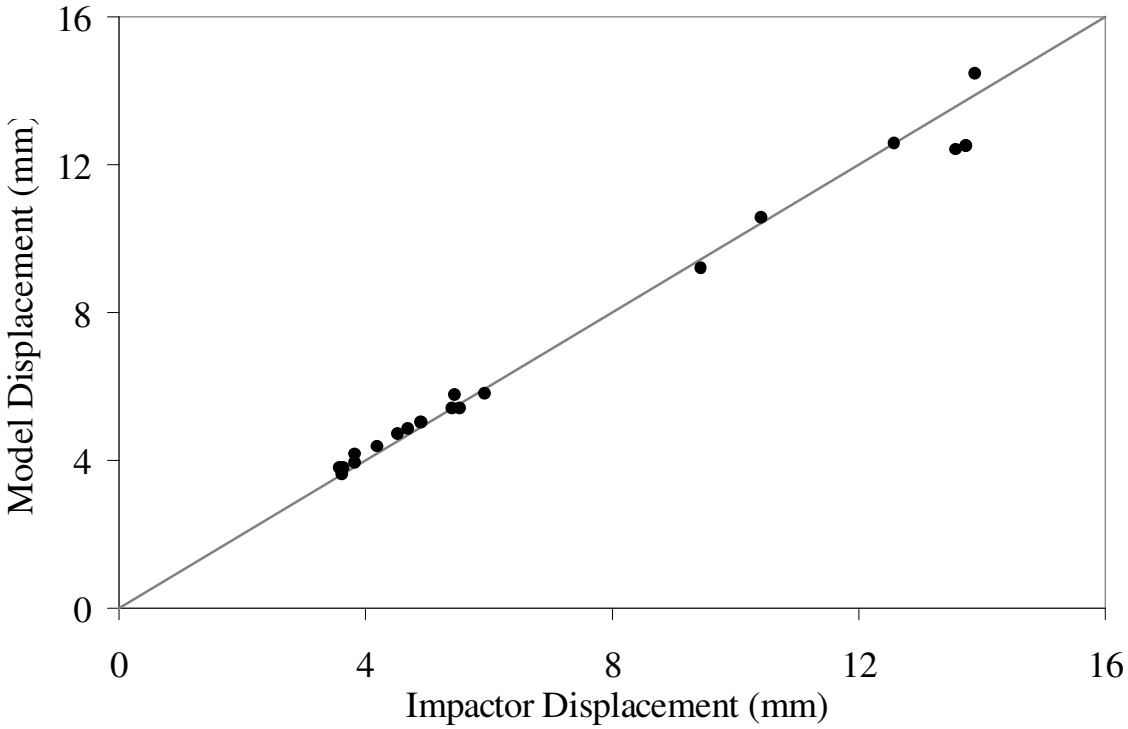

Figure 157: Impactor and optimized model displacement at peak force.

Optimizing the model by peak force, displacement and time resulted in a good overall match of the force-displacement response. Small deviations in stiffness were not

recreated by the model response (Figure 158). In general, the model tended to over-predict the duration of each impact (Figure 159).

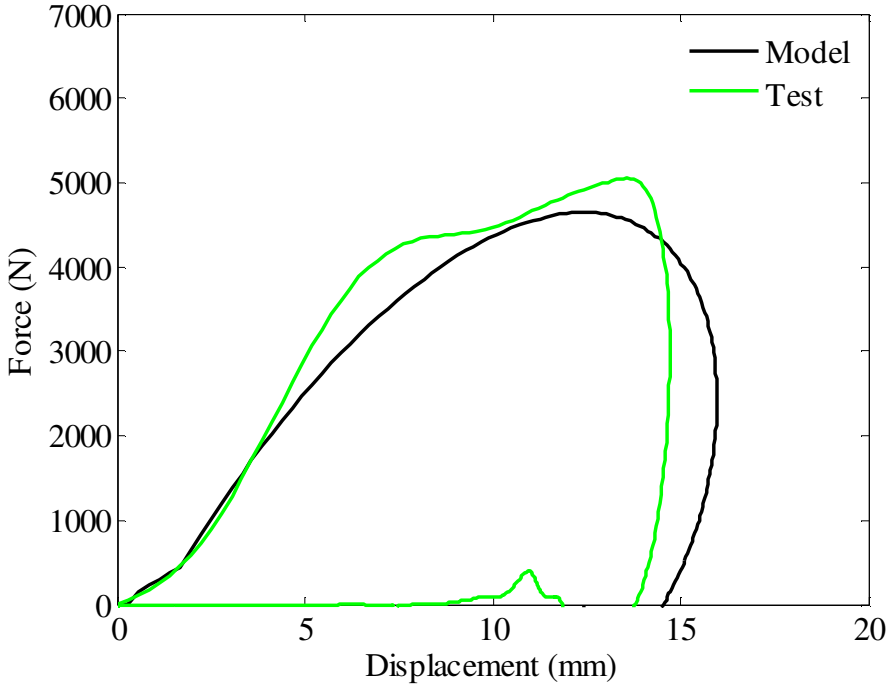

Figure 158: Force-displacement response of model using test parameters.

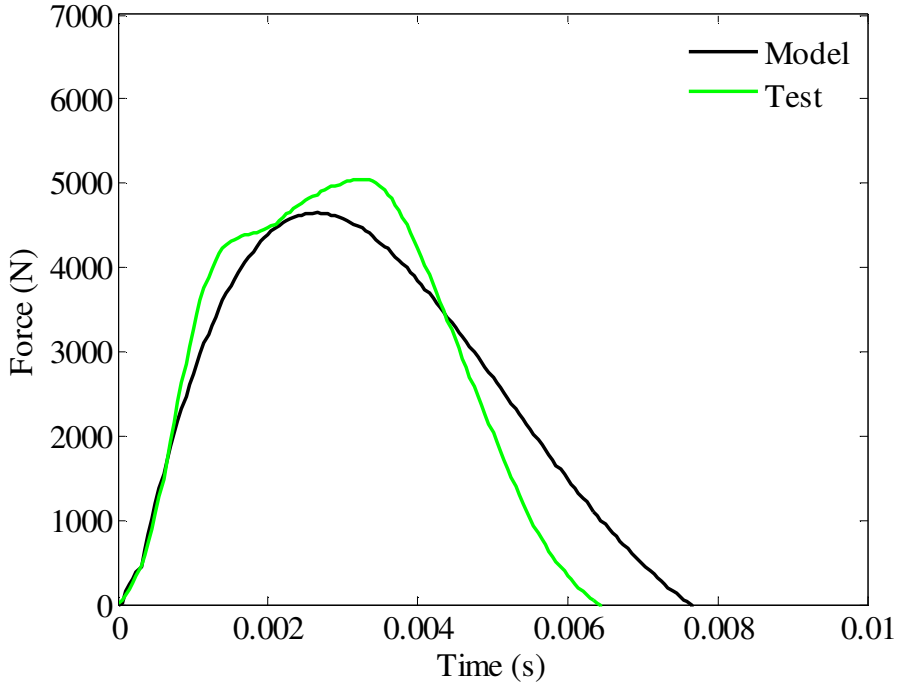

Figure 159: Impulse response generated by model using test parameters (same as Figure 158).

A general model was created by averaging the model parameters for all tests (Table 20). In some cases, the model parameters for a given model were not used due to an atypical response. The omitted tests had a larger than average variation between the change in impactor energy and energy under the force-displacement response. In these tests the impactor moved with respect to the head and, therefore, the resulting force-displacement response was not due to compression of the skull but a combination of skull deformation and impactor motion.

Table 20: Model parameters for frontal bone model achieved by averaging the optimized model parameters.

	Initial Stiffness (N/mm)	**Secondary Stiffness (N/mm)**	**Toe Length (mm)**	**Damping Factor (N-s/m)**
Mean	260	1450	2	1400
-1 Std. Dev.	150	910	1.5	700
+1 Std. Dev.	370	1990	2.5	2100

The model resulting from the averaged parameter values was used to estimate the peak force for each of the frontal bone impacts (Figure 160). Among the different impactor energy levels, the peak force produced by the generalized model was within 6 to 14% of the average peak force produced in the actual tests. On average the model was closer to the mean response for the higher impact severities. The generalized model was then used to simulate impacts performed by Nahum *et al.* (1968, 1975) by using the specified impactor mass and velocity as an input (Figure 161). On average the generalized model produced peak force values that were within 7 to 15% of the values reported. The impulse determined by the integral of the force-time history for the model was within 10% of the actual tests on average.

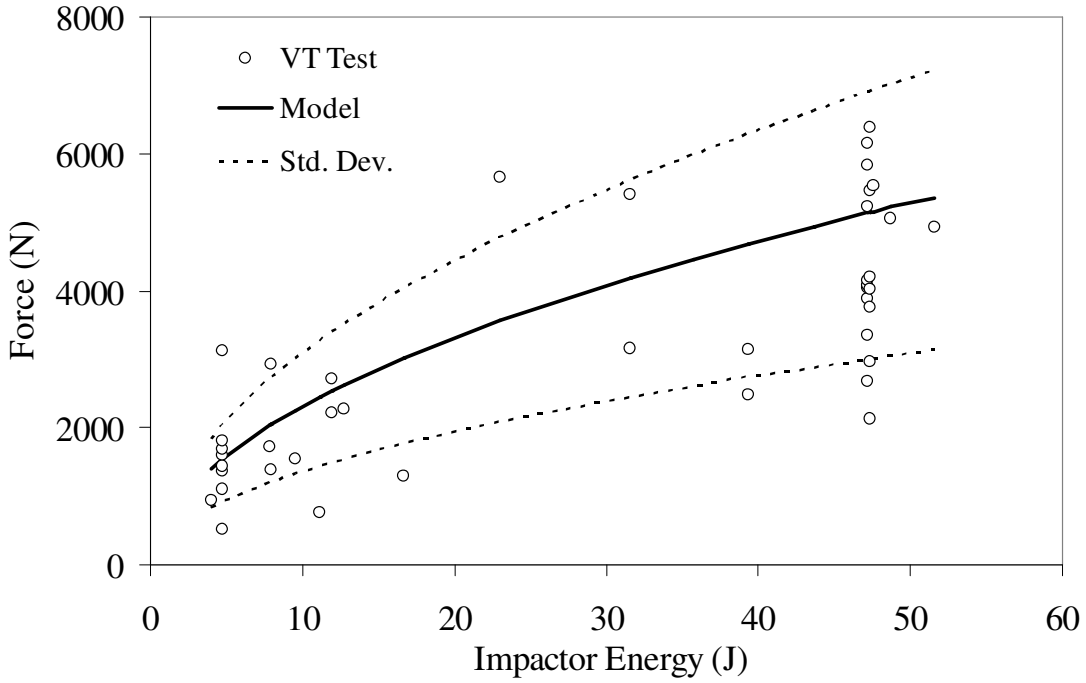

Figure 160: Results of generalized model using test parameters from current study.

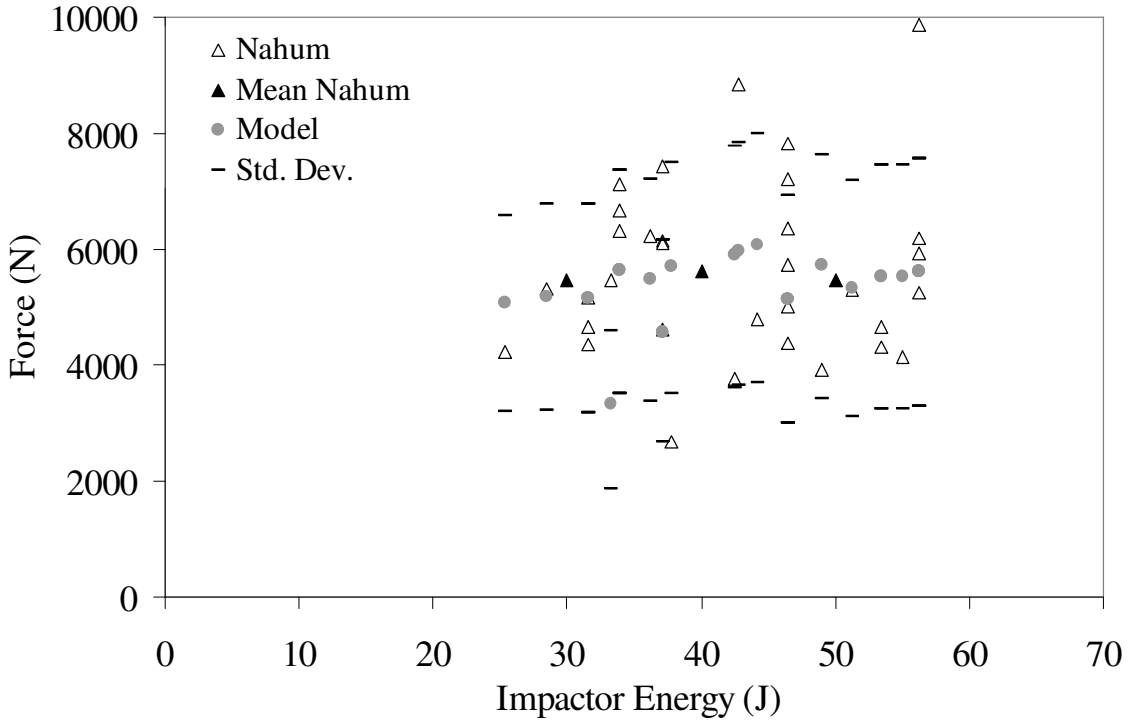

Figure 161: Nahum *et al.* (1968, 1975) data and model estimates of peak force.

The model was then modified to incorporate a free end condition rather than the fixed condition. This was done to evaluate the effects of the rigid constraint on the head and to

demonstrate changes in peak force if this constraint was eliminated. Since the actual head mass was not known a mass of 4.54 kg, the head mass of the 50th percentile male Hybrid III dummy was used. When using the optimized model parameters for each test, the unconstrained model produced force values that were 13% lower than the actual test (Figure 162, Figure 163). When using the average model parameters, the difference in predicted peak force with respect to the actual test data decreased with increasing impactor energy. Within the 22 tests performed at an impactor energy of 40 to 50 J, the average peak force produced by the model was within 24% of the test average. For impacts less than 10 J (n=15), the peak force predicted by the model was within 34% of the actual test, on average. The potential for the impacts in this study to produce brain injury was evaluated by calculating the HIC associated with each impact.

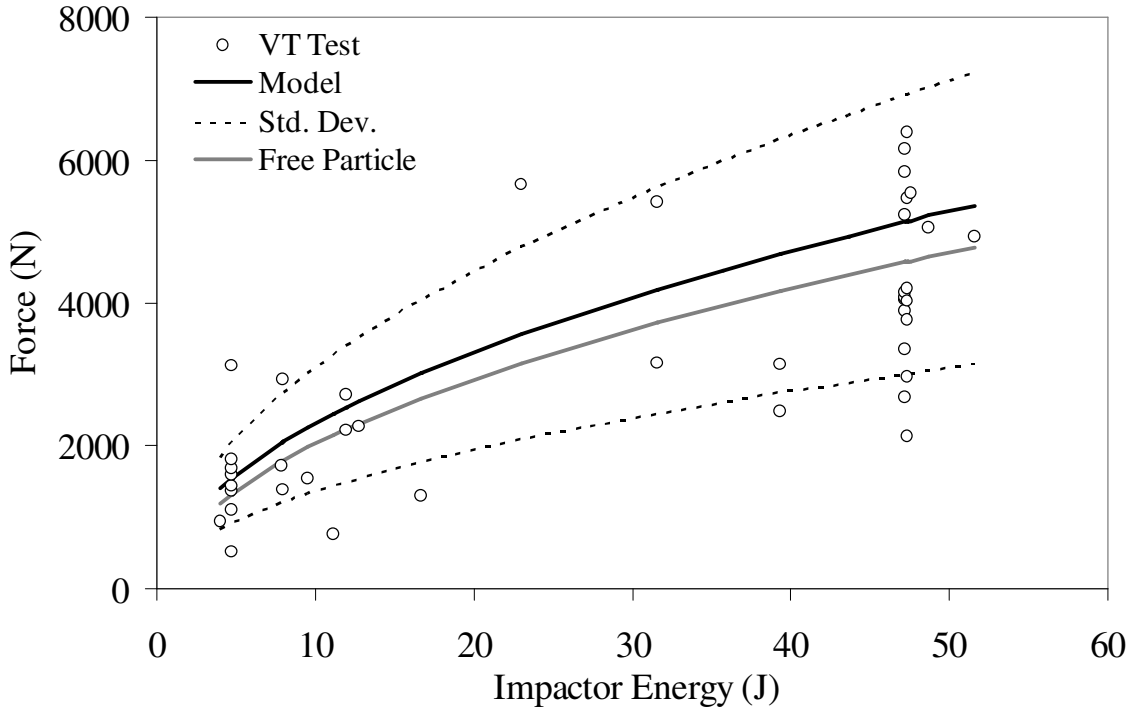

Figure 162: Estimated forces using a free particle end condition of the generalized model.

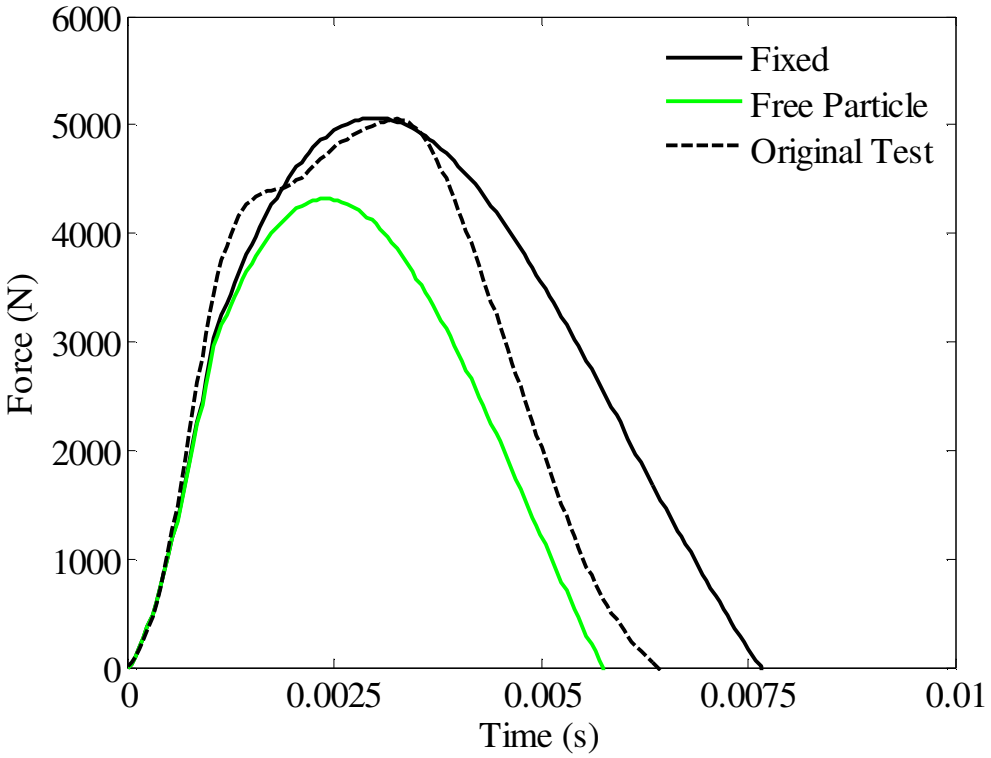

Figure 163: Response of model using free-particle end condition (same as Figure 159).

The HIC was estimated by applying the measured forces in each impact to an assumed unconstrained head (Figure 164). Since the force-time relationship from the actual test resulted from impact to a fully constrained head, the estimated HIC values will be higher than expected when striking an unconstrained head. The head mass was again assumed to be 4.54 kg. The optimized and averaged models were also used to estimate the HIC associated with each test. The model created using average parameters fit the mean peak force values of the actual test data well. On a test by test basis, the optimized model was within 25% of the actual test and the averaged model was within 40%. The effects of the rigid constraint were again assessed using the free-particle end condition. The optimized model and generalized model were run for each impact and the HIC was calculated based on the particle acceleration (Table 21). The HIC estimated by the free-particle model was approximately 60% lower than the fixed models and 50% of the actual test.

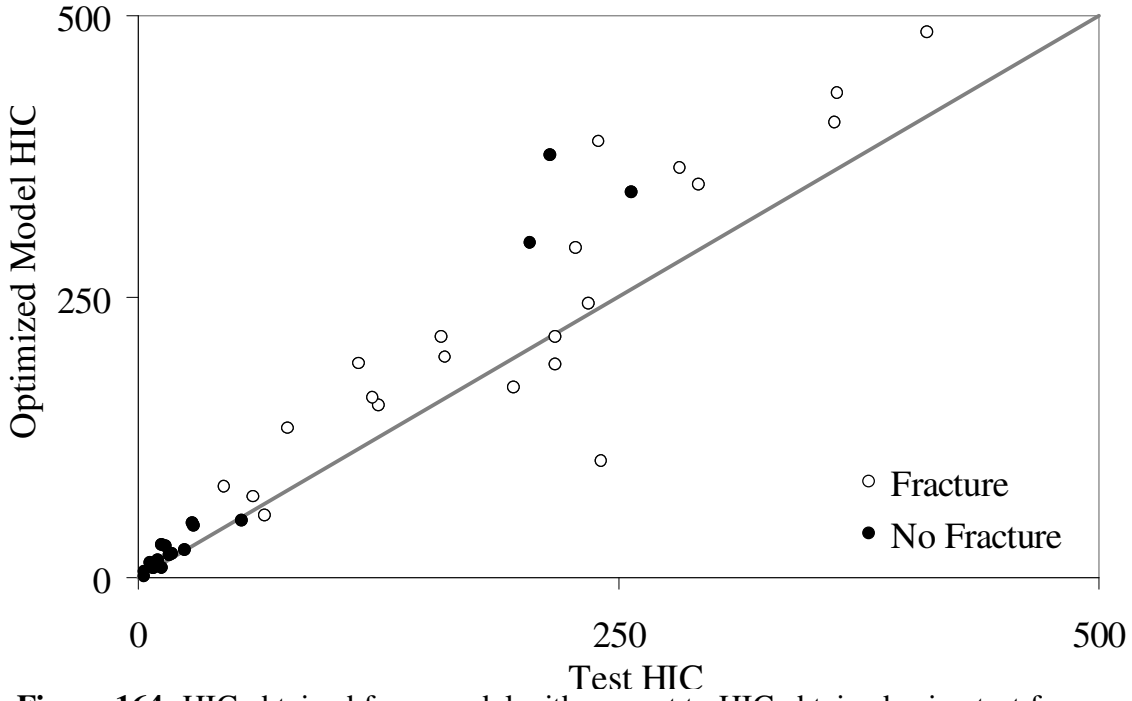

Figure 164: HIC obtained from model with respect to HIC obtained using test forces (assuming 50th percentile male head mass).

Table 21: Average of estimated HIC values from test and model head forces.

	Average HIC Value				
	Fixed Condition			Unconstrained	
Impactor Energy (J)	**Test**	**Optimized Model**	**Model**	**Optimized Model**	**Averaged Model**
< 10	16	18	16	12	10
10 - 40	115	159	99	59	63
> 40	288	372	294	153	168

The HIC values associated with this study were compared to those reported by Hodgson and Thomas (1973). In their study subjects were swung using a table such that the apex of the frontal bone struck a rigid surface. The peak forces reported in their study were much higher than the current study and, consequently, the HIC vales they obtained were higher as well (Figure 164).

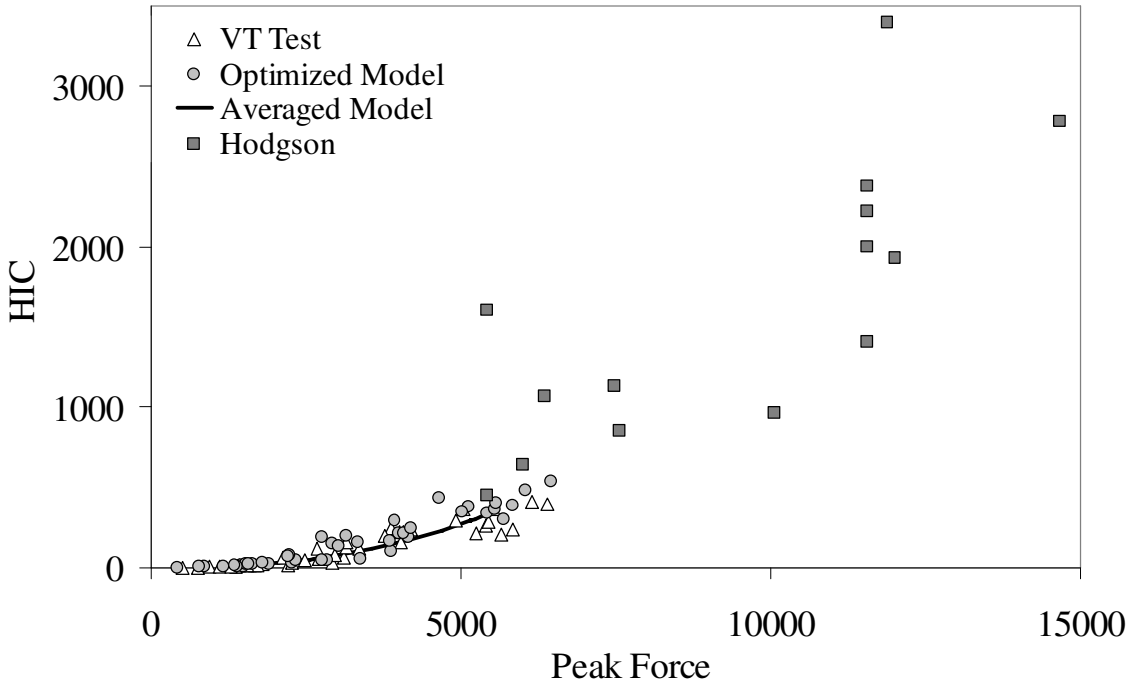

Figure 165: HIC values achieved at a given peak force in current tests, model and reported values by Hodgson and Thomas (1973).

Nasal Bone

The model was initially optimized to produce the maximum force achieved in each test (Figure 156). The bilinear force-deflection fit to the test data had an average correlation coefficient of 0.80 up to peak force. The peak force obtained from the model was within 10% of the peak force in all corridor tests.

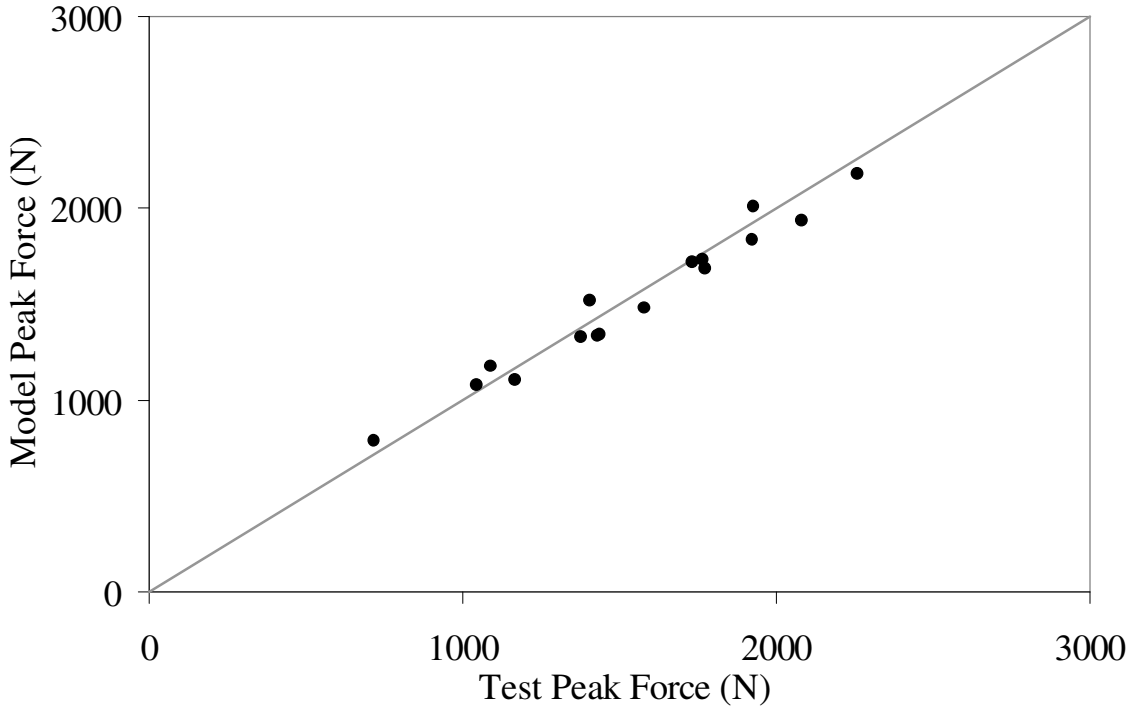

Figure 166: Results of numerical model optimized for each test.

A general model was created using the average model parameters generated by optimizing the model to individual tests (Table 22). This model was then used to estimate peak forces for all tests (Figure 167). The peak force predicted by the model was well within the range of measured forces in the actual tests. The same model was also used to predict the forces when applying the impactor mass and velocity utilized by Cesari *et al.* (1989) (Figure 168).

Table 22: Model parameters for the nasal bone model achieved by averaging the optimized model parameters.

	Initial Stiffness (N/mm)	**Secondary Stiffness (N/mm)**	**Toe Length (mm)**	**Damping Factor (N-s/m)**
Mean	22	251	6	1900
-1 Std. Dev.	5	133	3	299
+1 Std. Dev.	38	370	10	3501

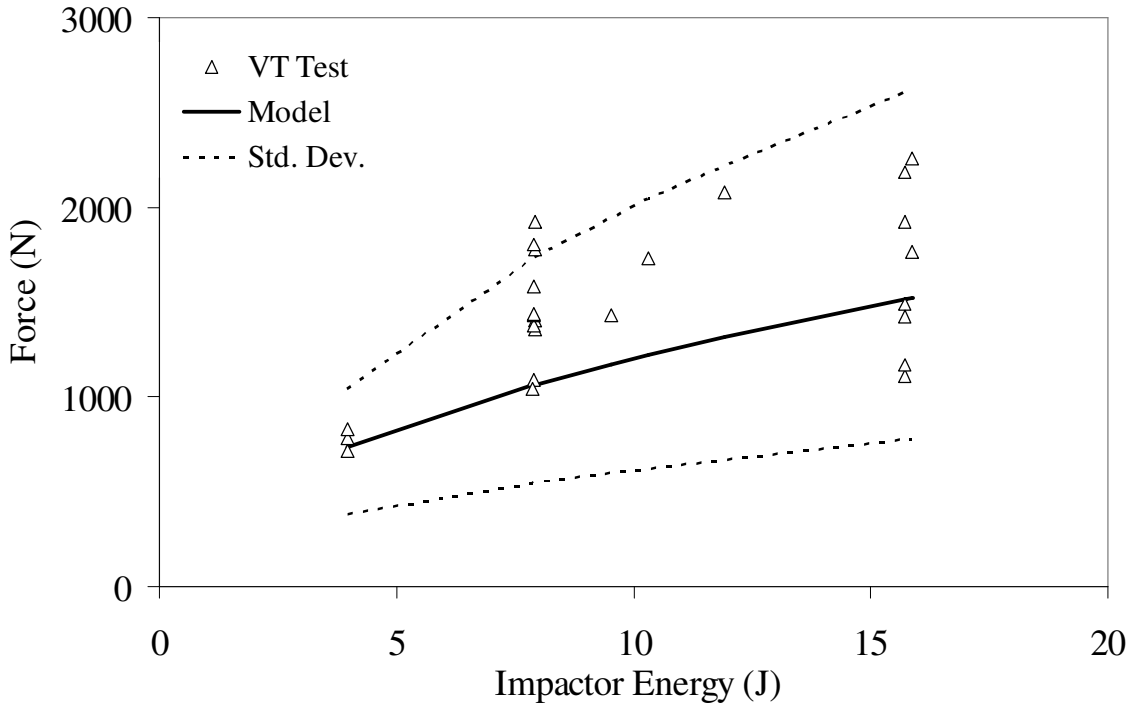

Figure 167: Results of numerical model for simulation of tests in current study.

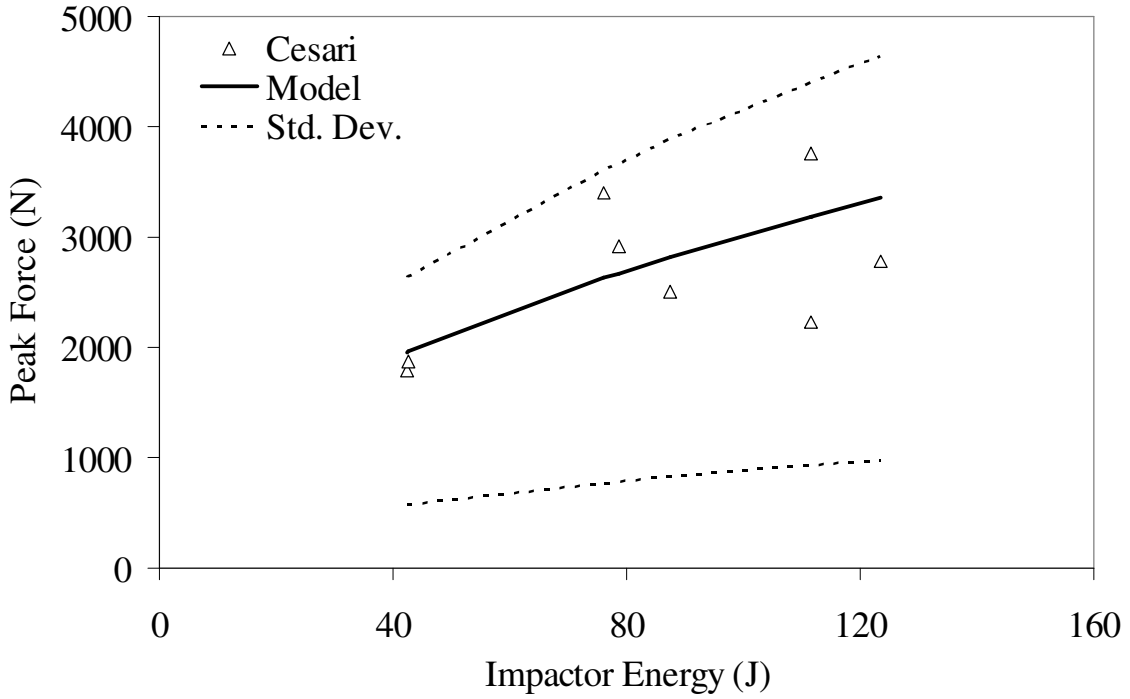

Figure 168: Cesari *et al.* (1989) data and numerical model results for simulated tests.

To evaluate the effects of the rigid constraint utilized in the current study the model was altered to allow the impactor force to be applied to a free head. As expected, the addition

of a free particle to the model produced lower peak forces for the same impact severity (Figure 169). Due to the use of a relatively free constraint in the study by Nyquist *et al.* (1986), the free-particle model was used to predict the forces obtained in their study using the impactor mass and velocity as inputs (Figure 170).

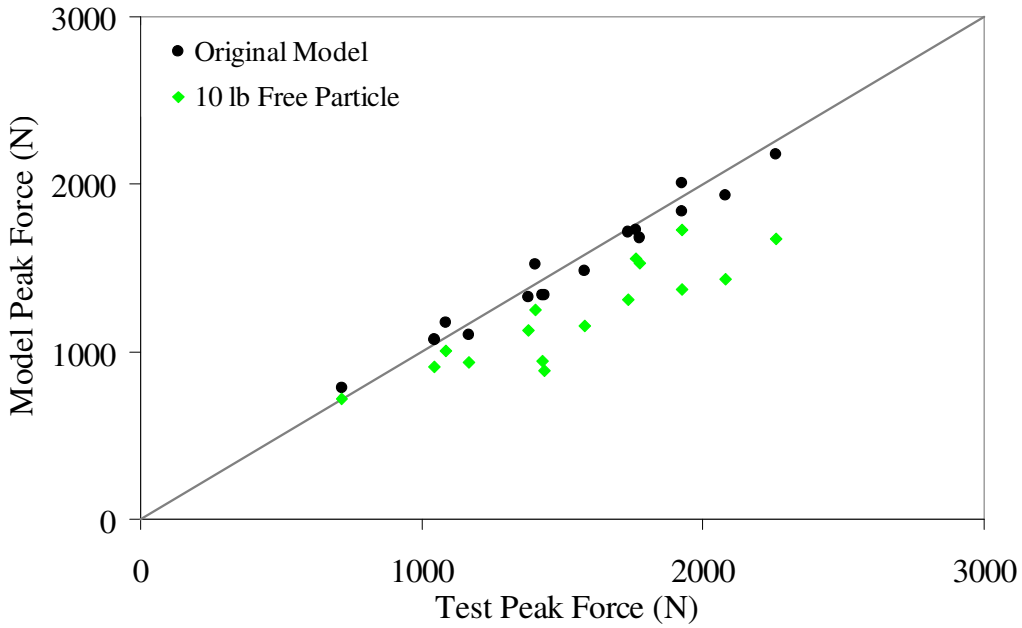

Figure 169: Change in predicted peak force when applying model to a free particle.

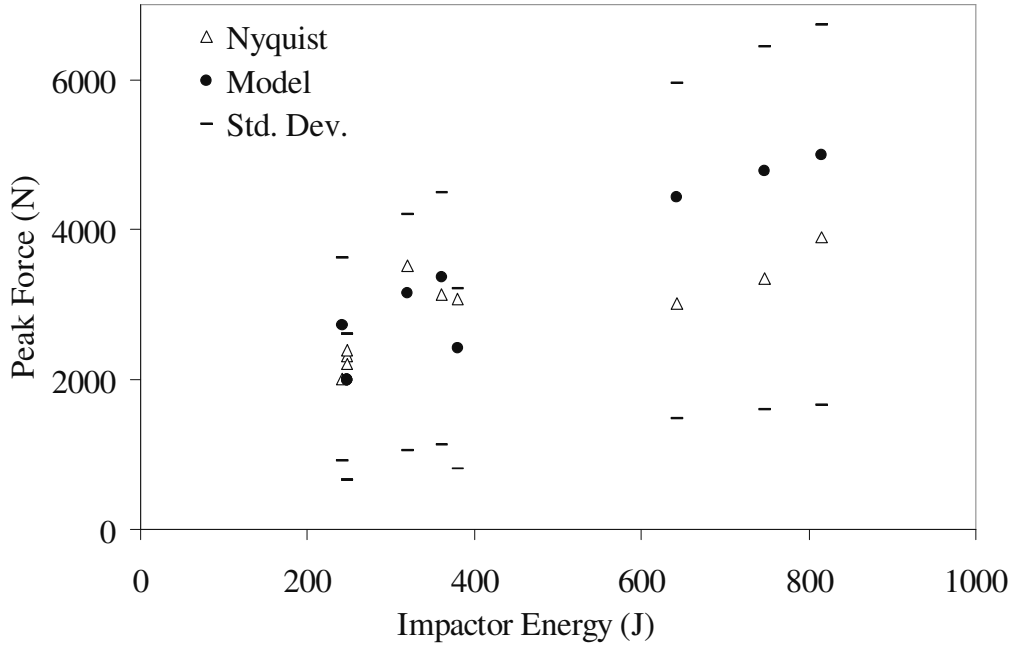

Figure 170: Simulation of Nyquist *et al.* (1986) tests using Maxwell model with a free particle mass of 4.54 kg.

To illustrate the influence of stiffness on the resulting HIC, the frontal and nasal bone models were compared. Each generalized model was modified to replace the rigid constraint with a free particle with a mass of 4.54 kg. Therefore, each model would simulate an unconstrained object being struck with the contact defined by either a frontal bone or nasal bone model. The inputs in the model were taken from the frontal bone impacts, which were more severe than the nasal impacts. The average HIC value obtained by the frontal bone model was 94 (std. dev. = 73) with a maximum of 218. On average the nasal bone model produced values which were approximately 70% of those obtained in the stiffer, frontal bone model. The nasal bone model had an average HIC of 63 (std. dev. = 49) and a maximum of 145. This 30% reduction in HIC resulted from an almost 6 times difference in stiffness between the frontal and nasal bone.

Maxilla

A numerical model of the maxilla impacts was created using a Maxwell material model. This model consists of a spring and damper in series. One end of the model was attached to the impactor mass with an initial velocity and the other end was rigidly constrained. The model was initially optimized to produce the maximum force achieved in each test (Figure 171). The bilinear force-deflection response fit the actual test response up to peak with an average correlation coefficient of 0.91. The peak force obtained from the model was within 7% (std. dev. = 6.7%) of the peak force in all tests. The model deflection at peak force was within 10% (std. dev. = 22%) of each test on average.

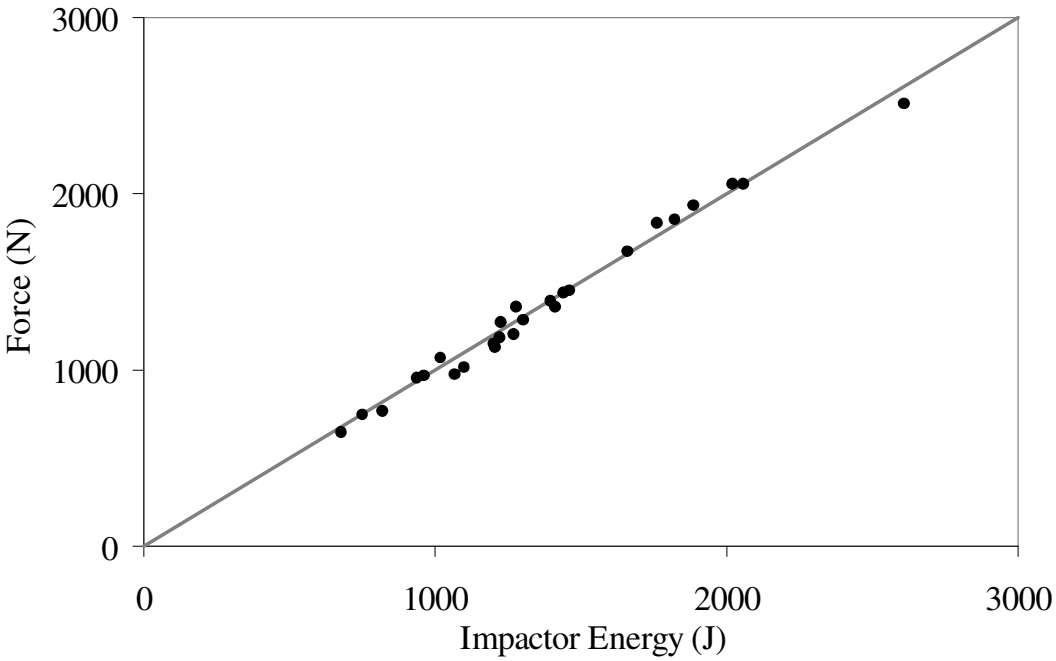

Figure 171: Results of numerical model optimized for each test.

The use of a bilinear fit for the spring stiffness creates an abrupt increase in force at the transition point which tends to result in an over-prediction in force immediately following the transition (Figure 172). The differences in force between model and test are more obvious in the force-displacement response than impulse (Figure 173).

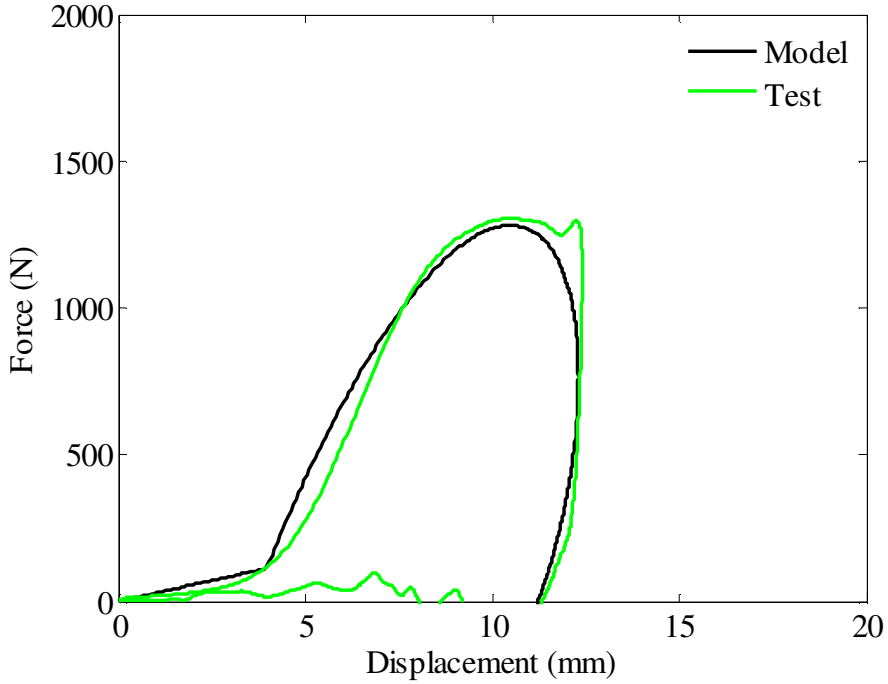

Figure 172: Test and model force-displacement response (H6 T4).

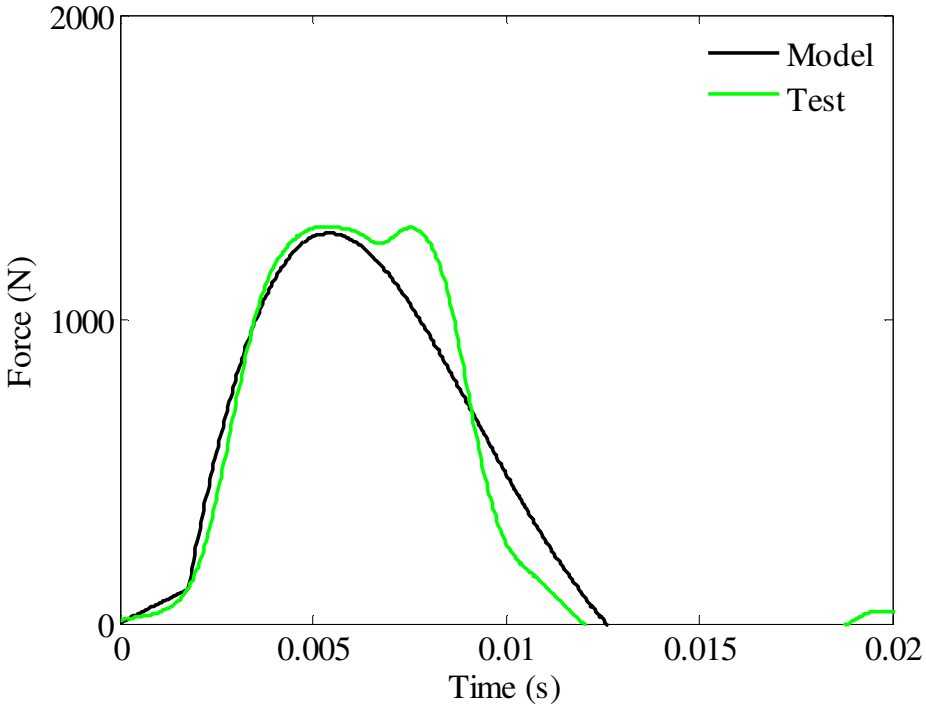

Figure 173: Test and model estimate of impulse response (Same as Figure 172).

The maxilla differed from the frontal bone and nasal bone response in that it exhibited a significantly different response due to fracture at higher energies. This was accounted for by creating two separate models (Table 23). In this study, all tests above an impactor

energy of 20 J resulted in a fracture, therefore this was used as the threshold between models. If the optimized model parameters were used to estimate maxilla response at the higher energy levels, the model would over-estimate peak forces significantly.

Table 23: Model parameters for the maxilla models achieved by averaging the optimized model parameters.

	Initial Stiffness (N/m)	Secondary Stiffness (N/m)	Toe Length (mm)	Damping Factor (N-s/m)	
Impactor KE < 20 J	34	302	3	821	Mean
	9	192	1	603	- 1 SD
	58	412	4	1039	+ 1 SD
Impactor KE > 20 J	41	381	4	502	Mean
	14	228	1	226	- 1 SD
	68	534	6	778	+ 1 SD

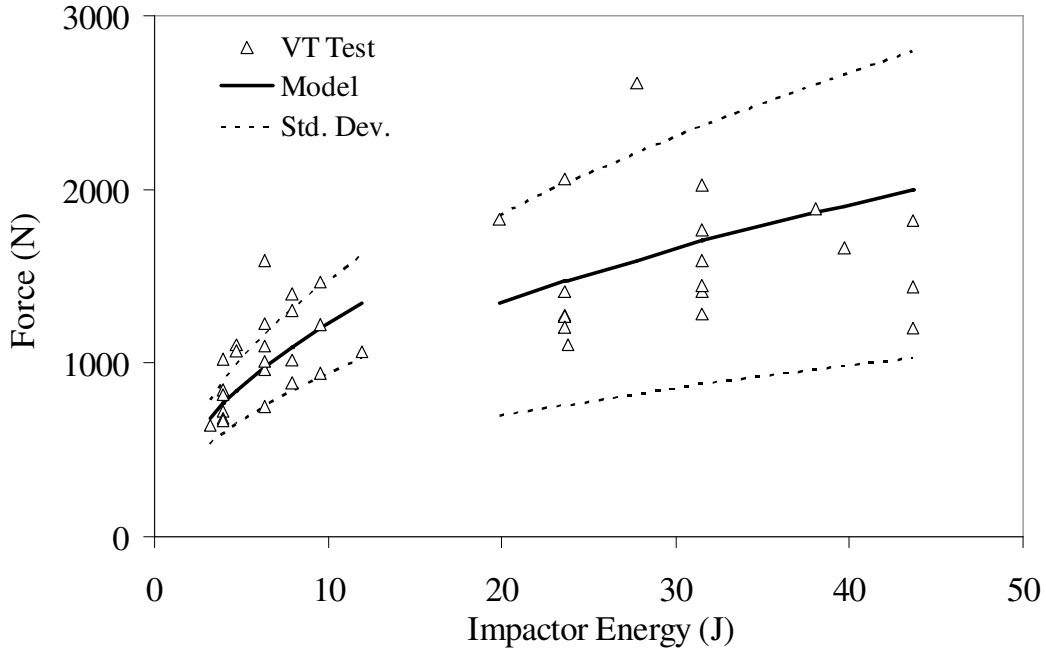

Figure 174: Generalized Maxwell models of maxilla impacts.

Overall, the model predicted the peak force in the Nahum *et al.* study with a difference of 20%. The average model fit the middle of the test response well and the standard deviation of the model parameters produced bounds that contained all but one test. Similar results were obtained when the model was used to simulate the impacts performed by Nahum *et al.* (1975). The mean response of the generalized model

matched the response of the Nahum tests well. On average, the model was within 20% of the peak force in the Nahum *et al.* study. The model performed better at the higher severities, with a difference of 10% for the impacts with an initial energy greater than 8 J (Figure 175).

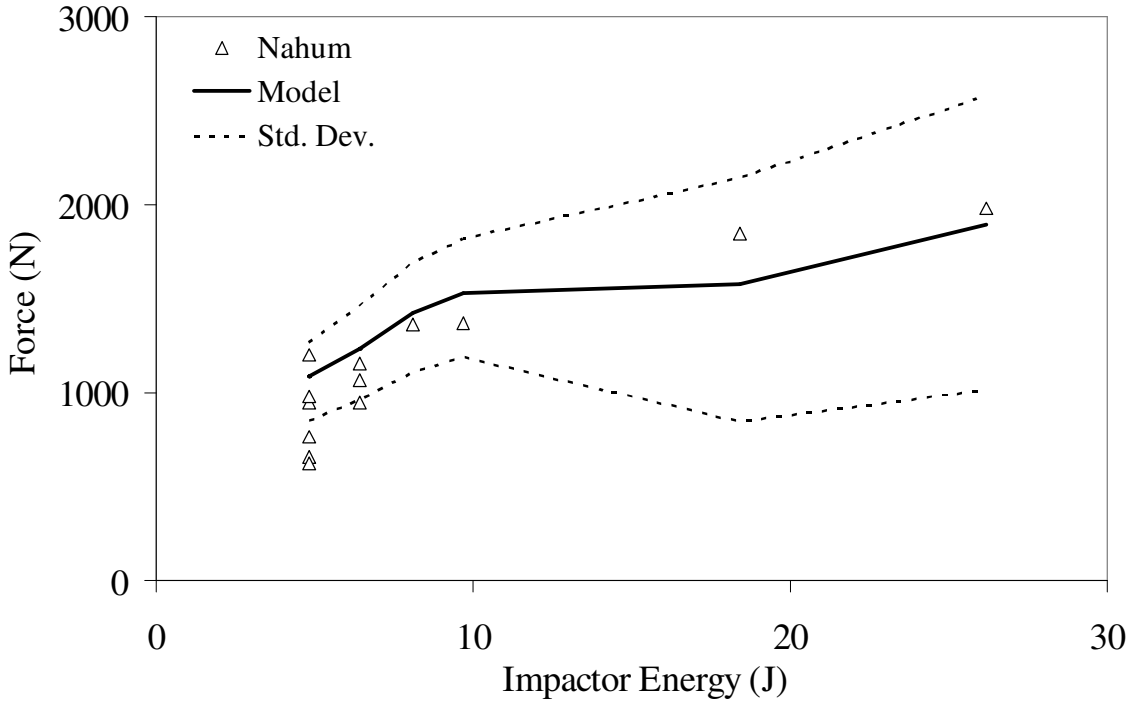

Figure 175: Model results using Nahum *et al.* impact conditions.

The studies by Bruyere *et al.* (2000) and Cesari *et al.* (1989) used similar methods, only with different impactor energies (Figure 176). The generalized model fits the average response of the Cesari *et al.* data fairly well with an average difference of 20%. The limitations of the model is apparent when compared to the Bruyere *et al.* (2000) data which was obtained at energy levels well above the current study.

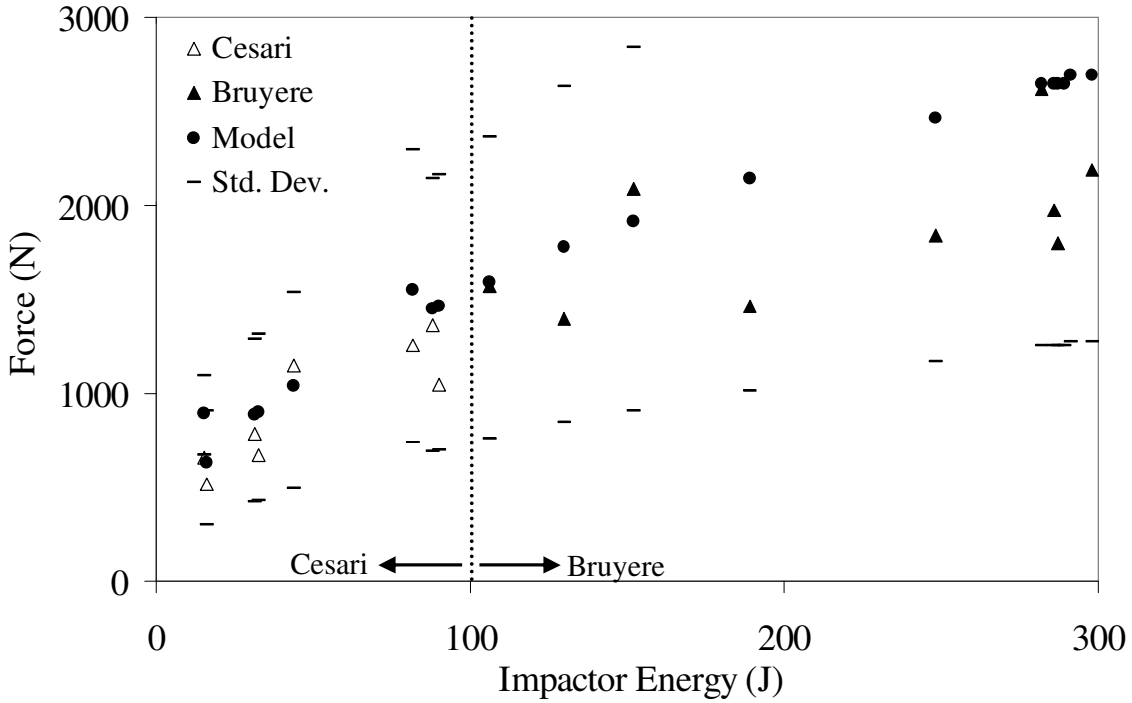

Figure 176: Model results using Cesari *et al.* and Buryere *et al.* impact conditions.

The model incorporating an unconstrained end condition under predicted the peak force by 13% on average (Figure 177). The unconstrained model exhibited a longer displacement than the fixed model (Figure 178), while decreasing the pulse duration of the impact (Figure 179).

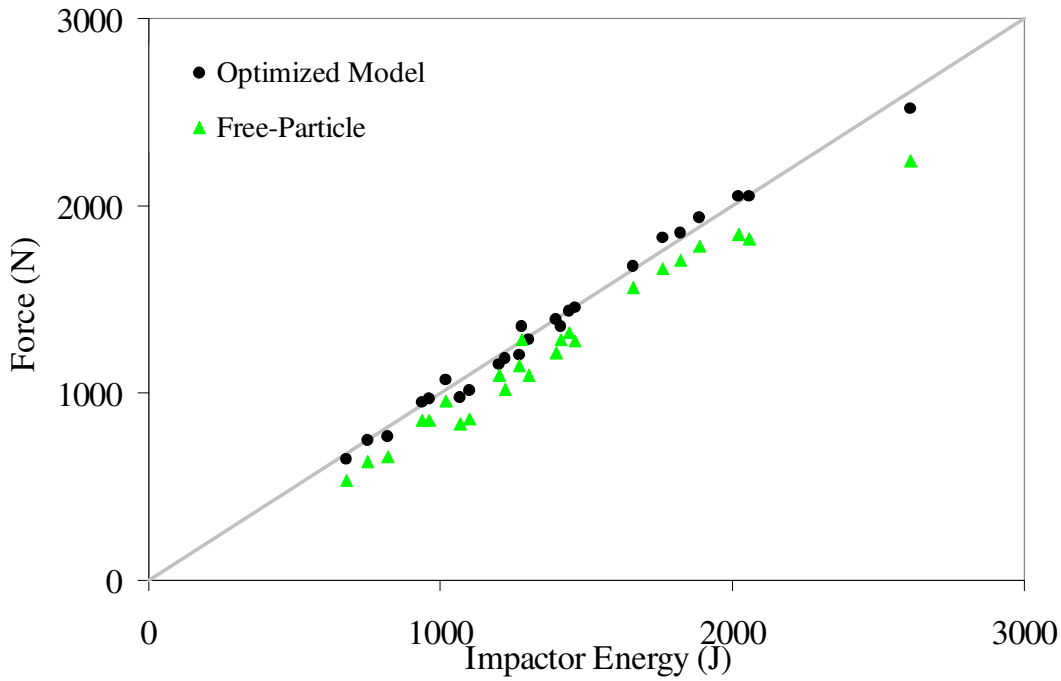

Figure 177: Model results using optimized parameters and free-particle end condition.

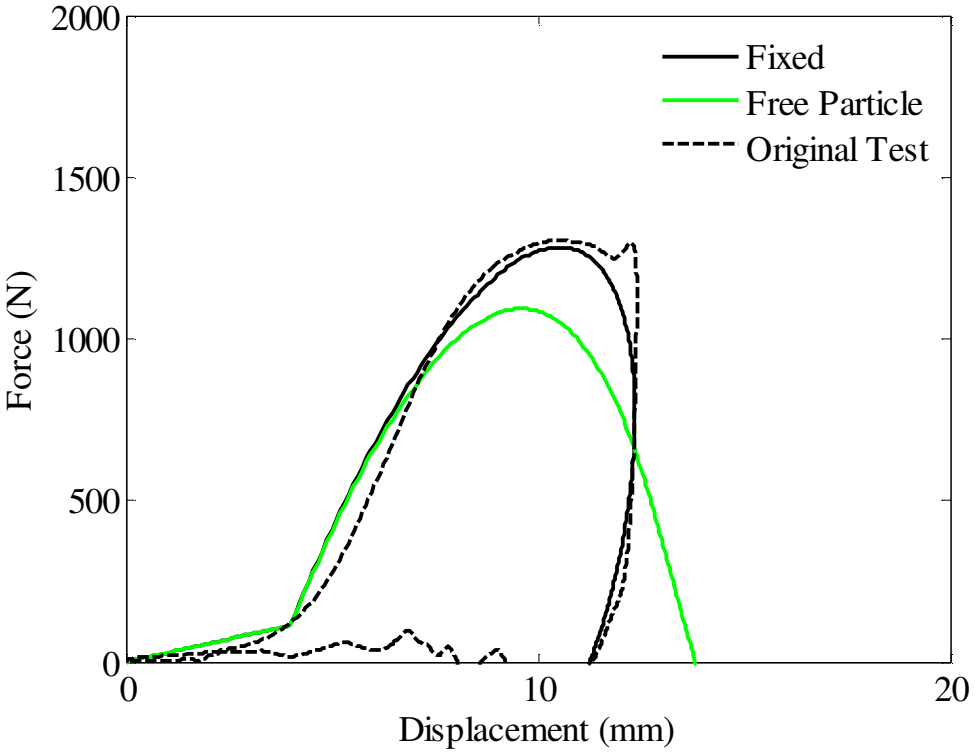

Figure 178: Model force-displacement response with and without free-particle end condition.

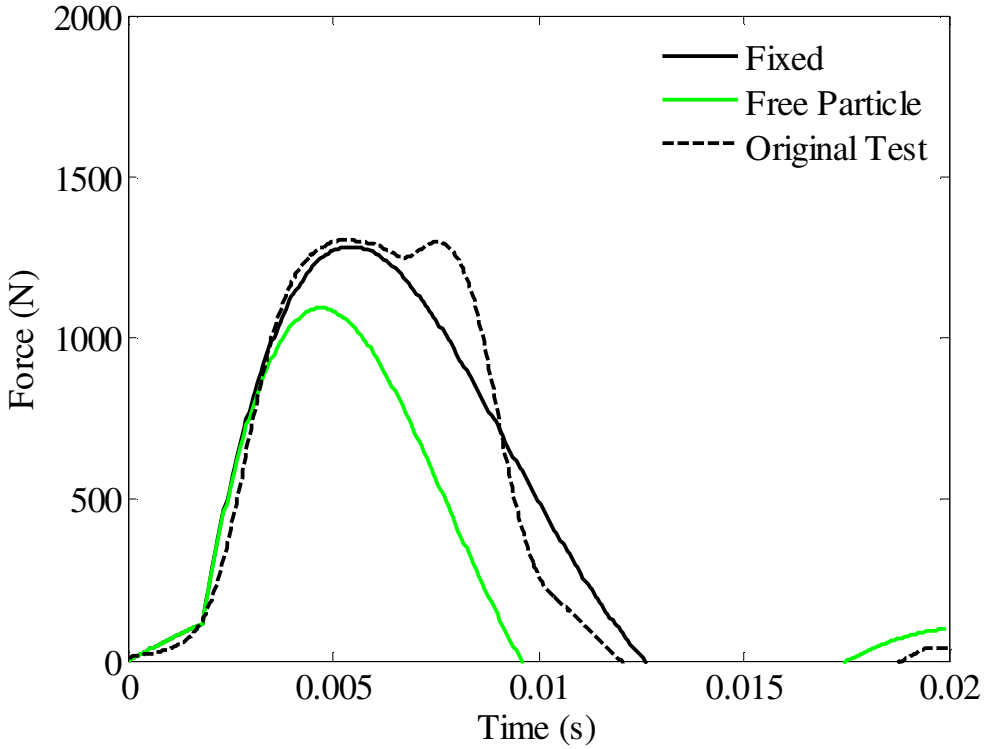

Figure 179: Model impulse with and without free-particle end condition.

The Bruyere *et al.* (2000) and Cesari *et al.* (1989) tests were re-run using the unconstrained model. This assumption was a better fit to their methods due to the use of a cervical collar to hold the cadaver head in place. So, in there study, the head constraint was more similar to a free particle than the rigid condition assumed with the original model. Using the free-particle end condition reduced the average percent error for the Bruyere *et al.* (2000) results from 21 to 19% and from 20 to 17% for the Cesari *et al.* (1989) tests.

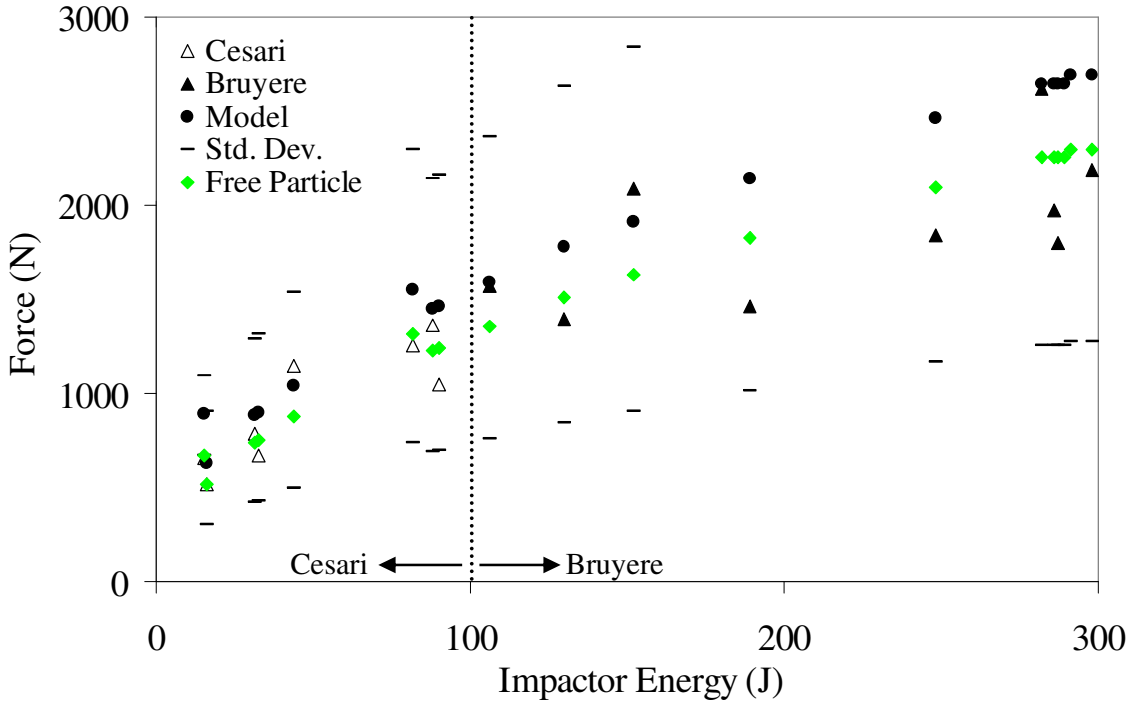

Figure 180: Free-particle model results using Cesari *et al.* and Buryere *et al.* impact conditions.

DISCUSSION

Frontal Bone

A Maxwell model of each impact was created and optimized to produce an estimate of the frontal bone response to impact. The optimized model predicted peak force and displacement values similar to those achieved in the actual test (Figure 156). In general, the model overpredicted the impulse of each impact, so that HIC values predicted by the model were higher than expected. Using the average of the test-specific parameters, a

generalized model was created which approximated the mean response of all tests (Figure 160). The model was used to asses the effects of allowing the head to translate freely rather than the fixed condition. A free particle with a mass of 4.54 kg (50^{th} percentile Hybrid III head mass) was attached to the Maxwell model. The unconstrained model demonstrated lower forces (Figure 162) and significantly lower HIC (Table 21) values for the optimized and general parameters

The Head Injury Criterion (HIC) values expected from the impacts performed in the current study were estimated by assuming each impulse was applied to an unsupported head. Since the actual head mass was not known, a mass of 4.54 kg, the head mass of the 50^{th} percentile male Hybrid III dummy was used. The resulting acceleration was used to estimate the HIC expected from each impact. The estimated HIC for fracture producing tests ranged from 45 to 411 with an average of 210. These values represent a relatively low risk of sustaining a concussion (Funk 2007). Regarding fracture, the estimated HIC values cannot be directly compared to the typically quoted value of 1000 as a 16% risk of fracture. The risk estimates utilizing HIC are based on several studies which utilized vastly different methods (Prasad and Mertz 1985). None of those studies utilized impactors with a similar size, nor was the frontal bone struck in a manner similar to the current study. The results of this study point to the limitations of the HIC in predicting skull fracture. The HIC is directly related to the impulse applied to the skull, but is not sensitive to the mechanism the impulse is applied to the head. The impulses in the current study were well over the threshold to cause fracture and had these impulses been applied to a Hybrid III dummy, the HIC values would have been well below 1000. Therefore, the HIC should not be utilized to estimate the risk of skull fracture without consideration for the actual stress imposed on the frontal bone, which will be directly related to impactor size and stiffness. The HIC values obtained by Hodgson and Thomas (1973) are questionable due to an inconsistency within the relationship between peak force and head acceleration. In their study, head acceleration was significantly higher than the value necessary to maintain the proper relationship between force and acceleration. On average, the head mass based on the ratio of force divided by acceleration was 38 kg. The peak forces reported in their paper were also significantly

higher than those in the current study and peak forces reported by Naham *et al.* (1968, 1975). The higher values reported by Hodgson and Thomas (1973) may be due to the use of a flat impactor, rather than the smaller, cylindrical shaped impactor of this study and Nahum *et al.* (1968, 1975).

Nasal Bone

To illustrate the relative severity of the impacts performed in the current study, the Head Injury Criteria (HIC) was calculated using the assumption that the measured impulse for each impact was applied to a free particle. The free-particle was assumed to have a mass of 4.54 kg, which is the head mass for the 50th percentile male Hybrid III dummy. Using these assumptions, the forces applied to each head would result in an average HIC value of 22 (std. dev.=12) with a maximum of 51 (fracture) and a minimum value of 3 (no fracture). It is clear from these values that the severity of the impacts in this series is not expected to cause brain injury. This is not a result of energy absorbing properties of the nasal structure, but rather is a result of the low severity of the impacts necessary to cause a nasal bone fracture. The energy dissipated by fracturing the nasal bone was small compared to the available kinetic energy just prior to impactor contact. The average change in impactor kinetic energy at the initial peak in impactor force was approximately 4 J, or 42% of the initial impactor energy for the impacts performed in this study. On average the maximum force achieved during the initial peak was 57% of the maximum force achieved during the entire impact. This lower initial force is consistent with the weaker structure of the nasal bones failing, followed by loading of the stronger posterior structures, thereby producing higher peak forces.

Maxilla

The maxilla response was unique in that it required two models in order to accurately simulate its response with and without fracture. This unique response is consistent with its structure. The maxilla is attached to the skull in such a way that once it fractures, it looses its load path to the skull. Therefore, once the fracture is severe enough, the maxilla can no longer support load and the remaining facial structures are not in a position to support additional impactor motion. By this mechanism, the maxilla can limit

the acceleration experienced by the skull, however as seen in this study, the forces necessary to cause a maxilla fracture are far lower than those expected to cause an inertial brain injury.

Limitations

The models developed in this study are limited to impactor energies similar to those utilized in the current study. When applied to other studies utilizing similar impactor energies, the model performed well and predicted peak forces within the average response of the previous studies. The optimized model developed in this study predicted displacement values similar to those of the actual tests, but its ability to estimate displacements in the literature is unknown due to the lack of data. Therefore, use of the model to estimate the expected displacement should be done with caution.

The HIC values estimated by assuming a free end condition produced an overestimate of the linear acceleration that would be experienced by an actual head. This is due to the higher forces created by utilizing a rigid support in the actual tests.

CONCLUSIONS

This chapter presented the development of a Maxwell model used to simulate impacts applied to the frontal bone, nasal bone and maxilla. The model was optimized based on the results of the respective chapters. Using the optimized model to simulate previous studies by using the impactor mass and velocity demonstrated that the model will provide a reasonable estimate of the average peak force expected during each impact. In some cases, the impactor energy used in the literature was considerably higher and the applicability of the model was diminished.

The model created for the frontal and nasal bones produced accurate results despite the fact that they are based on fracture and non-fracture tests. This is consistent with the results of the previous chapters which demonstrated that the peak force attainable during a frontal or nasal bone impact is not limited due to the occurrence of fracture. In the frontal bone, this phenomenon seems to be the result of its structure, which is generally

thicker and able to continue supporting load after the onset of fracture. In the nasal bone impacts, the presence of the maxilla and frontal bones provide additional support following structural failure of the nasal bones. The maxilla exhibited a different response to fracture which prevented the use of a single model to simulate its response to impact. The structure of the maxilla below the orbit is such that once fractured it will become detached from the skull and lose its ability to continue resisting impactor penetration. Comparing the peak forces achieved as a result of impact to each region demonstrates the overall lower peak forces achieved in the maxilla impacts (Figure 181). The nasal bone impacts tended to produce peak forces equal to and greater than those during maxilla impacts at half the impact energy.

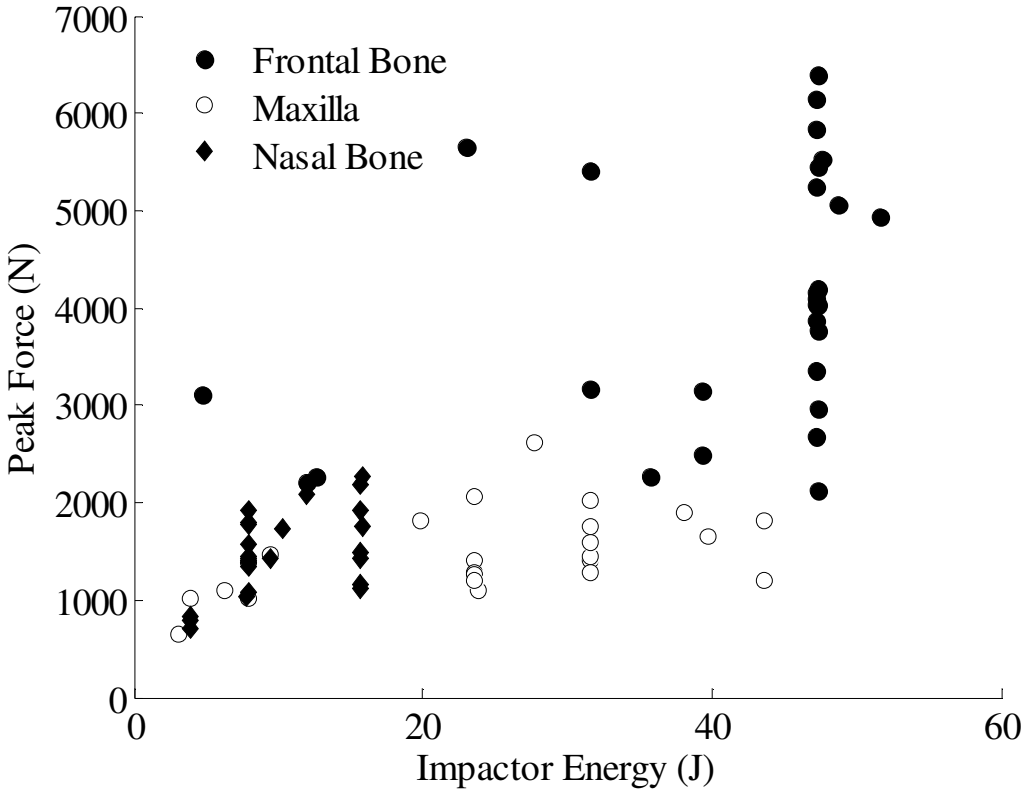

Figure 181: Peak force achieved as a function of impactor energy by facial region.

The HIC was estimated by applying the impulse measured during each test to an assumed free particle having a mass of the 50th percentile Hybrid III dummy. The results of this exercise demonstrated that HIC values normally considered to represent a low risk of injury actually resulted in fractures of the frontal bone. This does not reflect on the utility

of the HIC to predict brain injury or skull fracture. However, it does demonstrate the limitation of the HIC in that it does not account for the method of force application. The HIC was developed using a variety of different studies on the tolerance of the frontal bone, none of which were similar to the current study. Therefore, it would not be expected to perform correctly under the environment in the current study.

The models developed for the frontal bone, nasal bone and maxilla were optimized based on individual test results, then generalized based on the average parameter values. The output of the generalized model produced results at the average of the cadaver results when using the impactor velocity and mass as inputs. When applied to other studies, these models predicted similar peak forces as reported in studies with similar impactors as well dissimilar impactors. It appears that the difference between the flat face and rounded face of a cylindrical impactor is not pronounced enough to produce significantly different peak forces. The free-particle end-condition utilized in the model created results closer to those obtained in studies that utilized a less confining end condition than the rigid condition utilized in this study. The reduction in peak forces predicted by the free-particle model was less pronounced for the maxilla test than the frontal or nasal impacts.

The models developed in this study are based on a wide range of impactor energies and were shown to accurately predict peak forces in this study as well as previous work on the frontal bone, nasal bone and maxilla. These models can be useful in estimating the average cadaver response expected due to blunt impact. Therefore, if a particular impactor velocity and mass is of interest, these values can be applied to the model to determine the range of expected cadaver responses. Additionally, if a mathematical model of a given surface is known, it can be used in series with the current model to evaluate the influence of that surface on the impulse experienced by the head. In this way, the current models can be used in conjunction with a parametric analysis to optimize facial fracture countermeasures. As demonstrated in earlier chapters, the biofidelity of the FOCUS headform needs improvements and it is hoped that these models can assist in the optimization of the headform flesh to produce a more biofidelic response.

REFERENCES

Bruyere K, Bermond F, Bouguet R, Caire Y, Ramet M, Voiglio E: Human Maxilla Bone Response to 30 degree Oriented Impacts and Comparison with Frontal Bone Impacts, *Proceedings of the 44th Association for the Advancement of Automotive Medicine Conference*, 219-34; 2000.

Cesari D, Ramet M, Welbourne E: Experimental Evaluation of Human Facial Tolerance to Injuries, *Proceedings of the IRCOBI*, Stockholm, Sweden; 1989.

Funk J, Duma S, Manoogian S, Rowson S: Biomechanical Risk Estimates for Mild Traumatic Brain Injury, *Annual Proceedings of the Association for the Advancement of Automotive Medicine* 2007.

Nahum AM: The Biomechanics of Facial Bone Fracture, *Laryngoscope*, 85(1), 140-56; 1975.

Nahum AM, Gatts JD, Gadd CW, Danforth J: Impact Tolerance of the Skull and Face, *Proceedings of the 12th Stapp Car Crash Conference,* October 22-23, New York; 1968.

Nyquist GW, Cavanaugh JM, Goldberg SJ, King AI: Impact Tolerance and Response of the Face, *Proceedings of the Advances in Bioengineering Conference*, Anaheim, CA; 1986.

Prasad P, Mertz H: The Position of the United States Delegation to the ISO Working Group 6 on the Use of HIC in the Automotive Environment, *Society of Automotive Engineers*,(851246); 1985.

CHAPTER 10:
SUMMARY OF RESEARCH

MAJOR CONTRIBUTIONS

The proposed research will make several major contributions to the field of biomechanics:

1. An understanding of occupant, vehicle and collision descriptors which are associated with the occurrence of facial fractures.
2. The quantification of acoustic emission associated with facial impact by a blunt object and its association with fracture.
3. The determination of risk functions for the frontal bone, nasal bone, maxilla and mandible when subjected to focal blunt impact.
4. Force-displacement response corridors for the frontal bone, nasal bone, maxilla and mandible when subject to focal blunt impact.
5. Characterization of the FOCUS headform to further develop its utility in evaluating protective countermeasures.

The proposed research is expected to result in the publication of five journal articles with related conference publications as well (Table 24). It is expected that chapters four and five will be combined to create the submission for the Stapp Car Crash Conference.

Table 24: Proposed publication topics and journal submissions.

Chapter	Title / Topic	Journal	Conference
1	The Epidemiology of Facial Fractures in Automotive Collisions		Submitted – AAAM 2009
2	The Relationship Between Facial Fractures and Brain Injuries in Automotive Collisions.	Journal of Trauma	
3	A Review of Studies on Facial Tolerance	SAE Book	
4	Acoustic Emission in Fracture Detection	RMBS 2008	
5	The Tolerance and Response of the Frontal Bone to Blunt Impact	Stapp Car Crash Conference 2009	Ohio State: Injury Biomechanics Symposium 2009
6	The Tolerance and Response of the Nasal Bone to Blunt Impact		AAAM 2010
7	The Tolerance and Response of the Maxilla to Blunt Impact	J. Biomechanics	IRCOBI
8	The Biomechanical Response of the Mandible to Blunt Impact	J. Applied Biomechanics	IRCOBI
9	Mathematical Modeling of Facial Impacts	J. of Foresensic Sciences	Forensic Science Conference